Springer Series in
OPTICAL SCIENCES 140

founded by H.K.V. Lotsch

Springer Series in
OPTICAL SCIENCES

The Springer Series in Optical Sciences, under the leadership of Editor-in-Chief *William T. Rhodes,* Georgia Institute of Technology, USA, provides an expanding selection of research monographs in all major areas of optics: lasers and quantum optics, ultrafast phenomena, optical spectroscopy techniques, optoelectronics, quantum information, information optics, applied laser technology, industrial applications, and other topics of contemporary interest.
With this broad coverage of topics, the series is of use to all research scientists and engineers who need up-to-date reference books.

The editors encourage prospective authors to correspond with them in advance of submitting a manuscript. Submission of manuscripts should be made to the Editor-in-Chief or one of the Editors. See also www.springer.com/series/624

Vesselinka Petrova-Koch
Rudolf Hezel
Adolf Goetzberger

Editors

High-Efficient Low-Cost Photovoltaics

Recent Developments

With 144 Figures

Springer

Dr. Vesselinka Petrova-Koch
Gate East
Schleißheimer Str. 17, 85748 Garching, Germany
E-mail: vpkoch@yahoo.de

Professor Dr. Rudolf Hezel
Josef-Heppner-Str. 26, 82049 Pullach, Germany

Professor Dr. Adolf Goetzberger
the Fraunhofer Institute for Solar Energy Systems ISE
Heidenhofstr. 5, 79110 Freiburg, Germany
E-mail: goetzb@ise.fhg.de

Springer Series in Optical Sciences ISSN 0342-4111 e-ISSN 1556-1534
ISBN 978-3-540-79358-8 e-ISBN 978-3-540-79359-5

Library of Congress Control Number: 2008930093

Typesetting by the authors and VTEX, using a Springer LaTeX macro
Cover concept: eStudio Calamar Steinen
Cover production: WMX Design GmbH, Heidelberg

SPIN: 12191949 57/3180/Vtex
Printed on acid-free paper

9 8 7 6 5 4 3 2 1

springer.com

Preface

Global warming and climate change are a result of excessive emission of green house gases in the recent decades. During the same period we have experienced a dramatic *increase in energy demand to support the global industry and a* "*modern life style*". These events, combined with the astronomic increase of the *energy prices* since the beginning of the 21st century, make it obvious that the *global energy mix* needs to be changed in favor of *clean renewable energy sources*. At the same time we must improve the *energy efficiency* of all technologies.

Solar energy conversion, particularly *Photovoltaics* (PV) represents one of the most interesting and dynamically growing branches of the industry at the moment. Although today the cost of PV is still relatively high, it has dropped considerably in the past years and will continue to do so. A main driving force behind the development of solar energy is its enormous, practically unlimited potential. Unlike other renewable energy sources like wind or water, solar energy can be utilized everywhere on the globe. The cost of PV will have to continue to drop if the goal of economic viability is to be reached. Prices of PV modules and systems follow a well-determined learning curve. If present trends continue, it has been predicted that grid parity (cost of PV equal to grid electricity at the consumer's site) will be reached in about 10 years in favorable locations. An important aspect of the learning curve is that it includes not only scale effects of mass production but also technical advances and new concepts. It can be shown that for most applications *high efficiency* is a prerequisite *for lowering cost*. It is the purpose of this book to give a survey of the most important technologies for increasing efficiency and lowering cost of PV.

In the last five to six years the PV market has grown exponentially: not all over the world yet, but in some countries like Germany and Spain in the EU, and Japan in Asia. Japan and Germany may be considered as front-runners and engines of the newborn *PV Mega Industry.* The German *preferential feed-in tariff for solar electricity* and the new RES Law (*called EEG in German*) opened new market dimensions and made it possible that the German market outgrew a country like Japan, which was and is still the biggest PV producer worldwide. Germany reached this state in spite of the fact that it is not the sunniest part of Europe, due to the *joint efforts*

of politics, industry and academia. About one-fourth of all PV modules produced worldwide till the end of 2007 are installed in the southern part of Germany (mainly in Bavaria and Baden-Wuerttemberg)! The exceptionally successful *EEG* law also influenced many other countries. In the last five years more than 30 countries copied and/or modified it. In this way, a *PV network* was formed. This network spawned a very active PV development in several countries of the EU like Italy, Portugal, Greece, and even new member-states like Bulgaria. PV is becoming accepted also in countries like USA, Australia and Russia, as well as well as in the newly developing economies like China, India and Turkey, which are on their way to sign the Kyoto Protocol and to support the targets for Clean Energy.

So far the PV Market is dominated by the so called *first-generation* PV, the production and installation of which recently reached the gigawatt scale. First-generation PV, which can be seen on many solar roofs today, is based mainly on mono- and poly-crystalline Si, and these wafers are not made of low cost material. This generation is characterized by relatively low efficiencies of the cells and modules, considerably below the theoretical limits and below results that have been obtained in the laboratory. In spite of this fact, the demand for PV is increasing exponentially so that several crises along the value chain of the PV industry have occurred: for example the shortage of solar grade poly Si feedstock since 2005, or the one for solar glass, appearing on the sky-line now. The crises of the Si feed stock are causing a deviation from the learning curve. The fast growth of the PV demand at one side, and the shortage of Si at the other have generated not only supply problems, but they also led to a change of perspectives and to a search for innovative solutions, based on new materials, cells and module-systems. These new solutions are based on reduced consumption of expensive semiconductor material using for example *thin film PV technology* (*second-generation PV*), or on improved efficiency of crystalline cells and systems, while making use of cost effective *concentrators for solar radiation* (*third-generation PV*).

The aim of this book is to present some important trends and achievements that are shaping the *High Efficient Low Cost Photovoltaic* (*HELCPV*) *Industry*.

Our intention here is not to deal with the basics of PV, which are covered elsewhere. We also don't focus in this book on thin-film PV. Our ambition is to present here the most important strategies and developments in the *transition period for the PV industry between* 2000 *and* 2007 on its way *to a gigawatt industry*, and to predict some of the tendencies of development of the near future, focusing on innovative *highly efficient wafer-based solar cell* and innovative *modules* and systems, making use of *concentrated sun radiation.*

The book consists of 13 chapters, written by 25 authors. In chapter 1 an attempt is made to put together in a chronologic manner the milestones of the PV since the discovery of the photovoltaic effect in 1839 and to focus the attention on the important steps to develop a powerful and sustainable PV industry. In Chap. 2 a comprehensive review of PV for space applications as a for-runner of the PV Industry and its impact on the terrestrial PV is demonstrated. Chapter 3 focuses on the development of the terrestrial PV from a niche market in the beginning of the

21st century to one of the most important mainstream markets for electricity at the moment.

Chapter 4 reviews state of the art poly Si technology based on the Siemens process, which remains the major technology also after the recent shortage for poly Si. In Chap. 5 the recent advances of the so called ribbon technology, which gives the unique chance to reduce the consumption of Poly Si during wafer manufacturing are described. In Chap. 6 an unambiguous answer to the question "Why high efficient, bifacial c-Si PV cells?" is given, and a novel high-efficient rear contact c-Si cell with bifacial sensitivity and elegant simple manufacturing steps is described. Chapter 7 reviews the commercially available power c-Si PV cells, like the Point-Contact Solar Cell of Sun Power, the HIT Solar Cells of Sanyo and the Buried-Contact Solar Cell manufactured by BP. This gives opportunity to the reader to compare the concepts available already on the market with the one presented and analysed in Chap. 6.

Chapter 8 reviews the development of III–V multi-junction PV cells with efficiency close to 40%, on relatively less expensive c-Ge substrates. The ability of such cells to operate under extreme conditions (more than 1,000 suns) is emphasized. Cost effective concentrator systems based on Fresnel mini-lenses arrays, prepared out of silicone, and sun truckers for such concentrator modules are described here. In Chap. 9 the economic perspectives of the III–V concentrator PV when manufactured on megawatt scale is discussed and compared to the first generation c-Si PV. It is argued why CPV should be considered as a promising candidate on the market, capable to compete with the c-Si PV particularly in the very sunny regions in the solar belt-countries.

In Chap. 10 the attention is focused on an alternative device concentrating the sun radiation, named Fluorescent Concentrator, which is less popular than the one based on Fresnel-optics, but which is unique in its ability to concentrate diffuse radiation in a sophisticated way. The basics and the more recent advances to develop further and to simplify this device are reviewed in this part. Chapter 11 deals with a concept of a novel hybrid Photovoltaic/Thermal concentrator. Chapter 12 points the attention then to some innovative PV installation concepts and future PV applications.

Chapter 13 reviews the recent advances in the field of Organic Solar Cells and deals with some design rules, helping to make the organic PV relatively high efficient. We believe that OPV will continue to develop similar to the OLEDs and will be able to supply the market with high efficient low cost PV in a very near future.

Garching, Pullach, Freiburg,
July 2008

Vesselinka Petrova-Koch
Rudolf Hezel
Adolf Goetzberger

Contents

List of Contributors

Zh.I. Alferov
Ioffe Physico-Technical Institute
26 Polytechnicheskaya str.
St. Petersburg 194021
Russia
Zhores.Alferov@mail.ioffe.ru

V.M. Andreev
Ioffe Physico-Technical Institute
26 Polytechnicheskaya str.
St. Petersburg 194021
Russia
vmandreev@mail.ioffe.ru

C.J. Brabec
CTO Konarka Technologies Inc.
Altenbergerstr. 69
A-4040 Linz
Austria
cbrabec@conarka.com

G. Dennler
Konarka Austria GmbH
Altenbergerstr. 69
A-4040 Linz
Austria

A. Goetzberger
Fraunhofer Institute
for Solar Energy Systems
Heidenhofstr. 2
D-79110 Freiburg
Germany
adolf.goetzberger@
ise.fraunhofer.de

K. Hesse
Wacker Chemie AG
WACKER POLYSILICON
Johannes-Hess-Straße 24
D-84489 Burghausen
Germany
karl.hesse@wacker.com

G. Hey
DLR – Deutsches Zentrum
für Luft- und Raumfahrt e.V.
Direktion Raumfahrt
Postfach 30 03 64
D-53183 Bonn
Germany

R. Hezel
University of Hannover
Josef-Heppner-Straße 26
D-82049 Pullach
Germany
rudolf.hezel@t-online.de

W. Hoffmann
Vice President and CTO EES
Applied Materials GmbH & Co.KG
Siemensstraße 100
D-63755 Alzenau
Germany
winfried_hoffmann@amat.com

M. Koppe
Konarka Austria GmbH
Altenbergerstr. 69
A-4040 Linz
Austria

G. LaRoche
AZUR SPACE Solar Power GmbH
Theresienstr. 2
D-74072 Heilbronn
Germany

O. Mayer
GE Global Research
Freisinger Landstrasse 50
D-85748 Garching
Germany
oliver.mayer@research.ge.com

E.W. Merkle
Bayerische Solar AG
Dachauerstr. 37
D-80335 München
Germany
merkle@bayerische-solar.de

M. Morana
Konarka Austria GmbH
Altenbergerstr. 69
A-4040 Linz
Austria

D. Mühlbacher
Konarka Austria GmbH
Altenbergerstr. 69
A-4040 Linz
Austria

V. Petrova-Koch
Gate East
Schleissheimerst 17
D-85748 Garching/Munich
Germany
vpkoch@yahoo.de

K.-D. Rasch
AZUR SPACE Solar Power GmbH
Theresienstr. 2
D-74072 Heilbronn
Germany

V.D. Rumyantsev
Ioffe Physico-Technical Institute
26 Polytechnicheskaya str.
St. Petersburg 194021
Russia
rumyan@scell.ioffe.rssi.ru

M.C. Scharber
Konarka Austria GmbH
Altenbergerstr. 69
A-4040 Linz
Austria

I.A. Schwirtlich
SCHOTT Solar GmbH,
D-63755 Alzenau
Germany

G.F.X. Strobl
AZUR SPACE Solar Power GmbH
Theresienstr. 2
D-74072 Heilbronn
Germany

M. Sturm
Solar*Tec AG
Uhlandstr. 13
D-85609 Aschheim b. München
Germany
sturm@solartecag.de

R. Tölle
Solar*Tec AG
Uhlamstr. 13
D-85609 Aschheim b. München
Germany
toelle@solartecag.de

L. Waldmann
Public Relations
SCHOTT Solar GmbH
Carl-Zeiss-Straße 4
D-63755 Alzenau
Germany

D. Waller
Konarka Technologies Inc.
100 Foot of John Street
Boott Mill South, 3rd Floor
Lowell, MA 01852
USA

Z. Zhu
Konarka Technologies Inc.
100 Foot of John Street
Boott Mill South, 3rd Floor
Lowell, MA 01852
USA

1 Milestones of Solar Conversion and Photovoltaics

V. Petrova-Koch

1.1 Prehistory

Seventh century BC: In ancient *Egypt* the houses were built so that the solar radiation could be collected during the day and used during the night.

Fifth century BC: The *Greeks* oriented their houses so that they could receive solar energy in the winter time *to heat the buildings*.

Third century BC: *Archimedes* used *mirrors* to reflect *direct sun radiation* and to defend Syracuse from invasion by the Romans.

Second century BC: the first *windows* made out of *transparent mica* were inserted in houses in northern Italy, with the aim to increase the use of solar radiation in winter time.

First century AD: the so called *heliocaminos* started to be used. These solar baths with big mica windows oriented to the south found their maximum application in Italy around the fifth century.

Fourteenth century: the first *solar law* was introduced in Italy.

1767 in Russia: *M.V. Lomonossov* suggested the use of lenses to concentrate the solar radiation.

1767 in Switzerland: *Horace de Saussure* discovers the amplification and increased heat efficiency in Matjoshka-type five-folded glass boxes.

1830 in South Africa: *J. Hershel* uses the first *solar cooker*.

Around 1830: *H. Repton* constructs the first (*glass*) *greenhouses in Europe.*

1.2 Milestones of Photovoltaics

1839: *Alexandre-Edmund Becquerel*, a young experimental physicist in France, discovered the photovoltaic effect at age of 19, while assisting his father, experimenting with electrolytic cells made up of two metal electrodes.

1873: *W. Smith, working in the UK*, discovered the photoconductivity of selenium, which led to the invention of the photoconductive cell.

1876: *W.G. Adams and R.E. Day*, *USA*, observed the photovoltaic effect in solid selenium.

1883: *Ch. Frits*, an American inventor, described the first solar cell made from Se wafers.

1887: *H. Hertz* discovered in Germany that ultraviolet light altered the lowest voltage capable of causing a spark between two metal electrodes.

1888: *Ed. Weston* receives the first patent for solar cells (U.S. 389124 and US3891-25).

1904: *W. Hallwachs* discovered the photosensitivity in a copper/cuprous oxide pair.

1904: *A. Einstein* publishes his pioneering theoretical work on the photoelectric effect (he received the Nobel Prize in 1921 for this work).

1916: *R.A. Millikan* provides experimental proof of the photoelectric effect.

1916: *Y. Czochralski* (Polish scientist) develops a new method to grow single-crystal silicon.

1930: *W. Schottky* discovers a new cuprous oxide photoelectric cell.

1931: *A.F. Ioffe* guides a project at the Physico-Technical Institute in St. Petersburg on thallium sulphide photocells, which reach a record efficiency at that time of more than 1%. He submitted a proposal to the Soviet government concerning the use of solar PV roofs for providing electricity.

1932: *Audobert and Stora* discover the photovoltaic effect in CdS.

1948: *W. Schottky* presents the first theoretical concept for semiconductor PV.

1951: at *Bell Labs* the first p–n junction was grown in germanium.

1953: *D. Trivich* publishes the first theoretical calculations on the conversion efficiency of the solar spectrum with materials of different band gaps.

1953: *G. Pearson at Bell Labs* begins research of Li-doped Si solar cells.

1953: *D. Chapin*; *C. Fuller and G. Pearson* realized a two cm^2 Si solar cell with an efficiency of 4% (published on *NY Times* cover page).

1954: *D. Chapin*, *C. Fuller and G. Pearson* improve the efficiency of a Si Cell to 6%; first AT&T solar cell demonstration in Murray Hill, NJ.

1954: At *Siemens in Germany*, *G. Spenke* and his team develop an efficient *method for poly-Si growth*: Scientists and experts from *Wacker* and TU Munich participate in this work as part of a joint team with Siemens. The so-called *Siemens Method* is the main technology for the production of solar and semiconductor grade Si.

1954: *J.J. Loferski and Jenny* at RCA reported a pronounced PV effect in Cd*S*.

1954: *The International Solar Energy Society* (*ISES*) *was founded in Phoenix*, *AZ*, *1970. Its headquarters was later moved to Melbourne*, *Australia*, *and in 1995 it was moved again to Freiburg*, *Germany.*

1957–1959: *Hoffmann Electronics* achieves 8, 9 and 10% efficiency and develops the grid contact, significantly reducing the series resistance of the device.

1960: *Hoffmann Electronics* makes a jump to 14% efficient PV cells, mainly used for satellite technology and space applications.

1960/1961: *H. Mori* in Japan and *A.K. Zaitseva & O.P. Fedoseeva* in Russia independently proposed bifacial PV modules.

1961: *W. Shockley and H. Queisser* developed a thermodynamic theory on the principle of *detailed balance* for one-junction solar cell.

1961: *First IEEE PV Specialists Conf.* is initiated in *Philadelphia*, *USA*.

1963: *Sharp in Japan* installs the world largest array for *terrestrial applications*, with a power of 242 W!

1966: *The first 1 kW PV Array* was installed on the Orbiting Astronomic Observatory.

1966: *Zh.I. Alferov*, *V.B. Khalfin and R.F. Kazarinov* discovered "the superinjection-effect" in a *double heterostructure* (*DHS*).

1970: *Zh.I. Alferov*, *V.M. Andreev and a team* at Ioffe Institute St. Petersburg demonstrated the first efficient *GaAs heterostructure solar cell.*

1973: *Solarex was founded in the USA. This produced the first commercial polycrystalline solar cell and the first commercial amorphous solar cell. Solarex was later acquired by Amoco/Emron and then by BP Solar.*

1974: *Japan* formulates *Project Sunshine* at the beginning of the *first oil crisis.*

1976/1977: The first *fluorescent collector for solar applications* is suggested independently by *A. Goetzberger* and *W. Greubel*, and by *W.H. Weber* and *J. Lambe*.

1976: *D. Carlson and Ch. Wronsky at RCI*, *USA* demonstrate the first a-Si:H thin-film solar cell with an efficiency of around 1%.

1977: The *Solar Energy Research Institute* (*SERI*), later to become the *National Renewable Energy Laboratory* (*NREL),* opens in Golden, CO, USA.

1977: *EC PV Solar Energy Conference* starts *in Luxembourg.*

1978: The first lab *for Solar Energy and Renewable Energy Sources* (*SENES*) starts operations in Europe at the *Bulgarian Academy of Sciences in Sofia.*

1980: *M. Riel* starts the famous *1,000 solar roof program in Zurich*, Switzerland.

1980: *BP enters solar business*.

1981: *The Fraunhofer Institute for Solar Energy ISE* in Freiburg Germany founded by A. Goetzberger.

1981: *R. Hezel introduced Plasma Silicon Nitride* (*PECVD*) as *antireflection and passivation layer*, which is presently applied for almost all commercial silicon solar cells.

1981: *Reflective solar concentrators* used for the first time with solar cells at Ioffe Institute St. Petersburg.

1982: *The PV Production* worldwide reaches the value *of 10 MW*!

1982: *A 1-MW PV plant* – built by *ARCO Solar* with 100 Dual-Axis trackers with c-Si modules – goes online in *California.*

1983: The PV production worldwide exceeds *20 MW*, *and sales exceed* $250 million U.S.!

1983: *International Science and Engineering Conference* (the Asian ISE-Conference) is started.

1984: *M.A. Green and S. Wenham* introduced the *laser-grooved buried-contact* solar cell (*LGBC*).

1985: *M. Green* at the University of New South Wales Australia, *breaks the 20% efficiency barrier for c-Si solar cell under one sun* in the research lab.

1985: *R. Swanson* founded *Sun Power in CA* with the goal to commercialize the high-efficiency c-Si solar cell.

1986: *ARCO Solar* releases the first *commercial thin-film power module.*

1987: The Solar Challenge is inaugurated, and *PV-powered cars* race across Australia.

1989: *V.D. Rumyantsev at Ioffe Institute St. Petersburg* introduces a *solar concentrator lens-cell system with radically reduced size*.

1990: *ARCO Solar* is sold to *Siemens* and renamed *to Siemens Solar*.

1991: *Nukem GmbH* (*now Schott Solar*) built *1 MW pilot PV plant* out of *mono- and bifacial MIS-inversion-layer solar cells*, developed by the team of *R. Hezel at the University of Erlangen*.

1991: *M. Graetzel* invents the *dye-sensitized electrochemical solar cell.* An efficiency more than 10% was obtained within five years after the discovery.

1992: *BP* commercializes the *Laser Grooved c-Si Solar Cell* (*patented by M.A. Green and S. Wenham*).

1994: *NREL* develops and demonstrates *a two-terminal*, *high-efficiency GaInAsP/GaAs solar cell*, which under 180 suns shows more than 30% efficiency. The third generation CPV was born.

1997: *The biggest PV roof* with more than 3 MW is installed in Munich, Germany.

1997: *Sanyo* starts mass production of its *high-efficiency HIT c-Si/a-Si:H PV cells.*

1998: *SolarWorld A.G.* is founded in Germany, the *first vertically integrated PV company*.

1999: *M.A. Green and J. Zhao* achieved a *record efficiency of 24.7% for laboratory c-Si solar cells*.

1999: *Total PV power* installed worldwide exceeds *1 GW*!

2000: *April*: *Germany* introduces the *new EEG* (*feed-in law*), the law which, in 2008, was translated into more than 40 languages. Germany becomes the largest PV market worldwide.

2002: *First Solar Silicon Conference* dealing with the crisis of Si feedstock *was* organized by Photon in Munich, Germany.

2002: *Cypress Corp. and Sun Power* in the USA start pilot production of the high-efficiency c-Si Sun Power PV cell. Mass production set up in the Philippines.

2002: *Siemens Solar* sold its solar activities to *Shell Solar*, *in 2004 Shell Solar* c-Si solar cell activities were divested to *SolarWorld.*

2004: *General Electric* enters PV, after becoming owner of *AstroPower.*

2005: *Sharp* remains *the biggest producer* of PV cells worldwide.

2005: *Q-Cells*, which was founded in 2002, is the *fastest growing PV cell producer* worldwide.

2006: *A PV Roadmap for Europe* is proposed by WCRE.

2006: More than *25% of the PV Modules* produced worldwide are installed in Germany.

2006: *SolFocus in USA*, *Concentrix-Solar in Freiburg*, *Germany*, *and SolarTec AG in Munich*, *Germany*, start *pilot-production of concentrator III–V PV* (*CPV*). CPV Modules consisting of GaAs triple cells on Ge substrates with efficiency more than 35%, and Fresnel concentrator lenses made out of UV-resistive silicone, capable of providing up to 800 suns; system will be available in 2008.

2006: *Wacker* expands the production of solar-grade poly-Si in *Burghausen*, Germany, up to 16,000 tonnes per year to become the second biggest company in this field worldwide. The new investment is about 500 million €.

2006: *First Int. Solar Glass Conference* is organized by Photon in Munich.

2007: *Hemlock* announces its mega-expansion of poly-Si production up to 3,600 metric tonnes per year in *MI*, *USA*, and will start producing in 2010. The investment is about $1 billion U.S. Hemlock remains the biggest poly-Si producer worldwide.

2006: *InterSolar*, the *biggest International Solar Fair* takes place for a 10th and last time in Freiburg, Germany. In 2008 it will continue to operate in Munich.

2007: *SunPower* and *Sanyo* both announce the *highest efficiency* for mass produced Solar Cell under one sun solar radiation of *22%*.

2007: *Al Gore and IPCC* receive the *Nobel Peace Price.*

2007: *UN-Conference* devoted to climate change takes place *in Bali*.

2008: *Q-Cells* bypasses *Sharp* to becomes the world biggest PV cell producer.

2 From Extraterrestrial to Terrestrial Applications

G.F.X. Strobl, G. LaRoche, K.-D. Rasch, and G. Hey

2.1 Introduction

In the early 1950s, Bell Laboratories in the USA investigated possible applications of silicon semiconductors in electronics. While improving transistors, Bell scientists Gerald Pearson and Calvin Fuller invented the first silicon solar cell. That first effort was further improved for applications in remote humid locations by Darryl Chapin [1]. The first experiment with silicon yielded an efficiency of 2.3%. Improvements with regard to the dopants, the metallic contacts to the p- and n-side and the application of an antireflection coating led to efficiencies of 4%. In 1954, cells with 6% efficiency could be reliably manufactured.

The first solar battery was presented to the public by Bell Laboratories on April 25, 1954. The battery powered a 21-inch Ferris wheel one day and a solar-powered radio transmitter the next. Technical progress continued and the cell efficiency doubled within two years. Even then, Bell representatives dreamt of a limitless power supply. But this progress could be achieved only with high-purity, single-crystal silicon which was expensive. Thus, a commercial breakthrough was prevented with the exception of some applications by Western Electric to run telephone lines in rural areas. The price at that time was more than $300/W.

Commercialization efforts were undertaken by the National Fabrication Products Company with their chief Scientist Dr. Martin Wolf. But the company did not succeed in bringing the price down and was bought in 1956 by Hoffmann Electronics of El Monte, CA. They developed a 25 W sun-power-to-electricity converter module which no one bought. Its only application was in toys.

At the same time, the U.S. Army Signal Corps investigated possible applications for solar energy converters and found one preferred application: satellites in space! The U.S. Army signal corps was responsible for the design of a solar cell power system for the satellite project Vanguard to be built by the U.S. Navy. They contacted Hoffmann Electronics, and its chief engineer, Eugene Ralph, assembled some of their cells. On St Patrick's Day 1958, Vanguard 1, the first satellite with solar cells aboard, went into orbit. Two months later, SPUTNIK III, also equipped with silicon solar cells, was launched. After six years in orbit, Vanguard 1 was still sending radio messages back to Earth [2].

Despite some early applications on oil platforms, the astronomical price of silicon solar cells limited their use to space. So the onset of the Space Age was the

salvation of the solar cell industry (M. Wolf). From 1958 to 1969 the U.S. government spent more than $50 million on solar cell research and development.

2.2 Solar Cells for Space

Space cells had to be extremely overengineered to withstand the harsh space environment – charged particles, micrometeoroids, hard UV radiation, and temperature extremes due to change of daylight and eclipses all posed challenges. Those challenges required a special design for each satellite, due to individual layout, limited area, storage volume and mass. The solar cell power supplies grew steadily and reached 500 W with the Nimbus Spacecraft in 1964; 1,000 W on the Orbiting Astronomical Observatory in 1966; and 20 kW for the Orbiting Laboratory Skylab in 1972. The upper limit to the size of photovoltaic solar converter arrays in space was given by the capacity of the available launch vehicles. It was found that a high power-to-mass ratio of the solar array was the most important factor which could be increased by improving the solar cell efficiency and/or lowering the solar array mass.

In Germany on August 23, 1962, the "Gesellschaft für Weltraumforschung GfW" was founded to manage and coordinate space activities with the goal of building the first German satellite "AZUR". The satellite's mission was to study cosmic rays and their interference with the Earth's magnetosphere, the northern lights and the time variation of the solar wind due to solar flares. German industry was invited to develop and manufacture the required subsystems and to make the satellite ready for launch. It was launched on November 8, 1969, with a Scout rocket from Cape Canaveral. For this application the solar cell development also took place in Germany at Siemens and Telefunken. These activities benefited from progress made in the U.S. and published in dedicated technical journals and conference proceedings. Importantly, the cells delivered by Telefunken were 2 cm by 2 cm and delivered efficiencies of more than 10%. Moreover, with the introduction of titanium-silver contacts, a technology was developed that became the baseline for all future silicon solar cells for space applications.

Improved understanding of the theory of device operation led to increased efficiency and cost reduction of silicon solar cells (Fig. 2.1 from [2]). But the efficiencies achieved were still far below the theoretical ones. Moreover, theory stated that materials other than Si – like GaAs or CdTe – would give better efficiencies in the Sun spectrum, especially at increased temperatures (Fig. 2.2). Given that Si was the most developed and best understood material, most efforts were directed toward further improvements of Si solar cells. In parallel, other materials like cadmium sulfide, cadmium telluride, and gallium arsenide were investigated but did not achieve better results than silicon. Other thin-film technologies – one based on amorphous silicon and the other on the ternary compound $CuInSe_2$ (CIS) – found applications in electronics and to some extent in power plants.

One advantage of GaAs-based solar cells over Si was their better temperature stability and higher radiation resistance, giving them preference for special

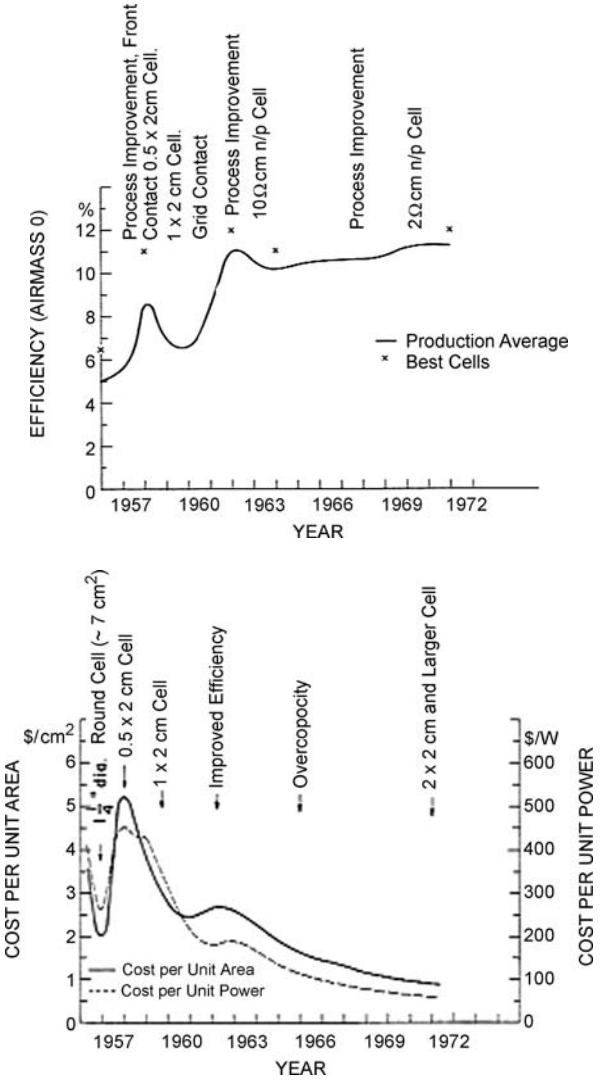

Fig. 2.1. Early historical development of silicon solar cell efficiency (*top*) and cell prices (*bottom*)

applications despite their higher costs. One of the first space applications of the temperature-stable GaAs solar cells took place on the Russian spacecrafts Venera-2 and Venera-3, launched in November 1965 to the "hot" planet Venus. The area of each GaAs solar array fabricated by the Russian Enterprise KVANT for these spacecrafts was 2 m^2. Then, the Russian moon cars were launched in 1970 (Lunokhod-1) and in 1972 (Lunokhod-2) with GaAs 4 m^2 solar arrays in each. The operating temperature of these arrays on the illuminated surface of the Moon was about 130 °C.

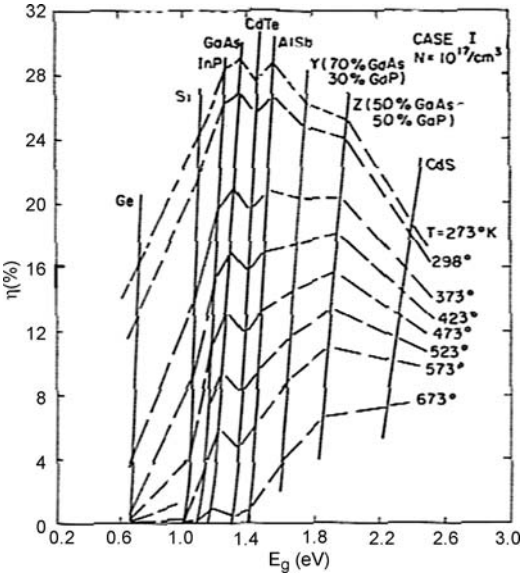

Fig. 2.2. Theoretical efficiencies of different materials at various temperatures (from [3])

The solar arrays demonstrated an efficiency of 11% and have provided the energy supply during the life-time of these moon cars [4].

Further progress was achieved by the development of AlGaAs/GaAs heterostructures, the combination of materials with different energy gaps. Their AM0 efficiency was increased up to 18–19% [5]. A solar array with a total area of 70 m^2 was installed in the Russian space station MIR launched in 1986 (Fig. 2.3). During 15 years in orbit, the array degradation appeared to be lower than 30% under hard operating conditions with appreciable shadowing, the effects of numerous dockings, and a challenging ambient environment of the station.

But GaAs solar cells were more expensive than Si solar cells by a factor 5 to 10, and therefore were used only for special applications. Compared to silicon, the use of GaAs solar cells was considered profitable only if their efficiency would exceed 20%. This was not realistic in the near-term. Therefore, main emphasis was given to further improving the Si technology.

2.3 Closer to the Limit

An analysis of the main loss mechanisms of Si solar cells by M. Wolf [6] yielded the following power-limiting factors:

1. Optical reflection of incident light on the cell surface.
2. Crystal quality limiting quantum efficiency of electron – hole pair production.
3. Loss of excess energy of the majority of absorbed photons necessary to generate electron – hole pairs.

Fig. 2.3. AlGaAs/GaAs solar array on the MIR Space Station (from [4])

4. Low optical absorption coefficient.
5. Recombination of minority carriers on the surfaces, by impurities, dislocations and on the back contact.
6. Reduced barrier height of the junction by the distance of the Fermi levels from the band edges.
7. Loss and leakage currents across the junction and recombination within the depletion layer.
8. Series resistances in the base region and the cell contacts.

The improvement of each factor should bring the real solar cell efficiency closer to the theoretical one. For space applications, the impact of charged particle irradiation had to also be considered. The following main developments were milestones in the improvement of Si solar cells to their present status.

2.3.1 Material Quality

Impurities in the solar cell material generally introduce traps into the crystal. These traps act as recombination centers. An increased density of such centers decreases the minority carrier lifetime and the cell efficiency. On the other hand, silicon must not only be very pure, but it must also be in a single-crystal form with essentially zero defects in the crystal structure. To achieve the required purity the metallurgical grade silicon extracted from silicon dioxide (quartzite) by reduction in large arc furnaces must be further purified by fractional distillation of the condensed volatile

compound $SiHCl_3$ and reduced by hydrogen. This semiconductor grade material is then melted in a crucible with trace levels of the dopant required (normally boron for p-type silicon) and, by means of a seed crystal, large cylindrical single crystals are pulled from the melt (Czochralski process). These so-called boules are sliced up into wafers forming the ingot for the manufacture of solar cells.

Refinements of the above processes improved the wafer quality continuously, allowing higher doping levels which resulted in remarkable efficiency improvements (10 Ω cm versus 2 Ω cm base resistivity). The increase of the crystal diameters from 5.0 cm to more than 12.5 cm allowed the manufacture of large-area solar cells. Though small cells are using the wafer area better (minimum material loss), large area cells were preferred for the subsequent processing steps of cover glassing, cell interconnection and substrate bonding due to cost savings.

2.3.2 Back Surface Reflector (BSR)

The absorption of photons from the incident sunlight depends on the absorption coefficient, which is high for short wavelengths and low for longer wavelengths. Accordingly red and infrared light penetrate deeper into the silicon material and a big portion is scattered or absorbed at the rear side contact. Polishing and coating the rear side with a thin aluminum reflector makes the back contact reflective giving the longer wavelengths a second chance at being absorbed and the energy which is not absorbed is re-emitted through the front surface leading to a reduction in cell absorbance. This is a critical parameter controlling the device's operating temperature.

Such back surface reflectors (BSR) gave a boost to the performance of thin cells and lowered the cell temperature considerably. Thin cells are making solar cells more resistant to charged particle radiation, since minority charge carriers have a higher chance of reaching the pn-junction even in the presence of recombination centers.

2.3.3 Back Surface Field (BSF)

The primary mechanism for the movement of minority carriers toward the pn-junction is the diffusion process. An additional moving mechanism was found to be the drift of minority carriers caused by a built-in electrostatic field arising from gradients of the impurity density. While a positive effect in the diffused region of the cell is found only with a deep junction, which stands against the enhancement of blue response (see violet cell), a drift field is advantageous in the bulk area in order to reduce minority carrier recombination at the rear side. It was found by Wolf [7] that the inclusion of a narrow layer with a drift field in the base region has a marked effect on the performance of the cell and the degradation rates due to nuclear particle radiation. The efficiency of silicon solar cells could be improved by the introduction of a back surface field by up to 17% (e.g., Spectrolab K4700- type compared to Spectrolab K6700-type [8]).

Technologies developed at Telefunken in Germany to form back surface fields consisted of boron diffusion, boron ion implantation and evaporated aluminum paste processes [9]. While the diffusion and implantation processes yielded equal efficiencies at beginning of life, implanted BSF cells showed lower degradation after particle irradiation (end of life EOL condition).

2.3.4 The Violet Cell [10]

Former cells were very limited in the short wavelength region and their diode characteristics were far from ideal. By the existing diffusion process the front regime of a cell consisted of three regions: a shallow region, called the dead layer, with an extremely short lifetime of the minority carriers. This was due to high dopant concentration above the solid solubility limit, a high field region maintained by the impurity profile, and the space charge region. An improvement of the short wavelength response had to eliminate the dead layer, and the recombination states in the space charge region caused by stresses and defects originating in the silicon front surface. Because the dislocation density decreases sharply toward the diffusion front, the dead layer could be eliminated by shallow diffusion. This minimized the total density of dislocations in the diffusion region. This reduction of the emitter thickness caused an increase in the lateral resistance which could be compensated for by increasing the grid lines, thus keeping the solar cell active area constant to avoid shading losses. These improvements in solar cell efficiency increase efficiency by 30% compared with typical commercial cells without changing the degradation behavior under particle irradiation.

2.3.5 Textured Surfaces

Aside from optical coating optimization, another approach to reduce reflection losses is to use textured surfaces. Texturization is achieved by creating a topology of small, densely packed tetrahedral grooves, V-grooves or random pyramids [11] that act as light traps on the solar cell's surface. When light impinges on this textured surface, reflection occurs at such an angle that it is deflected into a new point on the surface. Multiple interactions occur with the silicon, thus reducing the amount of light normally lost through reflection. Together with an antireflection coating the reflection of sunlight can be kept well under 3%, making the cell appear black ("black cell"). The textured surface also provides a reduction in path length to the junction which is most pronounced for longer wavelength light, thereby increasing longer wavelength collection efficiency (an important factor for thin devices) and radiation tolerance. As bulk region diffusion length is reduced by the effects of radiation, the reduced effective path length enables a contoured surface device to maintain more of the lower wavelength response than a comparable smooth cell.

Texturization increases solar absorbance also in the wavelength region not contributing to the carrier generation. To compensate for the resulting higher temperature special infrared (IR) or blue-red-reflecting (BRR) coverglass coatings have been developed.

2.3.6 Contacts

Titanium-silver and nickel-gold with solder on the interconnector pads were used for the solar cell contacts in the early stages [12]. Later, when the welding technique replaced the soldering technique, the solder layer was eliminated and the titanium was protected against electro-corrosion by an intermediate palladium layer. Today the standard contacts consist of Ti/Pd/Ag applied by vacuum evaporation with a subsequent sintering process and photolithographic process for grid forming. A similar process is applied for the rear side with an additional Al-layer serving as BSR.

2.3.7 Bypass Function [13]

Cell breakage or shadowing of solar cells could cause the solar cell to operate in reverse, forming a so-called "hot spot" with temperatures up to 400 °C. This unwanted effect can be avoided by applying a bypass diode in parallel to the cell but in opposite polarity. By special n^+/p^+-doping through the diffusion layer, this bypass diode could be integrated into the cell structure thus saving the additional expense for separate diode application. The application of a bypass function is an indispensable requirement for modern sophisticated GaAs-based multijunction solar cells.

2.3.8 Surface Passivation

Exposed surfaces – such as between gridlines at the top of the cell or the interface between ohmic metal contacts and semiconductor – are generally regions of high carrier recombination velocity. Drift fields prevent the minority carriers from reaching the wrong surface by forming an electric field between highly doped and lightly doped material like for the BSF; these are already effective at reducing recombination velocity.

Another effective method of surface passivation is the growth of a high purity siliconoxide coating in micro-electronic quality. The purer the oxide the higher the passivation effect. This requires special cleaning provisions prior to the growth of the oxide.

A combination of both methods is the local back surface field [14] minimizing recombination at the metallic rear side point contacts while the majority of the cell rear side is passivated by silicon oxide (Fig. 2.9).

2.3.9 Low-Intensity, Low-Temperature Operation

For the ESA deep space mission ROSETTA ASE, the former Telefunken developed a silicon solar cell which did not show power reduction effects under extreme low-intensity, low-temperature (LILT) conditions. The cell possessed all the characteristics for high efficiency, such as a shallow emitter, passivation oxides on front and rear side, textured front side with inverted pyramids, local back surface field and optimum gridline design realized by means of photolithography. The introduction

of a p^+-channel stopper in contact with the emitter provided very good diode characteristics and reverse protection because the n^+/p^+ diode operated like a Zener diode with reverse breakthrough voltages between −6 V and −8 V [15].

2.3.10 Solar Cell Assembly

For space applications, the solar cells use a coverglass for protection against charged particle irradiation and micrometeorites. The cells also require an interconnector to allow solar cell interconnection. The interconnector has to match the solar cell contacts and survive the thermal stresses which can cause multiple gap variations between adjacent cells. Therefore the preferred interconnector material is pure silver, silver coated Kovar or Molybdenum, the latter matching the thermal expansion coefficient of silicon very close. The interconnectors incorporate stress relief measures in order to withstand the mechanical and thermal stresses. In general, resistance welding is applied for the interconnector integration allowing, in connection with a thin interconnector thickness, a 100% coverage of the solar cell by the coverglass.

The coverglass is adhesively bonded to the solar cell front side. It is coated with an anti-reflection coating on the upper side and a UV-reflective coating on the inner side to protect the coverglass adhesive from darkening. Coverglasses with cerium oxide doping absorb the UV and don't need a UV-coating.

Bonding on the substrate, which is in general a carbon-fiber/Al-honeycomb structure with a polyimide foil insulation, is performed with an elastic cement leaving the gaps between the cells free in order to allow the cells undisturbed linear change. The costs for the silicon solar cell assembly and array integration and test are typically three to four times the solar cell costs.

2.3.11 High Efficiency Solar Cells

Figure 2.4a shows the advances in silicon solar cell performance that led to improved current and the voltage. Figure 2.4b shows improvements in electrical power, and Fig. 2.8 shows gains in efficiency. In Fig. 2.4b, 10 mW/cm^2 corresponds to an efficiency of 7.32% at standard air mass zero (AM0) illumination, averaging the sun spectrum and intensity in the air-free space close to the Earth. It should be pointed out that the reference sun spectrum and intensity for terrestrial applications (AM1.5) is different from the AM0 due to absorption and scattering in the atmosphere. This enhances the relative red portion in the spectrum leading to higher silicon solar cell efficiencies.

The production efficiency of a series product with optimized design (Fig. 2.5) achieved 17.5% in the 1980s (Sharp, Telefunken). At that point the development of space solar cells concentrated more and more on Gallium-Arsenide solar cells on Germanium substrate, which were offered by U.S. manufacturers Spectrolab and Tecstar with efficiencies over 19%. These cells were available for a reasonable price and had the potential to realize higher efficiencies. This potential was based on the possibility of using a special epitaxial process to grow several cells monolithically on top of each other, forming a so-called multijunction solar cell [16]. Such cells

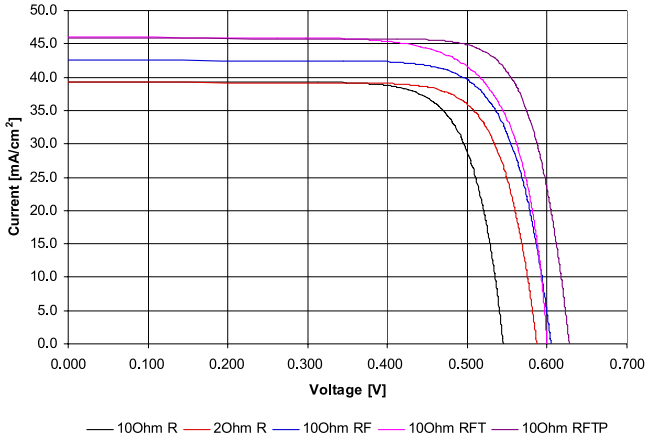

(a) IV-characteristics

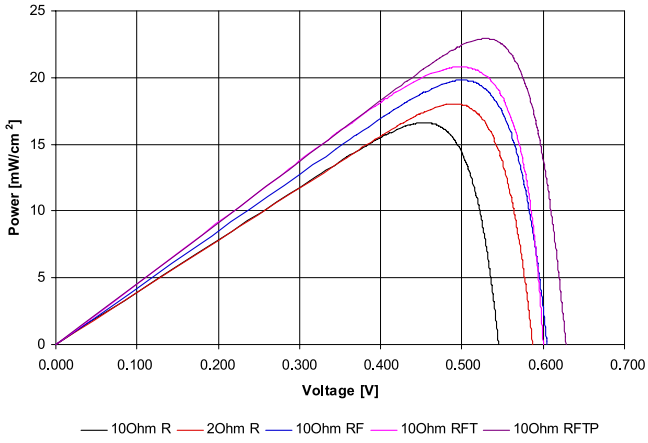

(b) PV-characteristics

Fig. 2.4. Advances in silicon solar cell performance valued at the IV and PV characteristics. Legend: R: back surface reflector; F: back surface field; T: texture; P: passivation

use the sun spectrum much better and operate at much higher voltages. As a consequence, in space applications, silicon solar cells were more and more replaced by GaAs-based solar cells. Nevertheless, the potential of silicon solar cells was not exhausted, and developers found a similar challenging field in terrestrial applications.

Manufacture of multijunction solar cells on the basis of materials from the III/V-groups of the periodic system is possible because the materials can be composed with different band gaps but identical lattice constant. This is necessary for monolithically growing materials on top of each other. Figure 2.6 shows that, for silicon, no suitable crystalline partner can be found limiting the efficiency of silicon solar cells to the monojunction maximum.

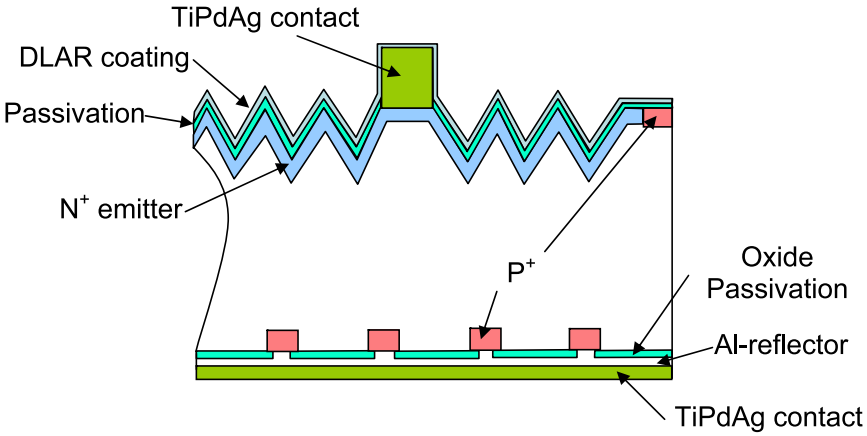

Fig. 2.5. Telefunken 17.5% high-efficiency space solar cell 2wiTHI-ETA®3-ID/ 130

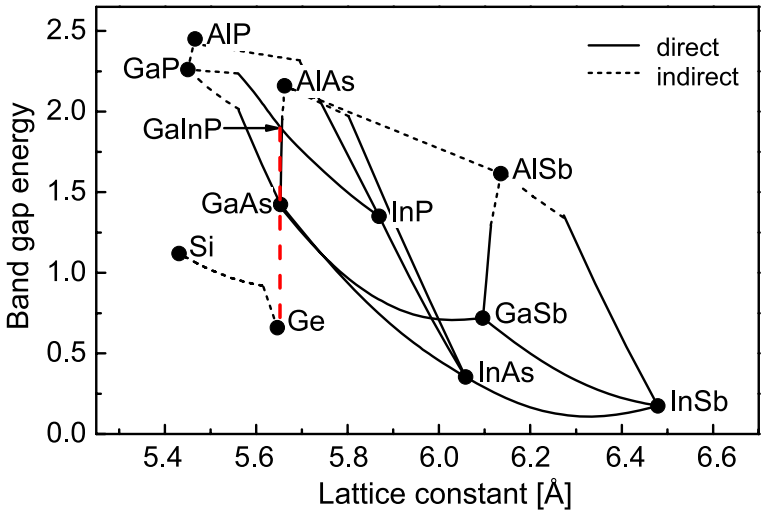

Fig. 2.6. Band gap of some semiconducting materials over their lattice constant. Only materials with same lattice constant like, e.g., Ge – GaAs – GaInP are intermateable

A multijunction solar cell is formed by stacking solar cells of different bandgap on top of one another. With the highest bandgap cell uppermost, light is automatically filtered as it passes through the stack. Each cell absorbs the light it can most efficiently convert, with the rest passing through to underlying cells (Fig. 2.7).

The first monolithic multijunction solar cells came onto the market in middle of the 1990s. These cells featured a dual junction solar cell consisting of a GaInP-top cell and a GaInAs-bottom cell epitaxially grown on a passive Ge-substrate by means of a chemical vapor deposition process using metalorganic precursors (MOCVD).

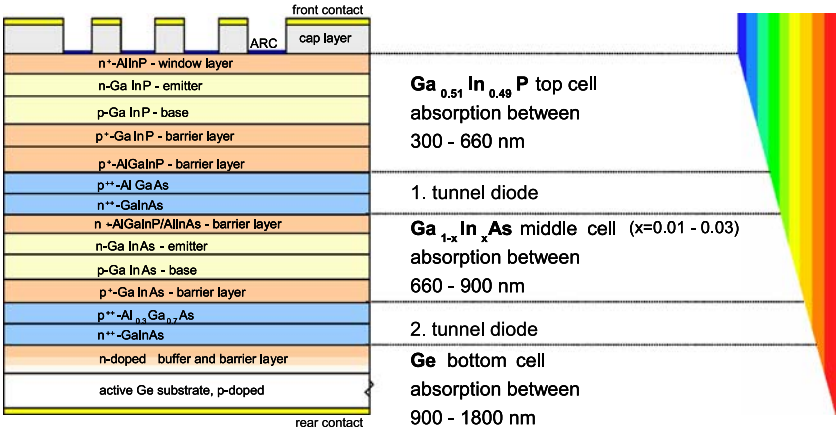

Fig. 2.7. Typical structure of a triple junction solar cell

The improvement compared to a single junction GaAs solar cell was more than 30% and yielded AM0-efficiencies of up to 24%. The first triple junction solar cells were developed at the end of the 1990s and consisted of a GaInP top cell, a GaInAs middle cell and a Ge bottom cell. By continuous improvements in the material, the growth conditions and especially the tunnel diodes separating the subcells from each other, the AM0-efficiency of triple junction cells has been improved from 25% in 2002 to 28.5% in 2006 (see Fig. 2.8). By optimizing the subcell design, the sensitivity to particle irradiation is only half that of silicon solar cells [17, 18]. Both high efficiency and high radiation hardness make the GaAs-based multijunction solar cells ideal for powering spacecrafts. But the price, which is more than five times that of a high-efficiency silicon solar cell (due to the sophisticated cell structure reflected in Fig. 2.7) limits terrestrial applications to concentrating systems.

Terrestrial applications started by adapting the technology developed for space as far as feasible. The developers of terrestrial photovoltaics did not have to consider the harsh space environment impacts and the mass requirements imposed on the design of space grade solar generators. Instead, the modules required encapsulation to protect the metallic cell contacts and interconnectors from corrosion and from mechanical damage caused by handling, hail, birds, and objects dropped or thrown on them. Additional requirements were UV stability, tolerance against terrestrial temperature extremes, abrasion hardness and self-cleaning ability. These requirements were met by a substrate consisting of aluminum, steel, epoxy board or window glass, a glass window, and as an encapsulant silicone adhesive or, alternatively, polyvinyl butyral (PVB) or ethylene/vinyl acetate (EVA).

But these solutions could not be realized in very large quantities at costs that allow solar-generated electricity to compete with wholesale electricity prices. To do so required not only low-cost approaches and low energy consumption during cell fabrication, but also high energy conversion efficiency to offset unavoidable area-related material and installation costs.

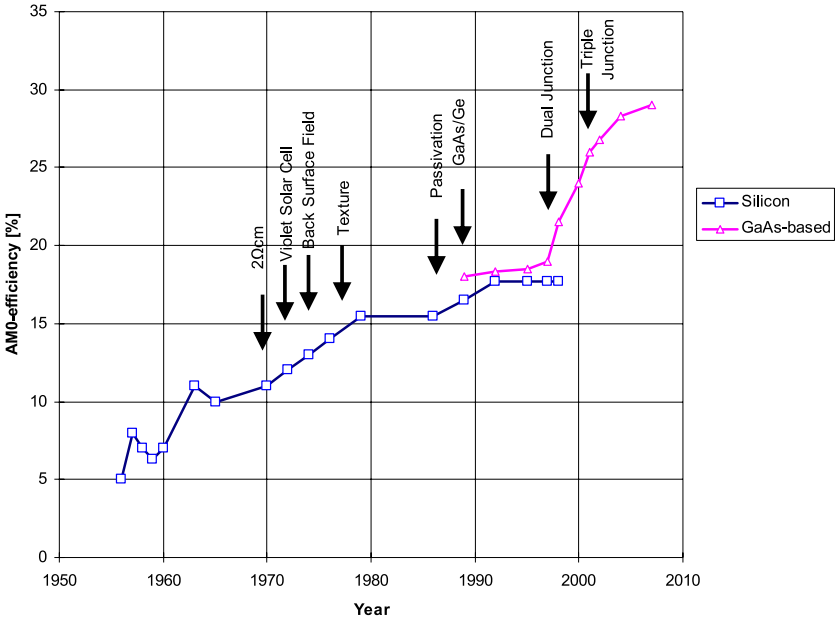

Fig. 2.8. Development of AM0-efficiency for space solar cells

To further improve the silicon solar cell efficiency, the following features have been introduced step-by-step:

- Highly doped bulk material (1 Ω cm base resistivity compared to 2–10 Ω cm for space solar cells).
- Use of float zone (FZ) silicon crystals instead of crucible grown (CZ). Due to the absence of oxygen in the molten silicon during the FZ process, there are no effects of thermal donors or oxygen precipitates. This produces a silicon wafer that has extremely stable resistivity performance and high carrier lifetimes. For space applications FZ material degrades more under combined particle/UV-radiation than CZ.
- Optimized emitter. In order to gain the full benefit of improved emitter surface passivation on cell performance, it is necessary to tailor the emitter doping profile so that the emitter is lightly doped between the gridlines, yet heavily doped under them.
- Shorter and narrower grid lines allow higher fill factors. Another approach for an improved fill factor is a shingled array design. Cells overlap in the module and the cell busbar area is shaded by the following row of cells. This allows a wide busbar design.
- Laser-grooved grid contacts followed by a second enhanced phosphorous diffusion producing selective doping in the contact areas.

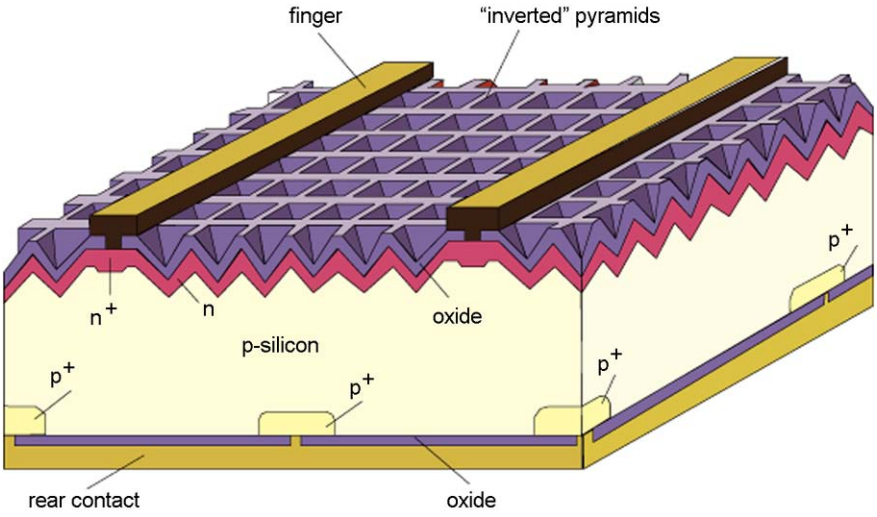

Fig. 2.9. Schematic of a PERL silicon solar cell (www.udel.edu/igert/pvcdrom)

A cell incorporating all of these improvements – in addition to the achievements of the space industry – is the passivated emitter with rear locally diffused (PERL) cell. This cell was developed by the University of New South Wales (Australia) (Fig. 2.9 and [19, 20]). It uses micro-electronic techniques to produce cells with efficiencies approaching 25% under the standard terrestrial AM1.5 spectrum. The passivated emitter refers to the high-quality oxide at the front surface that significantly lowers the number of carriers recombining at the surface. The rear is locally diffused only at the metal contacts to minimize recombination while maintaining good electrical contact.

Such extremely high-efficiency solar cells are very suitable for special applications, such as solar car racing, research and other applications where efficiency is the prime consideration. They are not a cost-competitive solution to most domestic and commercial solar cell applications. Achieving 23–25% efficiency, their price at ca. $400 U.S./W is about 100 times the cost of a standard commercial solar cell. They are cost prohibitive even for space applications.

The 1990 World Solar Challenge (WSC_solar-powered car race was won by "The Spirit of Biel" from the Engineering University of Biel, in Switzerland. Biel's winning time was 46 hours and eight minutes (65.3 ave. kmph). Biel's array was composed of laser-grooved aerospace cells that were connected by overlapping them in shingle style. The combination of high-efficiency cells with a high packing density (97.5%) resulted in an impressive 170 watts per square meter. The sleek, colorful, 182 kg solar racing car was clocked at 101 km/h during qualification trials and cruised at 72.4 km/h under mid-day sun [21].

2.4 Cost Reduction Measures

The efforts toward cost reduction had to consider design, materials and processes while keeping cell performance as high as possible. The most important parameter became the power-to-cost ratio replacing the power-to-weight ratio applicable for space solar generators. Compared with the highly sophisticated space technology, the following simplifications have been achieved step-by-step.

The major portion of the material costs is the expensive purification of the raw silicon and the single-crystal growing processes. Therefore numerous efforts have been undertaken to create basic material using less-pure silicon and a lower degree of crystalline perfection than the semiconductor-grade silicon.

2.4.1 Silicon Production

Alternative processes have been developed that, at a fraction of the cost of conventional semiconductor-grade silicon, create cells capable of adequate performance. The most common process applies the so-called fluid bed principle, using Trichlorosilane Cl_3HSi as the charge material which is then transferred into Monosilane SiH_4. From this the solar-grade silicon is extracted by cracking. This process is capable of reducing the costs required for semiconductor-grade material by 70%.

2.4.2 Bulk Material

A lot of material is lost by cutting the wafers into rectangular shapes. This waste of material can be avoided by using circular cells for the module assembly at the cost of low packing density. Waste can also be reduced by growing the ingots in square cross-sections to begin with. This can be achieved by casting silicon into boules or bricks. This process saves money compared to the CZ single-crystal growth technology but produces polycrystalline material instead of monocrystalline [22]. It has been demonstrated that a cell made of cast silicon can produce 12% to 14% efficiency and cost about 60% of a typical CZ cell. However, the slicing process is still necessary by which 50% of the material is lost.

A process that avoids material loss by slicing is the edge-defined, film-fed growth (EFG) of silicon [23]. This process consists of a slotted die of carbon or quartz which is partly dipped into molten silicon. The liquid silicon wets the die and is attracted into the slot by capillary action, forming a ribbon with the cross-section of the slot. Ten-cm wide ribbons at speeds up to 4 cm/min. were successfully grown in 1980 [24]. The process has been optimized by SCHOTT Solar (formerly RWE Solar), growing polycrystalline ribbons with a width of 15 cm at a growth speed of more than 10 cm/min. applying octagonally shaped dies.

2.4.3 Cell Contacts

Alternative developments replacing the expensive evaporation process were nickel plating followed by solder dipping and screen printing of metal pastes. Using the

latter method, thin layers of a paste with fine-grained metal powder are printed on the cell surface by silkscreen technique and fired afterwards in a continuous sintering furnace under inert atmosphere. Fine glass particles dispersed in the paste act as binders for the metal powder after firing. This process reduced costs by replacing the expensive, high-purity titanium – silver with an aluminum – silver mix and the discontinuous evaporation procedure by a continuous process. On the rear side, the addition of aluminum increases the doping level in the surface region with the alloy forming a back surface field. There are several disadvantages to this technology, including a restricted width of the gridlines, a high contact resistance between paste and silicon, and low conductivity of the sintered material.

These disadvantages were extensively reduced by employing a buried contact design. Grooves, cut into the top surface emitter by laser scribing, mechanical or chemical approaches, provide for increased contact area and grid finger cross-section. The metal application is either by screen printing or is electroless by immersing the wafers in a plating solution. Grooved contacts give a 30% performance advantage over screen printed cells without grooves.

2.4.4 Encapsulation

The encapsulation of the modules has to guarantee long life operation under extreme weather conditions. For the transparent front side, safety glass is commonly used; its thickness results from a trade-off between material cost savings and additional costs due to increased breakage rate. The rear side is made either of glass, like the front side, or of a weather- and waterproof foil back. The cells are embedded in silicone or in ethylene vinyl acetate (EVA). For edge protection and mounting the assembly is firmly bordered with a sturdy, fully closed aluminum frame. An automated production line with high throughput ensures consistent product quality and low costs.

2.5 Concentrating Systems – A New Opportunity for High Efficiency Space Solar Cells

The power-to-weight ratio of a terrestrial module is typically more than 10 W/kg compared to 100 W/kg for a typical space solar array. Launch costs in the range of 20,000 €/kg justify the application of highly sophisticated technology for space.

Nevertheless, high-efficiency space grade solar cells have a good chance of entering the terrestrial market. The primary impediment to direct application is the high price. But this can be drastically reduced by operating the solar cells in a concentrated system. This has two advantages: On the one hand, the cell size is reduced approximately proportional to the concentration factor; on the other hand, the efficiency is increased by a factor proportional to the logarithm of the concentration. These facts have prompted a resurgence of research in multijunction cells and commercial interest in concentrator III–V photovoltaics. Of particular interest are high

Fig. 2.10. 190 kWp power station by Solar Systems [27]

concentration systems. A record 40.7% efficiency at 240 suns was reported at the Madrid Conference in 2007 [25].

Over more than 30 years many research groups were engaged in developing concentrator photovoltaic systems (CPV). In the first concentrator modules and installations, large-area mirrors (0.5–1 m in diameter) focused the sunlight on cells of several square centimeters in area. Cooling by water or by means of thermal pipes was necessary [26]. Several reliable and efficient CPV power stations have been demonstrated, e.g., by Solar Systems in Australia (Fig. 2.10 and [27]). For this system, a new triple junction receiver was developed to replace the current silicon point-contact solar cells. The new receiver technology is based on high-efficiency (>35%) concentrator triple junction solar cells from Spectrolab, resulting in system power and energy performance improvement of more than 50% compared to the silicon cells. This is also due to the fact that multijunction cells exhibit lower ohmic losses because they operate at lower currents.

Appearance of the technology accessible for Fresnel lens fabrication has determined revision of the photovoltaic module design. Solar cells could be placed behind the concentrators in this case. The module housing could serve as a protector from the environment and provided for cooling by thermal conductivity. Since the Fresnel lenses had smaller dimensions (25×25 cm^2), the photocell dimensions were also decreased down to less than 1 cm^2.

In the late 1980s, the Ioffe Physico-Technical Institute, St. Petersburg [28] proposed the concept of a radical decrease in the concentrator dimensions while retaining a high sunlight concentration ratio. The first experimental modules of such a

Fig. 2.11. Array of the Ioffe full-size concentrator modules with small aperture area Fresnel lenses

type consisted of a panel of lenses, each of 1×1 or 2×2 cm^2, focusing radiation on AlGaAs/GaAs cells of submillimeter size. At that time, the main advantages of a module with small-aperture area concentrators were: the requirements imposed on the capability of heat-sinking material to conduct heat, on its thermal expansion coefficient and on its thickness are essentially relieved. The focal distance of such lenses appeared to be comparable with the structural thickness of the conventional modules without concentrators.

The team at the Ioffe Institute has developed concentrator modules [29] in which Fresnel lenses are arranged on a common superstrate to form a panel of 12×12 lenses. Cells as small as 2×2 mm^2 and 1.7 mm, in a designated area diameter and operating at a mean concentration ratio of about 700×, are used (Fig. 2.11). The lens profile was optimized, taking into account the refraction index of the lens material and its dependence on wavelength, focal distance, receiver diameter, sun illumination spectrum, and the sensitivity spectra of the subcells in a multijunction cell. The lens structure consists of a sheet of silicate glass and refracting microprisms formed of transparent silicone on the inner side of the glass. The microprisms themselves are formed by polymerization of the silicone compound directly on the glass sheet with the use of a negatively profiled mold. The advantages of this concentrator technology are based on the high UV stability of silicone, its excellent resistance to thermal shocks and high/low temperatures, good adhesive properties in a stack with silicate glass, simplicity and very high accuracy of the formation method. The accuracy of cell position is of great importance because each cell must be placed in the center of the focal spot of a corresponding lens. This accuracy has to be about 100 μm, which is realized by using automatic processes and standard electronic industry machines.

The overall module outdoor conversion efficiency as high as 24.6% was measured on a 2×4 lenses module. But the outdoor efficiency could exceed 28% at

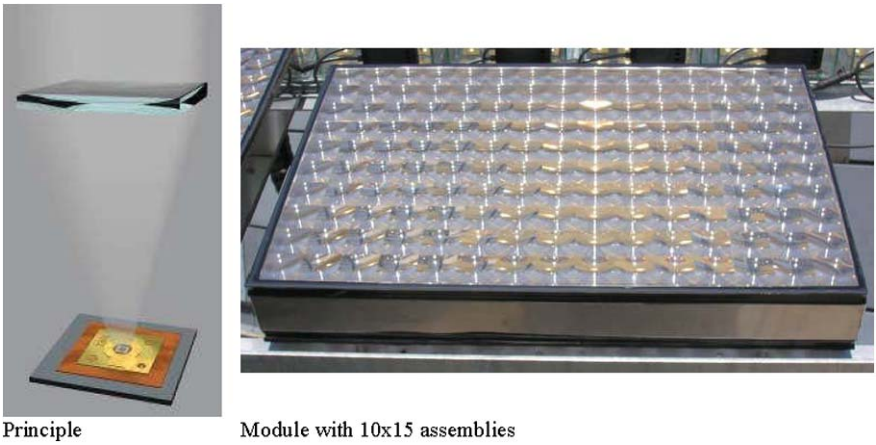

Fig. 2.12. FLATCON®-module Technology [31]

lower ambient temperature, or at the use of the cells with indoor efficiencies in the range of 39–40% instead of used ones with 32.34%.

Concentrix Solar, Germany, also uses high-efficiency triple junction solar cells in their FLATCON®-modules [30, 31]. Figure 2.12 shows the principle of the FLATCON technology and a photo of a module consisting of 150 Fresnel lenses made of embossed silicone on a $4 \times 4\,\mathrm{cm}^2$ glass plate equipped with circular triple junction cells with an active area diameter of 2.3 mm and a grid design optimized for the inhomogeneous illumination under the Fresnel lens. Under standard test conditions the efficiency is 33.0% at 300–500 suns. Typical operating module efficiency is 25.5%.

Most of the progress in solar cell development has been made for space use to the benefit of terrestrial applications. However, some of the technological improvements are starting to flow the other way, with discussion of solar cells made from copper-indiumdiselenide (CIS) material. This thin-film technology is very resistant to charged particle degradation and could be considered for space missions exposed to extremely difficult charged particle environment, e.g. those near the Jupiter moon Europa.

References

1. J. Perlin, *From Space to Earth: the Story of Solar Electricity, AATEC Publications* (Ann Arbor, Michigan, 1999). ISBN 0-937948-14-4
2. M. Wolf, Historical development of solar cells, in *Proc. 25th Power Sources Symposium*, 23–25 May 1972
3. J.J. Wysocki, P. Rappaport, Effect of temperature on photovoltaic solar energy conversion. J. Appl. Phys. **31** (1960)

4. Z.I. Alferov, V.M. Andreev, V.D. Rumyantsev, *III–V solar cells and concentrator arrays*, Ioffe Physico-Technical Institute, 26 Polytechnicheskaya str., St. Petersburg 194021, Russia
5. V.M. Andreev, V.R. Larionov, V.D. Rumyantsev, O.M. Fedorova, Sh.Sh. Shamukhamedov, P AlGaAs – pGaAs – nGaAs solar cells with efficiencies of 19% at AM0 and 24% at AM1.5. Sov. Tech. Phys. Lett. **9**(10), 537–538 (1983)
6. M. Wolf, A new look at silicon solar cell performance. Energy Convers. **11** (1971)
7. M. Wolf, Drift fields in photovoltaic solar energy converter cells, in *Proc. IEEE*, vol. 51, May 1963
8. Spectrolab Inc. Spectrolab production solar cell design data, 10 August 1981
9. G. Strobl et al., Experiences with implanted BSF solar cells, in *Proc. 4th European Symposium "Solar Generators in Space" Cannes*, 18–20 Sept. 1984 (ESA SP-210)
10. J. Lindmayer, J.F. Allison, The violet cell: an improved silicon solar cell, in *Ninth IEEE Photovoltaic Specialists Conference*, Silver Spring, Md., 2–4 May 1972
11. C.R. Baraona, H.W. Brandhorst, V grooved silicon solar cells, in *Proceedings of 11th Photovoltaic Specialists Conference*, 1975
12. P. Iles, Present state of solar cell production, in *Proc. 5th PVSC, NASA-GSFC*, Greenbelt, MD, 1965
13. T. Hisamatsu, H. Washio et al., Reverse bias characteristics of modules made of solar cells with and without integrated bypass function (IBF), in *Proc. 25th PVSC*, Washington, D.C., 13–17 May 1996
14. AZUR Patent DE 3815512C2
15. G. Strobl, H. Fiebrich, Production experience with LILT silicon solar cells for ROSETTA qualification, in *Proc. of 2nd WCPSEC*, Vienna, July 6–10 1998
16. B. Beaumont, J.P. Contour, P. Gibart, J.C. Guillaume, C. Vèrié, Conversion photovoltaique à haut rendement: le projet quadrispectral, in *Proc. 4th Europ. Symp. "Photovoltaic Generators in Space"*, Cannes, 18–20 Sept. 1984 (ESA – SP-210 Nov. 1984)
17. M. Meusel et al., Development status of European multi-junction space solar cells with high radiation hardness, in *Proc. 20th EPSEC*, Barcelona, 2005
18. G. Strobl et al., European roadmap of multijunction solar cells and qualification status, in *IEEE 4th World Conference on Photovoltaic Energy Conversion*, Waikoloa, Hawaii, 7–12 May 2006
19. J. Zhao, A. Wang, E. Abbaspour-Sani, F. Yun, M.A. Green, 22.3% efficient silicon solar cell module, in *25th PVSC*, Washington, DC, 13–17 May 1996
20. M.A. Green, *Silicon Solar Cells – Advanced Principles & Practice* (Sydney, 1996)
21. R.J. King, Recent car technology developments including Australian world solar challenge results, in *Proc. of 22nd IEEE PVSC*, 1991
22. K. Roy, K.-D. Rasch, H. Fischer, Growth structure of cast silicon and related photovoltaic properties of solar cells, in *Proc. 14th PVSC*, San Diego, CA, 1980
23. H.E. Bates, D.N. Jewett, V.E. White, Growth of silicon ribbon by edge defined, film-fed growth, in *Proc. 10th IEEE PVSC*, 13–15 Nov. 1973
24. J.P. Kalejs, B.H. Mackintosh, E.M. Sachs, F.V. Wald, Progress in the growth of wide silicon ribbons by the EFG technique at high speed using multiple growth stations, in *Proc. 14th IEEE PVSC*, San Diego, CA, 1980
25. R.R. King et al., Metamorphic concentrator solar cells with over 40% conversion efficiency, ECSC-4, in *4th International Conference on Solar Concentrators*, Madrid, 12–16 March 2007
26. Z.I. Alferov, V.M. Andreev, Kh.K. Aripov, V.R. Larionov, V.D. Rumyantsev, Pattern of autonomal solar installation with heterostructure solar cells and concentrators. Geliotechnica **2**, 3–6 (1981). Appl. Solar Energy **2** (1981)

27. P.J. Verlinden et al., Performance and reliability of multijunction III–V modules for concentrating dish and central receiver applications, in *IEEE 4th World Conference on Photovoltaic Energy Conversion*, Waikoloa, Hawaii, 7–12 May 2006
28. V.M. Andreev, V.R. Larionov, V.D. Rumyantsev, M.Z. Shvarts, High-efficiency solar concentrating GaAs-AlGaAs modules with small-size lens units, in *11th European Photovoltaic Solar Energy Conference and Exhibition – Book of Abstracts; abstract No. 1A. 15*, Montreux, Switzerland, 12–16 October 1992
29. V.M. Andreev, E.A. Ionova, V.D. Rumyantsev, N.A. Sadchikov, M.Z. Shvarts, Concentrator PV modules of "all-glass" design with modified structure, in *Proceedings of 3rd World Conference on Photovoltaic Energy Conversion 3P-C3-72*, 2003
30. A.W. Bett et al., High-concentration PV using III–V solar cells, in *2006 IEEE 4th World Conference on Photovoltaic Energy Conversion*, Waikoloa, Hawaii, on 7–12 May 2006
31. H. Lerchenmüller et al., From FLATCON® pilot systems to the first power plant, ECSC-4, in *4th International Conference on Solar Concentrators*, Madrid, 12–16 March 2007

3 PV Solar Electricity: From a Niche Market to One of the Most Important Mainstream Markets for Electricity

W. Hoffmann and L. Waldmann

3.1 General Overview

PV solar electricity is seen as one of the few booming markets, today and in the coming decades. This market has grown globally at a rate of about 40% per year over the past 10 years. Related industries have realized a two-digit, billion-dollar (U.S.) turnover worldwide. PV solar electricity is a high-tech industry with high performance potential in the coming decades, leaving even the electronics industries behind and approaching the automotive industry.

The PV history and future can be differentiated into the following four phases, each phase lasting roughly two decades.

1960 to 1980: PV solar technology was developed as an energy supply for satellites in the early 1960s. Companies like Tecstar in the United States, AEG (one of the roots of today's SCHOTT Solar) in Germany and Sharp in Japan were the leading manufacturers in this technology. This first phase ended in the 1980s, as PV technology for satellites was well established and feasible. In this period, the price per watt of PV power came down to earth.

1980 to 2000: This second phase can be characterized by tremendous progress in research, development and demonstration, driven by investment aimed at employing PV technology for terrestrial use. Pilot projects to manufacture solar cells and modules were tested. Sales mainly were in small kW applications with even some MW projects; for example, the 6 MW Carrissa Plains plant in the U.S. in the early 1980s. In remote areas, PV was already cost effective for many applications. Market activities increased markedly, first in the U.S. in the 1980s and followed by Germany in the 1990s. Japan also adopted a specific industry policy in the 1990s. With the market support programs in Japan and following in Germany (starting in 1990 and extended with the feed-in tariff by 2000) these three countries developed an emerging industry.

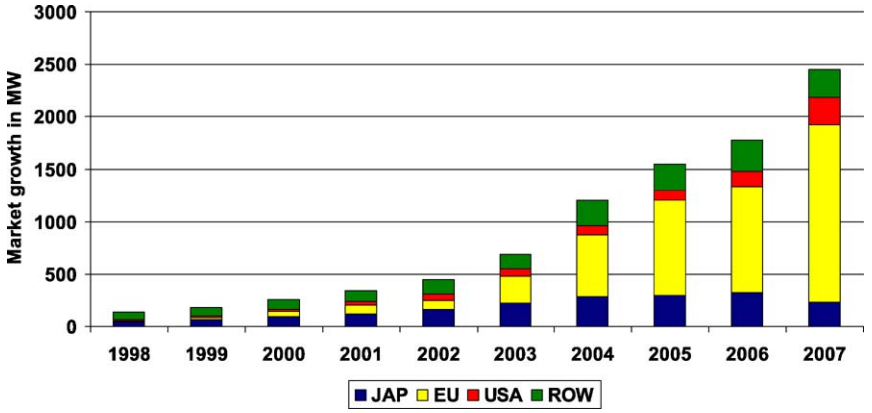

Fig. 3.1. Historical market development of PV solar electricity installation according to regions

2000 to 2020: This third phase could be named as a transition phase. In this period the benefits of the former political framework, as well as public awareness for the necessity of renewable energies go together with PV solar technology, which comes toward cost effectiveness in all market segments. Market support programs in more and more countries enable the local production industry for PV Solar technology to grow accordingly. With leading markets in Germany, the US and Japan, Spain, several new markets will emerge in Asia, Europe and the Americas.

2020 to 2040: In the fourth phase, finally PV solar electricity will be established on the world market. Due to the growing worldwide industrial production and thus falling costs, PV is competitive in all market segments and cost effective compared to most conventional energy sources.

PV solar electricity is a major technology and will play a significant role in the future development of economies worldwide. PV can help provide both industrial growth and the chance for at least 2 billion people to get access at all to energy by using clean electricity. In turn, this will open doors for education and development in poor and rural areas. Solar electricity technology might emerge as a key technology to represent the new industrial drive. Provided a growth rate of around 25% in the coming years, a total turnover of PV Systems worldwide can be estimated at around 100 billion Euros in 2020 and well above in the following years.

The PV vision of the European Commission for 2030 is to realize all the socio-economic benefits provided by (1) in the short-term, employment in large-scale, high-tech production; (2) in the mid-term, raising a viable industry that creates revenues and pays taxes; and last but not least (3) in the long-term supplying a significant contribution to global energy need with clean PV solar electricity. Thereby, in addition, PV contributes to reducing dependence on oil and gas imports and to help secure local energy supplies. Given recent political instability in the Middle

East, and after the crisis of gas supply between Russia and Ukraine, the premises of energy supply have changed crucially. Costs for risks and dependency have to be calculated on top of rising prices. The further growth will also cut significantly carbon dioxide emission by replacing power from fossil fuels.

The common goal of the PV industry and the European Commission is to create a self-sustaining market for solar electricity products by 2020. To attain this ambitious goal all instruments for market stimulation, technological development and system changes have to intertwine internationally.

3.2 PV Solar Electricity Market History

The annual market, which crossed the impressive number of one gigawatt, in average had an overall growth since 1998 by about 40%. The PV market for terrestrial applications may be divided into four major segments serving different customer needs:

- *Consumer*: Application in consumer goods such as calculators, wristwatches, garden lights, automotive applications etc.
- *Off-grid* Industrial: Remote industrial applications e.g. telecommunication repeater stations.
  Off-grid Residential: Rural electrification in developing countries providing for light, refrigeration and communication.
- *On-grid*: All applications connected to a national electricity grid.
- *High efficiency application*.

Consumer products powered by small solar applications will stay a niche market in terms of megawatt output. Nevertheless, intelligent housing and mobile communication provide growing demands for these applications in the future.

Also important are markets that are small in terms of number of applications, but that have high potential in terms of power output; this is the market for highest efficiency PV. Satellite powering and concentrator plants are typical applications for the highest efficiency segment.

While three market segments – off-grid industrial, residential and consumer – are already competitive today (these grew at a modest 18% p.a.), the fourth market segment of grid-connected systems increased by astonishing 63% p.a. The latter growth started in the USA in the 1980s, followed by Japan in the mid 1990s with Europe, in particular Germany, in the year 2000. The different growth rates catapulted the contribution of grid-connected systems in relation to the total market from about one quarter eight years ago towards more than three quarters today. The shares of these applications in the total market turned bottom up. The reason for this development is basically due to industry-politically induced market-support programs in the aforementioned countries. Today we find the feed-in tariff system in Germany, Spain, Italy, Greece, South Korea and India and some more to come in Europe as well as investment subsidies in Japan, U.S. and some other countries.

Fig. 3.2. Customer needs for different PV technologies

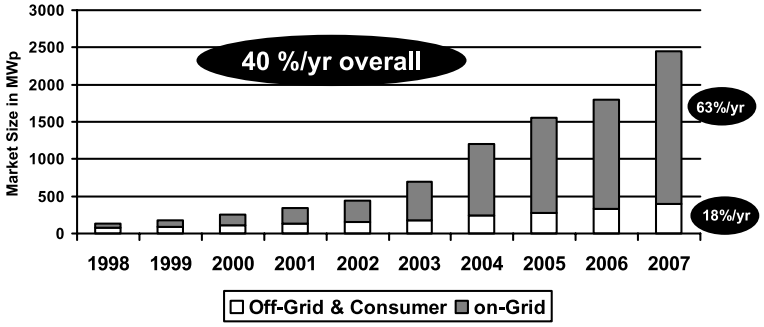

Fig. 3.3. Historic growth according to application

In 2004 Germany became the world leader in newly installed systems, with a total of more than 600 MW, leaving Japan far behind with 280 MW. But this development was not always foreseeable. The lessons learned from all the ups and downs in the German PV market can be summarized as follows: First, to create a fruitful environment and good conditions for a strong PV market, reliable long-term conditions must be requested. Second, financial incentives and an attractive feed-in tariff can actually compete with each other, especially when the financial incentive is restricted, capped or has to be applied for. In the latter case the customer follows the principle of maximizing benefits and waits for the additional incentive even when the feed-in tariff alone is sufficient for a return on investment rate of 6–8%. This effect is to be avoided. And third, the bureaucratic obstacles must be removed. In Spain, for example, it still takes more than 12 months to get all the permissions needed to install a PV plant.

These support schemes are necessary to have the market growth as described in the next section.

Table 3.1. Subsidy schemes of important European PV markets

	Feed in Tariff [€ct/kWh] Subsidy programm	Market size 2007	Targets
Germany	35.49–51.75	1,100 MWp	28% RES-E in 2020
Spain	23–44	623 MWp	400 MWp in 2010
Italy	36–49	50 MWp	3,000 MWp
France	31.19–57.19 50% tax reduction max 8000/16000 € grants in some regions	45 MWp	490 MWp in 2015
Greece	40–50 20%–60% grants for commercial plants	2 MWp (25% grid connected)	700 MWp in 2020

After all it has to be kept in mind that the estimated market growth in Europe can only be realized when the Spanish market opens up and other European countries follow. It is quite important to outline under which boundary conditions grid-connected systems will be competitive without support programs. The interaction of market growth, module price and competitiveness of PV solar electricity is discussed in Sect. 3.4.

3.3 Price and Competitiveness of PV Solar Electricity

In a more and more liberalized utility market, electricity produced by PV solar electricity systems worldwide will be able to compete with their generating cost first against peak power prices from utilities. This situation is most likely to happen within the next decade in more southern areas with higher solar irradiation (1,500–1,800 kWh/kW) while it may take about one decade more in places like Germany with lower insolation (800–1,000 kWh/kW). The point of time for this competitiveness is determined mainly by three major facts:

- Price decrease for PV solar electric systems leading to an equivalent decrease in the actual cost for PV generated electricity.
- Development of a truly liberalized electricity market.
- Correlation of higher priced peak power delivery from utilities and output of a PV solar electricity system.

Looking at electricity spot markets, clear price spikes can be seen that directly correspond with the energy yield of an installed PV solar array. The correspondence

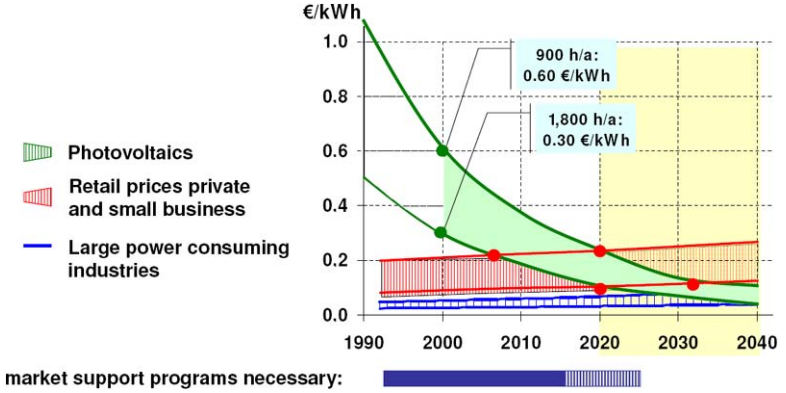

Fig. 3.4. Competitiveness of PV solar electricity

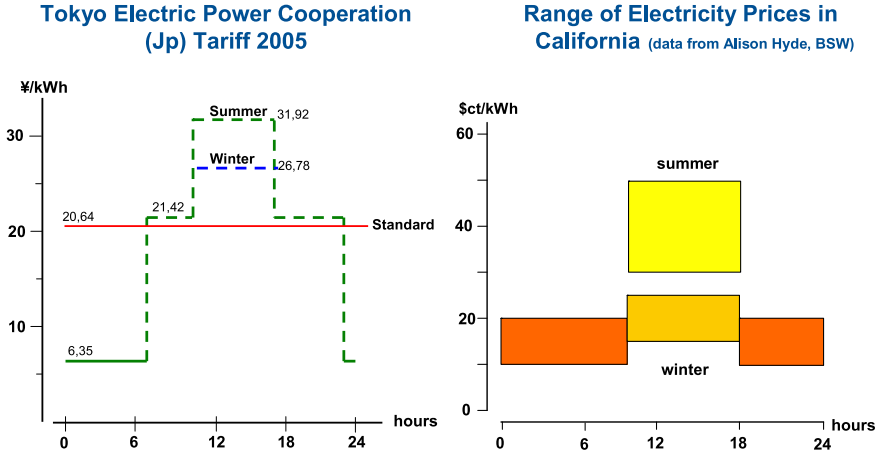

Fig. 3.5. Electricity retail prices for various countries

is remarkable with respect to time when one considers that the electricity is generated directly on the rooftop of the building where the energy is required. So the generation costs of PV solar electricity and the price of conventional electricity has to be compared at the point of sale, which is the power outlet. The electricity tariff of Tokyo Electric Power Corporation (TEPCO) provides a differentiated tariff that changes during the daytime and over the seasons. Thus, during the summer and at daytime, PV solar electricity in Tokyo is already cost effective for the customer. For this reason the Japanese market is still not collapsing, even though the incentives for PV in Japan went down to zero. A very similar situation can be observed in the liberalized electricity market of California. Differentiated tariffs show the highest price at summer during daytime. In these market situations, PV solar electricity is already cost competitive compared with the price at the private power socket.

Conventional energy costs are more likely to increase due to higher prices for gas, oil and coal and for the internalization of external costs as for the sequestration and storage of carbon dioxide. At the same time, prices for the technology-driven PV solar electricity will decrease. That gives us a clear picture for the future market.

For PV solar modules, there exists a good model for future price expectations derived from price experience curves. In analogy to production cost learning curves, a price experience curve in a double logarithmic plot shows the dependence of the component price versus the cumulative sold volume of said product. Typically one obtains a straight line whose slope determines the so-called experience factor, that being the price decrease in % by doubling the accumulated sold volume. This experience factor has been determined for a number of industries. The general finding is that for products where the smaller part of production cost is material-driven and the remaining, greater cost is "intelligence", one obtains experience factors at and above 30%. Examples are electronic devices with experience factors of 30 to 40% and, as a specific example, light-guided fiber cables with experience factors of 45%. Such experience factors in most cases typically stay constant for a given product and for quite a long time. In contrast, products with dominant material costs – e.g. float glass, steel, etc. – show almost no decrease in price; in fact, sometimes these products increase in price with more volume sold.

The price experience curve for PV solar modules currently shows a 20% decrease of price by doubling the cumulative volume. The material contribution for the product, the PV solar module, within the value-added steps is roughly two thirds for materials like glass, frame or plastic. The other one third is more "intelligence" driven, like cell efficiency or productivity by economy of scale. No surprise, in total there is then a 20% experience factor obtained.

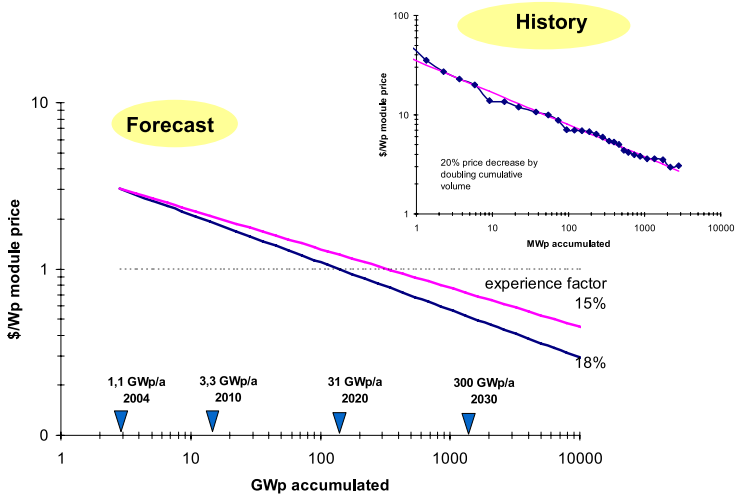

Fig. 3.6. Price experience curve for PV solar modules

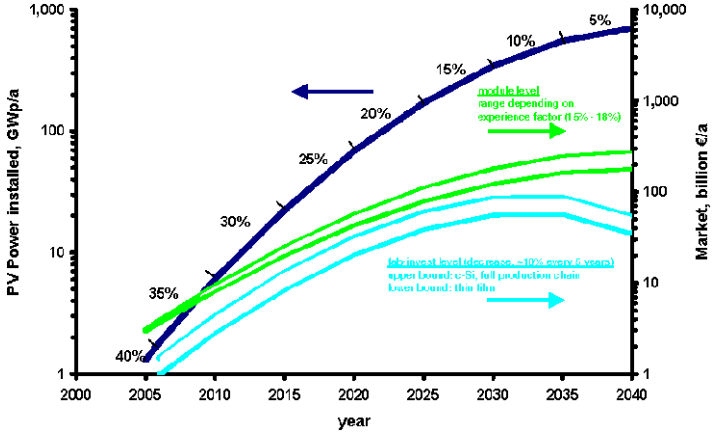

Fig. 3.7. Future growth of global PV solar electricity market in GWp and Bn€ turnover

As the proportion of material cost contribution increases with further production volumes, the experience factor may decrease from 20 to 18% or even 15%, just so we do not overestimate future cost decreases. On the shortfall of solar-grade poly silicon, a slight deviation of the ideal line is observed as the price for poly silicon more than tripled. After the massive investments and the boost in production capacity for poly silicon in 2008 the actual price points will most likely go back forwards the projected line. Whether Thin Film technologies will demonstrate a higher experience factor remains to be seen in the coming years.

It is important to realize that a price experience curve does not give us any answer as to the time when certain price levels will be reached. This can be obtained by assuming an annual growth rate from which an accumulated volume of sold products can be calculated and inserted as points in time when respective volumes will be reached. Taken together, the 25% annual growth and the experience factor of 15 to 18% would lead one to estimate an expected price decrease of about 5–7% per year, which is equivalent to half the price every 10 to 13 years.

The future generating cost for electricity was examined by the European Association of Utilities, Eurelectric, together with VGB Power Tech. As a result a study on electricity generation cost was released. The study compares different energy transforming processes:

- Fossil (coal, gas, lignite)
- Advanced fossil
- Nuclear
- Hydro
- Wind (off shore)

These processes were investigated at three different points in time: 2005, 2030 and 2050.

Price decrease by technological progress is taken into account, in addition to the development of prices for fuels and resources during that time period.

Table 3.2. Cost of electricity production with various technologies

	Cost of Electricity – Overlook			
	2005	2030	2030 CC	2050 CC
Hard Coal	4.11	6.18	6.72	6.46
Natural	4.44	6.95	7.06	8.76
Gas Lignite	3.72	6.47	6.21	6.19
IGCC	4.79	6.54	5.72	5.43
OxyFuel			6.09	5.95
Nuclear	4.30	4.70		4.90
Hydro run river	4.10		4.10+	
Wind off shore	7.62		7.57	

Cost of Electricity figures are in €-ct/kWh in prices of 2005

Source: Eurelectric 2007

Electricity generating cost [ct€/kWh]	Today 2005	Tomorrow 2030	Day after tomorrow 2050
Wind, off- on-shore	9/7.5*	6/5*	3/4
Solar thermal power	17*	6*	3
PV solar south/north	20/40	5/10	3/6

Source: Own estimates

* Eurelectric 2007

A clear increase is assumed in all fossil technologies. Today one kWh power output from coal or gas can be generated at a price level of 4 to 4.5 cent Euros. At 2030 this price will go up to 6–7 ct€ and leads to 6.5–9 ct€ in 2050.

The range for nuclear power starts at 4.3 ct€ and will likely stay stable until 2050 at 4.9 ct€. Hydro stays stable at 4.1 ct€ for the whole period.

Not surprisingly, wind power is represented by off-shore applications. But there is no significant price decrease through technological development indicated. Off-shore wind starts at 7.62 ct€, coming down to 7.57 ct€/kWh in 2030 and 2050.

Solar thermal power plants and PV solar electricity are not seen to have a significant contribution.

Other renewables were not subject to this study.

In fact there must be made some adjustments in this study from the point of view of the renewable energy sector.

As shown above the price experience curve will have its impact on the electricity generating cost. Of course, the rate is different with different technologies. PV solar electricity has a proven rate of around 20% price decrease by doubling the production output. Translated to a time scheme that assumes a growth rate of 25% for the PV sector, the 20% price experience curve leads us to estimate at least a 5% price decrease per year. That is to halve the generation cost every 12 years and, as a side effect, produce clean electricity without fuel cost. Solar thermal power plants today are calculated to have electricity generating costs at 17 ct€/kWh falling to 3 ct€ according to existing production and research-and-development roadmaps in this industry. At this point we want to appeal to the energy sector not to underesti-

mate the PV solar mainstream market power and the potential of concentrated solar thermal power.

3.4 Future Market Development

PV solar electricity in total has a huge potential to ease the upcoming energy problems. Looking closer into the PV solar electricity business we see several customer needs to be served by different technologies and products. These needs depend on the kind of application and the functions which are intended by using PV solar power. Each of these customer needs are covered by specific products and PV technologies. First and fastest growing today is the grid-connected segment. Here we see mainly rooftop applications, but also a growing awareness for building-integrated PV systems (BIPV). With BIPV, cost savings can be realized by replacing functional parts of a building with PV components and thus diminishing installation and material costs. Provided an existing feed-in tariff, the price per kWh tells the profitability of the investment in the PV system. The on-grid market definitely left the niche category in 2000 and entered the mainstream in 2004.

But in fact there are several other criteria the customer may have in mind depending on the purpose of the PV system. Off-grid applications are the second market. For an energy supply to a remote facility – for example, for a telecommunication repeater set in a desert area – long-term reliability will be taken into account. For rural electrification, the decentralized and modular structure of PV offers the best solutions, especially for light and small solar home systems. Having in mind the growing number of people without fair access to clean energy, we can assume that this segment will follow the on-grid segment, moving from niche status to mainstream. Rural electrification will become a real mainstream market in two decades. So the picture today will change from a few regional markets and low share for rural into many widespread markets and a 50% share for rural applications.

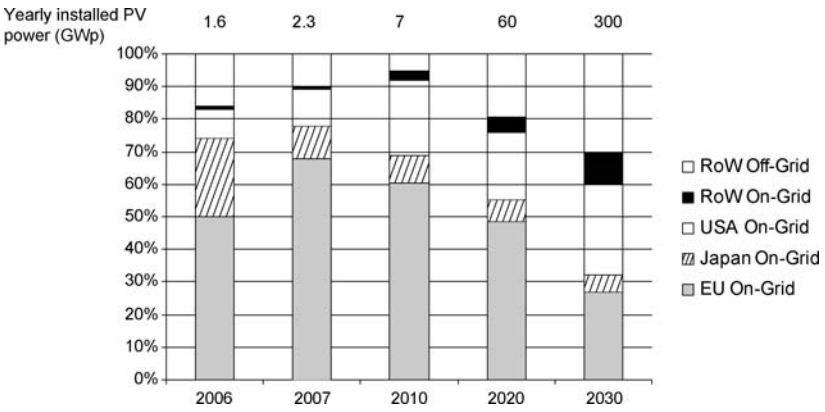

Fig. 3.8. Split of PV market according to region for on-grid and off-grid applications

Currently there are about 2–3 billion people in the world who are still without electric light and other amenities of the industrial world; this figure is not likely to change until 2030, due to the continuing population growth in these remote rural areas. Off-grid PV electricity supplies, such as PV-driven water-pumping systems, small solar home systems (SHS), and small village grids are aimed at greatly alleviating this situation.

For solar home systems in developing countries, both cost and service are important. The average monthly cost has been estimated by the Deutsche Gesellschaft für Technische Zusammenarbeit (GTZ), a federal Association for technical cooperation. For nonequipped homes the expenses for batteries, candles and kerosene amount to $6 to 8 (U.S.) per month. A 50 W PV solar electricity system with battery and charge controller represents an investment of about $500 (U.S.). That results in about $7 (U.S.) per month over six to eight years under the assumption of a low-interest loan (World Bank, national institutions, or banks supporting developing countries such as KfW). Microfinance is the core issue for this market segment. In the case of solar home systems, the performance, the operational lifetime and the price per service are more important than any considerations of PV module efficiency.

The need for solar villages in rural areas is eminently important due to the increase in global electricity consumption according to IEA, from 16,000 TWh in 2001 towards 36,000 TWh in 2040; the growth of the population in third-world regions will result in a need for more than 20,000 TWh within 35 years. More than half of the people will live in rural areas have not been connected to a main grid for decades due to prohibitive cost.

Decentralized power by renewable energies is the only choice. The PV solar technology employed for solar villages in rural areas is technology similar to grid-connected systems, e.g., in Germany. All cost and price decreases will be able to contribute to a faster and more widespread installation of decentralized power in these most needed applications.

3.5 Technology Evolution

All the existing technologies can be compared in terms of relative prices and module efficiencies. The crystalline wafer silicon technology with monocrystalline Czochralski wafers have a market share of around 30%; multicrystalline wafers make up around 60% of the market; and ribbon silicon wafers come close to 3% market share. These crystalline technologies (c-Si) show module efficiencies between 12 and 18% and have a total market share of 95%. The thin-film technologies like amorphous silicon with 4% market share and other thin-film technologies – e.g., CIS and CdTe – add up to the remaining 1% market share.

Setting a point of reference for module cost of 100% for modules containing ribbon silicon wafers with efficiency of 14.3%, the cost of the different technologies can be compared on relative terms. Modules with mainstream multicrystalline technology come to 111%, monocrystalline in conventional processing end up at 116%.

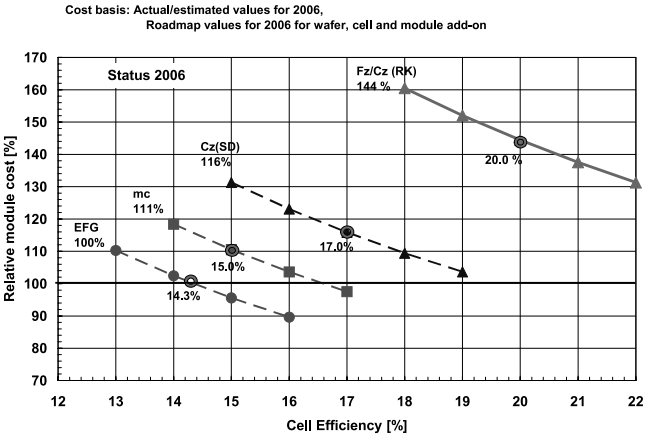

Fig. 3.9. Relative module cost by technology

In 2008 the curves will all be shifted by about 1.5% absolute to higher efficiencies, hence the same relative cost comparison applies.

Higher efficiencies lead to higher total cost by adding higher wafer and cell-processing cost and higher module add-on cost. Looking at the module cost relative to the efficiency of different technologies in 2006, the picture shows clear favorites. The very high efficiencies in monocrystalline cell technology – with 20% cell efficiency gained through rear contacting – have relative module costs that are up to 44% above the reference point of ribbon silicon technology, which has 14.3% cell efficiency. (Estimates by SCHOTT Solar on the basis of the technology roadmap.) This example shows that the technological pathway is also a function of market and economy. Highest efficiencies do not necessarily lead to lowest module prices per power output.

As time progresses, the module efficiencies will shift towards higher values and new technologies, like dye and organic cells may evolve.

To compare prices we set arbitrarily the highest price module with monocrystalline wafers and highest efficiencies to 100, then the price range shifts in relative terms from 70–100 in the year 2000 down to 35–60 in 2010 and 15–35 in 2020, corresponding well to the forecast in the price experience curve which we mentioned earlier. Looking to the split for the three major technologies we see 95% for c-Si and 5% for thin film in 2000. Toward 2020 we might find some two thirds c-Si technology and one third of thin film and new technologies, respectively. Even in 2030 we predict at least a share of one third for c-Si wafer technology. Altogether, there is good evidence that the price decrease for PV solar electricity produced kWh will decrease as assumed before.

Several side and synergy effects out of the TFT flat-panel display technology can be used for thin-film technology. Some of the processes handle similar material so basically the same machinery can be used.

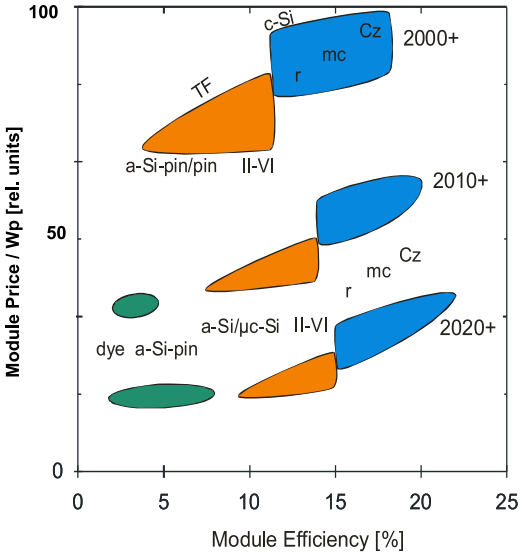

Fig. 3.10. Development for relative cost and module efficiency for various PV technologies

As a consequence of employing different technologies, different customer needs in separate markets can be served. The crystalline technology with high power per area and efficiencies between 25 and 40% will be a very niche product for space and concentrator applications.

The higher middle range, with efficiencies from 16 to 25% and premium price level covers the high power needs also in niche markets. The largest market share by far will have the mainstream multicrystalline and ribbon technology. With efficiencies from 14 to 16% these modules will be the PV workhorse in cost-effective applications. Both the high-efficiency and the medium-efficiency crystalline segment together will most likely take 95% of the market share within the next decade till 2015. Thin film and new concepts are going to catch up in the following decade until 2025, covering the largest market share starting in 2030.

With new concepts, in the future new materials and applications might be possible. Whereas the solar revolution in remote rural areas of our globe will literally mean ”power to the people”, the same solar revolution in industrialized areas must be a revolution of design in the building sector, urban planning and architectural solutions. This pathway has begun today.

This is in concert with a thorough study done by the German Advisory Council on Global Change (Towards Sustainable Energy Systems). In this study a share of more than one third of the global primary energy consumption in 2040 is predicted to be covered by renewable energies, in total with an approximate 10% share for combined PV solar electricity and solar thermal power stations. In 2100 the same study assumes an 85% coverage of primary energy consumption by renewables, with two thirds of that delivered by solar thermal power plants and PV solar elec-

Table 3.3. Various PV technologies in comparison

(a) Crystalline silicon		(b) Thin film	
Cz, Fz	High power/area @ premium price eta 16–25% space, niche markets	II–VI compound (CIS CTS) a-Si/µc-Si and thin Si films	Additional solutions for cost effective power applications eta 8–18%
mc & ribbon (EFG)	Cost effective power application eta 14–16% "The PV workhorse"	pin-ASI and ASI-THRU®	Low price/area @ low eta eta 4–6% "Solar electricity glass"
(c) III–V compounds (GaAs)		(d) New concepts	
Highest power/area @ very high price		Dye cells	"Color to PV" (eta 3–10%)
Multi bandgap	eta 25–40%	Organic cells	"Low material cost option"
	Space, concentrating systems	Scientific high eta approaches aiming for eta 30–60%	Utilization of hot electrons, intermediate band cells, up/down conversion, quantum wells, nanostructures etc.

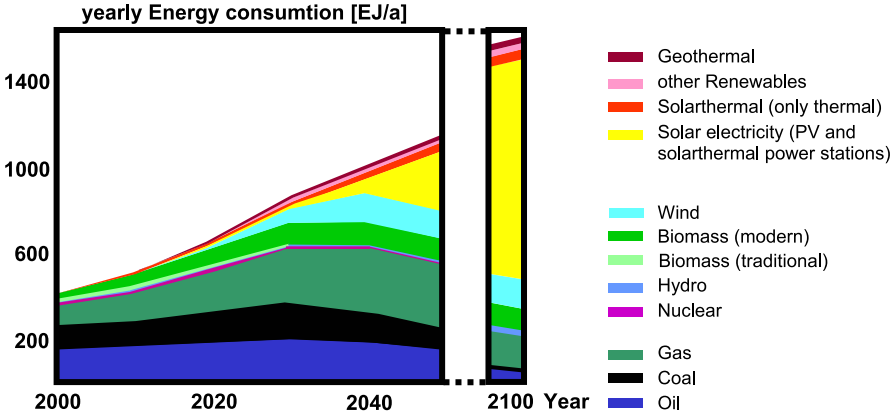

Fig. 3.11. Contribution of various technologies for global prime energy consumption

tricity systems. Although such long-term extrapolations always contain uncertainty, it is quite useful to examine highly probable boundary conditions – i.e. world population growth, prime energy split into applications and energy usage by region and application, environmental constraints etc. All these predictions tell us the tremendous need to act toward a major energy supply with PV solar electricity.

References

1. EPIA Roadmap, June 2004, http://www.epia.org/index.php?id=18
2. EREC "Renewable Energy Scenario to 2040", May 2004, http://www.erec.org/documents/publications/2040-scenario.html
3. German Advisory Council on Global Change, World in Transitions: Towards sustainable energy systems, Earthscan, London and Sterling, 2004
4. Sarasin Study "Solarenergie – ungetrübter Sonnenschein?", November 2004, Study "Solarenergie 2005", December 2005, Study "Solarenergie 2006", December 2006
5. SolarBuzz, MarketBuzz^{TM} 2005 "Annual World PV Solar Market Report 2005", March 2005 and MarketBuzz^{TM} 2006, "Annual World PV Solar Market Report 2006", March 2006
6. Strategies Unlimited, "Photovoltaics manufacturer shipments 2004, 2005 and 2006" published each April of following years

4 Advanced Solar-Grade Si Material

K. Hesse

4.1 Introduction

For three decades scientists around the world have been searching for the right technology to produce silicon feedstock for the photovoltaic industry, feedstock that fulfills the need for "low cost" as well as the need for sufficient quality. The urgency of this task has intensified since 1998, when it became clear that the PV demand could no longer be met with by-products from the electronics industry. The established producers of polysilicon developed specific products for the solar industry, but for the time being cannot catch up with the exploding demand. The actual Si shortage resulted in very high spot prices for solar-grade silicon and led to discussions on whether existing producers with their production methods will be able to cover the future demand of the solar industry. There are, again, opinions being expressed that alternative production methods are more suitable to fill the gap at lower costs. Here, requirements and possibilities have to be checked very carefully. In addition, old knowledge and experience about the different possibilities to produce silicon should not be forgotten. The future supply of silicon to the PV industry has to be seen in the tense environment of quality, costs and time of implementation.

4.2 Production Pathways for Solar Silicon Feedstock

4.2.1 Metallurgical Grade Silicon: Carbothermic Reduction of Silica as a Starting Point for Most Pathways

Most pathways for the production of solar silicon feedstock start with metallurgical silicon ("silicon metal", purity $> 98\%$) and end with hyperpure silicon (purity in the parts per billion range), so the challenge is to do this purification as efficiently as possible. The silicon metal is produced in submerged electric arc furnaces (electrical consumption between 10 to 30 MW) according to the formula

$$SiO_2 + 2C = Si + 2CO.$$

The feedstock includes woodchips, high-purity quartz lumps and high-purity coal, respectively charcoal and coke.

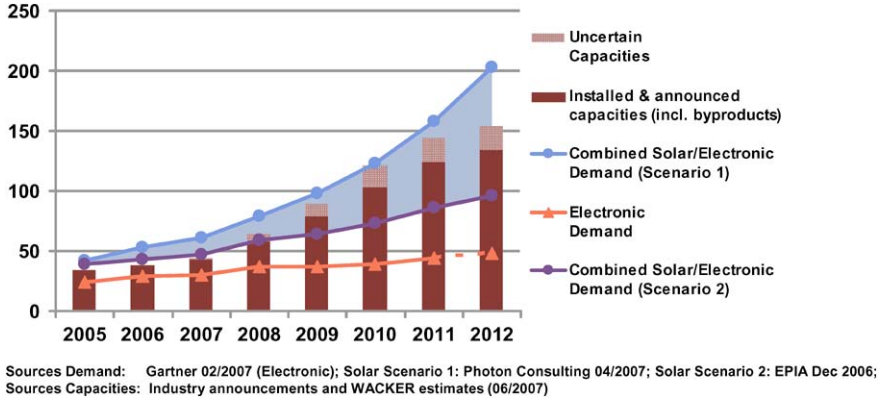

Fig. 4.1. Global polysilicon supply and demand (in ktons; mg-Si included) Status: June 2006

The silicon melt has to refined, is solidified in the casting process to get a multicrystalline structure and then crushed.

An important byproduct are silica fumes, formed in an side reaction according to the formulas

$$2\mathrm{Si} + \mathrm{O_2} = 2\mathrm{SiO},$$
$$2\mathrm{SiO} + \mathrm{O_2} = 2\mathrm{SiO_2}.$$

Due to economy of scale and process improvements, the electric consumption of 10–11 KWh per kg has been achieved, compared to more than 14 KWh/kg in the past [1].

As the worldwide production capacity for metallurgical silicon is far more than 1 mio mto/a (most of it for the metal/aluminum industry) there is no foreseen supply bottleneck.

Regarding the quartz as feedstock, it is certainly true that SiO_2 is one of the most abundant materials available on Earth (as sand). But if you are looking for high-purity quartz – as is necessary for high-purity metallurgical silicon – the availability is much more limited to special mines, e.g. in Spain or Brazil. This is not so much an issue of availability, but of costs (for mining and transport). So the often-used saying "from sand to electric energy" is misleading, because fine sand cannot be used easily in the furnaces and, in addition, usually has too many contaminants.

The purity of a typical metallurgical-grade silicon with respect to metallic impurities is approximately six orders of magnitude worse than that of a typical solar-grade silicon. So purification for solar needs is an inevitability.

4.2.2 Established Production Methods: Purification of Metallurgical Silicon via the "Silane Route" is Dominating

The extreme purity required for silicon in photovoltaic or electronics applications is achieved by converting metallurgical grade silicon into silanes (large scale industrial

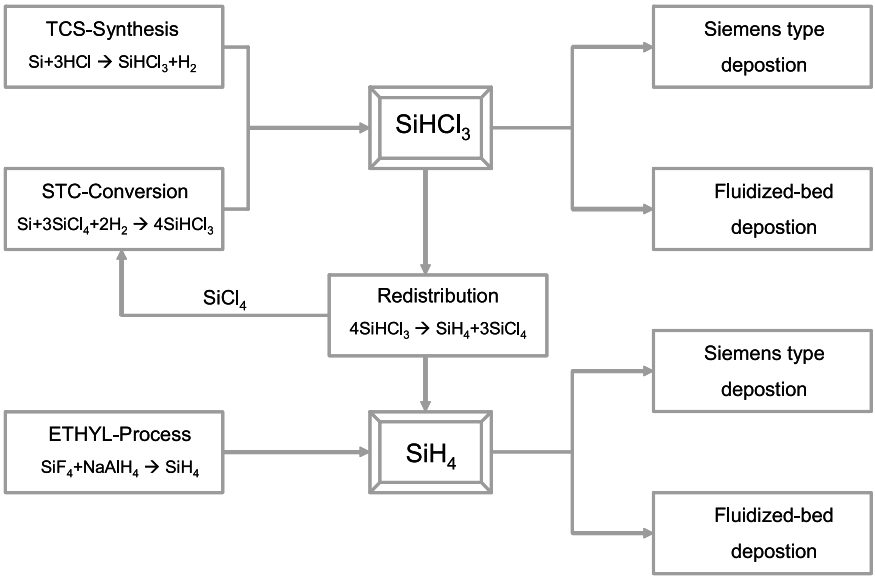

Fig. 4.2. Pathways for polysilicon production

processes are based on trichlorosilane or monosilane), which are then distilled and decomposed to yield hyperpure silicon. The conventional method is the so-called Siemens process, in which TCS is decomposed in bell jar-type reactors in the presence of hydrogen with the deposition of polysilicon on thin silicon rods [2]. The silicon tetrachloride (STC) produced as a byproduct is hydrogenated back to TCS or is used as a feedstock for pyrogenic silica. The fluidized-bed CVD process used to deposit polysilicon appears to be a very attractive alternative to the Siemens deposition process. WACKER has developed a successful fluidized-bed deposition process for granular solar-grade polysilicon based on TCS [3]. In contrast, two completely different processes use monosilane (SiH_4) as the feedstock for deposition of polysilicon. As shown in Fig. 4.2, one of these processes uses TCS as a feedstock to afford SiH_4, whereas the other process is based on SiF_4, a byproduct from the production of superphosphate fertilizers. Semiconductor-grade monosilane can be used in a modified low-temperature Siemens process or in a fluidized-bed deposition reactor to produce polysilicon.

According to a study by Pichel [4] in 2005, approximately 73% of the global capacity of polysilicon was produced using the Siemens process and TCS as a feedstock (Fig. 4.3).

4.2.3 Differences in Using TCS or Silane as Feedstock

Lobreyer [5] demonstrated that comparable qualities of semiconductor-grade polysilicon could be obtained from Siemens deposition of polysilicon, regardless of the type of silane feedstock (TCS or monosilane).

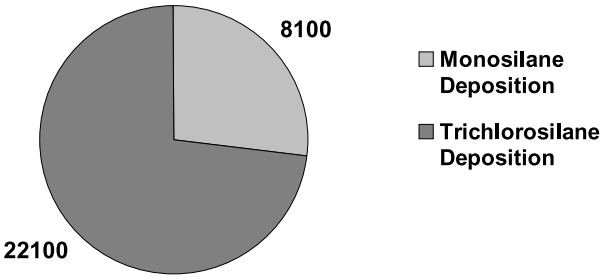

Fig. 4.3. Global capacity of polycrystalline silicon in 2005 [4]

There are pros and cons associated with the use of both monosilane and TCS to deposit polysilicon. Breneman [6] published a detailed review discussing the key advantages and disadvantages.

The deposition of polysilicon from monosilane can be carried out at a temperature as low as 650 °C, whereas temperatures >900 °C are necessary for TCS. If monosilane is used, the main problem appears to be the production of silicon dust by homogeneous vapor deposition, which decreases yields and limits deposition rates; it also negatively affects product morphology (pores, density, microroughness). If TCS is used, approximately 1/4 reacts to form silicon, 3/4 is converted into STC, and the remainder leaves the reactor as off-gas. On the other hand, if monosilane is used, conversion rates of nearly 100% are obtained and hydrogen is practically the only byproduct. The main pathway to produce monosilane is redistribution of TCS to monosilane and STC; here 1/4 of the TCS reacts to Monosilane and 3/4 is converted to STC; so the system with monosilane deposition has to deal with the same amounts of chlorosilanes as the TCS-based deposition system. There are also major differences in handling of the individual silanes. The self-ignition and the very low boiling point of monosilane necessitate extremely strict safety engineering requirements and a complex cryodistillation system.

Regarding the process complexity, the WACKER TCS-process achieves a closed loop production system based on only three chemical reactions:

$$\mathrm{mgSi + 3HCl \rightarrow SiHCl_3 + H_2} \quad \text{metallurgical Si to TCS,} \tag{4.1}$$

$$\mathrm{4SiHCl_3 \rightarrow Si + 3SiCl_4 + 2H_2} \quad \text{deposition of Si,} \tag{4.2}$$

$$\mathrm{3SiCl_4 + 3H_2 \rightarrow 3SiHCl_3 + 3HCl} \quad \text{hydrogenation of STC,} \tag{4.3}$$

$$\mathrm{mgSi \rightarrow Si} \quad \text{sum: purification of metallurgical silicon to hyperpure silicon, closed loops of hydrogen and chlorine}$$

So the decisive point appears to be how the polysilicon deposition process is integrated into the manufacturer's particular product flow. The objective here is to either recycle all byproducts and waste products or to use them to synthesize other products to minimize losses of silicon, chlorine and hydrogen. It is also important

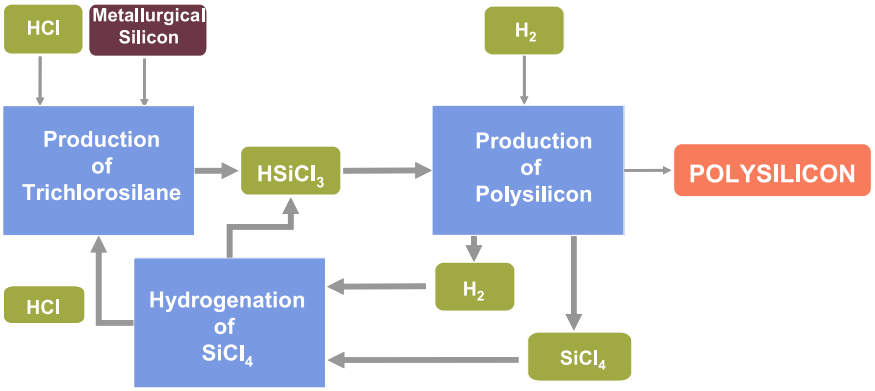

Fig. 4.4. WACKER polysilicon: Closed loops for hydrogen and chlorine yield significant cost advantages

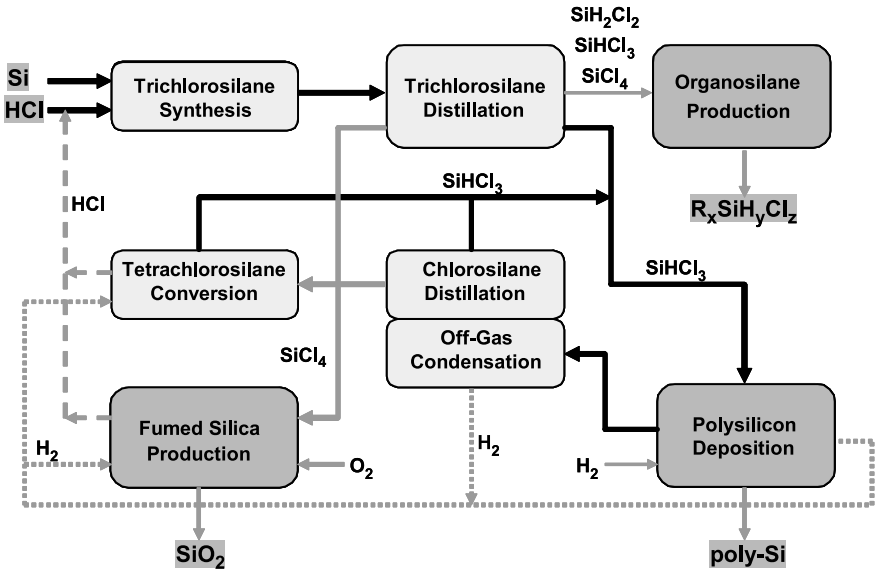

Fig. 4.5. Integrated product flow at Wacker Chemie AG, besides polysilicon, production of other value-added products is possible

to use any waste heat arising from the various processes within the integrated system.

The integrated product system used at the WACKER production site in Burghausen takes additional advantage of value-added products by linking the production of polysilicon to that of pyrogenic silica, organofunctional silanes, silicates and silicones (Fig. 4.5).

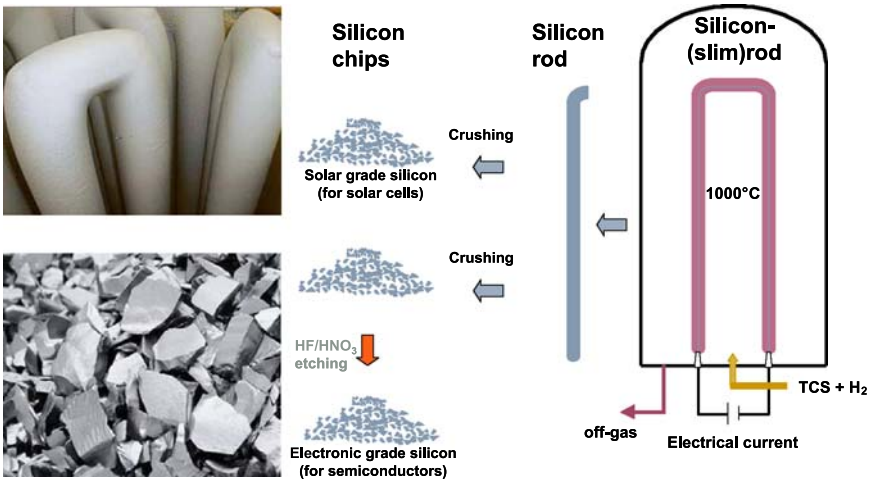

Fig. 4.6. Rod deposition: Optimized process of deposition handling and crushing for the solar industry

4.2.4 Accommodation of the Processes to the PV Requirements

An alternative to the "silane route" has been sought for many years, particularly for the production of solar-grade silicon. The purity of solar-grade silicon with respect to metallic impurities is approximately six orders of magnitude higher than that of a typical metallurgical-grade silicon. It is questionable as to whether there is an alternative to the "silane route" that can achieve this purity at acceptable costs. A very important parameter in PV applications is photovoltaic-system efficiency (generally 14–16%). The highest efficiencies with low specific material usage are possible only via high-quality feedstocks. For the production of solar grade feedstock, Wacker Chemie AG has optimized its production process taking into account the requirements of the solar industry for lower cost at somewhat lower quality requirements:

- The deposition process was modified for maximum deposition rate. The resulting rougher morphology does not impact the solar application.
- The purification of the surface by chemical cleaning or etching after crushing of the rods could be avoided by a new crushing process. This process leads to fewer contaminants, especially for metals, so that the solar requirements (metals contaminations in the low parts per billion per atom (ppba-) range can be fulfilled; the metal contamination of cleaned prime electronic-grade polysilicon are two orders of magnitude lower).

These modifications are allowing for economic production of solar feedstock, an important prerequisite for the actual capacity expansions at WACKER.

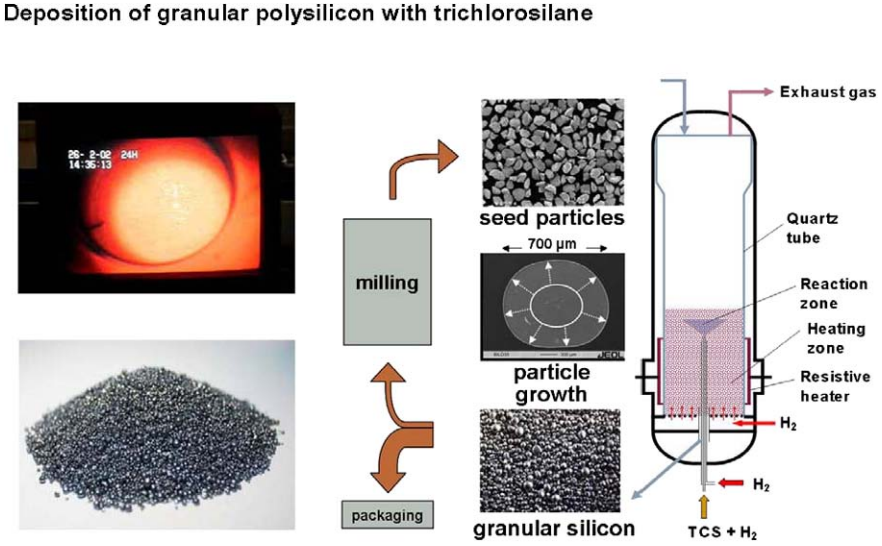

Fig. 4.7. Granular deposition

The fundamentals for cost-effective production of solar-grade silicon at WACKER POLYSILICON are:

- Highly integrated, but flexible production system: value-added use of byproducts.
- Economy of scale: investments, costs, productivity.
- Advanced reactor technology: high output, yield, quality.
- Flexible reactor technology: solar or electronic polysilicon according to demand.
- Fast realization time for new capacities with qualified personnel.

A fluidized bed deposition process might be a reasonable supplement to the "main route" rod deposition technology. In this process a fluidized bed of silicon particles is heated to the necessary decomposition temperature of the silicon containing gas which is passed through the bed. Ideally, elemental silicon is deposited on the silicon particles which hence are growing. It is possible to operate this process continuously by regularly withdrawing particles from the fluidized bed and adding smaller seed particles to the bed. The withdrawn particles are a ready-to-use product. Seed particles can be obtained, for example, by milling product granules. Besides the advantage of continuous operation, the process has the potential of lower specific energy consumption. For customers, granular polysilicon has a lot of advantages regarding handling, for high crucible filling grade (in combination with chunk material) and for applications that need a finely tunable continuous recharging. WACKER POLYSILICON is establishing this granular product to supplement its product portfolio.

4.2.5 The Myths of the "High-Energy/High-Cost" Rating of Established Silane-Based Polysilicon Deposition Technologies

There is a common perception that the production of solar- grade feedstock via gas-phase deposition is "too costly" because of the "high" energy consumption of the deposition process. And purification of silicon via metallurgical processes – i.e. different melting and crystallization steps, slag refining, treatment with different gases etc. – consumes much less energy and is therefore less expensive. But is this really true?

Myth 1: *High Temperature = high energy consumption*? The first misunderstanding is that high temperature in a process equals high energy consumption. But if there is no energy consuming reaction involved, the consumed energy is mainly influenced by the *energy losses* – a thermos bottle with hot fluid inside is also hot inside without being *"*energy intensive*"*. It is a similar situation with the gas-phase deposition. Energy consumption can be influenced a lot by scale, reactor design and process design. So the energy consumption figures given by Hunt et al. [2] are now much lower. Also the general belief that monosilane deposition is less energy consuming than trichlorosilane deposition, because of the lower deposition temperature, is not correct if you consider the maximum possible deposition rate: the trichlorosilane deposition rate can be much higher because the heterogeneous monosilane deposition rate is limited by the homogeneous gas-phase deposition (i.e. dust formation). The faster the deposition rate, the lower the energy losses. Also the high energy consumption for monosilane cryodistillation and storage has to be taken into account.

Myth 2: *The sum of chemical reactions, condensation and distillation steps of the silicon purification via silanes is more energy intensive than "direct" metallurgical purification.* Let us compare the trichlorosilane-based purification with a typical metallurgical purification involving at least two melting/crystallization steps (e.g. JFE-Process, Apollon Solar process [14, 15]) to reach the minimum required purity regarding metals by segregation. At WACKER the total energy consumption of the total TCS process is much lower than 100 kWh/kg with a total silicon yield of much more than 90%. In metallurgical refining, one melting /directed solidification step of silicon needs about 40 kWh/kg (relating to the usable end product). To reach a similar metal purity as the TCS-process you need at least three melting/solidification steps and still some elements cannot be efficiently removed due to their unfavorable segregation coefficient. In addition you have energy losses by treating the melt, e.g., with slag refining, gases, electron beam guns (for elimination of phosphorus), plasma torches (removal of boron) etc. to bring the dopant concentrations to an acceptable level. The remaining purity regarding carbon and dopants will still be worse compared to the TCS process. And you have high yield losses by slag and metal-contaminated parts after segregation. So there is no reason to condemn the "chemical" silicon purification methods in favor of "metallurgical" methods with respect to the needed energy or yield.

4.2.6 Alternative Technologies for the Production of Solar-Grade Feedstock: Purification of Metallurgical Silicon via Melt Treatment/Crystallization is Dominating

If you look at metallurgical methods you'll find that they need energy-intensive melting and crystallization processes and special treatments to remove dopants which are connected with yield losses. The achievable quality is still far lower as compared to gas-phase deposition processes. The situation is similar for the carbothermic direct reduction of pure quartz with pure carbon as well for the melt electrolysis of quartz. Other, previously evaluated and practiced methods – like the reduction of silicon compounds with metals, e.g. $SiCl_4$ with zinc in vapor phase or aluminothermic reduction – proved to be not competitive with regard to the achievable quality and costs. Important, limiting factors are the purities of the feed materials, contamination during the process steps, low yields of reaction steps and complex reprocessing of byproducts [9].

4.2.7 Alternative Vapor-Phase Deposition Technologies?

In a closed loop chlorosilane system the above-mentioned problems are already solved in large-scale production; the dominant technology is the heterogeneous vapor-phase deposition on rods. Thereby maximum purity is achieved. For solar-grade silicon, fluid bed deposition of granules is also a possibility. WACKER is testing this technology in a pilot project. Others are testing the deposition of silicon on hot surfaces with temperatures above melting point – "vapor-to-liquid" deposition [14]. The extremely corrosive nature of fluid silicon is limiting the achievable quality. The lowest energy consumption in deposition is reached in so-called "free space" reactors; here silanes are decomposed in a homogeneous gas phase reaction. But the resulting silicon is in the form of very fine particles ("dust"), which was not usable in the past because of the highly reactive oxidized surface and the low density which led to melting problems. There were also problems with contamination during handling of the material.

4.2.8 Time to Market

Very important is the period of time needed to develop new technologies to the point where they can be put into large-scale production. To come from a working concept in the lab to the pilot project and finally to production scale takes at least 10 years. This is a very long time frame compared to actual, extremely dynamic growth of the solar industry. That growth sets demanding targets regarding quality and especially costs. Based on its proven technology, WACKER actually almost tripled its capacity within four years, showing that it can keep up with the growth of the solar industry.

4.3 Summary

TCS will remain one of the semiconductor and photovoltaic industries' most important feedstocks in the future, regardless of whether it is used as a direct feedstock

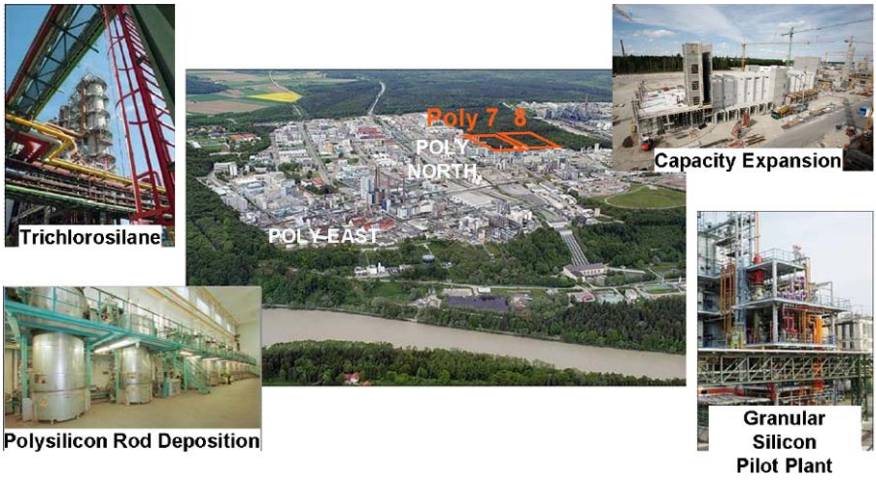

Fig. 4.8. Integrated polysilicon production of WACKER chemie AG in Burghausen, Germany

to produce polysilicon in the Siemens and granulated processes or as a raw material for monosilane production. For more than 50 years the WACKER group has used and improved polysilicon production based on vapor phase deposition of TCS in a closed loop process. Hydrogen and chlorine are processed in a cycle, and process heat is used efficiently in the chemical plant system. This process is safe and environmentally friendly and has further improvement potential. So it is suitable to meeting the future demand of the solar industry up to several hundred thousand tons. The capacity expansions to balance the actual shortage of polysilicon are under construction. In parallel, the downstream users are continuously improving the specific consumption of the precious polysilicon. Through higher cell efficiencies (based on high-quality feedstock), improved crystallization techniques, smaller wafer thicknesses, lower kerf loss during sawing and overall higher process yields, there is still the potential to lower the specific silicon consumption of about 10 g/Wp by almost half in the next several years [12].

References

1. A. Schei, J. Tuset, H. Tveit, *Production of High Silicon Alloys* (1998)
2. W.C. O'Mara, R.B. Herring, L.P. Hunt (eds.), *Handbook of Semiconductor Silicon Technology* (1990)
3. D. Weidhaus, E. Schindlbeck, K. Hesse, *Silicon for the Chemical Industry VII* (2004), p. 165, ISBN 82-90265-25-5
4. J. Pichel, M. Yang, *Renewable Energy Access*, Piper Jaffray, 11 January 2006
5. T. Lobreyer, K. Hesse, *Silicon for the Chemical Industry IV* (1998), p. 93, ISBN 82-90265-20-4
6. W. C Breneman, H.J. Dawson, *Silicon for the Chemical Industry IV* (1998), p. 101, ISBN 82-90265-20-4

7. I. Araki, T. Yamamoto, Y. Tokuda, H. Momose, *Silicon for the Chemical Industry VI* (2002), p. 197, ISBN 82-90265-24-7
8. H. Kohno, T. Kuroko, H. Itoh, *Silicon for the Chemical Industry II* (1994), p. 165, ISBN 82-519-1444-2
9. Flat-Plate Solar Array Project Final Report, vol. II: Silicon Material, JPL Publication 86-31, October 1986
10. Prometheus Institute, Polysilicon: Supply, Demand & Implications for the PV Industry, 2006
11. Ryan's Notes, Ferrous and Nonferrous News and Prices
12. EPIA, Capacity and market potential, Dez. 2006
13. Sun Screen II, CLSA, Juli 2005
14. 3rd Solar Silicon Conference, 2, München, April 2006
15. 21st European Photovoltaic Solar Energy Conference, Dresden, 4–8 Sept. 2006
16. Hesse, K.: Feedstock for the PV Industry. Photon 2nd Solar Silicon Conference, 11 April 2005
17. PHOTON International, May 2005

5 EFG Ribbon Technology

I.A. Schwirtlich

5.1 Introduction

Since the beginning of solar cell development based on crystalline silicon, there have been efforts to produce wafers directly from the melt instead of through crystallization of ingots. Ingots require slicing into the blocs and wafers which form the basis of solar cells. In the last 30 years, several dozen processes have been published that describe a variety of concepts. Only few of these processes could be developed to an acceptable degree of technical maturity. Among those successful technologies are the Dendritic Web process, the Edge Supported Pulling (ESP) process and the Edge-Defined-Film-Fed-Growth (EFG) process. The EFG Process was originally developed by Mobil Solar and, since the mid-1990s, belongs to SCHOTT Solar GmbH and its predecessors, respectively. The Ribbon Growth on Substrate (RGS) process was originally developed by Bayer AG and is now in a pilot project at the ECN, Petten. Considering the past 20 to 30 years, the EFG process has reached the most advanced state in terms of industrialization.

5.2 EFG process

The publicly known silicon ribbon growth processes can be categorized into two basic concepts despite their totally different designs:

(a) Pulling direction *vertical* to the melt surface
(b) Pulling direction *parallel* to the melt surface

Ribbon technologies belonging to category (a) are the ESP, Dendritic Web and the EFG processes. The RGS process should be placed in category (b) (see Fig. 5.1).

The processes due to concept (a) benefit from the good heat radiation by the two large surfaces of the ribbon. As the crystallization direction is directed into the melt, the segregation leads to enrichment of the remaining impurities in the residual melt. The feedstock material should therefore be relatively pure. The pulling speed and the crystallization speed are identical in absolute value but the direction is opposite. Processes following concept (b) have the advantage that the crystallization speed is

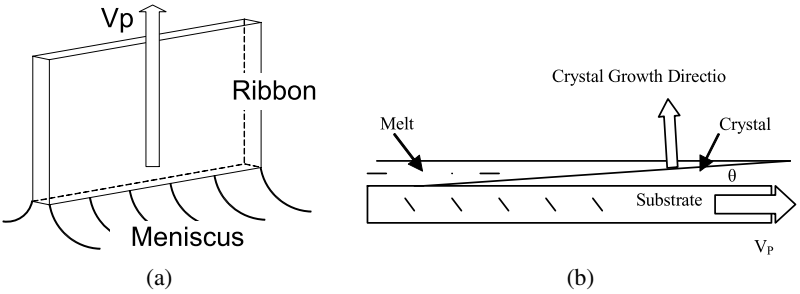

Fig. 5.1. Ribbon pulling direction vertical (**a**) and parallel (**b**) to the melt surface

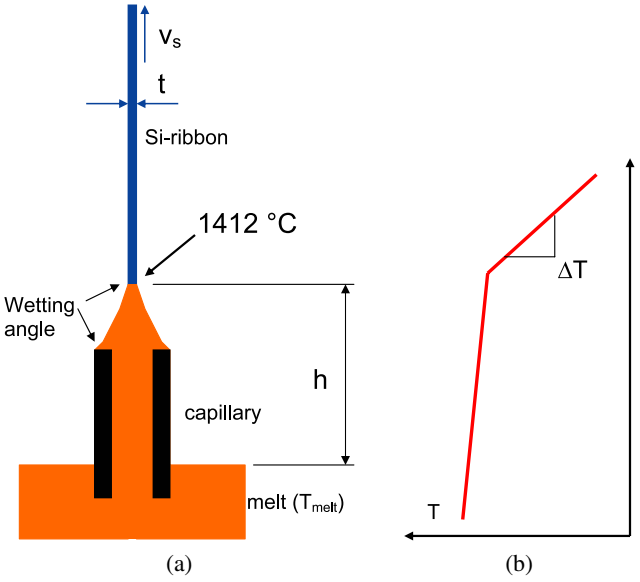

Fig. 5.2. Schematic drawing of the EFG process

directed nearly perpendicular to the pulling direction. As a consequence the segregation of impurities leads to a collection of impurities on the upper side of the ribbon that can be removed later by etching. Because of a potentially much higher pulling speed than crystallization speed, productivity can be much higher than in concept (a) processes. In addition to these basic differences, the quality of the produced wafers is decisive. Highest efficiencies – i.e., a conversion rate of sunlight into electricity of more than 15% – has been obtained with processes following concept (a).

To stabilize the melt meniscus, the EFG process uses a capillary die made of a material that is very well wetted by the melt. Due to the capillary effect of the wetting material the feeding of the meniscus with melt from the volume of the die is realized. Figure 5.2 shows this principle schematically.

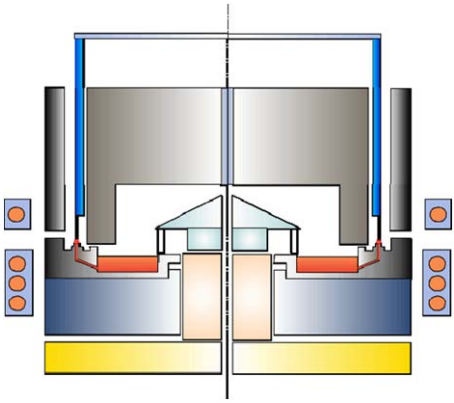

Fig. 5.3. Schematic drawing of the melt crucible with melt reservoir and capillary

Fig. 5.4. Simplified presentation of an EFG pulling device

The thickness of the ribbon depends on the wetting angle of the capillary material and the melt, the height h between meniscus and surface of the melt, the temperature difference ΔT between meniscus and crystal temperature as well as the pulling speed v_s.

A more detailed schematic drawing of the EFG crucible with capillary and melt reservoir is shown in Fig. 5.3. The crucible rests on a construction that carries the total set up including susceptor and cooling distance. Figure 5.4 shows a simplified presentation of the equipment as it is used in the production.

Fig. 5.5. View of the EFG production hall at SCHOTT Solar in Alzenau

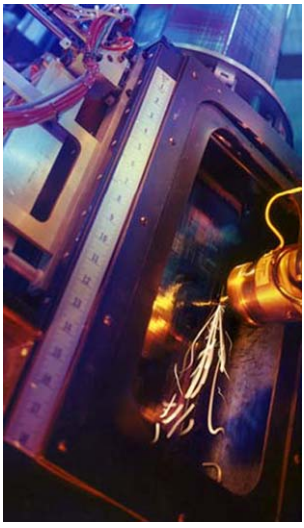

Fig. 5.6. Wafer production by separating

Figure 5.5 shows a view of the production hall at SCHOTT Solar in Alzenau, where octagon tubes with a length up to 6.5 m are produced. The control of the pulling process is mainly automatic.

The faces of the EFG-tubes are cut by laser beams into single wafers, shown in Fig. 5.6 along with details of the laser cutting equipment. Figure 5.7 shows an EFG wafer cut from one of the tube faces by laser.

To improve the productivity of the EFG process, developments have been made to extend the side facets of the tubes from 100 mm to 125 mm. 125-mm octagon

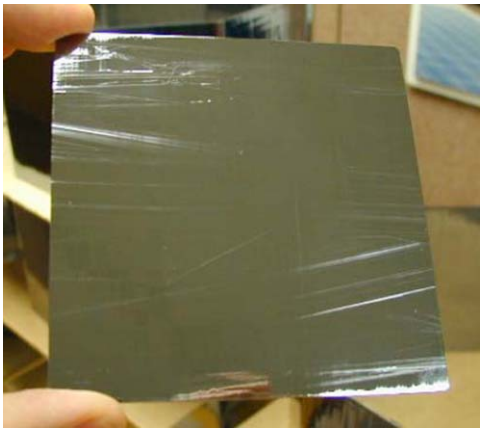

Fig. 5.7. EFG wafer produced by using a laser to cut the octagon tubes with a laser

Fig. 5.8. Octagonal tube with 8 × 125-mm wide facets

tubes are now the main production. The dimension of the wafers cut from these tubes is 125 mm × 125 mm.

Figure 5.8 shows an octagonal tube with 8 × 125-mm wide facets. The progress in productivity is shown by the increase in diameter from octagons with 8 × 10 cm faces to 8 × 125 mm up to the latest development to dodecagons with 12 × 125 mm faces (Fig. 5.9(a), (b)).

The wafers' electrical properties are important for the production of solar cells. The minority carrier lifetime is especially key for high efficiencies. Figure 5.10 shows a topography of the minority lifetime of an EFG wafer. Clearly visible are

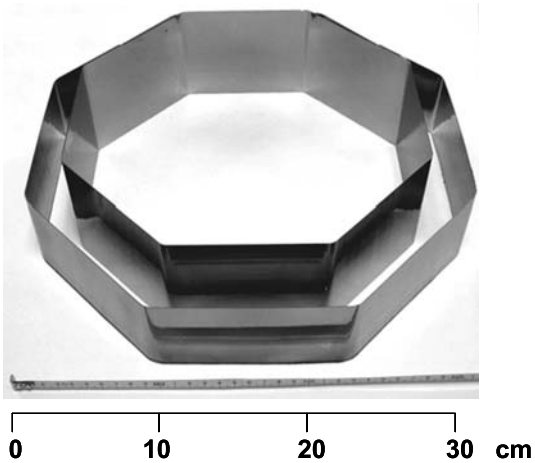

(a) Cross-section of a 8 × 100 mm tube put inside a 8 × 125 mm tube

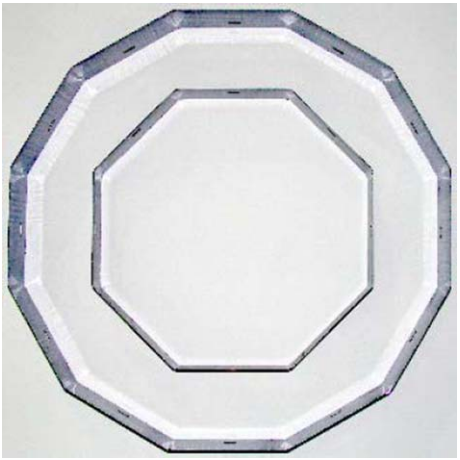

(b) Two cross-sections of tubes put together: A 8 × 125 mm tube inside a 12 × 125 mm tube

Fig. 5.9. (**a**) shows the difference in circumference of 8 × 100 mm tubes compared to 8 × 25 mm tubes. Because the tubes have the same growth rate, productivity is higher accordingly. The latest efforts to improve productivity resulted in the first experimental runs of dodecagon tubes with 12 × 125 mm facets grown at the same growth rate (**b**)

the different zones in the direction of crystal growing. The blue areas show good values at about 10 µs, the red in the range of 5 µs.

Solar cells produced from EFG wafers show efficiencies of up to 15% in production and offer an economical alternative to state-of-the-art multicrystalline wafers.

Research and development has obtained efficiencies of up to 18.2%, which shows the material's potential. Figure 5.11 shows the results obtained at NREL.

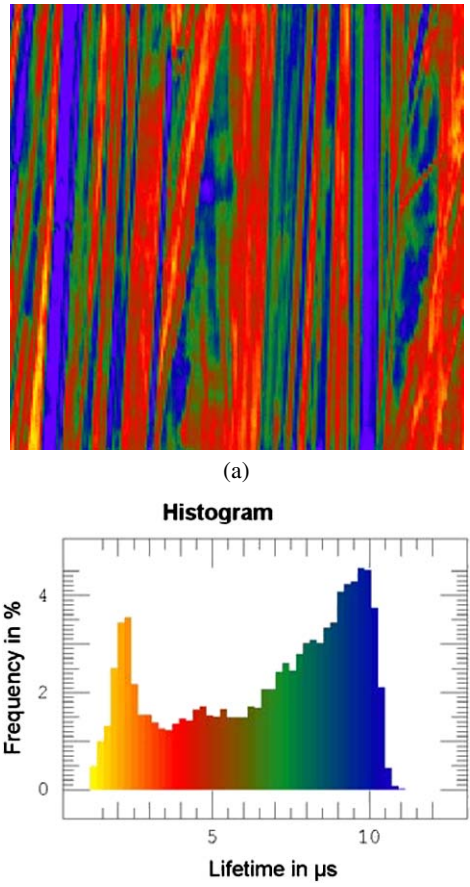

Fig. 5.10. Topography of minority carrier lifetime in EFG-ribbon-wafers. *The dark* areas show high quality material. (**a**) shows the topography (**b**) shows the statistical distribution of the data

This forms the best result within a development of several years, as indicated in Fig. 5.12.

Beside the efficiencies that can be obtained, potential cost savings in material are also very important. In EFG production the standard thickness today is 300 µm. In a pilot project, tubes with wall thicknesses around 200 µm have been manufactured and processed to solar cells. At present, a thickness of 80 µm seems to be possible. This would reduce the Si-consumption from about 7 g/Wp today to below 3 g/Wp tomorrow.

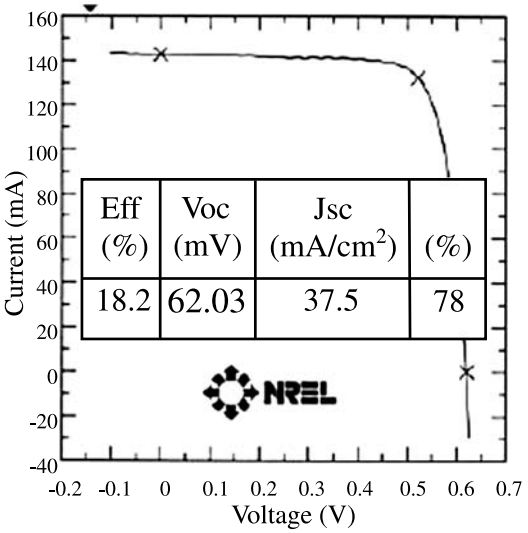

Fig. 5.11. Best EFG cell showing 18.2% efficiency obtained so far

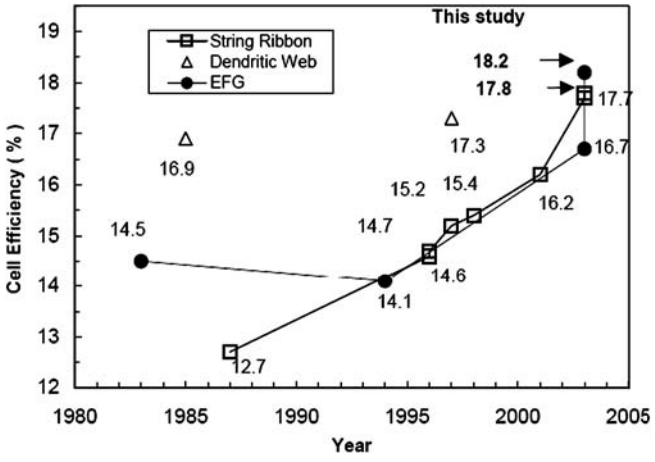

Fig. 5.12. Development of the ribbon material efficiencies

6 A Novel High-Efficiency Rear-Contact Solar Cell with Bifacial Sensitivity

R. Hezel

6.1 Introduction

At present, wafer-based silicon solar cells have a share of more than 90% of the photovoltaic market. Despite rapid growth in the manufacturing volume, accompanied by a significant drop in the module selling price, the high costs currently associated with photovoltaic power generation are one of the most important obstacles to widespread global use of solar electricity. Up to a certain level, a higher production volume is a key driver in cost reduction. However, apart from a drastic reduction of the silicon wafer thickness in conjunction with improved light-trapping schemes, innovative processing sequences combining very high solar cell efficiencies with simple and cost-effective fabrication techniques are needed to become competitive with conventional energy sources and thus to move solar energy from niche to mainstream.

The energy conversion efficiency has a great impact on the costs of a PV system. With a higher efficiency the module power density is increased, i.e. less cell and module area is required to achieve the same output power. Consequently all area-related costs are reduced, which make up more than 70% of the costs of a PV system. These include costs of the silicon feedstock, wafering, cell processing, module fabrication, installation and maintenance [1]. In particular, the silicon wafer contributes significantly to the module costs. Getting more power out of silicon is thus one of the most important challenges to realize an increase in efficiency. Reduction of the wafer thickness down to values of about 100 µm, as well as making the solar cell bifacially sensitive, are further means to reduce the cost of solar electricity.

As can be seen in Fig. 6.1, considerable progress in efficiency of crystalline silicon solar cells has been achieved in the past with laboratory cells characterized by high process complexity. A record efficiency of 24.7% has been obtained [2]. The theoretical limit of a silicon solar cell of 80 µm thickness and with Lambertian light trapping, an efficiency of 28.8% was determined [3].

The efficiencies of the majority of industrial solar cells are presently in the range of 13%–16% including monocrystalline Czochralski-grown and cast multicrystalline silicon as well as ribbon-grown silicon. These numbers clearly indicate the enormous potential for further efficiency improvement in commercial devices.

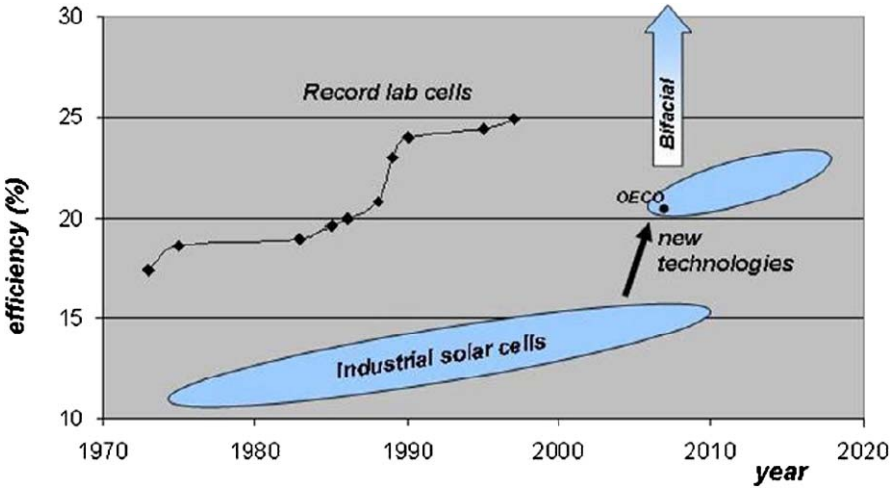

Fig. 6.1. Past, present and future of crystalline silicon solar cell efficiencies in the laboratory and in industry. Efficiencies exceeding 20% should be dominating the market in the near future. The novel bifacial OECO solar cells to be introduced in the following are potentially able to achieve effective cell efficiencies close to 35% by additionally using light impinging on the rear side

However, there are severe limitations to the standard screen printing approach [4]. Therefore it is indispensable to open up a new high-efficiency area above 20% in the near future with industrial crystalline silicon cells fabricated by novel cost-effective technologies (Fig. 6.1).

For some years promising candidates for this high-efficiency region have been commercially available. They are described in more detail in a separate section of this book. A recent comparative study of these devices including the novel obliquely evaporated-contact (OECO) solar cell should be mentioned [5].

The OECO solar cell, which will be extensively discussed in the following, is a completely different high-efficiency device characterized by a corrugated rear surface and both contact grid systems located at the rear side on the corresponding flanks of the ridges [6–8]. Bifacial sensitivity is automatically included together with the advantages of back-contact solar cells for efficiency, module fabrication and visual appearance. Efficiencies of 21.5% could already be obtained for front illumination [9]. High-efficiency and low-cost features are outlined together with the current fabrication sequence and the novel processing steps, including oblique contact-evaporation and surface passivation. The OECO cell is an all-silicon nitride-passivated device. Due to its importance to high-efficiency, the solar cells low-temperature surface passivation for front and rear side by plasma-enhanced chemical-vapor-deposited (PECVD) silicon nitride is also extensively discussed.

It should be emphasized that the bifacial sensitivity of the OECO cell with its potential for high rear-side contributions offers a simple way to effectively increase

cell efficiency. Effective efficiencies close to 35% should be achievable by proper module arrangement. A variety of possible bifacial applications is presented in the course of this article. As an interesting feature, from further improvements in rear-side efficiency the front-side efficiency will greatly benefit.

6.2 Structure of the Bifacial Rear-Contact Solar Cell

Figure 6.2 shows a schematic of the novel back-collecting and bifacially sensitive obliquely evaporated-contact (OECO) solar cell using p-type silicon [7–9]. The characteristic features include:

(i) A textured and well-passivated homogeneous front surface by PECVD silicon nitride, which simultaneously serves as antireflection layer.
(ii) A corrugated back surface with n-contact lines (emitter contacts) on one flank and p-contact lines (base contacts) on the opposite flank of the ridges. The flanks can be vertical, as shown in Fig. 6.2, or inclined, both resulting in very low grid shading of rear illumination.
(iii) A n^+ emitter generated at the rear surface except in the vicinity of the p-contacts.
(iv) The whole rear surface is covered by PECVD silicon nitride acting both as excellent passivation and antireflection layer for efficient utilization of light impinging on the rear side.

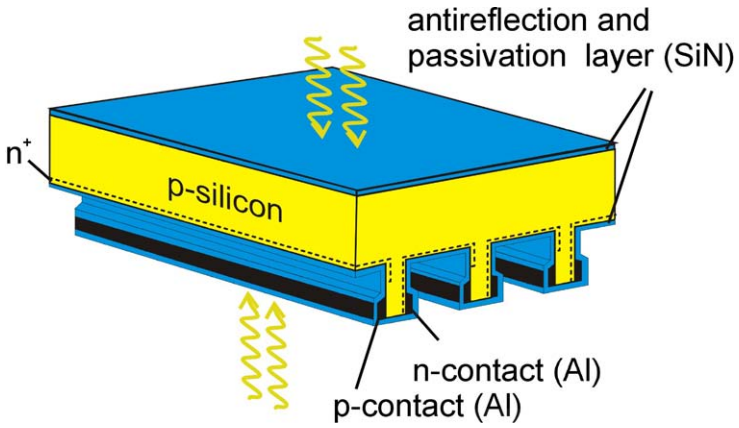

Fig. 6.2. Schematic of the high-efficiency bifacially sensitive OECO solar cell. Both contact lines are placed on the steep flanks of the ridges at the rear side. Also, light impinging on the rear side is efficiently used

6.3 High-Efficiency and Low-Cost Production Features

For advanced crystalline silicon solar cells, several efficiency-enhancing processing steps mainly focused on reducing carrier recombination are commonly applied [4, 10, 11]. Preferred implementations include: back surface field (BSF), selective emitter, floating junction and high-temperature thermal oxide passivation associated with narrow openings for point- or line-contact formation including complex alignment.

It is important to note that fabrication of the novel rear-contact OECO solar cells requires neither these costly, time- and energy-consuming high-temperature steps, nor does it require masks and alignment to achieve comparable one-sun front side efficiencies approaching 22%. A special feature of the OECO cells is their bifacial sensitivity, i.e. additional high power can be gained using the light directed onto the rear side.

Some of the unique high-efficiency and low-cost production features are:

- Absence of grid-shadowing on the front side.
- Effective cell efficiencies close to 35% are achievable due to bifacial operation, which is possible without additional processing. Rear-side efficiency can be close to that of the front side.
- The fabrication of the corrugated rear-side structure by one simple grooving step turns out to be highly cost-effective. In contrast to other approaches it allows, in a simple way, formation of both contact systems as narrow grid fingers at the corresponding flanks. By properly orienting the grooves, texturing of the flanks can be avoided in order to keep the contact area low.
- Simple and reliable separation of n- and p-contact lines, a small grid finger area as well as low metal consumption per cell are achievable by the novel self-aligned high-throughput oblique evaporation technique.
- The high-quality yet simple MIS-n^+p contact scheme gives two major advantages [12]. (i) Low-cost aluminum is applicable as contact grid metal and (ii) a selective emitter diffusion is not required to obtain high-efficiencies.
- Inherent passivation of the base contacts is provided by the rear-side design, thus replacing the boron diffusion process with its high thermal budget commonly used for the generation of a back surface field (BSF).
- Excellent low-temperature front- and rear-surface passivation is accomplished by plasma silicon nitride which simultaneously acts as antireflection coating.
- The back-contact cell design and "soft" processing are favorable for thin wafers. Substrate warpage does not occur. To a certain extent, the thinner the cells are the more efficient they become.
- The optimum base thickness is easily adjustable by the rear-side grooving process.
- Due to the special rear-side design characterized by narrow base regions without emitter coverage, lateral minority-carrier diffusion is negligible. As a consequence, in contrast to other back-contacted solar cells, neither additional lifetime requirements for the base material nor sophisticated tight rear-side patterning are of concern for the novel cells [11].

- Lower cell operating temperature and thus higher voltage results due to the "open" rear side. The long-wavelength radiation leaves the cell without being absorbed by a continuous rear metallization characteristic for most of the commercial solar cells.
- Since both contacts are on the rear side, module fabrication costs are reduced. High-throughput surface-mount automated assembly can be used.

6.4 Inherent Passivation of the Base Contacts

As a new characteristic for the back-contacted OECO solar cells, due to their geometrical arrangement at the flanks of the narrow ridges, the p-contacts collecting majority carriers are, to a large extent, screened against minority carriers without the presence of a local back-surface field. With proper cell design, the minority carriers (electrons) are, except in the V_{oc}-state, preferentially collected by the emitter running on both sides of the elevations. Thus, the carrier density in the vicinity of the base contacts is significantly reduced [7–9]. As a consequence, recombination at these contacts is sufficiently low. Therefore, in contrast to other high-efficiency solar cells, the complex formation of a local back surface field is not required. This

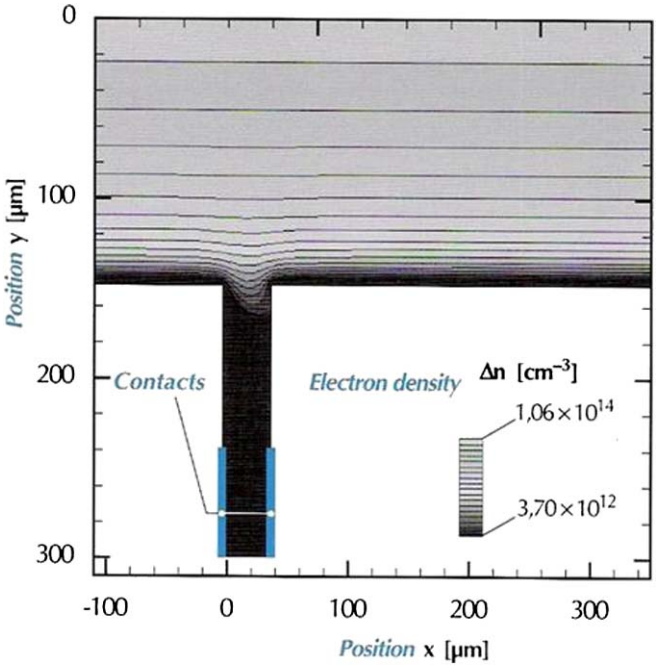

Fig. 6.3. Calculated two-dimensional electron density for a p-Si OECO solar cell under front side illumination and J_{sc} conditions. The extremely low density of electrons present in the narrow ridges results in a considerable reduction of carrier recombination at the base contacts

special feature of the back-contacted OECO cell was extensively investigated by two-dimensional calculations using DESSIS [8, 9].

As an example, Fig. 6.3 shows the calculated two-dimensional electron carrier density under front-side illumination and J_{sc} conditions for a properly designed rear-side structure with narrow ridges and wide grooves. The high injection level of $2 \times 10^{14}\,\mathrm{cm}^{-3}$ near the front surface decreases to $3 \times 10^{13}\,\mathrm{cm}^{-3}$ near the rear surface of the grooves. This behavior is characteristic for back-collecting solar cells with a planar rear side. Within the narrow ridge of the OECO cell, however, the minority carrier density is drastically reduced by more than a factor of 100 down to $2 \times 10^{11}\,\mathrm{cm}^{-3}$, leading to a considerable reduction of carrier recombination at the base contacts, which are located at the right flanks of the ridges. This shielding-effect for the minority charge carriers, acting as a kind of inherent passivation by geometric means, increases the short-circuit current density of the OECO solar cell by more than $2\,\mathrm{mA/cm}^2$ compared to a similar cell with a fully planar rear side. The fill factor is also increased by the extremely inhomogeneous minority-carrier distribution.

6.5 Processing Sequence

There are several options for the production of OECO solar cells. One example for the processing sequence is shown in Fig. 6.4, where only industrially feasible self-aligning mask-free steps are applied [8, 13]. First, the front surface of the wafer is textured with random pyramids, preferably by anisotropic etching (Fig. 6.4a). After the rear side is grooved, a diffusion barrier layer is deposited on the flanks of the ridges to prevent emitter formation in the vicinity of the base contacts (Fig. 6.4b).

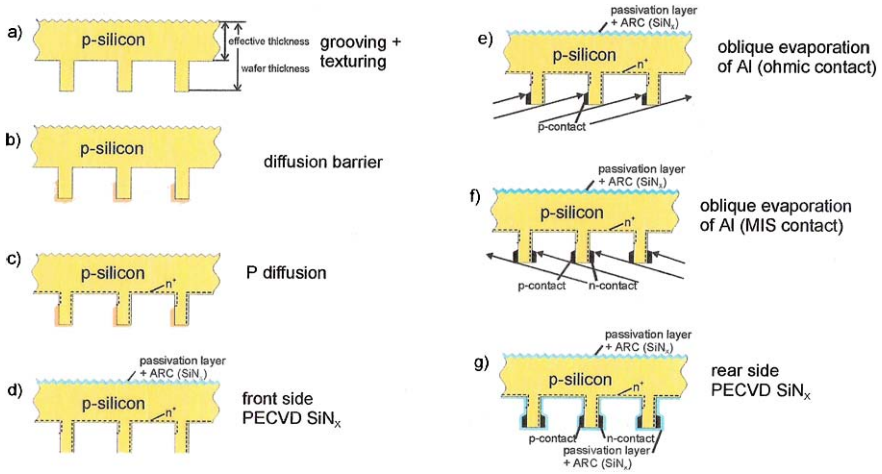

Fig. 6.4. Processing sequence for back-contacted bifacial OECO solar cells using only techniques feasible for industrial high-volume manufacturing

A conventional phosphorous diffusion follows at 890 °C to form the n^+-emitter, whereby the front side is protected against diffusion by proper positioning of the wafers (face to face) or by a diffusion barrier layer (Fig. 6.4c). A shallow emitter profile with a sheet resistivity around 90 Ω/sq is required, if comparable efficiencies for front- and rear-side illumination of the bifacial cell should be achieved. If only the efficiency for front-side illumination is to be optimized, a heavily doped emitter is preferable. Phosphorous glass and diffusion barrier are then removed. Low temperature (<400 °C) remote PECVD silicon nitride is used as front-surface passivation and antireflection layer (Fig. 6.4d).

Base-contact metallization is performed by oblique evaporation of aluminum (Fig. 6.4e). Ohmic contact formation and growth of an ultrathin (∼1.5 nm) oxide layer is simultaneously performed by a short annealing step at 500 °C.

A high-quality metal-insulator-silicon (MIS)-n^+p contact is obtained by oblique evaporation of aluminum from the direction opposite to the p-contact (Fig. 6.4f). As a nanolayer, the thin oxide serves two main purposes [12]: (i) it prevents Al from degrading the pn-junction, so that low-cost Al instead of expensive Ag can be used for reliable emitter contacts of solar cells [14]; and (ii) the majority carriers (holes) are blocked, whereas the minority carriers (electrons) are able to pass through the insulating layer by quantum-mechanical tunneling. Thus the simple-to-fabricate "tunnel" oxide replaces the high-temperature diffusion step usually applied to form a selective emitter.

Then the whole rear surface is covered with PECVD silicon nitride as passivation and antireflection layer (Fig. 6.4g). Finally the grid fingers of each polarity have to be connected by busbars running across the contact grid. For this purpose, after selective removal of the nitride layer from the respective grid fingers, busbar formation and tabbing are simultaneously performed by attachment of metal ribbons using conductive adhesives.

In conclusion, the relatively simple fabrication process exclusively uses industrially feasible, mask- and aligning-free processing steps such as surface grooving, emitter diffusion (n^+), self-aligned metallization and low-temperature passivation by silicon nitride on the front and rear side. Toxic materials are excluded. This underlines the high potential for OECO solar cells to be fabricated economically in an environmentally benign way.

6.6 Production Technology

6.6.1 Back-Surface Grooving

As the key feature of the back-contacted OECO solar cell, a corrugated rear surface has to be provided that consists of a set of parallel grooves forming specific elevations with steep side walls for the simple mask-free and self-aligned deposition of both contact line systems by oblique vacuum evaporation.

In general, the fabrication of the distinct back surface structure can be performed by various technologies, e.g., chemical etching, laser grooving or by a grinding technology.

Fig. 6.5. High-throughput grinding tool for surface grooving of OECO solar cells. A $10 \times 10\,cm^2$ wafer can be processed in a few seconds

The first approach, mechanical grooving with a fast rotating diamond-coated tool was developed. This method is a relatively simple and reliable process with high-throughput capabilities [15–18]. In order to demonstrate the industrial feasibility of the grinding technology, a novel high-throughput grinding system was constructed. The main feature of this equipment is a 150 mm wide grinding tool, which grooves silicon wafers up to $150 \times 150\,mm^2$ with one fast stroke. A section of this grinding tool is depicted in Fig. 6.5 [19].

By optimizing tool and process parameters the effect of crystal defects induced by mechanical abrasion is minimized [20]. As demonstrated by a large number of industrial-size wafers, breakage during the grinding process is negligible.

An important advantage of grooving for high-efficiencies is worth mentioning [8]. Whereas the cell surfaces are randomly textured with pyramids, the flanks can remain flat in order to keep the contact area low. This is accomplished simply by proper orientation of the grooves so that preferential etching does not occur at the flanks. As an example, for a (100) surface, the flank orientation should be of the (110) type.

Another cost-effective way for silicon surface grooving is based on chemical etching in conjunction with the definition of an etching mask by laser ablation or screen-printing [21].

An additional approach – direct laser ablation of silicon – can be used for groove formation. This is a well-known technology that has been successfully applied to mass production of buried contact solar cells [10].

6.6.2 Metallization by Oblique Evaporation

Oblique evaporation of contacts is the crucial step both for obtaining high-efficiencies as well as for simple, low-cost and reliable processing of the OECO solar cells [7]. In general, conventional vacuum evaporation with the wafers perpendicularly ori-

ented to the metal beam (mostly including mechanical masks or photolithography for structuring) cannot be regarded as a low-cost process for economic solar cell production. However, the situation is completely different for evaporation under a shallow angle, where the throughput of wafers can be drastically increased. The principle of the novel oblique-evaporation technique is shown in Fig. 6.6. It is based on the fact that vacuum evaporation is a directional process that allows us to make use of shadowing effects of a distinct surface structure to define the grid fingers. Using the self-shading effect, the metal fingers are deposited along the steep flanks of the ridges without any mask or alignment. The width of the fingers is simply adjusted by variation of the evaporation angle and thus the cross-section of the contact lines can be increased without significantly affecting light obscuration.

As a further, very important feature of the OECO technique, the separation of the n- and p-contact lines in order to avoid shunting is ingeniously simple and reliably accomplished without any masks or alignment [7]. As can be seen in Fig. 6.7, during evaporation first from the left side (p-contacts) and subsequently from the right side (n-contacts) even under a very shallow angle φ some metal is also deposited on the narrow tops of the ridges, thus connecting the two contact fingers. However, this metal layer is very thin (thickness $\sim a \sin(\varphi)$) compared to the grid-line thickness a and exhibits a porous columnar structure, so that it can easily be removed by a short etch without significantly reducing the thickness of the contact fingers. In the case of aluminum, the etch rate of the porous film obtained by evaporation under an angle φ of typically 4 °–8 ° is about three times higher than that of the nearly vertically deposited grid finger material [7].

An example of a high-throughput equipment for oblique vacuum evaporation is also schematically depicted in Fig. 6.6. The wafers are arranged in a vacuum chamber closely spaced on a rotating cylinder with their surface orientation deviating only slightly from being parallel to the evaporation beam. Thus the packing density and hence throughput is up to ten times higher compared to conventional vacuum

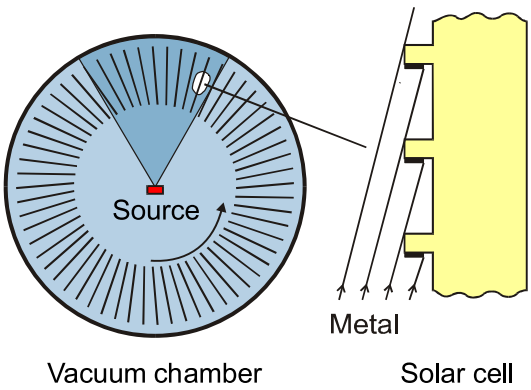

Fig. 6.6. Principle of oblique evaporation for contact metallization of OECO cells and arrangement of the wafers in the vacuum chamber. Self-alignment is provided by the shading effect of the groove tops

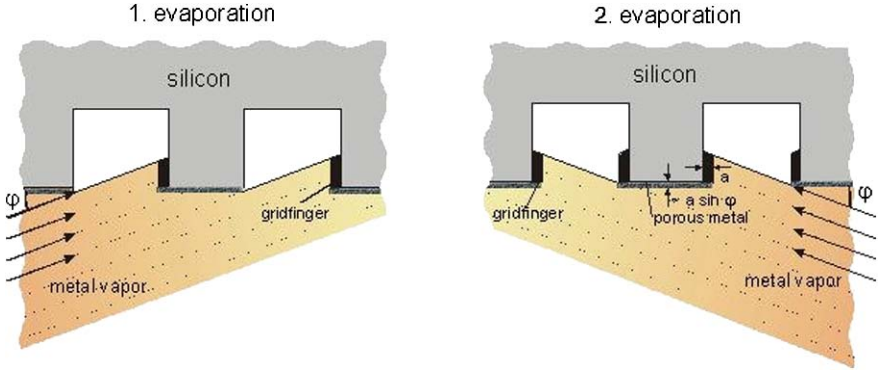

Fig. 6.7. Subsequent evaporation of both contact schemes. Separation of the n- and p-contact lines is reliably accomplished without any mask or alignment. Only a very thin porous metal film has to be removed from the ridge tops by a short etch

Fig. 6.8. Prototype of high-capacity oblique evaporation equipment for the metallization of OECO solar cells. Large wafer cassettes are arranged on a cylinder revolving around the evaporation source

evaporation, where the substrates are positioned perpendicular to the evaporation beam. Furthermore, metal wastage is prevented since nearly all the metal evaporated is used for the grid fingers. Electron beam or resistive heating can be applied for evaporation of the source material.

A high-capacity prototype of the evaporation equipment suitable for mass production was constructed according to the design shown in Fig. 6.8. A floor space of

only 2.5 m^2 is required for this system, whose capacity amounts to about 1,000 wafers of 10 × 10 cm^2 in size. Reliable operation was demonstrated in a pilot line [22].

6.6.3 Surface Passivation by PECVD Silicon Nitride

Passivation Mechanism and Film Properties

The achievement of high-efficiencies for crystalline silicon solar cells is highly dependent on the reduction of carrier recombination at the surface. Surfaces represent rather severe defects in the crystal structure and are the site of many allowed states within the forbidden energy gap of silicon. Excellent surface passivation achieved through the growth of dielectric films is thus of prime importance for high-efficiency solar cells. Furthermore, by passivation of the front and rear surface with dielectric layers – apart from serving as antireflection coatings – the internal optical reflection is also increased, resulting in good light-trapping properties. This is crucial to the future introduction of thinner and thus less-costly silicon substrates in solar cell manufacturing, so that lower wafer cost is not offset by efficiency losses [3].

Extrinsic silicon surface passivation by dielectric films is based upon the Shockley-Read-Hall theory [23, 24]. The recombination of charge carriers via surface states is dominated by the density of those centers that are located near the middle of the forbidden gap. The recombination rate at the silicon/insulator interface reaches its maximum value in case of depletion, when the electron and hole concentrations at the surface are equal. For strong accumulation or inversion, however, the concentration of majority or minority carriers, respectively, is prevailing. Under these conditions, the surface recombination rate is drastically reduced [3, 24]. Thus both the reduction of the surface state density and the presence of strong inversion or accumulation accomplished by fixed insulator charges can be used for surface passivation, characterized by the effective surface recombination velocity [25].

Two different techniques are hitherto applied to obtain low effective surface recombination velocities for high-efficiency solar cells [3, 24]: (i) growth of a thermal oxide film on silicon to reduce surface-state density and (ii) creation of a strong built-in electric field (high-low junction) in order to repel the minority carriers from recombination sites at the surface [26].

Thermally grown SiO_2 films provide very good surface passivation on n- and p-type Si-wafers and on phosphorous-diffused silicon wafers via an extremely low interface state density [24]. However, for solar cell application there are severe drawbacks. Due to their low refractive index of 1.46, they are not suitable for an efficient reduction of reflection losses. Furthermore, high temperature (>1,000 °C) processing is required, which is an energy- and time-consuming step. Since the oxide has to be grown before metallization, complex procedures have to be applied to open the film for contacting the underlying silicon.

The most promising alternative to thermally grown SiO_2 is amorphous silicon nitride fabricated at low temperature by plasma-enhanced chemical vapor deposi-

tion (PECVD). These films, first introduced and optimized for solar cells by the author's group in 1981, reveal excellent passivation of undiffused and diffused silicon surfaces, combined with optimal antireflection properties and low temperature processing [25, 27–31]. Furthermore PECVD silicon nitride is known from IC technology for its excellent impurity barrier properties, corrosion protection of the metallization, scratch- and crack-resistance and good step coverage [32]. Chemical, mechanical, electrical as well as optical properties of SiN films depend strongly on the preparation method and the particular process parameters used. Only a few dependencies which are relevant for the OECO cell fabrication shall be discussed.

Of all deposition parameters, temperature was found to be the most important [30]. Deposition temperatures around 400 °C provide optimal surface passivation, whereas at lower and higher temperatures the passivation quality is strongly decreasing. It is well known that a high amount of hydrogen (up to 25% H) is incorporated into the plasma silicon nitride films, partially forming Si–H and N–H bonds. The films are therefore often denoted as SiN_x:H, but in this work briefly, SiN. The saturation of unsaturated dangling bonds at the silicon surface by hydrogen is responsible for strong decrease of the surface state density in the range 350 °C–420 °C [30, 33]. At higher temperatures, both N–H and Si–H contents are lost and outdiffusion of hydrogen occurs.

The good AR coating properties of SiN films are due to the fact that the index of refraction n can be varied in a wide range from 1.7 to 3.0. An increase of n, which can be accomplished e.g. by increasing the SiH_4/NH_3 gas ratio, is correlated with a shift of the film composition toward silicon-rich films [34]. Very silicon-rich SiN films with a refractive index $n > 2.3$ were found to provide optimal surface passivation [30]. The more the SiN_x:H layers tend to resemble amorphous hydrogenated silicon, the better their surface passivation properties become. However, light absorption – particularly in the short-wavelength region – increases with Si content.

As to the amount of positive charges at the Si/SiN interface, it was found that the lower the amount of Si–H bonds the higher the positive interface charge density. If the amount of charges is sufficiently high, e.g. for nitride films with a low index of refraction, inversion can be achieved, where, as mentioned above, field effect passivation plays a significant role [25]. Such inversion layers accomplished by SiN antireflection coatings were successfully applied as emitters in MIS-inversion layer solar cells with efficiencies up to 19.6% [12, 35]. The excellent stability of the inversion layer is demonstrated by these cells encapsulated in novel large-area modules and installed since 1994 in many places, e.g., in the German-Spanish 1MW PV power plant in Toledo [36, 37].

With the present OECO cells, however, inversion layer formation may cause parasitic shunting which can be avoided by applying a more silicon-rich nitride layer with its higher index of refraction. It contains fewer positive charges and surface passivation is dominated by a reduction of interface–state density via hydrogen termination of Si-dangling bonds at the silicon surface.

It should be pointed out that nitride passivation is particularly well suited for use with multicrystalline substrates due to its consistency with hydrogenation of the bulk material resulting in a significant improvement of carrier lifetime [31].

Plasma Deposition Reactors for Silicon Nitride Layers

The properties of PECVD SiN depend strongly on the design of the reactor as well as on the deposition parameters. There are two fundamentally different reactor designs, parallel-plate (often referred to as "direct") and "remote".

In the parallel-plate version, the wafer is placed onto one of the two electrodes and is thus in direct contact with the plasma. It is important to note that the surface passivation properties of the SiN films depend strongly on the plasma frequency used. In the low-frequency (LF) mode (10–500 kHz), the ions in the plasma are able to follow the excitation frequency leading to surface damage and low-quality passivation. UV stability problems are a consequence of this surface damage with direct plasma SiN films [38, 39]. In the high-frequency (HF) regime (>4 MHz, typically 13.56 MHz) bombardment of the substrate surface is minimized since the ions in the plasma cannot follow the excitation of the electromagnetic field.

The second and most successful class of plasma reactors is formed by the downstream or remote system, which was introduced into photovoltaics in 1989 by the author's group at the University of Erlangen [38]. An important feature of the remote PECVD systems is that the Si wafer is located outside the plasma region, allowing for deposition of SiN films with no surface damage to the wafers and making the frequency relatively unimportant. Ammonia (NH_3) as one of the process gases is excited outside the deposition chamber by means of microwaves and mixed with silane (SiH4) in the chamber.

Up to now, the best surface passivation quality has been achieved with remote PECVD and parallel-plate HF reactors [30]. Figure 6.9 shows a schematic of the static laboratory-type remote PECVD system with downstream geometry (Oxford Plasmalab 80). It can be seen that the wafer is located outside the plasma. A mixture of ammonia (NH_3) and nitrogen (N_2) is excited by passing through a microwave cavity and mixes with silane (SiH_4) downstream of the plasma. The reaction takes place above the substrate which is placed on a heated plate.

In-line remote PECVD systems have been available to the PV industry for several years. Up to now they have been exclusively applied for the deposition of SiN antireflection coatings and as a source of hydrogen for the bulk passivation of multicrystalline silicon solar cells. Only recently have the surface passivation properties of SiN films deposited in such a large-area industrial PECVD system (SINA, Roth and Rau) been extensively studied [40].

The machine shown in Fig. 6.10 employs a 2.45 GHz linear microwave source for plasma excitation. In this source two quartz tubes are mounted perpendicular to the wafer transport direction. Ammonia is fed into the source above the tubes, whereas silane is added below at the sides of the plasma source. The wafers are placed on a carrier for transport through the processing chamber. Load looks at either end of the processing chamber are used for loading and unloading of the

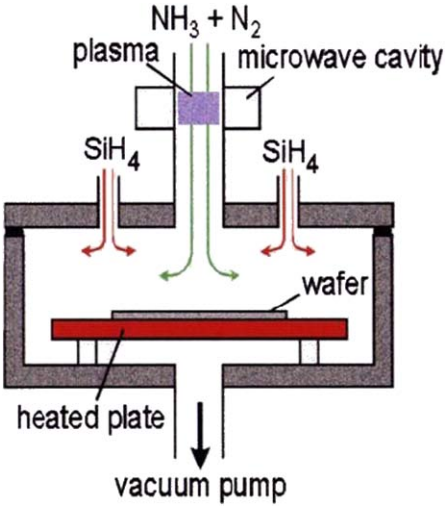

Fig. 6.9. Schematic of a static remote PECVD reactor

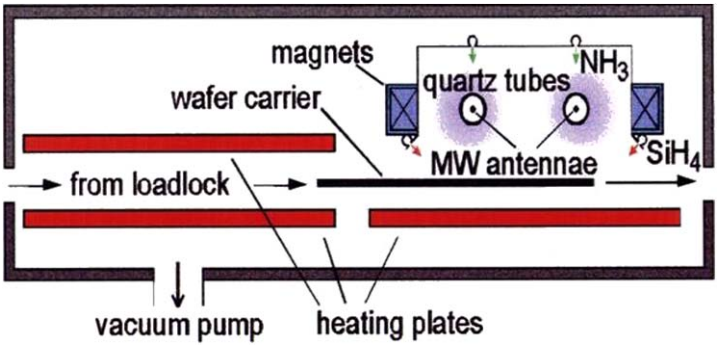

Fig. 6.10. Schematic cross-section of a microwave in-line remote PECVD system

carrier without breaking the processing vacuum. A detailed technical description of the complete inline system has been given elsewhere [40, 41].

The surface passivation properties of silicon nitride films could be optimized under dynamic deposition conditions in this reactor [40, 42]. Excellent results both on n^+-emitters and on low resistivity ($\sim$1 Ω cm) p-type silicon have been obtained, which are practically equivalent or even superior to those of the best laboratory reactors. It has been demonstrated that this industrial-scale, in-line deposition system is well suited for the passivation of advanced solar cells such as the OECO devices with efficiencies well above 20% [15, 22].

Front-Surface Passivation

Excellent passivation of the front surface is crucial to reach high-efficiencies, particularly for back-collecting solar cells [13]. Values of the effective front surface recombination velocity S_{eff} below 50 cm/s are required for high short-circuit current densities J_{sc} under front-side illumination. Record values below 10 cm/s could be obtained for silicon with resistivity above 1.5 Ω cm passivated by remote PECVD SiN layers [43]. However, these excellent surface recombination velocities were realized on planar silicon surfaces using silicon-rich SiN films with refractive indexes n above 2.4. The higher absorption of these films cause some losses in the short-circuit current density.

In order to achieve the highest possible cell efficiency, a layer with good optical properties and high passivation quality on a textured, low-resistivity silicon surface (∼0.5 Ω cm) is required.

With the commonly used SiN antireflection film (refractive index $n = 2.05$ and thickness $d_{2.05} = 105$ nm) only $S_{\text{eff}} = 240$ cm/s is achieved on a textured 0.5 Ω cm substrate. By this lower passivation quality the efficiency would be reduced by about 2% absolute. However, if a very thin silicon-rich SiN layer with $n = 2.5$ is deposited underneath, S_{eff} can be drastically reduced. This is demonstrated in Fig. 6.11 where the effective lifetime τ_{eff} and the surface recombination velocity S_{eff} are plotted as a function of the thickness $d_{2.5}$ of the silicon-rich layer, topped by a 70 nm thick nitride film with $n = 2.05$. The silicon nitride was deposited by remote PECVD at a temperature of 400 °C. The electrical properties were determined using injection dependent lifetime spectroscopy [8].

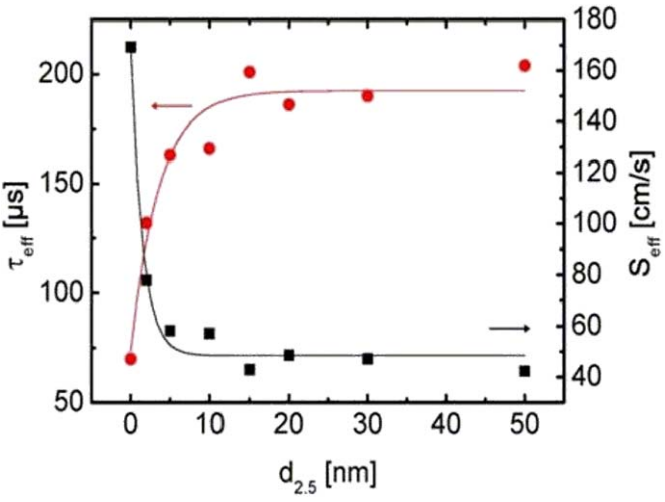

Fig. 6.11. Measured effective minority carrier lifetime τ_{eff} and surface recombination velocity S_{eff} for SiN double layers deposited at 400 °C on textured 0.5 Ω cm Si. The thickness $d_{2.5}$ of the Si-rich bottom nitride layer ($n = 2.5$) is varied, the top nitride layer ($n = 2.05$) has a constant thickness of 70 nm

As seen in Fig. 6.11, adding only a few nanometers of the silicon-rich nitride results in a steep increase in τ_{eff} up to a saturation value of about 200 µs for $d_{2.5} \geq 10$ nm. This corresponds to an excellent surface recombination velocity of 50 cm/s. From absorption measurements it was found that for $d_{2.5} > 10$ nm more than 5% of the sunlight is absorbed in the silicon-rich nitride film, which is not tolerable for highly efficient solar cells. For $d_{2.5} \leq 5$ nm, less than 2% is absorbed [9]. This small absorption is overcompensated for by the higher passivation quality. Thus, the cell efficiency shows a maximum for $d_{2.5} = 4$ nm with a gain of 1.1% absolute.

This newly developed silicon nitride double layer electrically outperforms the formerly used single silicon nitride film while preserving the excellent optical properties. Furthermore, the costly preparation of a floating junction, including a high-temperature diffusion step, is not required.

Rear-Surface Passivation

In the earlier development stage, the whole rear surface of the OECO cells was covered by a conventional PECVD SiN layer with a refractive index $n = 2.05$. A deposition temperature of 300 °C compatible with the MIS contacts had to be used. However, as was thoroughly investigated, due to their positive interface charges, these nitride layers create a conducting inversion channel between the diffused n^+-emitter and the ohmic base contact [44]. As a consequence, lower values of the shunt resistance and fill factor resulted. It was recently demonstrated with conventional rear-SiN passivated solar cells that this parasitic shunting can be eliminated by introducing a local back surface field (LBSF) [45].

Due to the unique features of the OECO cell, the generally applied back-surface field for passivation of the base contacts is not required. Therefore, we can avoid this extra processing step for the purpose of channel stopping.

Instead, in a more elegant way via an adapted processing and a new rear passivation scheme (consisting of a SiN double layer similar to that on the front side but deposited at the lower temperature of 300 °C) the parasitic shunting could be completely suppressed [9]. Shunt resistance values above 9 kΩ cm^2 are achieved. Furthermore, the surface recombination velocity is reduced by nearly a factor of 10, from 2,000 cm/s for the conventional SiN layer with $n = 2.05$ to 200 cm/s for the optimized double layer with $n = 2.5/2.05$. The high shunt resistance and thus the absence of parasitic shunting achieved by the SiN double layer is attributed to the fact that in the silicon-rich first nitride layer ($n = 2.5$) much fewer fixed positive charges are present resulting in a higher inversion-channel sheet resistance.

In conclusion, applying the optimized PECVD SiN double layers to the rear side of the OECO solar cells provides a simple way to improve the passivation quality of the rear surface while also reducing the shunting effect.

6.6.4 Interconnection Technology Based on Conductive Adhesives

In contrast to the conventional metallization by screen printing, the oblique evaporation process used for the OECO cells does not provide busbars which electrically

interconnect the grid fingers with each other and serve as solder areas for cell interconnection in module fabrication. Therefore, for OECO-type cells, an alternative technology is applied by which busbar formation and cell interconnection can be achieved using electrically conductive adhesives [15]. Their curing temperature is very low, typically below 200 °C, and the whole interconnection process is rather simple. After application of the adhesive – commercially available as a tape or as a one- or two-component paste – the metallic interconnectors (tabs or a prefabricated metal pattern) are attached to the cell and cured at the temperature specific for the adhesive.

This technique, already well established for chip mounting and in the automotive industry, has several advantages over traditional soldering. These advantages are particularly relevant for very thin and large as well as back-contacted silicon solar cells [46, 47]:

(i) As a low-temperature joining technique, it avoids build-up of mechanical stress on joints and cells which ultimately may cause breakage; thus, process yield and reliability increased.
(ii) Busbar formation and cell interconnection are accomplished in one process step.
(iii) The adhesives are nonpolluting (lead free!).

Conductive adhesives suited for contacting solar cells consist of a matrix, mostly an epoxy resin, and up to 80 wt% of conductive particles varying in size from several µm to several tens of µm. Electrical conductance is through side-to-side contact of the particles suspended in the epoxy matrix. Epoxies are easy to adjust, resistant to humidity and without hazardous out-gasing.

Since long-term stability of the interconnection has been proven by accelerated aging tests for some conductive adhesives, this novel technology appears to be a promising alternative to conventional soldering [15].

6.7 Cell Results

4 cm^2 solar cells were processed using 0.5 Ω cm FZ-silicon wafers with an effective base thickness of 150 µm. Only the front side was textured and, as outlined above, both sides were coated with double layer passivation stacks of PECVD silicon nitride.

The J–V curves under front- and rear-side illumination at STC (1 sun, AM1.5 G, 25 °C) are shown in Fig. 6.12 [9]. Efficiencies of 21.5% and 17.7% (independently confirmed at CalLab, Fraunhofer ISE, Germany) are achieved for front- and rear-side illumination, respectively (cell size: $2 \times 2\,cm^2$).

To our knowledge these are the highest efficiencies of back-contacted, bifacially sensitive solar cells fabricated without photolithography.

Remarkably high values of the short-circuit current density J_{sc} of 41.9 mA/cm^2 are achieved due to the excellent effective front-surface recombination velocity, very good optical properties and the inherent contact passivation provided by the narrow

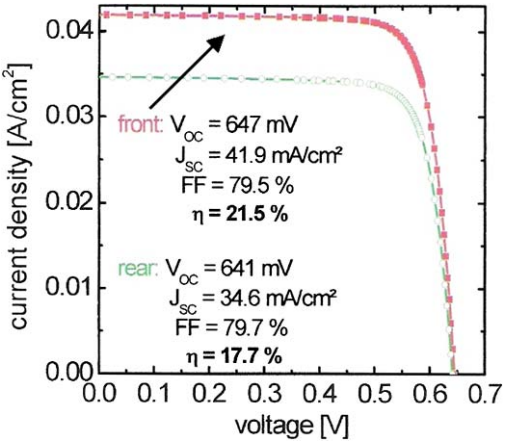

Fig. 6.12. Measured J–V-characteristics of back-contacted bifacial OECO solar cells. Efficiencies of 21.5% and 17.7% are achieved for front- and rear-side illumination, respectively

ridges. Although the rear side is not textured and both kinds of contacts are placed on this side, high J_{sc} values of 34.6 mA/cm^2 are realized under rear illumination. With a textured rear side and an optimized emitter diffusion, rear-side efficiencies up to 20% are expected.

The high fill factor of 79.5% is attributed to the absence of any parasitic shunt ($R_{sh} = 9\,\mathrm{k\Omega\,cm^2}$) and to a very low series resistance ($R_s = 0.4\,\Omega\,\mathrm{cm^2}$). The excellent quality of both surface passivations and evaporated contacts is reflected by the relatively high open-circuit voltage $V_{oc} = 647$ mV. It should be mentioned that due to the "open" rear side of the bifacial cell the operating temperature of the cell is lower compared to conventional cells with continuous rear metallization.

6.8 Efficiency Perspectives

In general, rear-contact solar cells have a key advantage. At least to a certain extent, the thinner they are, the more efficient they become. Figure 6.13 shows the efficiencies of back-collecting solar cells calculated as a function of the minority carrier diffusion length L_d for a base thickness of 50, 100, 200 and 300 µm, respectively [7]. Realistic conditions were used for the simulation, which led to efficiencies of 20.1% for $10 \times 10\,\mathrm{cm^2}$ front-collecting OECO cells and up to 21.2% for $4 \times 4\,\mathrm{cm^2}$ laboratory cells [22].

The efficiency of back-collecting solar cells depends strongly on the bulk diffusion length L_d and on the effective front-surface recombination velocity S_{front}. As can be seen from Fig. 6.13, with decreasing diffusion length the efficiency is sharply dropping, since the minority carriers generated mainly at the front side have to diffuse to the rear junction. High-efficiencies are achievable only if the bulk diffusion length strongly exceeds the base thickness. For high-quality material such as

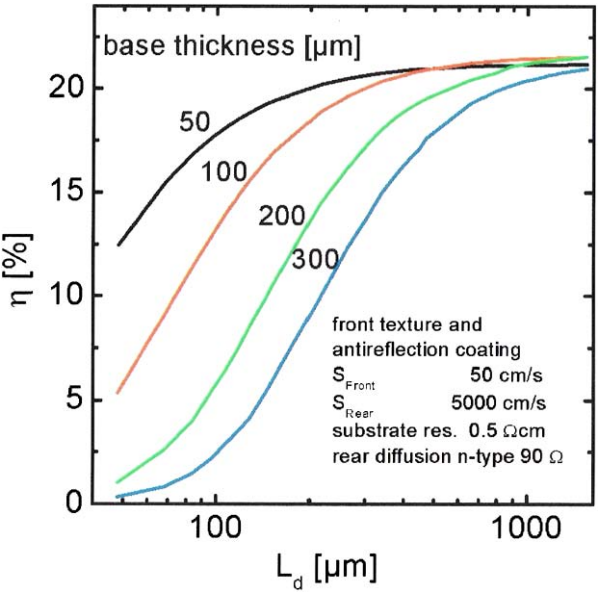

Fig. 6.13. Efficiency of back-collecting solar cells calculated as a function of the minority carrier diffusion length L_d and different base thickness. The thinner the cells, the more efficient they are

B-doped FZ–Si or Ga-doped Cz–Si with diffusion lengths above 800 µm, efficiencies approaching 23% are attainable. For material of lower quality such as B-doped Cz–Si (L_d ~250 µm) or multicrystalline silicon (L_d ~150–300 µm) the base thickness has to be reduced well below 200 µm to reach efficiencies up to 20%. Further details about these materials are presented in the following section.

Thus higher efficiencies can also be achieved for lower quality material if the base thickness is further reduced and optical confinement is provided. Efficient light trapping has recently been demonstrated for back-collecting OECO solar cells passivated on both sides by PECVD silicon nitride [48]. In the course of the rear-side grooving process of the OECO cell, the proper effective base thickness can also be adjusted. Even base thicknesses as low as 20 µm could be obtained without wafer breakage [18]. Excellent mechanical stability and flexibility is provided by the supporting ridges [49].

Thus, a starting wafer thickness down to values approaching 100 µm should be feasible in mass production with the effective base width of about 50 µm adjusted by grooving. It should again be noted that, in the case of the back-collecting OECO solar cells parallel to the reduction of the manufacturing costs by using thinner wafers, higher front-side efficiencies are realized.

For rear illumination the cells basically behave like conventional front-collecting devices. As already mentioned, efficiencies up to 20% are expected in the future despite the fact that both grid finger systems and busbars are placed on the rear side.

Shadowing by the grid fingers is almost negligible due to their vertical position on the flanks of the ridges.

6.9 Silicon Substrate Options

The high minority carrier lifetime of the silicon substrate is a prerequisite for high-efficiency solar cells. Due to the special rear-side design of the OECO cells, the requirements on the material quality are not as stringent in comparison to other back-contact solar cells, where a fraction of the minority carriers must diffuse laterally in addition to traversing the width of the cell [11].

Float-zone (FZ) silicon as the highest quality but most expensive single crystalline material has been, up to now, used mainly for laboratory devices and for niche applications to reach record cell efficiencies. However, only recently a novel photovoltaic-grade FZ–Si material was introduced for which, due to its high and stable carrier lifetime, high solar cell efficiencies can be demonstrated [50, 51]. The high production costs of FZ–Si caused by the fact that the starting material has to be in the form of an almost perfectly shaped polycrystalline rod could be drastically reduced and ingot prices comparable to those of Czochralski-grown (Cz) silicon should be within reach.

Currently, Cz-silicon is preferred for low-cost manufacturable single-crystalline silicon solar cells. Boron-doped Cz–Si has a market share up to 40% of the present world solar cell production. However, solar cells manufactured on B–Cz–Si have a serious problem: their initial efficiency degrades under illumination. For high-efficiency cells, a degradation of up to 10% relative has been reported. This is presently the main obstacle to making B–Cz–Si a perfect high-efficiency solar cell material. One approach to significantly reduce the effect of lifetime degradation on cell performance is to increase the ratio diffusion length/cell thickness by using thinner substrates; this is particularly beneficial for the back-collecting OECO solar cell [52].

The degradation effect is due to the activation of a specific metastable defect, which is correlated with the boron and oxygen concentration in the material [53]. Based on this knowledge several methods for completely eliminating the lifetime degradation in Cz–Si solar cells were proposed, whereby the two most promising approaches are (i) replacement of B with another dopant element such as Ga or P, and (ii) reduction of the oxygen concentration in the Cz material. The latter can be achieved by damping the melt flows with magnetic fields resulting in the so-called magnetic-field-assisted Cz (MCz) silicon with a very low oxygen concentration.

Surprisingly, Cz–Si doped with Ga has a stable lifetime on a much higher level than with B-doping and is thus absolutely comparable to the outstanding B-doped FZ–Si. The results of a comprehensive material study are shown in Fig. 6.14, where the efficiencies of front-collecting OECO-type solar cells on Ga-doped Cz–Si are plotted for the resistivity range of 0.08 Ω cm to 1.34 Ω cm together with some values for B-doped FZ–Si and Cz–Si [54]. Peak efficiencies of more than 21% could be obtained on 0.4 Ω cm Ga-doped Cz–Si as well as on 0.4 Ω cm B-doped FZ–Si,

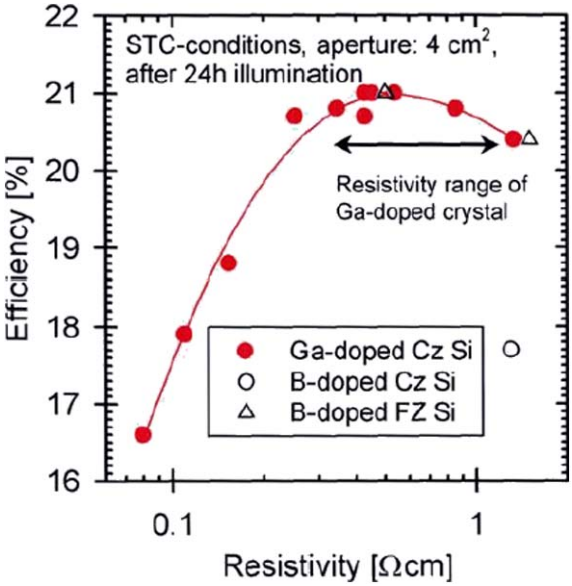

Fig. 6.14. Measured efficiencies of front-collecting OECO-type solar cells on Ga-doped Cz–Si and B-doped FZ–Si as a function of base resistivity. For both materials the same high performance is obtained. The inherent resistivity range of a Ga-doped Cz–Si crystal (see arrow) is tolerable for industrial production of high-efficiency solar cells

whereas a lower efficiency results for cells on B-doped solar grade Cz–Si mainly due to light-induced degradation.

As a consequence of the two orders of magnitude lower segregation coefficient of gallium in silicon compared to boron in silicon, the Ga-doped Cz–Si crystals exhibit a considerably higher variation in resistivity along their growth axis compared to B-doped crystals. Therefore the usability for high-efficiency solar cells of a complete 6″ Ga-doped Cz–Si crystal in the broad resistivity range between 0.25 and 1.34 Ω cm was investigated and the results are shown in Fig. 6.14. As can be seen, the efficiencies were found to reach more than 97% of the peak value, demonstrating that the inherent resistivity variations in Ga-doped Cz–Si crystals are well within the tolerable range for mass production of high-efficiency solar cells.

Other high-efficiency solar cell processes were also applied to the alternative Cz-materials at different institutes, and stable efficiencies well above 20% could be obtained on Ga-doped Cz–Si, B-doped MCz–Si and P-doped n-type Cz–Si [54–56].

In conclusion, there are several silicon material options for economic mass production of high-efficiency OECO solar cells, including B-doped Cz–Si, cast multicrystalline Si, Ga-doped Cz–Si and B-doped FZ–Si. Some alterations to the processing sequence are required for the use of n-type silicon.

As already mentioned, emphasis should be on the use of thin wafers. In addition to the high-efficiencies achievable for both sides of the bifacial OECO solar cell

even with B-doped Cz–Si this is another key issue to reduce silicon consumption and thus to drastically lower the cost/kWh solar electricity.

As to the availability of silicon, unlike the case of other semiconductors, there will basically be no shortage [57, 58]. Currently, silicon feedstock production and its supply to the PV industry is not sufficient to satisfy market demand. However, there is considerable growth in the world-wide silicon supply for solar application. This is partly due to capacity expansions by existing silicon producers and to new production facilities coming online [57].

6.10 Application of Bifacial Solar Cells

6.10.1 General Applications of Bifacial Flat Panels

Since bifacial solar cell designs offer a simple way of effectively improving cell efficiency, great efforts have been made in the past regarding both development as well as application of these devices for space and terrestrial systems, including concentrators [9, 14, 25, 28, 36, 59–65].

Up to now, however, large-scale installations could not be realized since bifacial solar cells with sufficiently high rear-side efficiencies were not commercially available. To underline the potential of bifacial cells in general, and that of the OECO cell in particular, we present the following examples of the many promising applications that provide power gains per unit area of the cells in the range between 30% and 70% compared to monofacial systems. Due to the high front efficiency exceeding 21% and the expected high rear-to-front-efficiency ratio close to 0.9 with the OECO cell, an extremely high power output can be achieved [9]. It should be mentioned that the operating temperature of bifacial cells and modules is lower, resulting in a higher open-circuit voltage [64, 66]. This is attributed to the "open" rear side of the bifacial cell, through which the long-wavelength radiation not used in the silicon leaves the cell without being absorbed by the continuous rear metallization, which is typical of conventional cells. Furthermore, in case of a reduced packing density of the bifacial cells, the heat can be better dissipated within the module [64].

Low-cost installations directing light onto the rear surface of the cells are required.

Figure 6.15 (left) shows the arrangement of relatively narrow bifacial modules in a certain distance parallel to a diffusely reflecting wall, such as a white-painted building façade [64]. Both the light impinging on the front side as well as the light falling between the modules on the white wall and scattered onto the rear side is used. There is ample room for different module configurations, e.g. to represent logos etc. [64]. Figure 6.15 (right) depicts the installation of a bifacial PV module inclined to a reflecting background. Another example particularly suitable for flat roofs of private and industrial buildings and for large standalone PV power plants is to simply mount bifacial PV modules in front of a high albedo background, such as sand, gravel, concrete, snow etc. (Fig. 6.16 (left)). In this context an interesting behavior of bifacial modules in winter and particularly in high altitudes should be

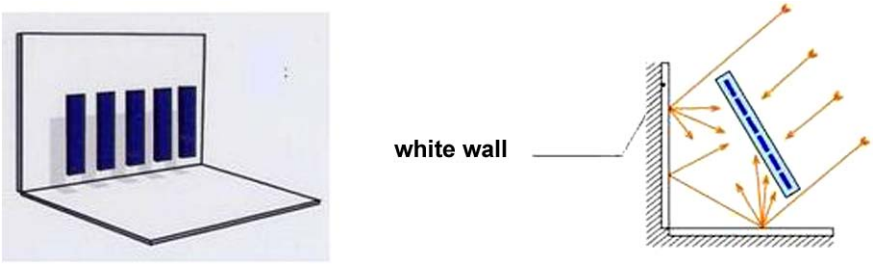

Fig. 6.15. Bifacial PV modules arranged in front of a diffusely reflecting background such as a white-painted building façade (*left*). Various arrays are possible, e.g., to represent logos etc. Installation of bifacial PV modules inclined to a white background (*right*)

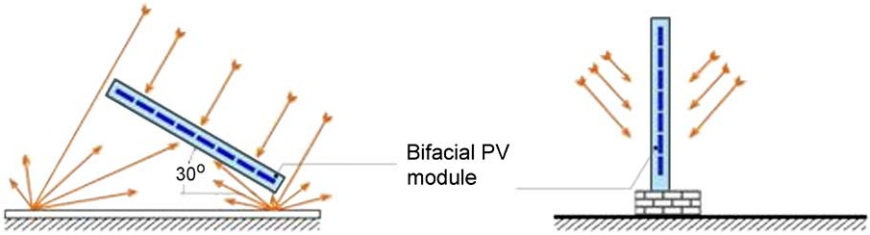

Fig. 6.16. Bifacial module on a floor consisting, e.g., of sand, gravel, concrete, snow etc. as light-scattering background (*left*). This configuration is particularly suitable for flat roofs and large standalone PV power plants. Vertical installation of bifacial modules with north–south orientation, e.g., on fences, railings or walls (*right*)

mentioned. When the front side is covered with snow and ice, electric power is still obtained by light reflected onto the rear side. As a consequence, cell and module temperature is raised thus helping to melt the front snow cover.

Further configurations with enhanced albedo for bifacial flat panels are discussed elsewhere [60, 61].

Vertical installation of bifacial modules, as shown in Fig. 6.16, is a suitable way of reducing the foundation area and of combining the panels with structural materials like fences, railings or walls. If oriented in a north–south direction, one side will be illuminated in the morning and the other side in the afternoon with a minimum at noon. As much energy output as a conventional optimally oriented PV module is delivered [63, 67]. There are several small demonstration projects including sound barriers on north–south motorways and vertical fence installations [63, 68].

6.10.2 Integration of Bifacial PV Modules in Low-Cost Concentrating Systems

The implementation of bifacial PV modules in highly reflective mirror systems is effective [60]. Figure 6.17 shows a representation of concentrators with small con-

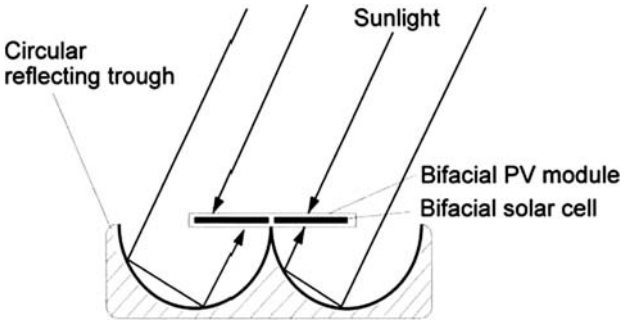

Fig. 6.17. Schematic cross-section of a static concentrator with bifacial solar cells

centration factors. The depicted Compound-Parabolic-Concentrator uses both direct and diffuse light, and all light rays either directly hit the front surface of the module or the rear side after one or more reflections [69]. Since the system tolerates a wide range of incoming light angles, tracking is not required. Several other configurations have been studied, including deviations from semicircular toward less-deep mirror structures [60, 61, 67].

6.10.3 Multifunctional Bifacial PV Elements

Bifacial PV Sun-Shading and Daylighting Element

A novel multifunctional sun-shading element was recently introduced which is based on sparsely packed, bifacially sensitive solar cells in combination with a white semi-transparent back sheet [64]. It is one part of the strategy to substitute expensive solar cells with cheap light-scattering material in order to raise the power output per cell and thus to increase the effective cell efficiency. On the other hand, apart from protecting against sun and rain, not only is sunlight collected by the front and rear surface of the cell efficiently converted into electricity, but also diffuse glare-free daylight is provided, thus preventing darkening of the room behind.

The principle is outlined in Fig. 6.18 (left). The sun-shading element consists of a set of parallel strings made up of bifacial solar cells, whereby the individual strings are arranged about one cell-width apart from each other. At about the same distance behind the module the white semitransparent reflector sheet is placed so that both the light falling directly on the front side as well as the light scattered by the sheet onto the rear side of the cell is used. There is ample room for other attractive cell arrangements within the module.

Figure 6.18 (right) shows an example of the shading element with each string consisting of 10 bifacial solar cells $10 \times 10\,\mathrm{cm}^2$ in size [14]. For comparison, two different reflector sheets made of PMMA were applied whereas the higher transmittance of the back sheet at the right-hand side can clearly be seen by the mirror image in the window behind. In this way daylighting and solar electricity generation can be varied within wide limits. From inside the room, the faint shadows cast by

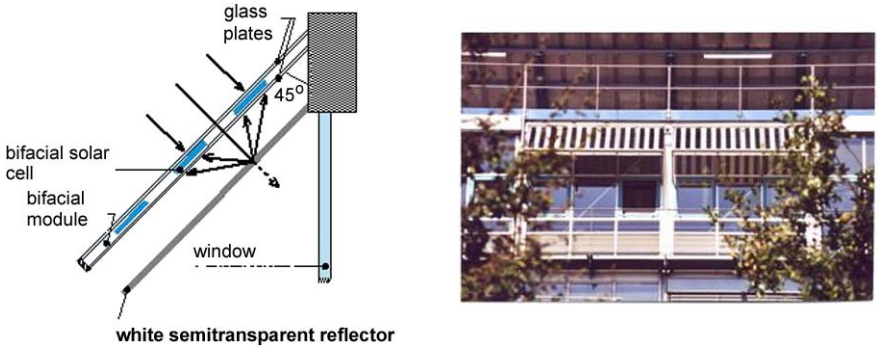

Fig. 6.18. Principle of the multifunctional PV sun-shading element with bifacial solar cells and semitransparent reflector sheet (*left*). Two prototypes of the PV element with bifacially active solar cells and different white back reflector sheets installed at a building façade (*right*). The higher transmittance of the reflector sheet of the right-hand module can clearly be seen by the mirror image in the window behind

the solar cells onto the white plate can be seen as they move according to the sun's position [64].

It's interesting to note that the power gain of the south-oriented bifacial sun shading element relative to monofacial operation was evaluated for symmetrical bifacial cells to about 50% at noon and increased up to 70% in the morning and afternoon hours, since at flat incidence relatively more light is scattered onto the rear side of the cells. Further details about the performance of these elements are presented elsewhere [64]. A broad spectrum of applications is possible, such as for shop windows, private homes, offices and industrial buildings.

Bifacial PV Facade Elements

Based on the same principle as the sun-shading module above, a bifacial PV element suitable for glass facades, entrance halls etc., is shown in Fig. 6.19.

For reflection of the light onto the rear of the cells, a white semitransparent (perforated) curtain is arranged behind the module which – besides daylighting – allows a clear view from inside through the façade. An important feature of the vertical arrangement of bifacial modules has to be mentioned. Generally for conventional PV modules placed on vertical facades, the output power is reduced by about 30% compared to the ideal inclination. This is due to the oblique incidence of sunlight. However, as shown in Fig. 6.19, this situation is favorable for the rear side of bifacial modules because, due to the shallow angle of the incoming light, a larger portion is scattered onto the back surface of the cell. Thus, for vertically oriented bifacial modules the decrease of power output by the front side is at least partly compensated by the increase in power output by the rear side.

In the case of a similar multifunctional bifacial PV façade element introduced recently, the curtain is replaced by diffusely reflecting venetian blinds arranged at

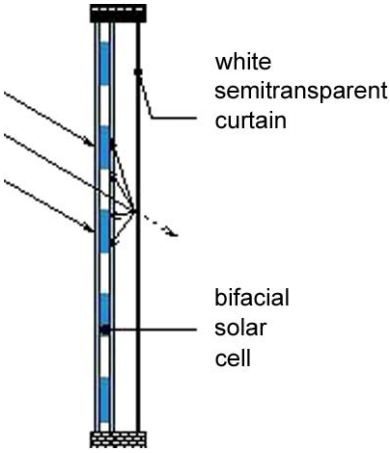

Fig. 6.19. Principle of a bifacial PV façade element. A white semitransparent curtain is arranged behind the module allowing a clear view from inside through the glass façade

a certain distance behind the module [70]. During times of high sun radiation, the blinds of a building are usually closed to avoid heating or dazzling. Here, the PV element will produce the maximum electric power on both the front and the rear side. At low radiation – like on a cloudy or rainy day – the blinds will be open and the solar cells receive light only on their front side. However, daylight will fall into the interior of the building. Varying the angle of the roller blinds, the electrical power output of the cells together with room illumination by daylight can be controlled [70].

Peak power values may particularly be realized with a similar arrangement, as shown in Fig. 6.18 but with cell size and lateral spacing reduced together with a reflector sheet attached closer to the rear side of the module. The considerably cheaper round or semicircular monocrystalline silicon wafers can be advantageously applied.

This may finally lead to a bifacial module with integrated diffuse reflector either opaque or semitransparent, which can be installed like any other conventional panel. Under optimized conditions it may provide up to 70% more power compared to a module made up of the same area of corresponding monofacial cells. With OECO cells, effective cell efficiencies approaching 35% should be within reach [9].

6.11 Conclusions

To address limits in efficiency and reduce the cost of current commercial solar cells, new cost-effective processing sequences are required. The OECO solar cells introduced in this paper are distinguished by the highest efficiencies of rear-contacted bifacially sensitive solar cells fabricated without photolithography.

Absence of shading losses on the front-side, uniform visual appearance and cost reduction in module assembly are the general advantages of rear-contact solar cells. In the future, however, further considerable cost advantages are expected for OECO cells as rear-contact devices. Particularly if lower-quality silicon can be used, reduction of the wafer thickness will result in higher front-side efficiencies. Thus, by saving expensive silicon material – which is crucial for the future of photovoltaics – cell performance is also improved. In this context, simultaneous busbar formation and cell interconnection using conductive adhesives has to be mentioned as a reliable cost-effective technique for thin OECO cells.

Together with the strength of silicon in terms of resource availability, nontoxicity and stability, the high-efficiency bifacial OECO solar cell with its economic and ecologically sound manufacturing process may significantly contribute to sustainable progress in photovoltaics. This refers to both one-sided and even more to double-sided applications, culminating in effective cell efficiencies up to 35%.

Acknowledgements. The OECO solar cell was developed at the Lower Saxonian Institute for Solar Energy Research (ISFH) at Hameln, Germany, when the author was Director of this institution and Professor of the Physics Faculty of the Hannover University. The author would like to thank J.W. Mueller, A. Merkle and all the members of the PV department at the ISFH for their valuable contributions to this work.

References

1. S.R. Wenham, M.A. Green, M.E. Watt, *Applied Photovoltaics*, Centre for Photovoltaic Devices and Systems, University of New South Wales, Sydney, Australia
2. J. Zhao, A. Wang, M.A. Green, Prog. Photovolt.: Res. Appl. **7**, 411 (1999)
3. M.A. Green, *Silicon Solar Cells: Advanced Principles and Practice* (Bridge Printery, Sydney, 1995)
4. M.A. Green, Prog. Photovolt.: Res. Appl. **8**, 127 (2000)
5. J. Bernreuter, *High, Higher, the Highest*, Photon International, May 2003 and *Hoch die Leistung*, Photon Mai 2003, Solarverlag Aachen
6. R. Hezel, Patent pending
7. R. Hezel, in *Proc. 29th IEEE Photov. Spec. Conf.*, New Orleans, 2002, p. 114
8. J.W. Müller, Dissertation, Univ. Hannover, Shaker Verlag Aachen, 2005
9. J.W. Müller, A. Merkle, R. Hezel, in *Proc. 20th Europ. Photov. Solar Energy Conf.*, Barcelona, 2005, p. 1020
10. M.A. Green, D. Jordan, Prog. Photovolt.: Res. Appl. **6**, 169 (1998)
11. K.R. McIntosh, M.J. Cudzinovic, D.D. Smith, W.P. Mulligan, R.M. Swanson, in *Proc. 3rd World Conf. on Photov. Energy Conversion*, Osaka, 2003, p. 971
12. R. Hezel, Prog. Photovolt.: Res. Appl. **5**, 109 (1997)
13. J.W. Müller, A. Merkle, R. Hezel, in *Proc. PV in Europe, Conf. and Exhibition*, Rome, p. 248, WIP, Munich, 2002
14. K. Jaeger-Hezel, W. Schmidt, W. Heit, K.D. Rasch, in *Proc. 13th Europ. Photov. Solar Energy Conf.*, Nice, 1995, p. 1515
15. A. Metz, R. Hezel, in *Proc. 17th Europ. Photov. Solar Energy Conf.*, Munich, 2001, p. 1359

16. H. Nakaya, M. Nishida, Y. Takeda, S. Moriuchi, T. Tonegawa, T. Machida, T. Nunoi, in *Proc. 17th Intern. Photov. Solar Energy Conf.*, Nagoya, 1993, p. 91
17. G. Willeke, H. Nussbaumer, H. Bender, E. Bucher, Sol. Energy Mater. Sol. Cells **26**, 345 (1992)
18. R. Hezel, R. Ziegler, in *Proc. 21th IEEE Photov. Spec. Conf.*, Louisville, 1993, p. 260
19. R. Hezel, Sol. Energy Mater. Sol. Cells **74**, 25 (2002)
20. A. Metz, R. Hezel, in *Proc. 28th IEEE Photov. Spec. Conf.*, Anchorage, 2000, p. 175
21. P. Engelhart, N.-P. Harder, T. Neubert, H. Plagwitz, B. Fischer, R. Meyer, R. Brendel, in *Proc. 21th Europ. Photov. Solar Energy Conf.*, Dresden, 2006, p. 773
22. R. Hezel, Adv. Sol. State Phys. **44**, 39 (2004); B. Kramer (Ed.), Springer, Berlin
23. W. Shockley, W.T. Read, Phys. Rev. **87**, 835 (1952)
24. A.G. Aberle, *Crystalline Silicon Solar Cells*, Centre for Photovoltaic Engineering UNSW, Sydney, NSW 2052, Australia (1999)
25. R. Hezel, K. Jaeger, J. Electrochem. Soc. **136**(2), 518 (1989)
26. J. Mandelkorn, J.H. Lamneck, J. Appl. Phys. **44**, 4785 (1973)
27. R. Hezel, R. Schoerner, J. Appl. Phys. **52**, 3076 (1981)
28. K. Jaeger, R. Hezel, in *Proc. 7th Europ. Photov. Solar Energy Conf.*, Sevilla, 1986, p. 806
29. A.G. Aberle, R. Hezel, Prog. Photovolt.: Res. Appl. **5**, 29 (1997)
30. T. Lauinger, J. Moschner, A.G. Aberle, R. Hezel, J. Vac. Sci. Technol. A **16**, 530 (1998)
31. A. Cuevas, M.J. Kerr, J. Schmidt, in *Proc. 3rd World Conf. on Photov. Energy Conversion*, Osaka, 2003, p. 913
32. A.K. Sinha, H.J. Levinstein, T.E. Smith, G. Quintana, S.E. Haszko, J. Electrochem. Soc. **125**, 601 (1978)
33. R. Hezel, K. Blumenstock, R. Schörner, J. Electrochem. Soc. **131**(7), 1679 (1984)
34. J. Robertson, Philos. May. B **63**, 47 (1991)
35. C. Peters, R. Meyer, R. Hezel, in *Proc. PV in Europe, Conf. and Exhibition*, Rome (WIP, Munich, 2002), p. 127
36. R. Hezel, W. Hoffmann, K. Jaeger, in *Proc. 10th Europ. Photov. Solar Energy Conf.*, Lisbon, 1991, p. 511
37. M. Alonso, R. Pottbrock, R. Voermans, J.J. Villard, B. Yordi, in *Proc. 12th Europ. Photov. Solar Energy Conf.*, Amsterdam, 1994, p. 1163
38. M. Rammensee, Doctoral thesis, University of Erlangen-Nürnberg, 1995
39. R. Hezel, R. Auer, M. Rammensee, *Progress in Plasma Processing of Materials* (Begell House Inc., New York, 1999), p. 891
40. J.D. Moschner, J. Henze, J. Schmidt, R. Hezel, Prog. Photovolt.: Res. Appl. **12**, 21 (2004)
41. K. Roth, F. Chen, M. Fritzsche, M. Kirschmann, J. Müller, H. Schlemm, in *Proc. 21st Europ. Photov. Solar Energy Conf.*, Dresden, 2006, p. 1137
42. J. Schmidt, J.D. Moschner, J. Henze, S. Dauwe, R. Hezel, in *Proc. 19th Europ. Photov. Solar Energy Conf.*, Paris, 2004, p. 391
43. T. Lauinger, J. Schmidt, A.G. Aberle, R. Hezel, Appl. Phys. Lett. **68**, 1232 (1996)
44. J.W. Müller, A. Merkle, R. Hezel, in *Proc. 19th Europ. Photov. Solar Energy Conf.*, Paris, 2004, p. 990
45. S. Dauwe, L. Mittelstädt, A. Metz, R. Hezel, Prog. Photovolt.: Res. Appl. **10**(4), 35 (2002)
46. J. Liu, Conductive adhesives for electronic packaging, Electrochemical Publications Ltd, Isle of Man (1999), ISBN 0-901150-37
47. J.H. Bultmann, M.W. Brieks, A.R. Burges, J. Hoornstra, A.C. Tip, A.W. Weber, Sol. Energy Mater. Sol. Cells **65**, 339 (2001)
48. J.W. Müller, A. Merkle, R. Hezel, in *Proc. 3rd World Conf. on Photov. Energy Conversion*, Osaka, 2003, p. 1399

49. L.W. Mittelstädt, A. Metz, R. Hezel, in *Proc. 16th Europ. Photov. Solar Energy Conf.*, Glasgow, 2000, p. 1340
50. J. Vedde, T. Clausen, L. Jensen, in *Proc. 3rd World Conf. on Photov. Energy Conversion*, Osaka, 2003
51. C. del Canizo et al., in *Proc. 19th Europ. Photov. Solar Energy Conf.*, Paris, 2004, p. 536
52. K.A. Münzer et al., in *Proc. 2nd World Conf. on Photov. Energy Conversion*, Vienna, 1998, p. 1214
53. K. Bothe, R. Hezel, J. Schmidt, Appl. Phys. Lett. **83**(6), 1125 (2003)
54. A. Metz, T. Abe, R. Hezel, in *Proc. 16th Europ. Photov. Solar Energy Conf.*, Glasgow, 2000, p. 1189
55. S.W. Glunz, S. Rein, J.Y. Lee, W. Warta, J. Appl. Phys. **90**, 2397 (2001)
56. J. Schmidt, Solid State Phenom. **95**, 187 (2004)
57. H.A. Aulich, F.W. Schulze, in *Proc. 21th Europ. Photov. Solar Energy Conf.*, Dresden, 2006, p. 549
58. J.H. Werner, Adv. Solid State Phys. **44**, 51 (2004); B. Kramer (Ed.), Springer, Berlin
59. A. Cuevas, A. Luque, J. Eguren, J. Del Alamo, Sol. Energy **19**, 419 (1982)
60. A. Luque, *Solar Cells and Optics for Photovoltaic Concentration* (Adam Hilger, Bristol, 1989)
61. A. Cuevas, in *Proc. 33rd Annual Conf. of the Australian and New Zealand Solar Energy Society*, Harbart, 1995, p. 983
62. A. Hübner, A.G. Aberle, R. Hezel, Appl. Phys. Lett. **70**(8), 1008 (1997)
63. T. Nordmann, A. Fröhlich, M. Dürr, A. Goetzberger, in *Proc. 16th Europ. Photov. Solar Energy Conf.*, Glasgow, 2000, p. 1777
64. R. Hezel, Prog. Photovolt.: Res. Appl. **11**, 549 (2003)
65. J. Coello, C. del Canizo, A. Luque, in *Proc. 21st Europ. Photov. Solar Energy Conf.*, Dresden, 2006, p. 1358
66. C.Z. Zhou, P.Y. Verlinden, R.A. Crane, R.M. Swanson, R.A. Sinton, in *Proc. 26th IEEE Photov. Spec. Conf.*, Anaheim, Ca, 1997, p. 287
67. A. Goetzberger, G. Walze, in *Techn. Digest of the International PVSEC-14*, Bangkok, 2004, p. 719
68. T. Joge et al., in *Proc. 29th IEEE Photov. Spec. Conf.*, New Orleans, 2002, p. 1549
69. B. Mayregger, R. Auer, N. Niemann, A.G. Aberle, R. Hezel, in *Proc. 13th Europ. Photov. Solar Energy Conf.*, Nice, 1995, p. 2377
70. R. Hezel, R. Auer, in *Proc. EUROSUN 96*, ed. by A. Goetzberger and J. Luther. International Solar Energy Society: Freiburg, 1996, p. 713

7 Commercial High-Efficiency Silicon Solar Cells

R. Hezel

7.1 Introduction

The present rapidly expanding photovoltaic market is dominated by mono- and multicrystalline silicon solar cells based upon the standard, decades-old screen-printing approach [1, 2]. Despite significant progress in both performance and cost reduction, there are limitations in efficiency that arise from using the screen-printing process to apply the front contact [1, 3].

Currently, there are three improved processing sequences for high-efficiency devices that are commercially available [1, 4]. These include the Point-Contact solar cell of Sun Power, the HIT cell of Sanyo Electric and the laser-grooved buried contact (LGBC) cell of BP Solar. Using completely different approaches in design and process technology, and deviating significantly from conventional silicon solar cells, these nonconventional cells have the potential to reach cell efficiencies beyond 20%. Details about the fabrication process are not available from the manufacturers. Basic features and properties of the high-efficiency structures are presented in the following.

7.2 The Point-Contact Solar Cell

The high-efficiency cell of Sun Power Corporation (founded 1988) is a simplified version of the highly sophisticated point-contact solar cell designed for concentrator applications. These cells were developed by Prof. Swanson together with NASA in 1973 and have been fabricated with conventional IC processing technology. They were successfully applied for niche applications, such as solar cars and solar airplanes [5].

Originally several photolithography steps were applied to define the rear features (i.e., diffusions, contact openings and fingers), so that one-sun efficiencies approaching 23% could be achieved. In order to reduce the fabrication costs and to make processing suitable for mass production, a novel screen-printing technology for masking purposes was developed [4, 6]. It is evident that these low-cost methods cannot define the rear features as tightly as photolithography, and therefore some changes in the design had to be made [6].

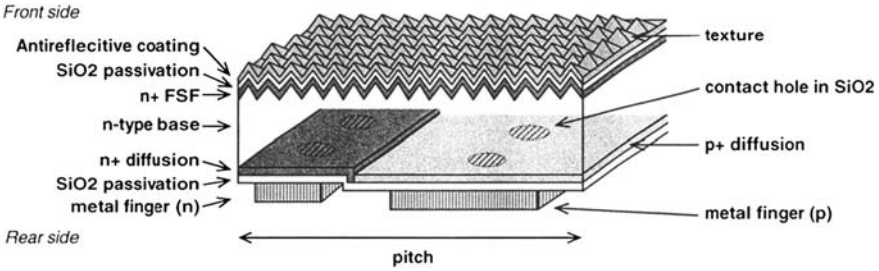

Fig. 7.1. Schematic diagram of the point-contact solar cell (Sun Power) [6]

The device is schematically depicted in Fig. 7.1. Both contact schemes are placed on the rear side. This is advantageous due to (i) improvement of efficiency since shading losses by the front grid are avoided; (ii) reduction of module fabrication costs as well as higher cell-packing density within the module; and (iii) better visual appearance of the modules due to the absence of the front metal grid.

High minority carrier lifetime and thus diffusion length is a prerequisite for any high-efficiency cell. However, back contacted solar cells are particularly sensitive to the minority carrier diffusion length, since most of the carriers are generated near the front surface and have to diffuse through the entire cell to the collecting junctions at the rear surface. Recombination of the charge carriers in the bulk should therefore be as low as possible.

Due to the relatively coarse contact geometry in the case of Sun Power's low-cost cell, some minority carriers must travel a significant lateral distance in addition to traversing the thickness of the cell to the collecting junction. As a consequence, extraordinarily high-quality silicon starting material with the lifetime >1 ms is required [6]. Low-cost photovoltaic float-zone silicon – available from Topsil – can meet these stringent lifetime requirements [7].

Furthermore, excellent front-surface passivation is provided by thermal SiO_2 together with a lightly n-doped front floating junction.

Interdigitated n^+ base and p^+ emitter diffusions and grid lines are used to collect the photogenerated carriers on the rear side. As an important high-efficiency feature, small-area contact holes are opened in the rear passivation SiO_2 film. Thus, localized point contacts are formed to reduce the metal-semiconductor contact area. This results in a low rear-surface recombination loss.

Since the back-surface has quite high reflectance due to the SiO_2 passivation layer, efficient light trapping occurs in the cell [1].

Recently the "surface polarization" effect was discovered by Sun Power in their back-contacted high-efficiency solar cells [8]. If the module is operated at a high positive voltage with respect to the ground, a negative charge is left on the antireflection coating due to the leakage current flowing from the cell through glass to the frame and ground. This negative surface charge attracts light-generated positively charged minority carriers (holes) to the surface of the n-type silicon substrate where they recombine with electrons and are thus lost.

When a module is operated at a negative voltage with respect to the ground, the surface polarization reverses and the performance of the module is not affected. Thus the surface polarization effect is completely reversible.

According to Sun Power, the polarization effect can be easily avoided by designing systems with proper grounding so that the modules only see negative voltage. Furthermore, work is under way to solve the problem by changing the cell design, so that grounding is not required.

With a cell efficiency of 22.4% Sun Power holds the record of all commercially produced silicon solar cells [9]. Modules are available with efficiencies ranging from 16.1% up to 19.3% [10].

7.3 The HIT Solar Cell

Based on experience with hydrogenated amorphous silicon films and solar cells, Sanyo Electric in 1990 launched basic research into a novel structure consisting of both monocrystalline and amorphous silicon. In 1997 a solar module with a conversion efficiency of 17.3% was commercialized. Since then considerable further progress has been made both in the laboratory and in mass production, culminating in a 21.8% efficient laboratory cell with a practical size of 100.4 cm^2 [11].

Of prime importance are (i) a high-quality amorphous-crystalline heterojunction due to the excellent surface passivation of crystalline silicon by intrinsic hydrogenated amorphous silicon (a-Si:H) layers and (ii) the use of n-type Cz–Si with its stable high minority carrier lifetime [12].

In Fig. 7.2 a schematic diagram of the HIT (Heterojunction with Intrinsic Thin Layer) solar cell is shown [13]. The cell is composed of a textured n-type Cz–Si wafer sandwiched between p/i a-Si:H films on the illuminated side and i/n a-Si:H

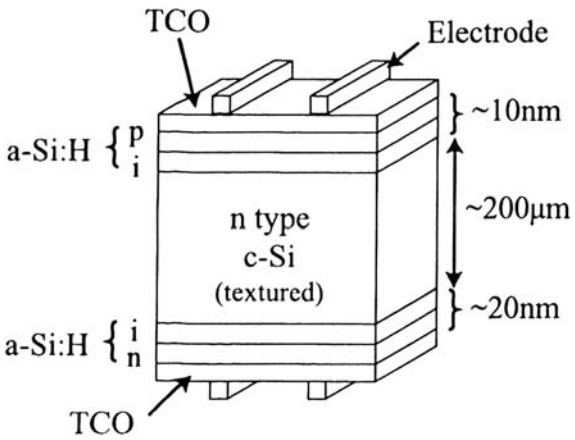

Fig. 7.2. Schematic diagram of the HIT Solar Cell (Sanyo Electric) [12]

films as a back surface field (BSF) structure on the rear side. Transparent conductive oxide (TCO) layers are deposited on both doped layers followed by a silver grid for current collection. TCO on the front side also serves as an antireflection (AR) layer. Spacing of the front grid fingers is narrower compared to conventional p/n diffused solar cells due to the relatively high sheet resistance of the TCO layer. Low-temperature processes (<200 °C) and the symmetrical structure of the HIT cells suppress both thermal and mechanical stress during production, which is advantageous for thin wafers. Furthermore, bifacial operation is possible [14].

Limitations in the short-circuit current of the cell may be given by the inherent absorption in the TCO layer and in the a-Si emitter layer. Further improvements are possible by developing high-quality widegap alloys for the reduction of the a-Si optical absorption, TCO with high carrier mobility, by optimization of the back surface field and by using finer grid-electrodes.

Very high open-circuit voltages can be obtained by plasma deposition of the intrinsic a-Si layer on a properly cleaned crystalline Si surface. Plasma and/or thermal damage to the crystalline Si surface during a-Si, TCO and Ag electrode fabrication has to be as low as possible.

For a high fill factor – in addition to a low resistance grid electrode material – a highly conductive window p-layer and a low sheet resistance of TCO is required.

A reduced temperature coefficient of −0.33%/ °C is a further advantage of the HIT cell [15]. The output power of most conventional crystalline modules drops by 0.4% to 0.5% per °C temperature increase.

At present HIT solar cell modules are commercially available with efficiencies ranging from 16.5% to 17.4%. The highest cell conversion efficiency in a mass produced HIT module is 19.5% [10].

7.4 The Buried-Contact Solar Cell

The laser-grooved buried-contact (LGBC) solar cell was introduced as a high-efficiency cell design in 1984 by M.A. Green and S. Wenham, University of New South Wales in Sydney, Australia. Manufactured by BP Solar in Spain since 1992 it was the first of the nonconventional cells to be commercialized [1, 3, 16].

The most striking feature of the buried contact cell are the fine contact lines which do not run on top of the cell surface, as is the case with conventional cells. Instead, a novel metallization scheme is applied, whereby deep and narrow grooves define the location and cross-sectional shape of the front metal conductors (Fig. 7.3). Grooves about 20 μm wide and up to 60 μm in depth are routinely obtained by using a laser scriber. Thus much higher values of the aspect ratio are obtained compared to conventional metallization. The advantages are low grid shadowing and low resistance losses in the finger metallization, boosting both short-circuit current and fill factor of the cells.

A two-step emitter is formed by heavily doping the contact region with phosphorous (n^{++} local emitter) whereas the rest of the surface is lightly diffused to obtain a shallow n^+p junction. This lowly doped n^+-emitter is effectively passivated with

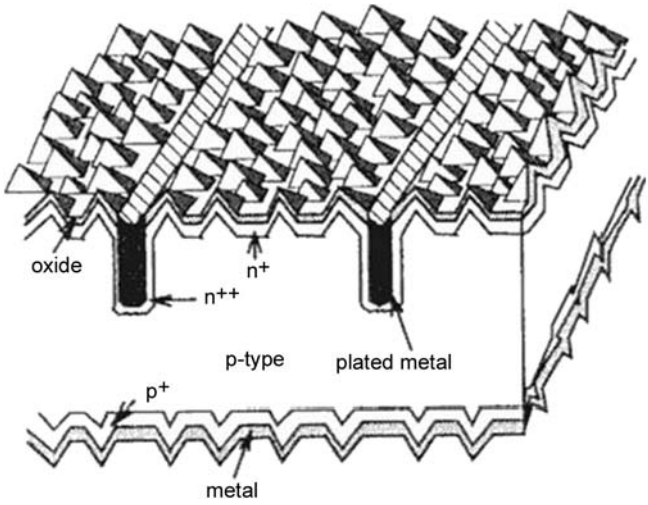

Fig. 7.3. Schematic diagram of the laser-grooved buried-contact (LGBC) solar cell (BP Solar) [17]

silicon nitride, which simultaneously serves as an excellent antireflection coating. The two-step emitter structure, together with a random pyramid textured surface, results in an optimum spectral response and minimum contact resistance of the cell. Furthermore, only a small contribution to the cell saturation current density is given, which determines the open-circuit voltage of the cell.

A p^+-region acting as back-surface field is incorporated by aluminum alloying in order to reduce recombination of the electron–hole pairs at the rear side.

The contacts on both sides of the cell are obtained by self-aligning electroless plating of nickel, followed by copper. Additional electrolessly plated layers such as silver can be applied. The insulating silicon nitride restricts the plating to the grooved areas and to the rear of the wafer.

The technology of the buried-contact cell has been described in detail elsewhere [16]. At present LGBC modules ("Saturn") produced by BP Solar are commercially available with efficiencies ranging from 13.9% to 15.5% [10].

Recently, cell efficiencies of 18.3% were obtained in a pilot line on 147.5 cm^2 boron-doped Czochralski-silicon wafers [17]. By improving the rear structure, 20.1% efficient large-area laser-grooved buried-contact solar cells were realized in the laboratory on 140 μm thick boron-doped float-zone silicon wafers [18]. The best laboratory result reported for LGBC cells (area 12 cm^2) on FZ-Si wafers was achieved in 1991 with an efficiency of 21.3% [19].

References

1. M.A. Green, *Silicon Solar Cells: Advanced Principles and Practice* (Bridge Printery, Sydney, 1995)

2. C. Podewils, Photon, Das < Solarstrom Magazin 3/2007, Solar Verlag Aachen
3. M.A. Green, Prog. Photovolt.: Res. Appl. **8**, 127 (2000)
4. J. Bernreuter, Photon International 5/2003 and Photon 5/2003, Solar Verlag Aachen
5. P.J. Verlinden et al., Prog. Photovolt.: Res. Appl. **2**, 143 (1994)
6. W.P. Mulligan, D.H. Rose, M.J. Cudzinovic, D.M. De Ceuster, K.R. McIntosh, D. Smith, R.M. Swanson, in *Proc. 19th Europ. Photov. Solar Energy Conf.*, Paris, 2004, p. 387
7. J. Vedde, T. Clausen, L. Jensen, in *Proc. 3rd World Conf. on Photov. Energy Conversion*, Osaka, 2003
8. Photon 4/2006, Solar Verlag Aachen
9. Denis De Ceuster et al., in *Proc. 22nd Europ. Photov. Solar Energy Conf.*, Milan, 2007, p. 816
10. Photon 6/2007, Solar Verlag Aachen
11. E. Maruyama et al., in *Proc. 4th World Conf. on Photov. Energy Conversion*, Hawaii, 2006, p. 1455
12. J. Schmidt, Solid State Phenom. **95–96**, 187 (2004)
13. M. Tanaka et al., in *Proc. 3rd World Conf. on Photov. Energy Conversion*, Osaka, 2003, p. 955
14. M. Taguchi et al., Prog. Photovolt.: Res. Appl. **8**, 503 (2000)
15. M. Taguchi et al., in *Proc. 31st IEEE Photov. Spec. Conf.*, 2005, p. 866
16. T.M. Bruton et al., in *Proc. 11th Europ. Photov. Solar Energy Conf.*, Amsterdam, 1994, p. 761
17. T. Bruton et al., in *Proc. 3rd World Conf. on Photov. Energy Conversion*, Osaka, 2003, p. 899
18. N. Mason et al., in *Proc. 21st Europ. Photov. Solar Energy Conf.*, Dresden, 2006, p. 521
19. J. Zhao et al., in *Proc. 22nd IEEE Photov. Spec. Conf.*, Las Vegas, 1991, p. 399

8 III–V Solar Cells and Concentrator Arrays

Z.I. Alferov, V.M. Andreev, and V.D. Rumyantsev

8.1 Introduction: Early History of Heterostructures and III–V Solar Cells

Semiconductor heterostructures allow us to solve the problems of controlling the fundamental parameters of the semiconductor devices. These heterostructures provide the ability to change the electronic band structure, band gaps and refractive indices of the material itself during epitaxial growth, as well as to control the effective masses and mobilities of the charge carriers in it. The development of the physics and technology of semiconductor heterostructures has resulted in remarkable changes in our everyday life. Heterostructure electronics is widely used in many areas. It is hardly possible to imagine our life without double heterostructure (DHS) laser-based telecommunication systems, heterostructure solar cells (HSSCs) and light-emitting diodes (LEDs), heterostructure bipolar transistors and low-noise, high-electron mobility transistors for high-frequency applications including, for example, satellite television. Now DHS lasers exist in practically every home in CD players. Heterostructure solar cells are widely used for space and terrestrial applications.

The idea of using heterojunctions in semiconductor electronics was put forward at the beginning of the electronics era. W. Shockley, in his first patent concerned with p–n-junction transistors, proposed a wide-gap emitter to obtain unidirectional injection of charge carriers [1]. A. Gubanov was the first to analyze theoretically current–voltage characteristics of isotype and anisotype heterojunctions [2]. However, the most important theoretical investigations at this early stage of heterostructure research were done by H. Kroemer, who introduced the concept of quasi-electric and quasi-magnetic fields in a graded-band heterojunction and made an assumption that heterojunctions might exhibit extremely high injection efficiencies in comparison to homojunctions [3]. In the same period, various concepts were developed regarding application of heterostructures in semiconductor solar cells. The next important step was taken several years later when the concept of double-heterostructure lasers had been formulated independently by Alferov [4] and Kroemer [5]. In 1966, it was predicted that the density of injected charge carriers could be higher – by several orders of magnitude – than the carrier density in the wide-gap emitter (“superinjection”

effect) [6]. In the same year, the main advantages of the DHS concept were summarized [7] for the use in various devices, especially lasers and high-power rectifiers.

At that time, general skepticism surrounded the possibility of creating an "ideal" heterojunction with a defect-free interface, where theoretically predicted excellent injection properties would be realized. In fact, the pioneering study of the first lattice-matched epitaxial single-crystal Ge–GaAs heterojunctions by Anderson [8] gave no proof of nonequilibrium charge carrier injection in heterostructures. Mostly owing to this general skepticism, only a few groups tried to find an "ideal couple", which seemed to be a quite difficult problem. Many conditions of compatibility between thermal, electrical, and chemical properties, as well as the crystalline and band structures of the contacting materials were to be met.

A lucky combination of properties in gallium arsenide – i.e., small charge carrier effective mass and wide energy gap, effective radiation recombination, sharp optical absorption edge due to the "direct" band structure, high electron mobility at the absolute minimum of the conduction band and its strong reduction at the nearest minimum at the (100) point – ensured this material would be under "active investigation" in different electronic devices, even at that initial stage of research. Since the maximum effect would be achieved by using it in the heterostructures with wide band-gap materials, the most promising systems considered at that time were GaP–GaAs and AlAs–GaAs. To be "compatible," materials of the "couple" must have, as the first and the most important condition, close lattice constants; therefore, heterojunctions in the AlAs–GaAs system were preferable. However, prior to starting the work on preparation and study of these heterojunctions, one had to overcome a certain psychological barrier. By that time, AlAs had long been synthesized, but many properties of this compound remained poorly studied, since AlAs was known to be chemically unstable and to decompose in moist air. The possibility of preparing the stable and applicable heterojunctions in this system seemed to lack promise.

Initially, the attempts to create double-heterostructures were related to a lattice-mismatched GaAsP system. Alferov et al. succeeded in fabricating the first DHS lasers in this system by vapor phase epitaxy. However, due to lattice mismatch, the lasing occurred only at liquid nitrogen temperature, similar to the behavior of the homojunction lasers. At the same time, it was discovered that small crystals of AlGaAs solid alloys of different compositions, which had been prepared by growing from a melt, were stable for at least two years. It immediately became clear that AlGaAs is suitable for preparing durable heterostructures and devices. Studies of the phase diagrams and growth kinetics in this system and the development of a version of the liquid-phase epitaxial growth method resulted soon in the fabrication of the first lattice-matched AlGaAs heterostructures [9, 10].

Then the progress in the semiconductor heterostructure field was very rapid. The following properties and effects had been experimentally proved: unique injection properties of a wide-gap emitter and the effect of superinjection [11]; stimulated emission at recombination [12]; the band-diagram of the AlGaAs–GaAs heterojunction and carefully studied luminescence properties [13]; and the effect of carrier diffusion in a graded-band heterostructure. At the same time, the majority of

the most important devices were created, realizing many of the main advantages of the heterostructure concept: low-threshold, room-temperature lasers [14–17]; high-efficiency LEDs [10, 18]; solar cells [19]; bipolar transistors [20]; and p–n–p–n switching devices [21].

At that early stage in heterostructure physics and technology, it became clear that new lattice-matched structures were needed in order to cover a wider range of the wavelength spectrum. The first important step was in the works [22, 23], in which the various lattice-matched heterojunctions based on quaternary III–V solid solutions were proposed for independent variation of the lattice constant and the band gap. Soon, InGaAsP compositions were recognized as one of the most important materials for many different practical applications: InGaAsP/InP for lasers in the infrared intervals suitable for fiber optics communications [24]; and InGaP/InGaAsP/GaAs lasers in the visible region [25]. In the early 1970s, ideal lattice-matched heterostructures were limited to only the mentioned materials. Later this "world map" of the III–V heterostructures was drastically expanded.

Since the first solar-powered satellites, Vanguard-1 and Sputnik-3, were launched in 1958, solar cells based on Si had become the main sources of electricity on the spacecrafts. The first space arrays were based on single crystal silicon solar cells characterized by efficiency of about 10%. During the 1960s and 1970s, considerable improvements in the Si cell design and technology were introduced, which allowed increases in the efficiency up to 18%. These improvements were due to, e.g., fabrication of "violet" cells with increased short-wavelength photosensitivity, formation of so-called back-surface field, the application of photolithography to ensure optimal front grid pattern, reduction of optical losses by front surface texturing and improved antireflection coating deposition. These advanced Si cells are still used for space missions that do not strictly require III–V solar cells with their higher efficiency and better radiation stability [26, 27].

At the beginning of the 1960s, it was found that GaAs-based solar cells with the Zn-diffused p–n junction ensured better temperature stability and higher radiation resistance. One of the first scaled applications of the temperature-stable GaAs solar cells took place on the Russian spacecrafts Venera-2 and Venera-3, launched in November 1965 to the "hot" planet Venus. The area of each GaAs solar array fabricated by the Russian Enterprise KVANT for these spacecrafts was 2 m^2. Then the Russian moon cars were launched in 1970 (Lunokhod-1) and in 1972 (Lunokhod-2) with GaAs 4 m^2 solar arrays in each. The operating temperature of these arrays on the illuminated surface of the Moon was about 130°C. Therefore, silicon-based solar cells could not operate effectively in these conditions. GaAs solar arrays have shown efficiency of 11% and have provided the energy supply during the lifetime of these moon cars.

The first AlGaAs/GaAs solar cells with passivating wide bandgap window were created in 1970 [19]. In the following decades, by means of the liquid-phase-epitaxy (LPE) of AlGaAs/GaAs heterostructures [19–36], their AM0 efficiency was increased up to 18–19% [34–38] owing to the intensive investigations in the fields of physics and technology of space solar cells [39–42]. These investigations were

Fig. 8.1. Command module of MIR Space Station was launched into orbit on March 13, 1986, with a PV array based on AlGaAs/GaAs solar cells developed by the Ioffe Institute and fabricated in NPO Kvant. The array operated during the entire 15-year space station mission

stimulated and supported by ambitious space programs in the former USSR [33] and in the USA [26, 27].

High efficiency and improved radiation hardness of the AlGaAs/GaAs solar cells stimulated the large-scale production of AlGaAs/GaAs space arrays for the spacecrafts launched in the 1970s and 1980s. For example, an AlGaAs/GaAs solar array with a total area of 70 m^2 was installed in the Russian space station MIR launched in 1986 (Fig. 8.1). During 15 years in orbit, the array degradation appeared to be lower than 30% under conditions that included appreciable shadowing, the effects of numerous dockings, and a challenging ambient environment. At that time, it was the best large-scale demonstration of AlGaAs/GaAs solar cell advantages for space applications. Further improvement of the LPE technology allowed obtaining [43, 44] the efficiencies of 24.6% (AM0, 100 suns) on the basis of the heterostructures with an ultra-thin AlGaAs window layer and a back surface field layer.

Since the late 1970s, AlGaAs/GaAs heterostructures were also produced by the metal organic chemical vapor deposition (MOCVD) technique [45, 46]. The advantage of MOCVD is the possibility to fabricate multilayer structures in high-yield reactors with layers of a specified composition and precise thickness that can vary from 1–10 nm to several microns. AlGaAs/GaAs heterostructures with an ultra-thin ($\sim$0.03 μm) top window layer and with a back surface wide-bandgap barrier were fabricated by MOCVD for space cells. AlGaAs/GaAs 4 cm^2 space solar cells with efficiencies of 21% [47] and 21.7% [48] were fabricated on the base of these structures.

Enhanced light absorption was provided in the cells with an internal Bragg reflector [49–51]. This dielectric mirror increases the effective absorption length of sunlight within the long-wavelength part of the photoresponse spectrum and allows making the base layer thinner. In this case, the cell efficiency is more tolerant to reduction of the carrier diffusion length and, as a result, these cells are more radiation resistant [51].

Due to the fact that MOCVD is capable of producing single-crystal layers on silicon and germanium substrates, it has the potential for fabrication of low-cost, high-efficiency III–V solar cells on these substrates. The lattice-mismatch of 4% between Si and GaAs does not allow growing GaAs on Si with sufficient quality. However there is a progress in improving the GaAs/Si structure quality by using special structures and growth techniques: strained superlattice, thermo cyclic growth and cyclic structure annealing.

Ge is a quite good lattice-match to GaAs material. Therefore high-quality epitaxial growth of GaAs was realized by MOCVD, which is now the basic technique for growing multilayer AlGaAs/GaAs/Ge single-junction and GaInP/GaAs/Ge multijunction solar cells. This method provides epitaxial structures with good crystal quality on Ge substrates, with high productivity and good reproducibility.

Among other single-junction cells, the InP-based cells are rather promising for space applications because InP has a higher radiation resistance [27, 52, 75] than GaAs. However, there are certain obstacles for the scale application of InP-based cells in space arrays. First, there is no lattice-matched wide-bandgap window for InP to make stable passivation of the front surface. Second, it is difficult to grow this material with high quality on the Ge and Si substrates due to lattice-mismatches as high as 8% between InP and Si and 4% between InP and Ge.

Multijunction (tandem) cells ensured the further increase in III–V solar cell efficiencies. Despite a large number of theoretical studies of tandem solar cells [53–56], their efficiencies remained low for a long time, since the ohmic and optical losses in available designs were unacceptably high. Monolithic and mechanically stacked tandem cells with increased efficiencies were developed in the beginning of the 1990s. In mechanically stacked tandems with GaAs top cells and GaSb (or InGaAs) bottom cells [57–59, 62, 65–67], efficiencies exceeding 30% were achieved under concentrated sunlight. Monolithic tandem cells have been developed and fabricated by MOCVD on the structures of GaInAs/InP [64], Si/AlGaAs [68], AlGaAs/GaAs [69, 70], GaAs/Ge [71–74], GaInP/GaAs [60, 61, 63, 76, 77] GaInP/GaAs/Ge [78–84], GaInP/GaInAs [85] and GaInP/GaInAs/Ge [81, 82, 86, 87, 99–103] heterostructures.

8.2 Single-Junction AlGaAs/GaAs Concentrator Solar Cells

The creation of AlGaAs/GaAs heterostructure solar cells opened up new possibilities for increasing the efficiency of solar energy conversion. The idea of wide-band gap window was realized for solar cells, which allowed protecting the photoactive

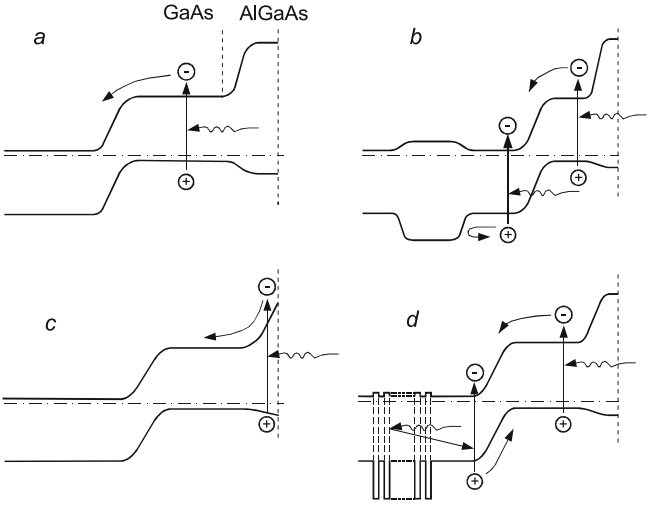

Fig. 8.2. Energy band diagrams of solar cells based on AlGaAs/GaAs heterostructures: (**a**) Structure with a p–n junction in GaAs and with a frontal wide-gap "window" of p-AlGaAs. (**b**) Structure with a back potential barrier in the n-region. (**c**) Structure with a frontal p-AlGaAs layer of variable composition. (**d**) Structure with a Bragg mirror

region of the cells against the influence of surface electronic states. Defect-free heterojunctions between AlGaAs (wide-gap window) and p–n GaAs (photoactive region) were successfully formed, which provided ideal conditions for the photogeneration of electron–hole pairs and their collection by the p–n junction. Since solar cells with a GaAs photoactive region turned out to be even more radiation-resistant, they quickly found an application in space solar arrays, despite their significantly higher cost compared to silicon cells.

First, the developments of AlGaAs/GaAs solar cells were based on relatively simple structures and technologies. Also, a relatively simple LPE technique was applied. Only one wide-gap p-AlGaAs layer had to be grown, whereas the p–n junction was formed by the diffusion of a p-type impurity from the melt into the base material of n-GaAs (Fig. 8.2(a–c)). From the middle of the 1980s, high-tech methods began to penetrate the sphere of semiconductor solar photovoltaics. The progress in the field of GaAs-based solar cells was stimulated by the application of new epitaxial techniques for heterostructure growth. The main achievement here was metal-organic chemical vapor deposition.

New technologies have led to improvements in the solar cell structure parameters. First, the wide-gap AlGaAs window was optimized, and its thickness became comparable with that of the nanosized active regions in heterolasers. The AlGaAs layer also served as the third component in the triple-layered interference antireflection coating (ARC) of a cell. A prismatic cover was applied to reduce the shadowing losses on the top grid finger contacts in concentrator solar cells (Fig. 8.3(a)). A heavily doped GaAs contact layer was grown on top of the wide-gap AlGaAs

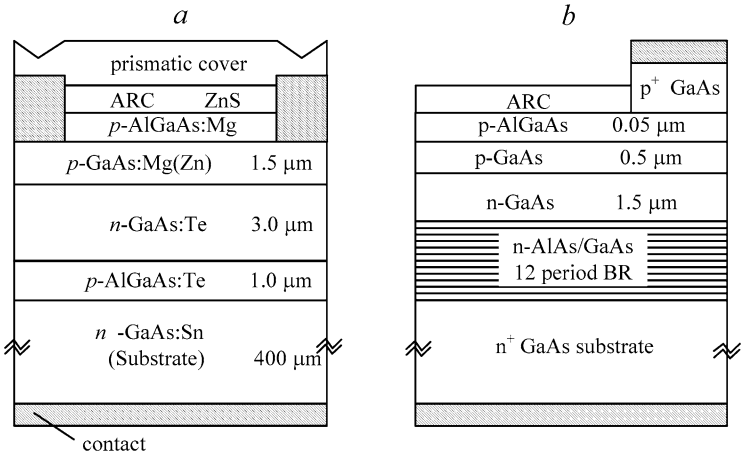

Fig. 8.3. Heterostructure of the AlGaAs/GaAs-based solar cells. (**a**) Prepared by LPE with thick (3 μm) base n-GaAs layer. (**b**) Prepared by MOCVD with internal Bragg reflector and thin (1.5 μm) base n-GaAs layer

window, and it was removed during the postgrowth treatment in the areas between the contact stripes (Fig. 8.3(b)). Second, a back (behind the p–n junction) wide-gap layer was introduced, which ensured, along with the front wide-gap layer, a double-sided confinement of photogenerated carriers within the region of light absorption (Fig. 8.2(b) and Fig. 8.3). The recombination losses of carriers before their collection by the p–n junction were reduced. At this stage of the optimization of single-junction AlGaAs/GaAs photocell heterostructures, the modified low-temperature LPE technique was still competing with the newly developed MOCVD technique.

For these structures the record efficiency of 27.8% for illumination with the concentrated (216 suns, AM1.5d) sunlight was measured in MOCVD-grown solar cells [88]. At the same time, the record efficiency of 24.6% for single-junction cells at illumination with a 100× concentration of AM0 sunlight (Fig. 8.4) still belongs to LPE-grown solar cells [89, 90]. Also, the highest efficiencies for high concentration ratios in the range of 1,000–2,000 suns (AM1.5d) were measured in the LPE grown AlGaAs/GaAs single-junction cells (Fig. 8.4): 26.2% (1,000×) and 25.0% (2,000×) [91]. These cells can operate under ultra-high sunlight concentration with efficiency as high as 23% at 5800 suns (AM1.5d) [92].

In MOCVD-grown AlGaAs/GaAs solar cell structures, a single wide-bandgap AlGaAs layer, which forms the back potential barrier, can be replaced by a system with pairs of AlAs/GaAs layers making a Bragg mirror (Fig. 8.3(b) and Fig. 8.5) [93]. The wavelength of the reflection peak for such a mirror is chosen in the vicinity of the absorption edge of the photoactive spectrum region, so that the long-wavelength light that was not absorbed in this region can be absorbed during the second passage after reflection from the mirror (Fig. 8.2(d)). At the same time, the wide-gap mirror layers continue to serve as the back potential barrier for photogenerated carriers.

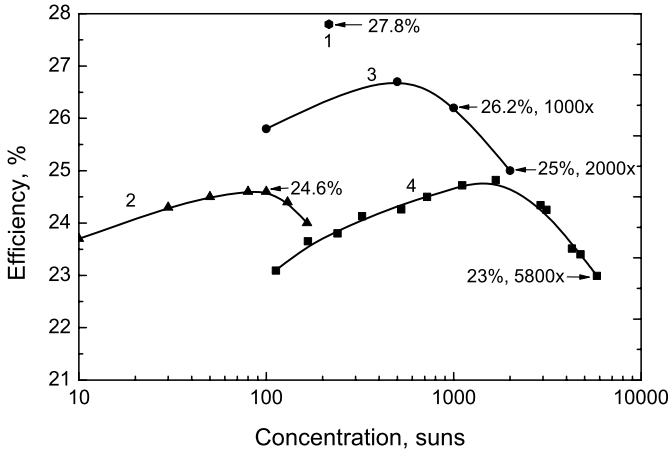

Fig. 8.4. Highest efficiencies in the MOCVD (*1*) and LPE grown AlGaAs/GaAs single-junction concentrator solar cells under AM0 (curve *2*) and AM1.5d (*1, 3, 4*) spectrum irradiation [88–92]

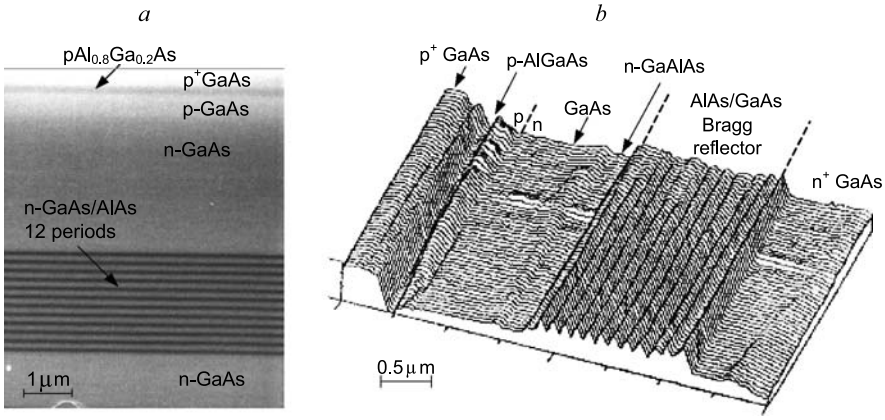

Fig. 8.5. SEM (**a**) and STM (**b**) images of the solar cell heterostructure with internal Bragg reflector

In these conditions, the thickness of the photoactive region can be reduced by half without loss of current as compared to the thickness of structures without a mirror (Fig. 8.3(b)). This factor led to a significant increase in the radiation resistance of such photocells, because the amount of lattice defects generated under irradiation by high-energy particles decreases proportionally to the thickness of the photoactive region.

More complicated structures with several Bragg reflectors [94] tuned for several IR bands of solar radiation allow us to increase the reflection of the sub-bandgap

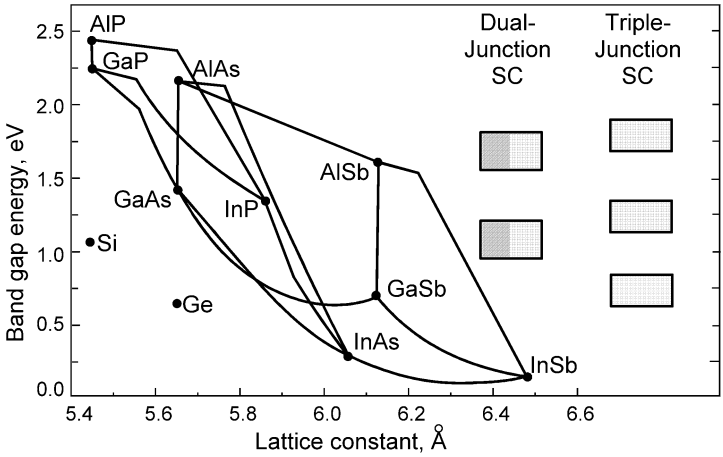

Fig. 8.6. Band gaps of III–V compounds and their solid solutions vs. the lattice constants of these materials. The optimum E_g are shown for the dual- and triple-junction solar cells

IR-radiation to reduce cell operation temperature and, as a result, to increase the cell efficiency.

8.3 Multijunction Solar Cells

The idea of tandem solar cells began to be discussed in the early 1960s and was considered to be promising. However, increasing the efficiency seemed a long way away. The situation started to change in the late 1980s, when many research groups concentrated their efforts on developing different types of multijunction solar cells. The optimal band gaps for dual and triple-junction cells are shown in Fig. 8.6.

At the first stage, the best results on efficiency were obtained through the mechanically stacked multijunction cell concept started in 1989 by Fraas and Avery; that effort resulted in a 32.6% (AM1.5D, 100×) efficient concentrator GaAs/GaSb mechanically stacked dual-junction cell [59]. However, everyone understood that the really promising cells would be those with a monolithic structure.

The first high-efficiency monolithic tandem cells were fabricated by MOCVD on GaInAs/InP [95], GaAs/AlGaAs [96]. To prepare GaInAs/InP tandem cells [95], GaInAs n- and p-layers are grown on an InP substrate to form the bottom cell. InP n- and p-layers were grown on top of this structure to form the top cell. The contacts were made according to a three-terminal scheme: one back contact covering the entire surface and two ridge-like contacts to the illuminated surface. One of them served to connect the top of the bottom cell and the back of the top cell. The cell efficiencies were 8.9% for the bottom GaInAs cell and 22.9% for the top InP cell, the total efficiency being as high as 31.8% AM 1.5 at concentration ratio of 50×.

High-efficiency AlGaAs/GaAs monolithic tandem cells have been made with GaAs bottom and $Al_{0.37}Ga_{0.63}As$ top subcells [96]. An efficiency of 27.6% mea-

sured under AM1.5G spectrum irradiation was achieved in this tandem (top cell: $E_g = 1.93$ eV). The component cells were electrically connected by a metallic contact fabricated during the post-growth processing.

Two-terminal monolithic tandem solar cells based on AlGaAs/GaAs heterostructures were fabricated by low-temperature LPE [97]. The top and bottom cells were connected by a tunnel junction formed in GaAs. The heterostructure was grown by a two-stage LPE procedure. The bottom GaAs-based cell structure was grown at the first stage. Heavily doped p^+-GaAs and n^+-GaAs layers were grown on this structure to prepare a tunnel junction. Their thickness was chosen as thin as possible (8–10 nm) to minimize the sunlight absorption losses within a GaAs-based subcell. The doping levels were as high as 10^{20} cm^{-3} when Ge or Te was added to the melt. This is quite sufficient to form a tunnel junction. The top AlGaAs layer was grown to protect the tunnel diode during the second LPE growth. Reference samples of such GaAs subcells (without p^+ and n^+ layers and with thin $pAl_{0.9}Ga_{0.1}As$ window layer) have demonstrated outdoor efficiency exceeding 27% (AM1.5, 100–300 suns). At the second stage, the top AlGaAs subcell was grown with the photoactive region made of $Al_xGa_{1-x}As$ ($x > 0.3$). These cells demonstrated rather high external quantum yield of 80–90% in the spectral range of 650–450 nm. The open-circuit voltage of 2.53 eV and the fill factor of 0.8 at 50 suns were obtained in these tandem cells. Further developments of monolithic tandem solar cells by LPE were not continued because the reproducibility of two-stage LPE progress was not ensured.

Researchers from the NREL (National Renewable Energy Laboratory, USA) were the first to obtain the sufficient efficiency increase in the monolithic dual-junction solar cells [98]. Using the MOCVD technique, they grew GaInP/GaAs structures matched by their lattice constants, in which the top photocell had a p–n junction in $In_{0.5}Ga_{0.5}P$ and the bottom one was in GaAs. The cells were electrically connected in series by means of a tunnel p–n junction specially formed between the cascades. Efficiency of 30.2% (AM1.5d, 180×) was obtained in these dual-junction cells.

At the same time, the interest in triple-junction cells was growing. As a consequence of well-directed efforts, efficiency as high as 35–40% was demonstrated in monolithic GaInP/Ga(In)As/ Ge cells [99–103].

8.3.1 GaInP/GaAs Dual-Junction Solar Cells

Figure 8.7 shows a monolithic dual-junction GaInP/GaAs cell structure. At the Ioffe Institute, such structures were grown by a low-pressure AIX 200/4 reactor equipped with EpiRas 2000TT unit (real time in-situ epitaxy monitoring tool). It should be noted that the EpiRas system provides simultaneous measurements of the different characteristic parameters by the following three methods: normalized reflection spectroscopy, reflection anisotropy spectroscopy (RAS), and emissive pyrometry. This allows us to obtain data on real temperature of the growth surface, growth rate, thickness of the layers, composition of ternary alloys, doping levels, surface reconstruction and interface quality. Permanent recording of the RAS signal during the wafer heating process makes it possible to measure the wafer deoxidation

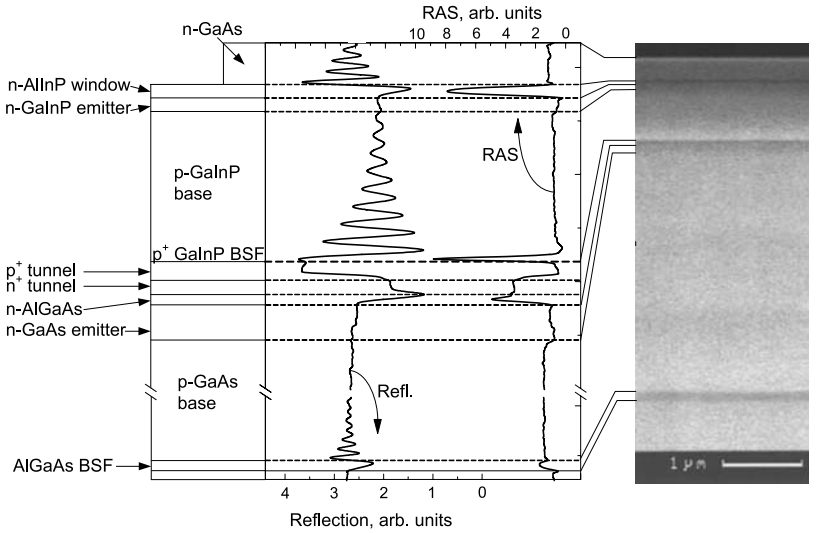

Fig. 8.7. GaInP/GaAs monolithic dual-junction cell structure: cross-sectional diagram (*left*); time-resolved curves of light reflection (at $h\nu = 2\,\mathrm{eV}$) and RAS (at $h\nu = 3.5\,\mathrm{eV}$) recorded during the structure growth (*in the middle*); scanning electron microscope image of the grown structure (*right*)

temperature. The surface and interface roughness can be estimated as well. Due to the difference in refraction indices of the growing materials, oscillations arise on the time-resolved light reflection curve. Attenuation of these oscillations due to an increase in absorption in the growing layer is used to determine the composition in the case of the ternary alloys, whereas the period of oscillations is used for growth rate and layer thickness calculations. Layer parameters calculated with the help of these data are in good agreement with those measured by means of the scanning electron microscopy, secondary ion mass spectroscopy (Figs. 8.7, 8.8) as well as by x-ray diffractometry, photoluminescence and other methods.

The structures of multijunction solar cells are among the most complicated of all semiconductor devices. Nevertheless, it can be "deciphered" by using the whole store of the modern diagnostic equipment. These methods allow us to obtain comprehensive information about the structure layers. However, there is a problem of precise measurements of the doping level in the thin (10–15 nm) layers of tunnel diodes.

The modes of MOVPE reactor operation were varied to adjust the conditions for growth of photoactive (AlInP, GaInP, GaAs, etc.), tunnel, buffer and spacer layers and to seek reproducible technological processes for fabrication of GaInP/GaAs dual-junction cells of p-on-n and n-on-p polarities. Since monolithic dual-junction (DJ) solar cells are two current sources connected in series, the overall current in the outer circuit will be equal to the minimum current generated in one of the junctions. The current value will be the highest one, when the photocurrent values of the top

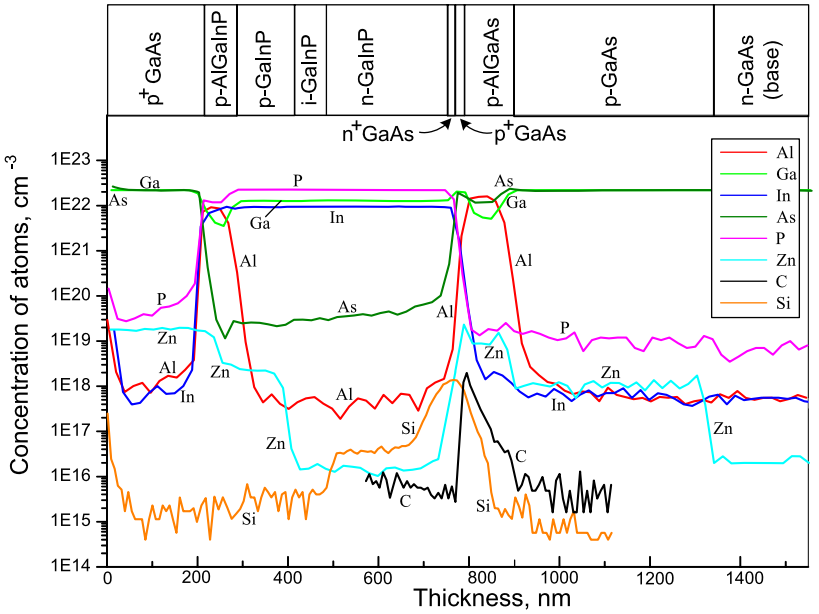

Fig. 8.8. SIMS distributions of P, As, In, Al, Ga, Zn, C, Si and structure scheme of p-on-n dual-junction GaInP/GaAs solar cell, also interpreted through use of Raman spectroscopy, SEM and EBIC methods. The structure is shown from the front surface of the top cell to the base n-GaAs layer of the bottom cell

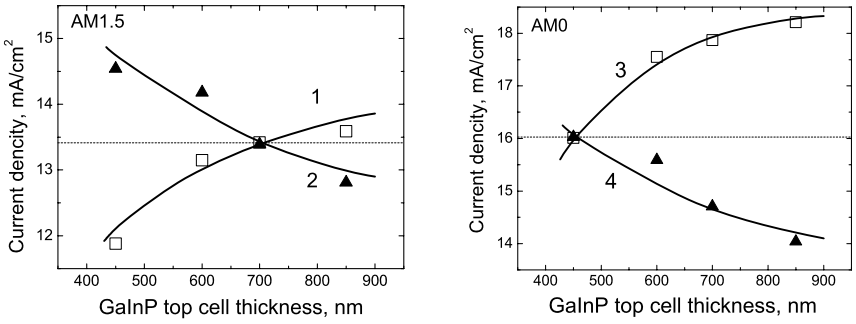

Fig. 8.9. Photocurrent densities in the GaInP top (curves *1, 3*) and GaAs bottom (*2, 4*) cells vs. thickness of GaInP cell for AM1.5 (*left*) and for AM0 (*right*) spectra [104]

and bottom cells are matched and maximal. Current matching can be achieved by varying the top cell thickness, since the amount of light absorbed by the bottom cell depends on the top cell thickness (Figs. 8.9, 8.10). In the case of the AM0 spectrum conversion, the equality in the currents of the GaInP and GaAs junctions is possible at converting the solar spectrum part with photon energies higher than 1.9 eV in the bottom GaAs junction. This is achieved by means of decreasing the top cell thick-

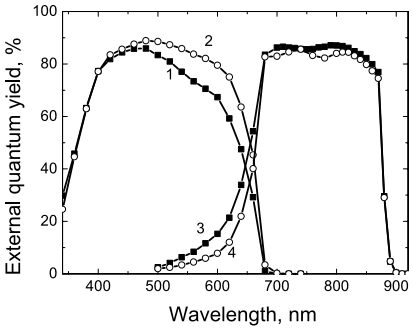

Fig. 8.10. External quantum yield in GaInP top (curves *1, 2*) and GaAs bottom (*3, 4*) cells of a dual-junction monolithic GaInP/GaAs solar cell with different thicknesses of the GaInP top cell: *1, 3* – 450 nm, *2, 4* – 700 nm [104]

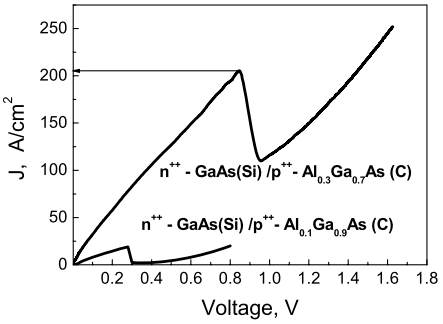

Fig. 8.11. I–V curves of tunnel diodes based on n^+-GaAs (Si) /p^+-AlGaAs (C) structures with different Al content developed for dual-junction GaAs/GaInP solar cells [104]

ness. Otherwise, at the complete absorption of photons with the energy higher than 1.9 eV by the top GaInP cell, its current will be higher than that of the bottom GaAs cell. For the terrestrial AM1.5 sunlight characterized by less ultraviolet radiation, the current correlation in a solar cell is achieved at a larger thickness of the top GaInP cell (Figs. 8.9, 8.10). At the GaInP cell thickness of 450 nm, the matching between currents of the top and bottom cells has been achieved: $J_{\mathrm{GaInP}} = 16.01\,\mathrm{mA/cm^2}$, $J_{\mathrm{GaAs}} = 16.03\,\mathrm{mA/cm^2}$ (AM0 spectrum). The current matching for the AM1.5d spectrum was achieved at the GaInP thickness of 700 nm: $J_{\mathrm{GaInP}} = 13.39\,\mathrm{mA/cm^2}$, $J_{\mathrm{GaAs}} = 13.42\,\mathrm{mA/cm^2}$ [104].

The tunnel diode for DJ concentrator solar cells should operate at high light intensity. In the growing technique for such tunnel diodes the doping p-AlGaAs layers with C was used at the smallest ratio of V/III (<2.5) at various Al contents. As a result of optimizing technological processes, a tunnel diode based on the n^+-GaAs(Si)/p^+-$Al_{0.3}Ga_{0.7}As$ structure with the peak current density above $200\,\mathrm{A/cm^2}$ was fabricated (Fig. 8.11); this ensured the operation of the developed DJ cells at a high concentration level.

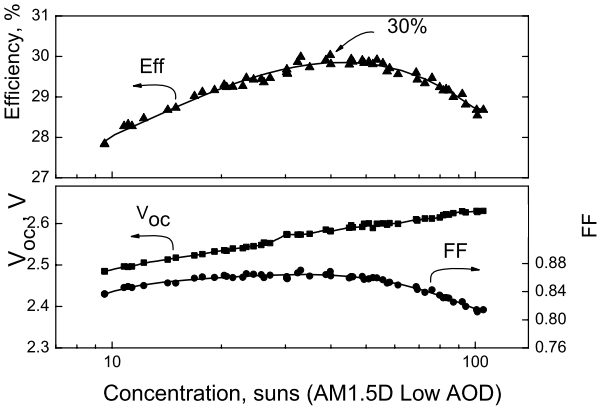

Fig. 8.12. Efficiency, V_{OC} and FF versus concentration for the n-on-p GaInP/GaAs dual-junction solar cells [104]

The I–V measurements of DJ cells under concentrated light were performed using developed at the Ioffe Institute three-channel pulsed solar simulator with a tunable blue/red ratio. Figure 8.12 shows V_{OC}, FF and efficiency values versus sunlight concentration for a terrestrial DJ cell. The maximum efficiency is above 30% at the concentration ratio of 30–50 X has been measured in this cell [104].

8.3.2 Hybrid Triple-Junction GaInP/GaAs–GaSb Monolithic/Mechanically Stacked Solar Cells

One way to increase tandem cell efficiency is the fabrication of hybrid cells with a monolithic GaInP/GaAs IR transparent top cell mechanically stacked with an IR-sensitive bottom cell. An essential aspect of this cell concept is the optical transmittance of the top cell. The interference effects in the multilayer structure and light adsorption in the GaAs substrate material result in the main optical losses of IR light passing through the top cell to the bottom one. When the top cell is operating in the mechanically stacked tandem, its transmittance could be improved in two ways: (1) thinning the GaAs substrate and (2) reducing the base doping level. For both these cases, the optimization of ARC properties on the top and bottom sides of the top cell should be done.

Because of the high light absorption by free charge carriers in the p-doped GaAs material, the DJ cell of n-on-p polarity was grown on an IR transparent n-GaAs substrate. An additional tunnel diode between the n-GaAs substrate and the n-on-p DJ cell was inserted in these structures [104]. The measured transmittance spectra for top cells as a function of substrate doping and thickness show that at simultaneous decreasing the doping level and thickness of the GaAs substrate, the interference effects become more pronounced, and the interference optical losses remain substantial in spite of transmittance improvement. Nevertheless, more than 85% of the

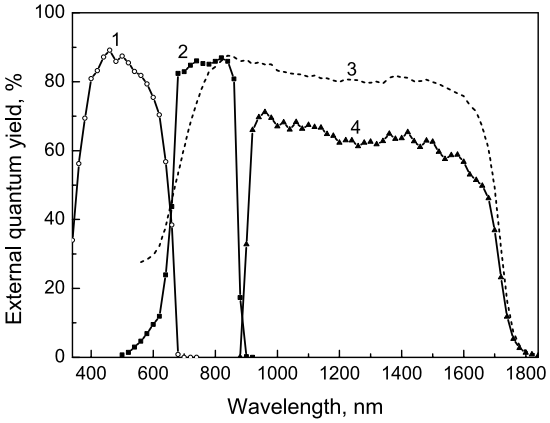

Fig. 8.13. Spectral response of a hybrid GaInP/GaAs (monolithic)/GaSb mechanically stacked triple-junction cell. Curves *1, 2*: spectra of top GaInP (*1*) and middle GaAs (*2*) sub cells. Curve *3*: GaSb cell as it is, Curve *4*: GaSb cell behind GaInP/GaAs top cell based on 380 μm thick IR-transparent GaAs substrate

infrared light passes through the InGaP/GaAs top cell and reaches the GaSb bottom cell.

Solar cells based on GaSb intended for mechanically stacked tandems were fabricated by the Zn diffusion into the n-GaSb front epitaxial layer grown by LPE on the heavily doped n^+-GaSb substrate. The GaSb cells based on epitaxial layers are characterized by the higher photosensitivity in comparison with the cells based on the "bulk" material [105, 106]. Application of the epitaxial technology for the fabrication of GaSb cells together with the optimization of the antireflection coating of both the top and bottom cells allows for gains in the external quantum yield in the spectral range of the top cell transparency; that improvement gives an increase in the generated photocurrent (Fig. 8.13). The cells with an epitaxial layer grown on a heavily doped substrate are characterized by the fill factor of 0.68–0.70, which does not decrease with the increase of light concentration up to 300 suns (Fig. 8.14). As a result these cells demonstrate higher values of the efficiency compared to those of the cells earlier fabricated by zinc diffusion into the GaSb wafer.

The maximum achieved efficiencies for the top and bottom cells arranged in a triple stack is 30.2% (40 suns) for the DJ cell and 5.9% (420 suns) for the GaSb cell. The best efficiency of 35% was obtained for GaInP/GaAs–GaSb mechanical stacks based on well-matched current top DJ cells [104]. The recent improvements of the GaSb cell show really optimistic results for it, placed behind the IR-transparent DJ cell: 17.7 mA/cm^2, FF = 0.72 and 6.2% (AM1.5D, Low AOD, 290 X) efficiency. Thus, the efficiency above 38% (AM1.5) seems to be achievable in the improved concentrator hybrid cell based on GaInP/GaAs top and GaSb bottom subcells.

Efficiency as high as 34% (15 suns, AM0) has been achieved in the hybrid triple-junction monolithic/mechanically stacked voltage-matched circuits based on

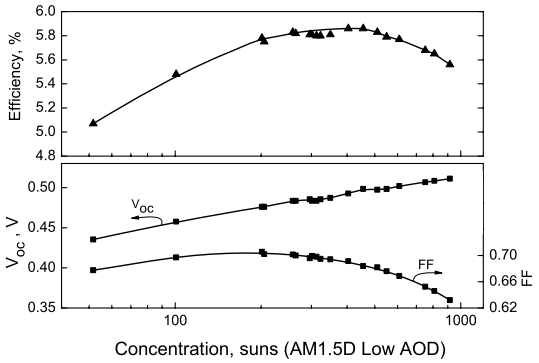

Fig. 8.14. Efficiency, V_{oc} and FF versus concentration for the GaSb bottom cell illuminated through GaInP/GaAs DJ cell with 380 μm n-GaAs ($n = 2 \times 10^{16}$ cm^3) substrate [104]

a GaInP/GaAs monolithic top cell and a GaSb bottom cell [107]. Efficiencies of 27.5% in the top GaInP/GaAs cell and of 6.5% in the bottom cell were achieved. To arrange two-terminal circuits, seven GaSb cells were connected in series ensuring output voltage (V_{mp}) slightly exceeding the V_{mp} of GaInP/GaAs cells connected in parallel.

The quadruple GaInP/GaAs–AlGaAsSb/GaInAsSb cells can ensure further efficiency increase up to 40% and more at concentrated AM1.5d sunlight. This can be achieved owing to a possible efficiency increase in the monolithic dual-junction bottom cell based on lattice-matched AlGaAsSb/GaInAsSb structures with band gaps of ~1 eV in the top subcell and ~0.6 eV in the bottom subcell [108].

Unfortunately, complicated assembly of the mechanically stacked cells and difficulties of heat removal from the top cell at sunlight concentration ratio exceeding 100 suns are obstacles to industrializing this approach.

8.3.3 Monolithic GaInP/Ga(In)As/Ge Triple-Junction Solar Cells

Efficiencies of 35–40% was obtained recently [99–103] in the monolithic GaInP/Ga(In)As/Ge concentrator triple-junction cells (see Fig. 8.15). Top and middle subcells include the following layers: back-surface field (BSF) layer, base, spacer, emitter and window. The Ge-subcell consists of a base (substrate), a diffused emitter and a window. Subcells are connected in series by tunnel diodes, which in turn include highly doped thin (10–20 nm) layers. Combination of the lattice matched GaInP top cell, GaAs middle cell and Ge bottom cell divides the solar spectrum into three parts at excess photocurrent density in the Ge-cells (Fig. 8.16). Current matching can be improved if the middle cell has lower band gap (for instance, 1.2–1.3 eV) in the lattice-mismatched (metamorphic) GaInP/GaInAs/GaAs structure [87, 99, 100]. The problem of the crystal quality arises during the growth procedure development for such metamorphic solar cells. It should be noted that GaInAs with a near to ideal band gap of 1.1 eV has the lattice mismatch of 1.6% with the Ge substrate. In spite

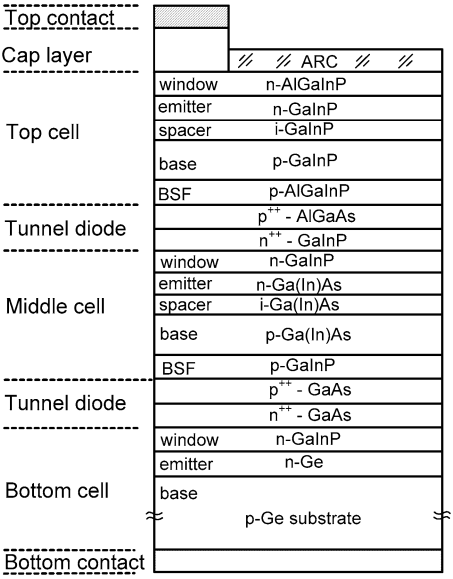

Fig. 8.15. Typical GaInP/Ga(In)As/Ge structure of a monolithic triple-junction solar cell on p-Ge substrate

of the higher theoretical efficiency of such metamorphic cells, the achieved cell efficiencies are approximately equal to those for lattice matched cells. Nevertheless, the highest efficiency (>40%) was reached by Spectrolab, Inc. in the metamorphic $Ga_{0.44}In_{0.56}P/Ga_{0.92}In_{0.08}As/Ge$ three-junction concentrator solar cells [103].

Multijunction solar cells are characterized by a complicated structure. In a triple-junction cell, three photoactive p–n junctions are connected in series by two intermediate n^+–p^+ tunnel junctions, biased by voltage in the forward direction. Very high doping concentrations of the tunnel junction regions require small thicknesses of the corresponding layers in the structure to reduce the nonphotoactive light absorption. In addition, two enclosing barrier layers designed to minimize dopant diffusion from the n^+ and p^+ layers in both tunnel junctions should be introduced in a multijunction solar cell structure. Very often technological difficulties associated with formation of the tunnel junctions are the reason for lower conversion efficiency of a cell. This is especially true in the case of the cells intended for operation under high sun concentration conditions.

If the generated photocurrent density in a cell exceeds the density of the peak tunnel current (J_p) of one or both tunnel junctions, in this case there exists a part of the I–V curve near the open circuit voltage point, where a trace from the action of the internal tunnel diode(s) can be revealed. The J_p value is an important parameter of a cell, establishing the limit in the photocurrent density for efficient operation. Figure 8.16 shows a family of the illuminated I–V curves for a TJ cell. It was measured at different light intensities from a high-power flash solar simulator [109].

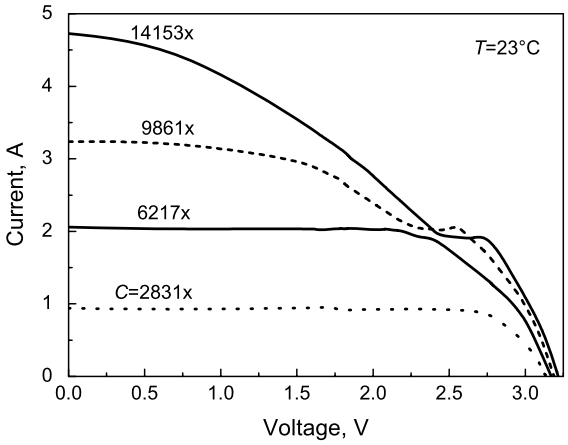

Fig. 8.16. A family of illuminated I–V curves at different light intensities from the high-power flash solar simulator for TJ cell (designated illumination area is 2 mm in diameter) [109]

A tunnel peak is revealed at sun concentration beginning from ~9800×. Resolution of the tunnel peaks is difficult, when I–V curves are strongly deformed due to obvious action by the cell's internal resistance. The value of J_p as high as 65 A cm^{-2} has been calculated from I–V curve for $C = 9861\times$, when considering only the designated illumination area.

The main result of Fig. 8.16 is that TJ cells can operate at illumination intensities as high as several thousand suns. Tunnel peaks have a tendency to move toward the open circuit voltage point, when illumination increases. At the same time, peak current decreases. This is probably caused by overlapping of the tunnel curves, with part of the curve related to the photoactive junctions being more vertical near the open circuit point at higher photocurrents. Other reasons may be regarded as well. Among them is a parasitic photoactivity of the tunnel junctions, when generated photocurrent reduces peak current. Another reason can be associated with the carrier transport through the cell structure, where the thickness of all the layers is smaller than the diffusion length of the photogenerated carriers, or potential barriers are not high enough. Further investigations could resolve the causes of this phenomenon.

A reduction in ohmic losses is obtained by lowering both series and sheet resistances; this ensures a high fill factor value exceeding 0.87 at concentration ratios up to 1,000 suns and FF = 0.8 at 4,000 suns (Fig. 8.17). Efficiencies of about 37% at 1,000×, 36% at 2,500× and 34.5% at 4,000× have been measured in one of the Spectrolab's cells available in the market.

The following statements may be formulated on the basis of the presented data: heterostructures of high-efficiency, multijunction solar cells are the most complicated structures among all semiconductor devices. The confirmation of this declaration is as follows.

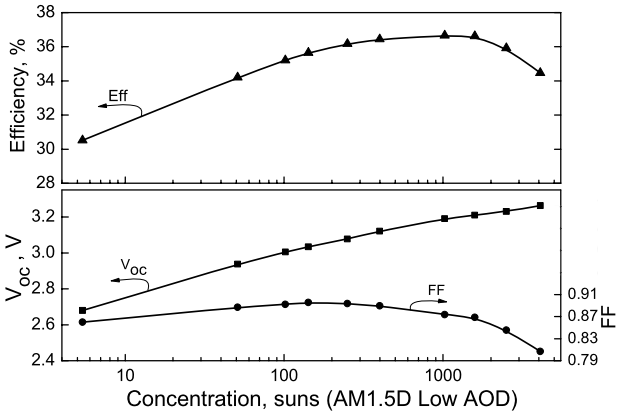

Fig. 8.17. Efficiency (Eff), fill factor (FF) and open circuit voltage (V_{oc}) vs. sunlight concentration ratio for a triple-junction GaInP/GaInAs/Ge Spectrolab's solar cell (area is 4 mm^2 and designated illumination area is 1.7 mm in diameter)

- Full range of the III–V materials in view of the binaries and solid alloys is involved in formation of the multijunction solar cell structure (including nitrides for advanced cells). A very wide range of the layer band gaps covering photon spectrum from UV to IR should be ensured. All the layers are lattice matched, or moderately metamorphic.
- A triple-junction cell consists of about 20 layers and the quantity of layers will be larger in advanced 4–6-junction cells, or in the cells with Bragg reflectors, as well as in the cells incorporating superlattices and quantum dots. Layer thickness is varied in a very wide range from 10 nm in the tunnel diodes up to a few micrometers in the photoactive regions.
- Doping level is varied from 10^{15}–10^{16} cm^{-3} in the spacer layers up to 10^{19}–10^{20} cm^{-3} in commutating tunnel diodes. A drastic change in the doping level should be ensured in the tunnel diodes and this sharpness should be conserved in the structure during further crystallization at high growth temperatures. Also, the operating capacity of the tunnel junctions should be ensured during the lifetime of outdoor cell operation at various temperatures and high photocurrent densities.
- III–V cell structures are grown on Ge substrate, being the foreign material in relation to the cell material. A number of additional technological problems are expected if the Ge substrate is substituted for the Si substrate, which is more promising from economical point of view.
- Individual cell dimensions are varied from 1 mm^2 in the terrestrial concentrator modules with mini-lenses up to about 30 cm^2 in arrays without concentration for space application. It means that extremely high quality of growth and post-growth technologies must be ensured.

- Solar cells are among such semiconductor devices which operate under difficult climatic conditions. A thin glass sheet or dielectric layer is the only barrier between the environment and the cell structure.
- In concentrator cells, optically transparent protectors and front layers are subjected to the action of highly intensive light (up to 1,000 suns and higher in the center of the focal spot), so that a radiation resistance of corresponding materials should be ensured.
- Conflicting demands on the cell structure are accompanied by a requirement to provide the lowest cell cost as an essential issue in reducing the system cost of solar electricity.

In spite of the complexity of MJ cell structures and technology, a number of new companies have been formed to organize the production of concentrator PV installations based on multijunction cells. This expansion is driven by the new perspectives for significant efficiency increase and reduction in the costs of solar electricity.

It is clear that solar cells are the key elements in the concentrator PV installations. Table 8.1 summarizes the efficiencies of terrestrial single- and multijunction III–V concentrator solar cells achieved in the period of 1989–2006. Cell producers, sunlight concentration ratios (suns), conditions at measurements (air mass) and the cell structure (type of solar cells) are shown in the table. The cells in the upper part of the table are characterized by rather high efficiency. However, in the 1990s there was no production of such cells. Getting the high-power companies (Spectrolab, AZUR Space, EMCORE Photovoltaics, Sharp, etc.) involved in "terrestrial" concentrator activity allowed for large-scale production of MJ concentrator solar cells for concentrator modules. This means that an opportunity arises for expanding the concentrator PV industry in the near future [110–114].

8.4 Concentrator PV Modules and Installations with III–V Solar Cells

The concentrator approach is the only way for large-scale use of high-efficiency III–V cells for terrestrial applications. Indeed, optical elements made of relatively cheap materials can focus the sunlight on small-area cells, which allows for drastically reduced consumption of semiconductor materials in production of the solar arrays. The costs for optical elements and mechanical sun-tracking systems are covered by the expense of the larger amount of "solar" electricity produced in higher-in-efficiency cells and owing to normal positioning of the PV modules with respect to sunrays during the daytime. For more than 30 years many research groups were engaged in developing concentrator PV systems. Under development were the solar cell structure and fabrication technology, effective concentrator optical systems, module design, and sun trackers [28, 40, 115, 116]. Interest in concentrator PV grew substantially after the higher-in-efficiency multijunction solar cells promised to achieve photovoltaic conversion efficiencies near 35–40% at high levels of sunlight concentration.

Table 8.1. Selected efficiencies of the concentrator solar cells based on III–V compounds

Year	Producer	Eff (%)	Suns	Air mass	Type of solar cell	Ref.
1989	Boeing	32.6	100	AM1.5	GaAs/GaSb, mech. stacked	[88]
1991	Spire	27.6	255	AM1.5	AlGaAs/GaAs, single-junction	[88]
1991	NREL	31.8	50	AM1.5	InP/InGaAs DJ, monolithic	[88]
1994	IOFFE	24.6	100	AM0	AlGaAs/GaAs, single-junction	[43]
1994	NREL	30.2	180	AM1.5d	GaInP/GaAs, DJ, monolithic	[88]
1999	IOFFE/IES-UPM	24.8	1,680	AM1.5d	AlGaAs/GaAs, single-junction	[92]
		23	5,800			
2001	Fraunhofer ISE	30.2	300	AM1.5d	GaInP/GaInAs DJ, monolithic	[88]
2001	IOFFE/IES-UPM	26.2	1,000	AM1.5d	AlGaAs/GaAs, single-junction	[91]
		25	2,000			
2001	JX Crystals	34	15	AM0	GaInP/GaAs-GaSb, TJ hybrid circuit	[107]
2005	Fraunhofer ISE RWE-SSP	35.2	600	AM1.5d	GaInP/GaInAs/Ge, monolithic	[111]
2006	IOFFE	35	50	AM1.5 low-AOD	GaInP/GaAs/GaSb, TJ hybrid monolithic/mech.stacked	[104]
2006	Toyota TI Sharp Corp.	38.9	489	AM1.5g	GaInP/GaInAs/Ge, TJ monolithic	[102]
2006	Spectrolab	39.3	179	AM1.5 low-AOD	GaInP/GaInAs/Ge, TJ monolithic	[88]
2006	Spectrolab	40.7	240	AM1.5 low-AOD	GaInP/GaInAs/Ge, TJ monolithic	[103]

Fig. 8.18. Concentrator PV installation with four parabolic mirrors and AlGaAs/GaAs cells mounted on the heat pipes, 1981 [117]. In photo: Rumyantsev

Fig. 8.19. Solar PV installation with AlGaAs/GaAs solar cells and parabolic mirrors, 1981 [118]. In photo: Alferov (*on the right*), Rumyantsev (*in the center*) and Tuchkevich, former director of Ioffe Institute

In the first concentrator modules and installations, large-area mirrors (0.5–1 m in diameter) focused the sunlight on cells of several square centimeters in area. Cooling by water or by means of thermal pipes was necessary [115–118] (see Figs. 8.18, 8.19). The appearance of Fresnel lens fabrication technology has required revision of the photovoltaic module design. Now, solar cells could be placed behind the concentrators. The module housing could serve as a protector from the environment (Fig. 8.20). Since the Fresnel lenses had smaller dimensions ($25 \times 25\,\text{cm}^2$), the photocell dimensions were also decreased down to less than $1\,\text{cm}^2$. The characteristics of such photocells were improved due to lower internal ohmic losses and simplified assembly. For cooling the cells, it was sufficient to use the heat conductivity of the module's metallic housing [119].

Fig. 8.20. Solar PV installation with 16 Fresnel lenses ($25 \times 25\,\text{cm}^2$ each) and AlGaAs/GaAs cells, 1986 [119]

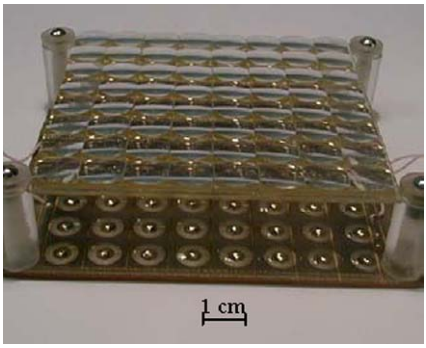

Fig. 8.21. Concentrator PV module employing small- aperture area smooth-surface lenses and AlGaAs/GaAs cells, 1989 [120, 121]

In the late 1980s, a concept was proposed that meant a radical decrease in the concentrator dimensions and retention of a high sunlight concentration ratio [120, 121]. The first experimental modules of this type consisted of a panel of lenses, each of 1×1 or $2 \times 2\,\text{cm}^2$, focusing radiation on the AlGaAs/GaAs cells of submillimeter size (see photograph in Fig. 8.21). There are several advantages of a module with small-aperture area concentrators: the requirements imposed on the capability of heat-sinking material are essentially relieved such as requirements for the thermal expansion coefficient and thickness. The focal distance of lenses appears to be comparable with the structural thickness of the conventional modules without concentrators.

The advantages of the small-size concentrator cells are the following: low ohmic losses at collection of low current at nonuniform light intensity distribution and high local photocurrent density; high cell chip throughput from a wafer; and the possibility of applying the highly productive mounting methods. Somewhat later this approach resulted in creation of the "all-glass" photovoltaic modules with III–V cells and panels of small-aperture area Fresnel lenses (each lens is $4 \times 4\,\text{cm}^2$). The

Fig. 8.22. Array of the full-size concentrator modules with small aperture area Fresnel lenses [130]

lens panels had a "glass-silicone" composite structure. This work was carried out through close cooperation between the research teams from the Ioffe Institute (St. Petersburg, Russia) and Fraunhofer Institute for Solar Energy Systems (Freiburg, Germany) [122–125].

In recent years, the team at the Ioffe Institute developed the concentrator modules [126–129], in which Fresnel lenses are arranged on a common superstrate in the form of a panel of 12 × 12 lenses. The cells are as small as 2 × 2 mm^2 and 1.7 mm in designated area diameter operating at mean concentration ratio of about 700× [130] (see photograph in Fig. 8.22).

For the use of the monolithic multijunction cells, the following fundamental advantage should be noted. They operate at lower photocurrent, so that ohmic losses, say, in a five-junction cell, would be lower than the losses in a one-junction cell operating within the same spectral range by a factor of 5. Nonuniformity in the illumination distribution along the cell surface is a negative feature of concentration. For multijunction cells, an important factor is chromatic aberrations in concentrators of the refractive type. Negative influence of this type of illumination nonuniformity cannot be compensated for by using a more dense contact grid, because lateral currents arise between subcells inside the cell structure. Small-size cells have certain advantages in this respect. On the other hand, parameters of a concentrator as an element of a PV system should be optimized in the required way.

8.4.1 Concentrator Modules with Mini-lens Panels: Design and Fabrication

Comprehensive analysis has been done regarding concentration properties of the Fresnel mini-lenses operating with III–V triple-junction cells [131]. The lens profile optimization was carried out taking into account the refraction index of the lens material and its dependence on wavelength, focal distance, receiver diameter, sun illumination spectrum, and sensitivity spectra of the subcells in a multijunction cell.

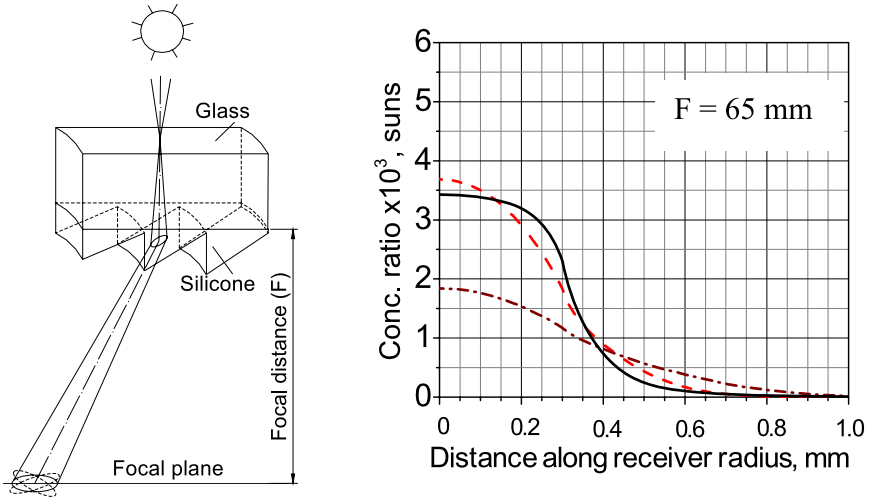

Fig. 8.23. Optical layout of a Fresnel lens fragment with a composite structure (*on the left*), and calculated light intensity distributions along the receiver diameter for spectral bands corresponding to three cascades in a triple-junction cell (*on the right*: *solid line* for top sub-cell; *dashed* and *dash-dotted lines* for middle and bottom sub-cells, respectively). Lens aperture area is $40 \times 40\,\text{mm}^2$ at focal distance F = 65 mm and groove pitch of 0.25 mm [131]

Lens structure consists of a sheet of silicate glass and refracting microprisms formed of transparent silicone on the inner side of the glass. The microprisms themselves are formed by polymerization of the silicone compound directly on the glass sheet with the use of a negatively profiled mold. The advantages of this concentrator technology are based on a high UV stability of silicone, its excellent resistance to thermal shocks and high/low temperatures, good adhesive properties in a stack with silicate glass, simplicity and very high accuracy of the formation method. Small mean thickness of the prisms ensures negligibly low absorption of the sunlight in comparison with Fresnel lenses made of bulk acrylic with a "regular" total thickness of about 3 mm.

Figure 8.23 shows the optical diagram of the Fresnel lens operation. Sunrays with divergence, corresponding to the sun disk size, are incident upon the lens surface. The overlap of the elliptical light spots from different parts of the lens forms distribution of light intensity along the focal plane. A receiver of diameter d can accept a certain part of light. This amount of light, divided by total amount of light, incident within lens aperture area and spectral range of receiver sensitivity, is defined as lens optical efficiency with respect to given receiver diameter.

Figure 8.23 (right) shows an example of light intensity distributions along the receiver radius for spectral bands corresponding to three cascades in a triple-junction cell. It is seen that a concentration ratio as high as 3,500 suns can occur in the receiver center. Averaged lens optical efficiencies versus receiver diameter for focal distances of F = 45, 65 and 85 mm are shown in Fig. 8.24 (on the left). It was

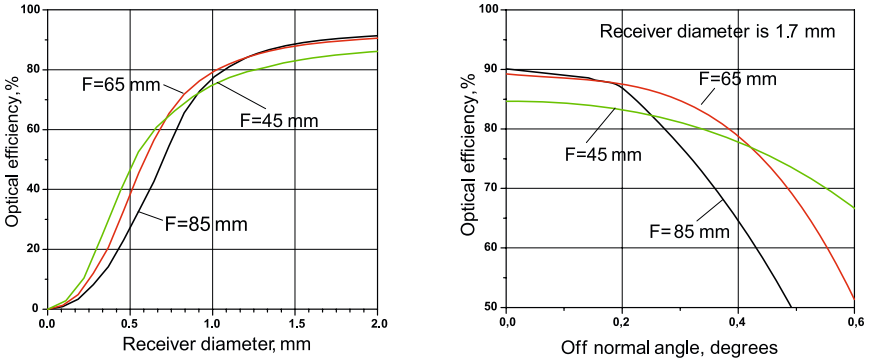

Fig. 8.24. Dependences of lens optical efficiency on receiver diameter at a normal angle of incidence (*on the left*) and those at off-normal angles for the case of 1.7 mm receiver diameter (*on the right*)

assumed in calculations that there exists a balance between photocurrents in the top and middle subcells, but an excess of photocurrent in the bottom subcell, as one can estimate from the cell photoresponse curves. Therefore, lens optical efficiency may be calculated only for top and middle subcells.

At real operation of the concentrator modules, the incidence angle of the sunrays upon the lens surface is under variation. Off-normal behavior of the concentrator systems with different focal distances, but alike receiver diameters of $d = 1.7$ mm, is shown in Fig. 8.24 (on the right). One can see that the off-normal curve is wider for shorter focal distances, but an advantage in acceptance angle at F = 45 mm is revealed, when absolute optical efficiency is low enough – near 75%. In this case, the local concentration ratio in the center of the light spot is near 4,500 suns. In contrast, for the case of F = 85 mm concentration in the center is only 2,500 suns at the highest (among others) lens optical efficiency in the normal position. A narrower acceptance angle for lenses with long focal distance can be compensated by more accurate tracking to the sun.

A full-scale $50 \times 50\,\text{cm}^2$ module (see photograph in Fig. 8.22) includes a 144-lens panel and a corresponding quantity of properly mounted cells. The accuracy in positioning the cells is of great importance because each cell should be situated in the center of the focal spot of a corresponding lens. This accuracy has to be about 100 μm, which can be realized by using automatic processes and standard electronic industry machines. Two versions of the cell mounting are shown in Fig. 8.25.

On the left side of Fig. 8.25, flat copper plates 0.5 mm thick provide initial distribution of heat from a solar cell. In the case of the small-aperture area submodules, a very stable and cheap silicate glass may be used in a stack with a relatively thin heat sinking material (copper or steel). In spite of the low thermal conductivity of glass, waste heat can be dissipated to ambient air, as it occurs in regular flat-plate modules without concentration. Superior insulating properties of glass allow connecting the cells in an electric circuit of any configuration ensuring electrical safety of a mod-

Fig. 8.25. Small-size ($2 \times 2\,mm^2$) cells mounted by soldering to: flat copper plate (*left*) and trough-shaped copper plate (*right*). In the latter case, a heat-sinking trough with a string of cells can be placed behind a glass sheet

ule as a whole. Even walls of a module housing may be made of glass, justifying this approach as "all-glass" module design. On the left side of Fig. 8.25, the glass base plate also serves for hermetical sealing of the cells mounted on trough-like heat sinks. These troughs with strings of cells are glued on the outer side of the module cabinet behind the glass plate. Positioning of the troughs with mounted cells is not an elaborate procedure even when using manual fabrication techniques if a special template is applied. Hermetic sealing is provided for the thin air body inside the troughs, whereas the entire volume between the front and rear glass sheets of the module housing is connected with atmosphere. Special tubes are used to prevent dust from penetrating the module. The tubes are situated in diametrically opposite corners of module housing, thus providing an exit for condensed water. After affixing the troughs, connecting electrically the cell strings and assembling the module, the rear module side is coated with a hermetic sealing compound.

8.4.2 Outdoor Measurements of the Test Modules with Mini-lens Panels

Operational abilities of the modules of the "all-glass" design have been checked in respect to overall conversion efficiency by fabrication and outdoor measurements of test modules of reduced sizes [131]. The modules were equipped with GaInP/GaAs/Ge triple-junction cells produced by Spectrolab, Inc. In the module, described below, the cells were characterized by conversion efficiencies of 32–34% (AM 1.5d) at flash measurements with uniform distribution of incident light and the concentration ratio of about $1{,}000\times$.

In a module with an eight-lens panel (2×4 lenses) the cells of 2 mm in diameter were used, being connected in parallel. The sealed module was installed on a sun-tracking system. After the outdoor I–V measurement, the module was characterized indoors using a large-area flash solar tester [128] to compare corresponding results for outdoor and indoor measurements (Fig. 8.26).

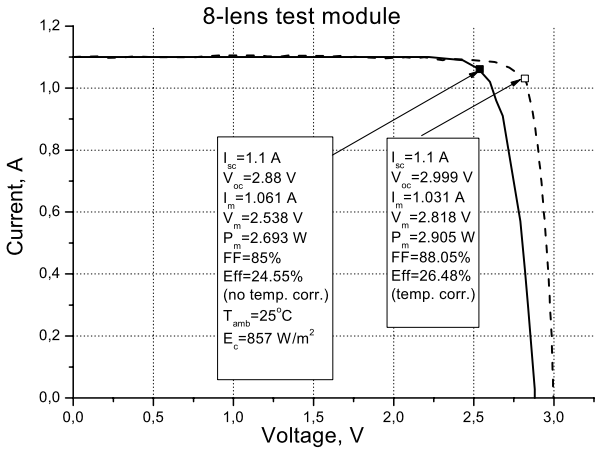

Fig. 8.26. I–V curves measured on the eight-lens test module outdoors (St. Petersburg, June 16, 2006, 16 h. 43 m., ambient $T = 25\,^{\circ}\mathrm{C}$, *solid line*) and indoors by a flash solar tester (*dashed line*). Cell temperature is about 50 °C outdoors and 25 °C indoors

Overall module conversion efficiency as high as 26.5% was measured at typical cell temperature of 25 °C in the indoor test. It should be noted that actual outdoor efficiency for modules could exceed 28% at lower ambient temperature, or with the use of the cells with indoor efficiencies in the range of 39–40%. Applying antireflection coatings on optical elements of such a module can help to increase the overall module efficiency up to 30–32%.

Solar PV modules with small-aperture area concentrators are compact, simple in structure and are characterized by lower material consumption in comparison with previous module designs. They ensure an "ideal" situation for the conversion of sun power, when a high optical concentration of sunlight is performed, but the distributed character of heat dissipation persists, inherent in the flat-plate photovoltaic modules without concentrators.

8.5 Perspectives of the Efficiency Increase in III–V Solar Cells

Figure 8.27 demonstrates the dynamics of the efficiency increase for III–V solar cells, single-crystal Si as well as thin-film Si solar cells during the last 50 years. Further, expected efficiency increase is shown by dashed curves. It is seen that efficiencies of the cells, based on thin-film and crystalline silicon ("one-sun" and concentrator cells) have almost reached their limit. The thin-film approach is the promising way to reduce the cost of solar electricity. Concentrator III–V arrays open the same opportunity due to the possibility of realizing a cost lower than that of crystalline Si arrays at module efficiencies higher than 30%.

The experience to date in the development of the triple-junction solar cells gives us reason to hope for achieving higher efficiency in four-, five- and, maybe, even

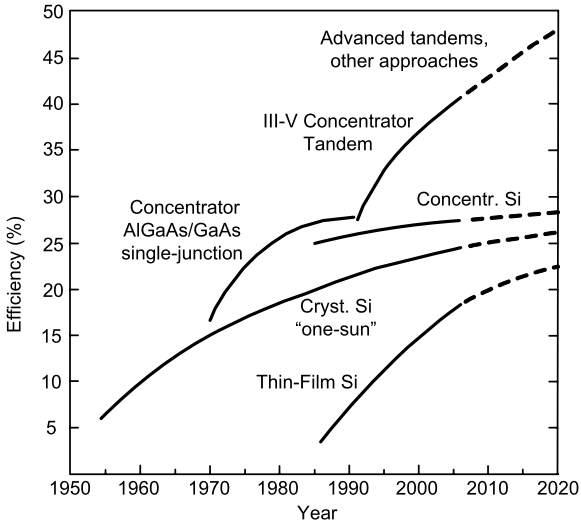

Fig. 8.27. Evolutions of achieved efficiencies till 2006 and predicted efficiencies of different types of solar cells (illumination under AM1.5 solar spectrum conditions)

more-junction structures. There are no scientific or theoretical doubts that these hopes will be justified when appropriate quality materials for intermediate cascades are found and grown. The search for these structures is under way, and several areas may be singled out. To increase the quantity of p–n junctions in MJ cells, the cost of such structures does not increase, because the total structure thickness remains the same owing to the possibility of reducing layer thickness in each cascade absorbing and converting a "narrower" part of the solar spectrum.

Complexity of the solar cell structures, namely, the multijunction structures, reduces the requirements for the bulk properties of the materials used. Indeed, the larger the number of junctions, the thinner the photoactive region in each junction and the weaker the effect of such a parameter as the minority carrier diffusion length on the efficiency of the device. The method for compensating insufficiently good bulk properties of a material by technological perfection of the multijunction cells has also begun to be used in the development of new types of thin-film solar arrays.

Solar thermophotovoltaics (TPV) [132, 133] is based on the principle of intermediate conversion of highly concentrated sunlight into radiation of a selective emitter heated up to 1200–1800 °C. At the second stage, photovoltaic conversion of this radiation occurs in a low-bandgap ($E_g = 0.5$–0.8 eV) photocell. Significant reserves for the increase in solar TPV efficiency lie in possibilities for the back effect of a photoconverter on radiation source (emitter of photons): the nonused photons can be reflected back to the radiator keeping it hot. Such a possibility is completely absent in current solar power systems. Therefore, the TPV generator is a complex system which should be more effective, if the principle of radiation recirculation is involved. A promising way for TPV converter efficiency to increase is the devel-

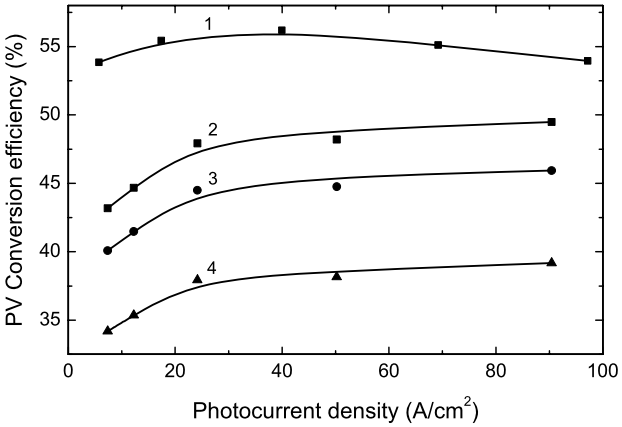

Fig. 8.28. Conversion efficiencies of GaAs (curve *1*) and GaSb (curves *2–4*) PV cells (designated illumination area is about 2 mm^2) as a function of the photocurrent density at monochromatic irradiation with wavelengths: *1* – 850 nm, *2* – 1680 nm, *3* – 1550 nm, *4* – 1315 nm

opment of selective emitters matched to PV cells. Such a selective emitter should radiate intensively at $h\nu > E_g$ and weakly at longer wavelengths. A similar role is played by an optical filter. This component is usefully included in a TPV system to return subbandgap-energy photons back to the emitter. It can be made as a dielectric stack (deposited on the cell or emitter surface, or arranged as a separate component), or as a metallic reflector on the rear surface of the cells. In other words, combining the filters, metal reflectors on the cell back and selective emitters, one has considerable room to shape the energy spectrum accepted by a cell. Theoretical conversion efficiency of the TPV approach is 84.5% and expected in practice is about 40%.

The possibility of high-efficiency PV conversion of selective radiation has been confirmed by experiments with PV conversion of the monochromatic radiation with the photon energy just a little higher than the cell band gap [134]. An efficiency of 56% was measured in GaAs-based cells under monochromatic illumination with wavelength of 850 nm, and efficiency of 49% was detected in a GaSb cell at $\lambda = 1680$ nm (Fig. 8.28).

Photocells with a graded bandgap in the photoactive region give additional possibilities for efficiency increase at a high excitation level, where the quantity of generated electron–hole pairs is higher than quantity of majority carriers. If a cell heterostructure has a gradient of the bandgap (ΔE_g) with a decrease in E_g from the front surface, the additional voltage arises owing to separation of electrons and holes, generated by photons of different energies in the different parts of the graded bandgap layer. In the case of a very high excitation level, the value of this additional voltage can be close to $\Delta E_g/q$ [135]. The theoretical efficiency limit in this approach is the same as for the infinite tandem cell stack. However, to use this effect, new semiconductor materials with special properties should be developed. Low-dimensional quantum well/dot structures open the door to preparation of such

materials and cells. Short-period superlattices were grown by MBE for fabrication of the graded band gap layers in the laser structures [136]. Excellent heterointerface smoothness has been obtained, resulting in high internal quantum efficiency of radiation recombination. The low threshold current in these lasers was the world record for a long time and served as a good demonstration of the superlattice application for fabrication of graded bandgap layers of high quality.

Hot carrier cells should use the energy of photogenerated carries before their thermalization and collection by a p–n junction. The efficiency limit in this approach is the same as that for tandem cells. However, to realize this approach, carrier cooling rates should be reduced sufficiently, or radiative recombination rates should be sufficiently accelerated. Thus, special materials with particular band structures should be developed for these cells.

Multiple electron–hole pair cells with quantum efficiency higher than unity also allow for increase in efficiency. The theoretical efficiency for an idealized cell of such a type is the same as for the infinite tandem cell stack. Several electron–hole pairs should be generated by each incident photon in this case. The higher-than-one quantum efficiency behavior was actually found, although very close to one, for high-energy visible photons and for UV photons. However, competitive processes of the carrier energy relaxation are too efficient, which have not allowed for noticeable improvement in solar cell performance until now.

Analyzing current trends in physics of semiconductors, for instance, progress in the development of third-generation injection lasers, one finds primarily wider use of the quantum dot (QD) heterostructures [137]. A new approach involving the use of materials with QDs has been proposed for solar cell development as well: the creation of an photoactive medium with an "intermediate band" [138]. A semiconductor material for such cells should have an intermediate half-filled (or metallic) band close to the center of the forbidden gap. In addition to the conventional abandoning electrons from the valence to the conduction band by absorption of high-energy photons, abandoning to/from intermediate band to the conduction band can be realized by absorption of low energy photons. This three-photon effect ensures a better utilization of the sunlight energy. Voltage degradation is expected to be prevented by the existence of three separated quasi-Fermi levels, each one related to every existing band. The maximum efficiency of 63% was calculated for a cell with the bandgap of 1.95 eV and intermediate band Fermi level located at 0.71 eV from one of the bands. The generalization of this concept to more than two intermediate bandgaps (multiband solar cells) gives maximum theoretical efficiency as high as 86.8%, which is identical to the efficiency of a large stack of tandem cells. Low-dimensional structures can constitute a way for engineering the intermediate band concept. In addition, quantum mechanical calculations have shown that, in principle, it is possible to arrange atoms of a bulk material in such a way that it can exhibit the required intermediate band.

8.6 Conclusion

At present, III–V heterostructure solar cells are already widely used for space applications. Progress in terrestrial applications of III–V solar cells is associated with the development of cells with efficiencies exceeding 45% at the concentrated sunlight. These devices can form a technical basis for large-scale solar power engineering in the future. In this case, a considerable amount of electrical energy supplying our homes will be generated by heterostructure solar cells illuminated by the sun through the concentrators.

There are legends to the effect that, in the antique times, priests used concentrated sunlight during ritual ceremonies for setting the Holy Fire in temples. From that arose the traditional way to set the Olympic Fire. Historically, the first utilitarian use of concentrated sunlight took place for military purposes: Grecians, on Archimedes' initiative, set fire to the ships of Romans who besieged Syracuse in 212 B.C. The Grecian soldiers directed the sunbeams toward the targets using a great number of polished metallic shields. Only in recent history have people again turned to the idea of the practical application of concentrated sunlight, creating solar furnaces for highly refractory materials, as well as solar power plants with steam cycles. It might be well to point out that the direct conversion of concentrated sunlight into electric power by means of highly efficient cascade solar cells is, as we have seen from the above, one of the main ways for satisfying the power demands of the mankind. It is significant that at present there is no particular application of this technology for creating weapons – now, and also in the foreseeable future. Hence, development, harnessing and fostering widespread use of the technology are not burdened by additional risks for humanity. Quite the contrary, this will aid in reducing the presently discussed greenhouse effects.

There are other alternative, yet also promising technologies for future power generation. For example, one could use atomic energy. At the very beginning, this technology was intended to create a new type of weapon. This was soon realized with the creation of bombs with unprecedented destructive power. The military aspect of this technology remains quite actual and, for many, attractive. And this precarious situation persists today, although atomic power plants were also built during a very short period of time. Thus, hopes have arisen of creating an inexhaustible power source using thermonuclear reactions. If the risks associated with plausible catastrophes on atomic plants, and the problems of the radioactive waste burial, are added to the risk of nuclear weapon proliferation, the public anxieties connected with atomic technology development become understandable.

On the other hand, a generalized situation with energy could be outlined in the following way. Why build many dangerous nuclear reactors on our planet Earth if there already exists a huge, safe and inexhaustible reactor – the sun – which sends an abundance of power to the Earth in the form of sunlight? Our task rests "only" on the reasonable and effective use of this power.

References

1. W. Shockley, Circuit Element Utilizing Semiconductor Material. U.S. Patent 2269347, September 25, 1951
2. A.I. Gubanov, Theory of the contact between two semiconductors with different types of conduction. Zh. Tekh. Fiz. **20**, 1287 (1950)
3. H. Kroemer, Theory of a wide-gap emitter for transistors. Proc. IRE **45**, 1535 (1957)
4. Z.I. Alferov, The double heterostructure: concept and its applications in physics, electronics and technology. Les prix Nobel, Norstedts Tryckeri, Stockholm, 2001, pp. 65–93
5. H. Kroemer, A proposed class of heterojunction injection lasers. Proc. IEEE **51**, 1782 (1963)
6. Z.I. Alferov, V.B. Khalfin, R.F. Kazarinov, A characteristic feature of injection into heterojunctions. Fiz. Tverd. Tela **8**, 3102–3105 (1966) [Sov. Phys. Solid State **8**, 2480 (1967)]
7. Z.I. Alferov, Possible development of a rectifier for very high current densities on the bases of a p–i–n (p–n–n^+, n–p–p^+) structure with heterojunctions. Fiz. Tekh. Poluprovodn. **1**, 436–438 (1966) [Sov. Phys. Semicond. **1**, 358–361 (1967)]
8. R.L. Anderson, Germanium-gallium arsenide heterojunctions. IBM J. Res. Develop. **4**, 283 (1960)
9. Z.I. Alferov, V.M. Andreev, V.I. Korol'kov, D.N. Tret'yakov, V.M. Tuchkevich, High-voltage p–n junctions in $Ga_xAl_{1-x}As$ crystals. Fiz. Tekh. Poluprovodn. **1**, 1579–1581 (1967) [Sov. Phys. Semicond. **1**, 1313–1314 (1968)]
10. H.S. Rupprecht, J.M. Woodall, G.D. Pettit, Efficient visible electroluminescence at 300 K from $Ga_{1-x}Al_xAs$ p–n junctions grown by liquid-phase epitaxy. Appl. Phys. Lett. **11**, 81 (1967)
11. Z.I. Alferov, V.M. Andreev, V.I. Korol'kov, E.L. Portnoi, D.N. Tret'yakov, Injection properties of n–$Al_xGa_{1-x}As$-p-GaAs heterojunctions. Fiz. Tekh. Poluprovodn. **2**, 1016–1017 (1968) [Sov. Phys. Semicond. **2**, 843–844 (1969)]
12. Z.I. Alferov, V.M. Andreev, V.I. Korol'kov, E.L. Portnoy, D.N. Tret'yakov, Coherent radiation of epitaxial heterojunction structures in the AlAs–GaAs system. Fiz. Tekh. Poluprovodn. **2**, 1545–1547 (1968) [Sov. Phys. Semicond. **2**, 1289–1291 (1969)]
13. Z.I. Alferov, V.M. Andreev, V.I. Korol'kov, E.L. Portnoi, D.N. Tret'yakov, Recombination radiation in epitaxial structures in the AlAs–GaAs system, in *Proc. IX Int. Conf. on the Physics of Semiconductors*, Moscow, 1968, 1 (Nauka, Leningrad, 1968), pp. 504–510
14. Z.I. Alferov, V.M. Andreev, E.L. Portnoy, M.K. Trukan, AlAs–GaAs heterojunctions injection lasers with a low room-temperature threshold. Fiz. Tekh. Poluprovodn. **3**, 1328–1332 (1969) [Sov. Phys. Semicond. **3**, 1107–1110 (1970)]
15. I. Hayashi, Heterostructure lasers. IEEE Trans. Electron Devices **ED-31**, 1630–1645 (1984)
16. Z.I. Alferov, V.M. Andreev, D.Z. Garbuzov, Y.V. Zhilyaev, E.P. Morozov, E.L. Portnoi, V.G. Trofim, Investigation of the influence of the AlAs–GaAs heterostructure parameters on the laser threshold current and the realization of continuous emission at the room temperature. Fiz. Tekh. Poluprovodn. **4**, 1826–1829 (1970) [Sov. Phys. Semicond. **4**, 1573–1575 (1971)]
17. I. Hayashi, M.B. Panish, P.W. Foy, S. Sumski, Junction lasers which operate continuously at room temperature. Appl. Phys. Lett. **17**, 109–111 (1970)

18. Z.I. Alferov, V.M. Andreev, V.I. Korol'kov, E.L. Portnoi, A.A. Yakovenko, Spontaneous radiation sources based on structures with AlAs–GaAs heterojunctions. Fiz. Tekh. Poluprovodn. **3**, 930–933 (1969) [Sov. Phys. Semicond. **3**, 785–787 (1970)]
19. Z.I. Alferov, V.M. Andreev, M.B. Kagan, I.I. Protasov, V.G. Trofim, Solar-energy converters based on p–n $Al_xGa_{1-x}As$–GaAs heterojunctions. Fiz. Tekh. Poluprovodn. **4**, 2378–2379 (1970) [Sov. Phys. Semicond. **4**, 2047–2048 (1971)]
20. Z.I. Alferov, F.A. Ahmedov, V.I. Korol'kov, V.G. Nikitin, Phototransistor utilizing a GaAs–AlAs heterojunction. Fiz. Tekn. Poluprovodn. **7**, 1159–1163 (1973) [Sov. Phys. Semicond. **7**, 780–782 (1973)]
21. Z.I. Alferov, V.M. Andreev, V.I. Korol'kov, V.G. Nikitin, A.A. Yakovenko, p–n–p–n structures based on GaAs and on $Al_xGa_{1-x}As$ solid solutions. Fiz. Tekn. Poluprovodn. **4**, 578–581 (1970) [Sov. Phys. Semicond. **4**, 481–483 (1971)]
22. Z.I. Alferov, V.M. Andreev, S.G. Konnikov, V.G. Nikitin, D.N. Tret'yakov, Heterojunctions on the base of III–V semiconducting and of their solid solutions, in *Proc. Int. Conf. Phys. Chem. Semicond. Heterojunctions and Layer Structures*, Budapest, 1970, 1, ed. by G. Szigeti (Academiai Kiado, Budapest, 1971), pp. 93–106
23. G.A. Antipas, R.L. Moon, L.W. James, J. Edgecumbe, R.L. Bell, In Gallium Arsenide and Related Compounds. Conf. Ser. IOP **17**, 48 (1973)
24. A.P. Bogatov, L.M. Dolginov, L.V. Druzhinina, P.G. Eliseev, L.N. Sverdlova, E.G. Shevchenko, Heterolasers on the base of solid solutions $Ga_xIn_{1-x}As_yP_{1-y}$ and $Al_xGa_{1-x}Sb_yAs_{1-y}$. Kvantovaya Electron. **1**, 2294 (1974) [Sov. J. Quantum Electron **1**, 1281 (1974)]
25. Z.I. Alferov, I.N. Arsent'ev, D.Z. Garbuzov, S.G. Konnikov, V.D. Rumyantsev, Generation of coherent radiation in $pGa_{0.5}In_{0.5}P$–$pGa_{x\sim0.55}In_{1-x}As_{y\sim0.10}P_{1-y}$–$nGa_{0.5}In_{0.5}P$. Pisma Zh. Tech. Fiz. **1**, 305–310 (1975) [Sov. Phys. Tech. Phys. Lett. **1**, 147–148 (1975)]
26. D. Flood, H. Brandhorst, Space solar cells, in *Current Topics in Photovoltaics,* vol. 2, ed. by T.J. Coutts, J.D. Meakin (Academic, New York, 1987), pp. 143–202
27. S.G. Bailey, D.J. Flood, Space Photovoltaics. Prog. Photovolt.: Res. Appl. **6**(1), 1–14 (1998)
28. V.M. Andreev, V.A. Grilikhes, V.D. Rumyantsev, *Photovoltaic Conversion of Concentrated Sunlight* (Wiley, New York, 1997)
29. H.J. Hovel, J.M. Woodall, High-efficiency AlGaAs–GaAs solar cells. Appl. Phys. Lett. **21**, 379–381 (1972)
30. V.M. Andreev, T.M. Golovner, M.B. Kagan, N.S. Koroleva, T.A. Lubochevskaya, T.A. Nuller, D.N. Tret'yakov, Investigation of high efficiency AlGaAs–GaAs solar cells. Sov. Phys. Semicond. **7**(12) (1973)
31. Z.I. Alferov, V.M. Andreev, G.S. Daletskii, M.B. Kagan, N.S. Lidorenko, V.M. Tuchkevich, Investigation of high efficiency AlAs–GaAs heteroconverters, in *Proc. World Electrotechn. Congress*, Moscow, 1977, Section 5A, report 04
32. H.J. Hovel, *Semiconductors and Semimetals*, ed. by Willardson, R.K., Beer, A.C. Solar Cells, vol. 11 (Academic, New York, 1975)
33. V.M. Andreev, III–V heterostructure photovoltaics in Russia, in *Proceedings of 17th European Photovoltaic Solar Energy Conference*, 2000, pp. xxxi–xxxii
34. J.M. Woodall, H.J. Hovel, An isothermal etchback-regrowth method for high efficiency $Ga_{1-x}Al_xAs$–GaAs solar cells. Appl. Phys. Lett. **30**, 492–493 (1977)
35. V.M. Andreev, V.R. Larionov, V.D. Rumyantsev, O.M. Fedorova, S.S. Shamukhamedov, P AlGaAs–pGaAs–nGaAs solar cells with efficiencies of 19% at AM0 and 24% at AM1.5. Sov. Tech. Phys. Lett. **9**(10), 537–538 (1983)

36. H.J. Hovel, Novel materials and devices for sunlight concentrating systems. IBM J. Res. Dev. **22**, 112–121 (1978)
37. E. Fanetti, C. Flores, G. Guarini, F. Paletta, D. Passoni, High efficiency 1.43 and 1.69 eV band gap Ga_{1-x} Al_xAs–GaAs solar cells for multicolor applications. Solar cells **3**, 187–194 (1981)
38. R.C. Knechtly, R.Y. Loo, G.S. Kamath, High-efficiency GaAs solar cells. IEEE Trans. Electron Dev. **ED-31**(5), 577–588 (1984)
39. H.S. Rauschenbach, *Solar Cell array Design Handbook. The Principles and Technology of Photovoltaic Energy Conversion* (Litton Educational Publishing, New York, 1980)
40. A. Luque, *Solar Cells and Optics for Photovoltaic Concentration* (Adam Hilger, Bristol, 1989)
41. L.D. Partain (ed.), *Solar Cells and Their Application* (Wiley, New York, 1995)
42. P.A. Iles, Future of photovoltaic for space applications. Prog. Photovolt.: Res. Appl. **8**, 39–51 (2000)
43. V.M. Andreev, A.B. Kazantsev, V.P. Khvostikov, E.V. Paleeva, V.D. Rumyantsev, M.Z. Shvarts, High-efficiency (24.6%, AM0) LPE grown AlGaAs/GaAs concentrator solar cells and modules, in *Conf. Record First World Conference on Photovoltaic Energy Conversion*, 1994, pp. 2096–2099
44. V.M. Andreev, V.D. Rumyantsev, A^3B^5 based solar cells and concentrating optical elements for space PV modules. Solar Energy Mater. Solar Cells **44**, 319–332 (1996)
45. R.D. Dupuis, P.D. Dapkus, R.D. Vingling, L.A. Moundy, High-efficiency GaAlAs/GaAs heterostructure solar cells grown by metalorganic chemical vapor deposition. Appl. Phys. Lett. **31**, 201–203 (1977)
46. N.J. Nelson, K.K. Jonson, R.L. Moon, H.A. Vander Plas, L.W. James, Organometallic-sourced VPE AlGaAs/GaAs concentrator solar cells having conversion efficiencies of 19%. Appl. Phys. Lett. **33**, 26–27 (1978)
47. J.G. Werthen, G.F. Virshup, C.W. Ford, C.R. Lewis, H.C. Hamaker, 21% (one sun, air mass zero) 4 cm^2 GaAs space solar cells. Appl. Phys. Lett. **48**, 74–75 (1986)
48. S.P. Tobin, S.M. Vernon, S.J. Woitczuk, C. Baigar, M.M. Sanfacon, T.M. Dixon, Advanced in high-efficiency GaAs solar cells, in *Conf. Record 21st IEEE Photovoltaic Specialists Conference*, 1990, pp. 158–162
49. S.P. Tobin, S.M. Vernon, M.M. Sanfacon, A. Mastrovito, Enhanced light absorption in GaAs solar cells with internal Bragg reflector, in *Conf. Record 22nd IEEE Photovoltaic Spesialists Conference*, 1991, pp. 147–152
50. V.M. Andreev, V.V. Komin, I.V. Kochnev, V.M. Lantratov, M.Z. Shvarts, High-efficiency AlGaAs–GaAs solar cells with internal Bragg reflector, in *Conf. Record First World Conference on Photovoltaic Energy Conversion*, 1994, pp. 1894–1897
51. M.Z. Shvarts, O.I. Chosta, I.V. Kochnev, V.M. Lantratov, V.M. Andreev, Radiation resistant AlGaAs/GaAs concentrator solar cells with internal Bragg reflector. Solar Energy Mater. Solar Cells **68**, 105–122 (2001)
52. M. Yamaguchi, Space solar cell R&D activities in Japan, in *Proceeding 15th Space Photovoltaic Research and Technology*, 1997, pp. 1–10
53. C.C. Fan, B.-Y. Tsaur, B.J. Palm, Optimal design of high-efficiency tandem cells, in *Conf. Record 16th IEEE Photovoltaic Specialists Conf.*, 1982, pp. 692–698
54. M.A. Green, *Solar Cells* (Prentice-Hall, New Jersey, 1982)
55. M.F. Lamorte, D.H. Abbott, Computer modeling of a two-junction, monolithic cascade solar cell. IEEE Trans. Electron. Dev. **ED-27**, 231–249 (1980)
56. M.B. Spitzer, C.C. Fan, Multijunction cells for space applications. Solar Cells **29**, 183–203 (1990)

57. L.M. Fraas, High-efficiency III–V multijunction solar cells, in *Solar Cells and Their Applications*, ed. by L.D. Partain (Wiley, New York, 1995), pp. 143–162
58. R.K. Jain, D.J. Flood, Monolithic and mechanical multijunction space solar cells. J. Solar Energy Eng. **115**, 106–111 (1993)
59. L.M. Fraas, J.E. Avery, J. Martin, V.S. Sundaram, G. Giard, V.T. Dinh, T.M. Davenport, J.W. Yerkes, M.J. O'Neil, Over 35-percent efficient GaAs/GaSb tandem solar cells. IEEE Trans. Electron. Dev. **37**, 443–449 (1990)
60. S.R. Kurtz, D. Myers, J.M. Olson, Projected performance of three- and four-junction devices using GaAs and GaInP, in *Proc. 26th IEEE Photovoltaic Specialists Conf.*, 1997, pp. 875–878
61. M. Yamaguchi, Multi-junction solar cells: present and future, in *Technical Digest 12th International Photovoltaic Solar Energy Conference*, 2001, pp. 291–294
62. A.W. Bett, F. Dimroth, G. Stollwerk, O.V. Sulima, III–V compounds for solar cell applications. Appl. Phys. **A69**, 119–129 (1999)
63. M. Yamaguchi, A. Luque, High efficiency and high concentration in photovoltaics. IEEE Trans. Electron Devices **46**(10), 41–46 (1999)
64. M.W. Wanlass, J.S. Ward, K.A. Emery, T.A. Gessert, C.R. Osterwald, T.J. Coutts, High performance concentrator tandem solar cells based on IR-sensitive bottom cells. Solar Cells **30**, 363–371 (1991)
65. V.M. Andreev, L.B. Karlina, A.B. Kazantsev, V.P. Khvostikov, V.D. Rumyantsev, S.V. Sorokina, M.Z. Shvarts, Concentrator tandem solar cells based on AlGaAs/GaAs–InP/InGaAs (or GaSb) structures, in *Conf. Record First World Conference on Photovoltaic Energy Conversion*, 1994, pp. 1721–1724
66. V.M. Andreev, V.P. Khvostikov, E.V. Paleeva, V.D. Rumyantsev, S.V. Sorokina, M.Z. Shvarts, V.I. Vasil'ev, Tandem solar cells based on AlGaAs/GaAs and GaSb structures, in *Proc. 23d International Symposium on Compound Semiconductors*, 1996, pp. 425–428
67. V.M. Andreev, R&D of III–V compound solar cells in Russia, in *Technical Digest of 11th International Photovoltaic Solar Energy Conference*, 1999, pp. 589–592
68. M. Umeno, T. Kato, M. Yang, Y. Azuma, T. Soga, T. Jimbo, High efficiency AlGaAs/Si tandem solar cell over 20%, in *Conf. Record First World Conference on Photovoltaic Energy Conversion*, 1994, pp. 1679–1684
69. B.-C. Chung, G.F. Virshup, M. Ladle Ristow, M.W. Wanlass, 25.2%-efficiency (1-sun, air mass 0) AlGaAs/GaAs/InGaAsP three-junction, two-terminal solar cells, in *Conf. Record 22nd IEEE Photovoltaic Specialists Conference*, 1991, pp. 54–57
70. V.M. Andreev, V.P. Khvostikov, V.D. Rumyantsev, E.V. Paleeva, M.Z. Shvarts, Monolithic two-junction AlGaAs/GaAs solar cells, in *Proc. 26th IEEE Photovoltaic Specialists Conference*, 1997, pp. 927–930
71. M.L. Timmons, J.A. Hutchley, D.K. Wagner, J.M. Tracy, Monolithic AlGaAs/Ge cascade cell, in *Proc. of 21st IEEE Photovoltaic Specialists Conference*, 1988, pp. 602–606
72. S.P. Tobin, S.M. Vernon, C. Bajgar, V.E. Haven, L.M. Geoffroy, M.M. Sanfacon, D.R. Lillington, R.E. Hart, K.A. Emery, R.L. Matson, High efficiency GaAs/Ge monolithic tandem solar cells, in *Proc. 20th IEEE Photovoltaic Specialists Conference*, 1988, pp. 405–410
73. P.A. Iles, Y.-C.M. Yeh, F.N. Ho, C.L. Chu, C. Cheng, High-efficiency (>20% AM0) GaAs solar cells grown on inactive Ge substrates. IEEE Electron Device Lett. **11**(4), 140–142 (1990)

74. S. Wojtczuk, S. Tobin, M. Sanfacon, V. Haven, L. Geoffroy, S. Vernon, Monolithic two-terminal GaAs/Ge tandem space concentrator cells, in *22nd IEEE Photovoltaic Specialists Conference*, 1991, pp. 73–79
75. P.A. Iles, Y.-C.M. Yeh, Silicon, gallium arsenide and indium phosphide cells: single junction, one sun space, in *Solar Cells and Their Applications*, ed. by L.D. Partain (Wiley, New York, 1995), pp. 99–121
76. J.M. Olson, S.R. Kurtz, A.E. Kibbler, P. Faine, Recent advances in high efficiency $GaInP_2$/GaAs tandem solar cells, in *Proc. 21st IEEE Photovoltaic Specialists Conference*, 1990, pp. 24–29
77. K.A. Bertness, S.R. Kurtz, D.J. Friedman, A.E. Kibbler, C. Kramer, J.M. Olson, High-efficiency GaInP/GaAs tandem solar cells for space and terrestrial applications, in *Conf. Record First World Conference on Photovoltaic Energy Conversion*, 1994, pp. 1671–1678
78. P.K. Chiang, D.D. Krut, B.T. Cavicchi, K.A. Bertness, S.R. Kurtz, J.M. Olson, Large area GaInP/GaAs/Ge multijunction solar cells for space application, in *Conf. Record First World Conference on Photovoltaic Energy Conversion*, 1994, pp. 2120–2123
79. P.K. Chiang, J.H. Ermer, W.T. Niskikawa, D.D. Krut, D.E. Joslin, J.W. Eldredge, B.T. Cavicchi, Experimental results of $GaInP_2$/GaAs/Ge triple junction cell development for space power systems, in *Conf. Record 25th IEEE Photovoltaic Specialists Conference*, 1996, pp. 183–186
80. R.R. King, N.H. Karam, J.H. Ermer, M. Haddad, P. Colter, T. Isshiki, H. Yoon, H.L. Cotal, D.E. Joslin, D.D. Krut, R. Sudharsanan, K. Edmondson, B.T. Cavicchi, D.R. Lillington, Next-generation, high-efficiency III–V multijunction solar cells, in *Proceedings of 28th IEEE Photovoltaic Specialists Conference*, 2000, pp. 998–1005
81. R.R. King, C.M. Fetzer, P.C. Colter, K.M. Edmondson, J.H. Ermer, H.L. Cotal, H. Yoon, A.P. Stavrides, G. Kinsey, D.D. Krut, N.H. Karam, High-efficiency space and terrestrial multijunction solar cells trough bandgap control in cell structures, in *Proc. 29th IEEE Photovoltaic Specialists Conference*, 2002, pp. 776–779
82. R.R. King, R.A. Sherif, D.C. Law, J.T. Yen, M. Haddad, C.M. Fetzer, K.M. Edmondson, G. Kinsey, H. Yoon, M. Joshi, S. Mesropian, New horizons in III–V multijunction terrestrial concentrator cells research, in *Proceedings of 21st European Photovoltaic Solar Energy Conference*, Dresden, 2006, pp. 124–128
83. P.K. Chiang, C.L. Chu, Y.C.M. Yeh, P. Iles, G. Chen, J. Wei, P. Tsung, J. Olbinski, J. Krogen, S. Halbe, S. Khemthong, Achieving 26% triple junction cascade solar cell production, in *Proc. 28th IEEE Photovoltaic Specialists Conference*, 2000, pp. 1002–1005
84. H.Q. Hou, P.R. Sharps, N.S. Fatemi, N. Li, M.A. Stan, P.A. Martin, B.E. Hammons, F. Spadafora, Very high efficiency InGaP/GaAs dual-junction solar cell manufacturing at Emcore Photovoltaics, in *Proc. 28th IEEE Photovoltaic Specialists Conference*, 2000, pp. 1173–1176
85. A.W. Bett, F. Dimroth, G. Lange, M. Meusel, R. Beckert, M. Hein, S.V. Riesen, U. Schubert, 30% monolithic tandem concentrator solar cells for concentrations exceeding 1000 suns, in *Proc. 28th IEEE Photovoltaic Specialists Conference*, 2000, pp. 961–964
86. F. Dimroth, U. Schubert, A.W. Bett, J. Hilgarth, M. Nell, G. Strobl, K. Bogus, C. Signorini, Next generation GaInP/GaInAs/Ge multijunction space solar cells, in *Proc. 17th European Photovoltaic Specialists Conference*, 2001, pp. 2150–2154
87. R.R. King, M. Haddad, T. Isshiki, P. Colter, J. Ermer, H. Yoon, D.E. Joslin, N.H. Karam, Metamorphic GaInP/GaInAs/Ge solar cells, in *Proc. 28th IEEE Photovoltaic Specialists Conference*, 2000, pp. 982–985

88. M.A. Green, K. Emery, D.L. King, Y. Nishikawa, W. Warta, Solar cell efficiency tables (version 29). Prog. Photovolt.: Res. Appl. **15**, 35–40 (2007)
89. V.M. Andreev, A.B. Kazantsev, V.P. Khvostikov, E.V. Paleeva, V.D. Rumyantsev, M.Z. Shvarts, High-efficiency (24.6%, AM0) LPE grown AlGaAs/GaAs concentrator solar cells and modules, in *Proceedings of 1st World Conference on Photovoltaic Energy Conversion*, Hawaii, 1994, pp. 2096–2099
90. S.G. Bailey, D.J. Flood, Space photovoltaics. Prog. Photovolt.: Res. Appl. **6**, 1–14 (1998)
91. C. Algora, E. Ortiz, I. Rey-Stolle, V. Diaz, P. Pena, V.M. Andreev, V.P. Khvostikov, V.D. Rumyantsev, A GaAs solar cell with efficiency of 26.2% at 1000 suns and 25.0% at 2000 suns. IEEE Trans. Electron Devices **48**(5), 840–844 (2001)
92. V.M. Andreev, V.P. Khvostikov, V.R. Larionov, V.D. Rumyantsev, E.V. Paleeva, M.Z. Shvarts, C. Algora, 5800 Suns AlGaAs/GaAs concentrator solar cells, in *Technical Digest of the International Photovoltaic Science and Engineering Conference*, Sapporo, Japan, 1999, pp. 147–148
93. M.Z. Shvarts, O.I. Chosta, I.V. Kochnev, V.M. Lantratov, V.M. Andreev, Radiation resistant AlGaAs/GaAs concentrator solar cells with internal Bragg reflector. Solar Energy Mater. Solar Cells **68**, 105–122 (2001)
94. V.M. Andreev, I.V. Kochnev, V.M. Lantratov, S.A. Mintairov, V.D. Rumyantsev, M.Z. Shvarts, Ultra-violet sensitive infra-red reflective AlGaAs/GaAs solar cells with two Bragg reflectors, in *Proc. of the 16th European Photovoltaic Solar Energy Conference*, Glasgow, 2000, pp. 1019–1021
95. M.W. Wanlass, J.S. Ward, K.A. Emery, T.A. Gessert, C.R. Osterwald, T.J. Coutts, High performance concentrator tandem solar cells based on IR-sensitive bottom cells. Solar Cells **30**, 363–371 (1991)
96. B.-C. Chung, G.F. Virshup, S. Hikido, N.R. Kaminar, 27.6% efficiency (1 sun, air mass 1.5) monolithic $Al_{0.37}Ga_{0.63}As$/GaAs two junction cascade solar cell with prismatic cover glass. Appl. Phys. Lett. **55**, 1741–1743 (1989)
97. V.M. Andreev, V.P. Khvostikov, E.V. Paleeva, V.D. Rumyantsev, S.V. Sorokina, M.Z. Shvarts, V.I. Vasil'ev, Tandem solar cells based on AlGaAs/GaAs and GaSb structures, in *Proc. 23rd International Symposium on Compound Semiconductors*, St. Petersburg, Russia, Sept. 23–27, 1996
98. D.J. Friedman, S.R. Kurtz, K.A. Bertness, A.E. Kibbler, C. Kramer, J.M. Olson, D.L. King, B.R. Hansen, J.K. Snyder, GaInP/GaAs monolithic tandem concentrator cells, in *Proceedings of the 1st World Conference on Photovoltaic Energy Conversion*, Waikoloa, Hawaii, USA, 1994, pp. 1829–1832
99. R.R. King, D.C. Law, C.M. Fetzer, R.A. Sherif, K.M. Edmondson, S. Kurtz, G.S. Kinsey, H.L. Cotal, D.D. Krut, J.H. Ermer, N.H. Karam, Pathways to 40%-efficient concentration photovoltaics, in *Proc. 20th European PVSEC*, Barcelona, Spain, 2005, pp. 6–10
100. F. Dimroth, R. Beckert, M. Meusel, U. Schubert, A.W. Bett, Metamorphic $Ga_yIn_{1-y}P/Ga_{1-x}In_xAs$ tandem solar cells for space and for terrestrial concentrator applications at $C > 1000$ suns. Prog. Photovolt.: Res. Appl. **9**(3), 165–178 (2001)
101. D.J. Aiken, M.A. Stan, S.P. Endicter, G. Girard, P.R. Sharps, A loss analysis for a 28% efficient 520x concentrator module, in *Proceedings of the IEEE 4th World Conference on Photovoltaic Energy Conversion*, Hawaii, 7–12 May 2006, pp. 686–689
102. M. Yamaguchi, Y. Okada, A. Yamamoto, T. Takamoto, K. Araki, Y. Ohshita, Novel materials and structures for high efficiency multi-junction solar cells, in *Proceedings at the 21st European Photovoltaic Solar Energy Conference*, Dresden, 2006, pp. 53–56

103. R.R. King, D.C. Law, K.M. Edmondson, C.M. Fetzer, G.S. Kinsey, D.D. Krut, J.H. Ermer, R.A. Sherif, N.H. Karam, Metamorphic concentrator solar cells with over 40% conversion efficiency, in *Proceedings for 4th International Conference on Solar Concentrators (ICSC-4)*, El Escorial, Spain, 2007, pp. 5–8
104. M.Z. Shvarts, P.Y. Gazaryan, V.P. Khvostikov, V.M. Lantratov, N.K. Timoshina, InGaP/GaAs–GaSb and InGaP/GaAs/Ge–InGaAsSb hybrid monolithic/stacked tandem concentrator solar cells, in *Proceedings at the 21st European Photovoltaic Solar Energy Conference*, Dresden, 2006, pp. 133–136
105. V.M. Andreev, V.P. Khvostikov, V.D. Rumyantsev, O.A. Khvostikova, P.Y. Gazaryan, A.S. Vlasov, N.A. Sadchikov, S.V. Sorokina, Y.M. Zadiranov, M.Z. Shvarts, Termophotovoltaic converters with solar powered high temperature emitters, in *Proceedings of the 20th European Photovoltaic Solar Energy Conference*, Barcelona, June 2005, pp. 8–13
106. V.M. Andreev, A.S. Vlasov, V.P. Khvostikov, O.A. Khvostikova, P.Y. Gazaryan, N.A. Sadchikov, Sun powered TPV converters based on GaSb cells, in *Proceedings at the 21st European Photovoltaic Solar Energy Conference*, Dresden, 2006, pp. 35–38
107. L.W. Fraas, W.E. Daniels, H.X. Huang, L.E. Minkin, J.E. Avery, M.J. O'Neill, A.J. McDanal, M.F. Piszczor, 34% efficient InGaP/GaAs/GaSb cell-interconnected-circuits for line-focus concentrator arrays, in *Proceedings of the 17th European Photovoltaic Solar Energy Conference*, Munich, 2000, pp. 2300–2303
108. V.M. Andreev, V.P. Khvostikov, V.D. Rumyantsev, S.V. Sorokina, M.Z. Shvarts, Single-junction GaSb and tandem GaSb/InGaAsSb & AlGaAsSb/GaSb thermophotovoltaic cells, in *Proc. of the 28th IEEE PVSC*, Alaska, September, 2000, pp. 1265–1268
109. V.M. Andreev, E.A. Ionova, V.R. Larionov, V.D. Rumyantsev, M.Z. Shvarts, G. Glenn, Tunnel diode revealing peculiarities at I–V measurements in multijunction III–V solar cells, in *Proceedings of the IEEE 4th World Conference on Photovoltaic Energy Conversion*, Hawaii, 2006, pp. 799–802
110. Z.I. Alferov, V.M. Andreev, V.D. Rumyantsev, III–V heterostructures in photovoltaics, in *Concentrator Photovoltaics*, ed. by A. Luque and V. Andreev. Springer Series in Optical Sciences, vol. 130 (2007)
111. A.W. Bett, F. Dimroth, G. Siefer, Multi-Junction concentrator solar cells, in *Concentrator Photovoltaics*, ed. by A. Luque and V. Andreev. Springer Series in Optical Sciences, vol. 130 (2007)
112. M. Yamaguchi, K. Araki, T.T. Takamoto, Concentrator solar cell modules and systems developed in Japan, in *Concentrator Photovoltaics*, ed. by A. Luque and V. Andreev. Springer Series in Optical Sciences, vol. 130 (2007)
113. N.H. Karam, R.A. Sherif, R.R. King, Multijunction concentrator solar cells, an enabler for low-cost concentrating photovoltaic systems, in *Concentrator Photovoltaics*, ed. by A. Luque and V. Andreev. Springer Series in Optical Sciences, vol. 130 (2007)
114. M. Yamaguchi, K. Araki, T.T. Takamoto, Concentrator solar cell modules and systems developed in Japan, in *Concentrator Photovoltaics*, ed. by A. Luque and V. Andreev. Springer Series in Optical Sciences, vol. 130 (2007)
115. G. Sala, A. Luque, Past experiences and new challenges of PV concentrators, in *Concentrator Photovoltaics*, ed. by A. Luque and V. Andreev. Springer Series in Optical Sciences, vol. 130 (2007)
116. V.D. Rumyantsev, Terrestrial concentrator PV systems, in *Concentrator Photovoltaics*, ed. by A. Luque and V. Andreev. Springer Series in Optical Sciences, vol. 130 (2007)
117. Z.I. Alferov, V.M. Andreev, Kh.K. Aripov, V.R. Larionov, V.D. Rumyantsev, Pattern of autonomous solar installation with heterostructure solar cells and concentrators. Geliotechnica **2**, 3–6 (1981). Appl. Solar Energy, **2** (1981)

118. Z.I. Alferov, V.M. Andreev, Kh.K. Aripov, V.R. Larionov, V.D. Rumyantsev, Solar Photovoltaic installation with 200 Watt output based on AlGaAs-heterophotocells and reflective concentrators. Geliotechnika **6**, 3–6 (1981). Appl. Solar Energy, **6** (1981)
119. A.A. Vodnev, A.V. Maslov, V.D. Rumyantsev, Sh.Sh. Shamukhamedov, Experience on creation of the solar installations based on AlGaAs/GaAs-photocells with concentrators, in *Sunlight Concentrators for Photovoltaic Power Installations*, ed. by V.A. Grilikhes, Leningrad, Energoatomizdat, 1986, pp. 25–29 (in Russian)
120. V.M. Andreev, A.A. Alaev, A.B. Guchmazov, V.S. Kalinovsky, V.R. Larionov, K.Y. Rasulov, V.D. Rumyantsev, High-efficiency AlGaAs-heterophotocells operating with lens panels as the solar energy concentrators, in *Proc. of the all-Union Conference "Photovoltaic phenomena in semiconductors"*, Tashkent, 1989, pp. 305–306 (in Russian)
121. V.M. Andreev, V.R. Larionov, V.D. Rumyantsev, M.Z. Shvarts, High-efficiency solar concentrating GaAs–AlGaAs modules with small-size lens units, in *11th European Photovoltaic Solar Energy Conference and Exhibition – Book of Abstracts*; abstract No. 1A. 15, Montreux, Switzerland, 12–16 October, 1992
122. Project: INTAS96-1887, 1997–2000 years, Photovoltaic installation with sunlight concentrators. Final Report, 2000
123. V.D. Rumyantsev, M. Hein, V.M. Andreev, A.W. Bett, F. Dimroth, G. Lange, G. Letay, M.Z. Shvarts, O.V. Sulima, Concentrator array based on GaAs cells and Fresnel lens concentrators, in *Proceedings of the 16th European Photovoltaic Solar Energy Conference and Exhibition*, Glasgow, United Kingdom, 1–5 May 2000
124. V.D. Rumyantsev, V.M. Andreev, A.W. Bett, F. Dimroth, M. Hein, G. Lange, M.Z. Shvarts, O.V. Sulima, Progress in development of all-glass terrestrial concentrator modules based on composite Fresnel lenses and III–V solar cells, in *Proceedings of the 28th PVSC*, Anhorage, Alaska, 2000, pp. 1169–1172
125. A.W. Bett, C. Baur, F. Dimroth, G. Lange, M. Meusel, S. van Riesen, G. Siefer, V.M. Andreev, V.D. Rumyantsev, N.A. Sadchikov, FLATCON^{TM} – modules: technology and characterization, in *Proceedings of 3rd World Conference on Photovoltaic Energy Conversion 3O-D9-05*, 2003
126. V.M. Andreev, E.A. Ionova, V.D. Rumyantsev, N.A. Sadchikov, M.Z. Shvarts, Concentrator PV modules of "all-glass" design with modified structure, in *Proceedings of 3rd World Conference on Photovoltaic Energy Conversion 3P-C3-72*, 2003
127. Z.I. Alferov, V.D. Rumyantsev, Trends in the development of solar photovoltaics, in *Next Generation Photovoltaics*, IoP, 2004, pp. 19–49
128. V.D. Rumyantsev, N.A. Sadchikov, A.E. Chalov, E.A. Ionova, D.J. Friedman, G. Glenn, Terrestrial concentrator PV modules based on GaInP/GaAs/Ge TJ cells and minilens panels, in *Proceedings of the IEEE 4th World Conference on Photovoltaic Energy Conversion*, Hawaii, 2006, pp. 632–635
129. V.D. Rumyantsev, A.E. Chalov, E.A. Ionova, V.R. Larionov, N.A. Sadchikov, V.M. Andreev, Practical design of PV modules t for very high solar concentration, in *Proc. on CD of the Third Int. Conf. on Solar Concentrators for the Generation of Electricity or Hydrogen*, Scottsdale, Arizona, May 2005
130. V.D. Rumyantsev, N.A. Sadchikov, A.E. Chalov, E.A. Ionova, V.R. Larionov, V.M. Andreev, G.R. Smekens, E.W. Merkle, Pilot installation with "all-glass" concentrator PV modules, in *Proceedings at the 21st European Photovoltaic Solar Energy Conference*, Dresden, 2006, pp. 2097–2100
131. V.D. Rumyantsev, A.E. Chalov, N.Y. Davidyuk, E.A. Ionova, N.A. Sadchikov, V.M. Andreev, Solar concentrator modules with fresnel lens panels, in *Proc. of the Fourth Int. Conf. on Solar Concentrators for the Generation of Electricity or Hydrogen*, El Escorial, Spain, 2007, pp. 33–36

132. P.A. Davies, A. Luque, Solar thermophotovoltaics: brief review and a new look. Solar Energy Mater. Solar Cells **33**, 11–22 (1994)
133. V. Andreev, V. Khvostikov, A. Vlasov, Solar thermophotovoltaics, in *Concentrator Photovoltaics*, ed. by A. Luque and V. Andreev. Springer Series in Optical Sciences, vol. 130, 2007
134. V.M. Andreev, V.A. Grilikhes, V.P. Khvostikov, O.A. Khvostikova, V.D. Rumyantsev, N.A. Sadchikov, M.Z. Shvarts, Concentrator PV modules and solar cells for TPV systems. J. Solar Energy Mater. Solar Cells **84**, 3–17 (2004)
135. Z.I. Alferov, V.M. Andreev, Yu.M. Zadiranov, V.I. Korol'kov, N. Rahimov, T.S. Tabarov, Photo-EMF in $Al_xGa_{1-x}As$ graded band-gap heterostructures. Pisma Z. Tech. Fiz. **4**, 369–372 (1978) [Sov. Tech. Phys. Lett. **4**(4), 149–150 (1978)]
136. Z.I. Alferov, A.M. Vasiliev, S.V. Ivanov, P.S. Kop'ev, N.N. Ledentsov, M.E. Lutsenko, B.Y. Melser, V.M. Ustinov, Reducing the threshold in GaAs–AlGaAs DHS SCH quantum well lasers ($j_{th} = 52$ A/cm^2, $T = 300$ K) with quantum well restriction by short period superlattice of variable period. Pisma Z. Techn. Fiz. **14**, 1803–1806 (1988) [Sov. Tech. Phys. Lett. **14**, 782 (1988)]
137. Z.I. Alferov, N.A. Bert, A.Y. Egorov, A.E. Zhukov, P.S. Kop'ev, A.O. Kosogov, I.L. Krestnikov, N.N. Ledentsov, A.V. Lunev, M.V. Maksimov, A.V. Sakharov, V.M. Ustinov, A.F. Tsatsul'nikov, Y.M. Shernyakov, D. Bimberg, An injection heterojunction laser based on arrays of vertically coupled InAs quantum dots in a GaAs matrix. Fiz. Tekh. Poluprovodn. **30**, 351–356 (1996) [Semiconductors, **30**, 194–196 (1996)]
138. A. Marti, L. Guadra, A. Luque, Intermediate-band solar cells, in *Next Generation Photovoltaics. High Efficiency trough Full Spectrum Utilization*, ed. by A. Marti, A. Luque (Institute of Physics, Bristol, 2004), pp. 140–164

9 The Economic Perspective: Is Concentrator PV Capable of Breaking the Economic Barrier

E.W. Merkle, R. Tölle, and M. Sturm

PV will contribute to the new energy mix only if we manage the transition from a subsidy-driven to a cost-effective method of producing solar electricity

9.1 Climate Change and Depletion of Fossil fuels

The provision of clean, sustainable energy is the paramount issue of this century! Due to the discussion of climate change and the depletion of natural energy sources, there is worldwide support for renewable energy.

The International Energy Agency (IEA) predicts a significant increase in world-wide energy demand. Due to the depletion of fossil resources and the problems of climate change, this demand will have to be satisfied by renewable energy sources in the future.

Only the energy of the sun – 15,000 times the amount which is needed – has the potential to meet the demand. It is obvious that within a few decades solar energy has to replace all fossil fuels.

According to industry analysts, The growing concern about climate change due to CO_2 emissions combined with the steep rise in prices for fossil fuels will lead to much higher growth in PV installations in the following decades.

9.1.1 Photovoltaic as Part of Global Energy Trends

The perspectives of the global PV markets are subordinate to the long-term energy perspectives. It is a fact that all fossil energy sources, to varying extents, are unsustainable.

The UN Climate Report makes clear that the growing use of climate-destroying energy sources on an industrial level and also by private households demands a redirection of climate politics. Furthermore it can be stated that the specific sourcing cost of fossil energy sources rise disproportionate.

In many cases, access to the still-existing fossil resources is possible only in politically unstable regions with unsatisfactory production infrastructure.

Considering this background photovoltaic is one of the sustainable options for generating energy besides wind, hydro- and geothermal energy, biomass or the conventionally based generation of energy.

The goal of 20% renewable energies, which was decided on the EU Climate summit, will be a great catalyst for the PV industry, raising it far above average development potential. The expected rise in prices of conventionally generated electricity makes photovoltaic an increasingly competitive form of sustainable energy generation.

9.1.2 Growth Perspective of Photovoltaic

The growth forecasts for PV have been surpassed by the actual growth for the last decade.

With a current market of around 2 Gigawatt (GW), forecasts for the year 2030 currently range from a market volume of 170 up to 1,000 GW of installations per year with a sales volume of $500 to $2,000 billion per annum in 2030.

The latter figures were published by Rogol of Photon Consulting, a leading PV analyst [2]. The more conservative figures were published by research analysts from the capital market environment (e.g., Bank Sarasin [3]).

Even the conservative figures estimate a 100-fold growth of the industry within the next 22 years.

By then the market share of PV-produced electricity, which is now only 0.2%, will be in the range of 20 to 40%.

The drivers of this extraordinary growth perspective are the following:

1. The steep rise in costs of conventional energy and reduction of costs of solar power
2. Direct or feed-in subsidies
3. PPA (power purchase agreement) and reverse metering
4. New markets
5. Trading of CO_2 credits

Here, we analyse all five drivers for the future growth of the PV industry.

Steep Rise in Energy Costs and Reduction of Costs of Solar Power

During the last few years, a steep rise in the cost of energy has taken place. Due to growing demand and depletion of fossil fuels this increase will most likely accelerate.

In contrast to this rise, there is a similar steep drop in the price of PV-produced electricity – an 85% reduction between 1982 and 2007. Even the rather conservative Deutsche Bank predicts that solar power will be cheaper than other sources of energy within a decade [1].

Both developments lead to a convergence, as shown in Fig. 9.1.

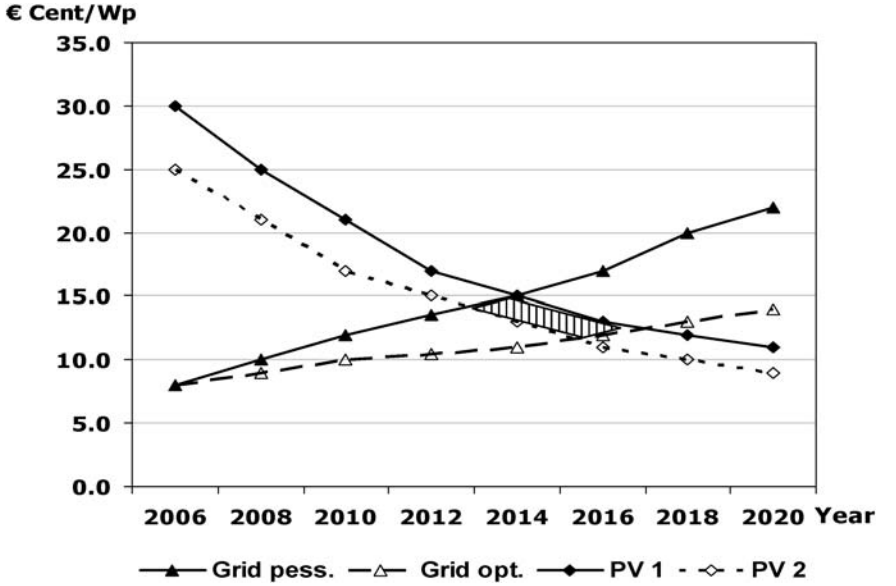

Fig. 9.1. Depending on optimistic (PV 2) and pessimistic (PV 1) scenarios, "grid parity" will be reached in most countries with high sun exposure, i.e. >1500 kWh per m^2 and year, between 2,013 and 2,017. Source: IEA, own calculations

Direct or Feed-in Subsidies

The growth of PV installations started with incentive programs for rooftop installations in Japan and Germany. While those direct subsidies were related only to the initial investment, the real success story started with the inauguration of the Renewable Energy Law (EEG) in 1999 and revised in 2003. Through this law, a feed-in tariff of more than 0.5 EUR was given to the investors for each kWh produced by PV in Germany. This law was so successful that more than 50% of all worldwide PV installations in 2006 were in Germany. This law has meanwhile been copied, with local adaptations, by close to 60 nations. The feed-in tariff remains stable and is guaranteed for 20 years once the installation is connected to the grid. But the tariff was lowered annually by 5–6.5% in the past few years and the digression of the feed-in tariff will accelerate in the coming years. This system is giving security to investors at a level similar to real estate investments, but also poses a strong incentive to lower the prices of PV systems. Whereas in the first stage mostly small rooftop installations were built, the focus has changed to large field installations in Germany and recently in other European markets like Spain and Italy.

Power Purchase Agreement (PPA) and Reverse Metering

A big advantage of PV is the production of energy at the place where it is needed. Here a tremendous market is foreseen. In the western states of the U.S., two sys-

tems are in operation. PPAs have been brought into public focus through retail outlets like Wal-Mart. They signed a 10–20 year agreement to buy the electricity produced by the solar panels at a fixed price. The owners are capital investors. This model will become more and more profitable as PV module prices decrease. With thin-film modules a return on investment (ROI) of 7% can be realized without subsidies. More than 100 cities in the U.S. and Hawaii already operate these PPAs.

A second and similar system was put into operation mainly for homeowners: reverse metering. With this system a private homeowner can feed the electricity produced by his PV modules back into the grid. The meter then runs backwards, for example, during daytime hours when nobody is at home and not much electricity is used. On sunny days in Arizona, California and other sun-belt states, homeowners produce all the electricity they need for the evening hours. Because demand in electricity frequently peaks during hot summer days around noon time, utilities need not invest into additional power plant capacity once this system reaches a critical volume of several 10,000 homes.

In a growing number of states like Arizona and California, where state rebates and federal tax credits can be added, PV systems at the presently high price of around $6,500 U.S. already generate an ROI of up to 7%. If prices continue to go down, PV will become a mainstream investment for millions of households. Already premiums are being paid for houses with solar installations.

New Markets/New Regulations

New markets will arise when alternatives for fossil fuels must be found. PV installations can replace millions of diesel generators all around the world. Electricity and thus the chance for a civilized life can be brought to 2–3 billion people who do not currently have access to the grid. New thin-film modules with sizes of $260 \times 220\,\mathrm{cm}^2$ enable use in buildings. Those building-integrated PV systems (BIPV) will have a tremendous market. Most buildings can generate most of their electricity though integration into walls or semitransparent modules instead of shaded solar glass. The costs may even be less than standard glass windows once a critical volume for those modules is achieved. The German government is currently discussing a new regulation, which would require new buildings to produce 15% of their energy requirement by renewable energy sources. This new regulation will jump start the BIPV market.

A huge demand will come once plug-in hybrid cars become popular. With the solar energy generated through a solar roof on the carport or shaded parking area, most of the energy can be generated needed to power a car for 95% of its use (daily mileage 50 miles).

There will be many new markets coming up once a change in thinking has taken place and energy prices keep sky rocketing and climate problems reach new heights.

Trading of CO_2 Credits

The trading of CO_2 credits is becoming more popular in the world. The simple fact that PV systems produce CO_2-free electricity may have an additional market value, thus promoting the investments into PV power installations.

In the following sections the authors present their own opinion about the future potential of three different PV technologies, i.e. the first-generation crystalline silicon flat plate, the second-generation thin-film and the third-generation concentrator PV (CPV) technologies. Within this article CPV refers only to high-concentration technologies above 500× based on III–V compound solar cells. The potential of low-to-medium silicon concentration technologies (below 100×) would require an article in itself, since the technological variations are huge and complex.

9.2 Cost Reduction as the Major Target

9.2.1 Cost Potentials of the Current Technologies

Ever the first modern silicon wafer-based solar cell was developed 50 years ago, the perception has been that using it to produce electricity would be expensive.

However, these rather high costs are due to the fact that the industry has not reached its stage of maturity yet. Small business units are still prevailing. Only recently have large industrial units been built, achieving considerable reductions in costs.

However, the different technologies have different potentials for cost reduction.

1. The first generation: Silicon flat-plate technology, which has used the abundant supply of off-quality silicon wafers for decades, now suffers from high prices of feedstock and a large number of production processes.
2. The second generation: Thin-film technology has better options to reduce costs due to low material consumption (1% of first-generation use of semiconductor material) and automatic coating processes.
3. The third generation: Concentrator technology (CPV) has the lowest material consumption and also excellent options for fully automated production lines.

The raw material consumption necessary for 100 GWp assumed for 2020 of the different PV generations is shown in Table 9.1 and is compared to the 2006 world total production of the same material.

In the case of CPV, the worldwide Germanium reserves are currently estimated at 8,200 metric tons. According to Umicore, the market leader in Germanium refining, all waste streams in the Germanium production are recycled [4]. The recycling of end-of-lifetime CPV modules is needed to extend the Germanium reach. From all the technologies described in Table 9.1, the third-generation CPV has the second lowest raw material capacity expansion requirements after the second-generation amorphous silicon thin-film technology. For all technologies shown in Table 9.1 only the bulk semiconductor material has been taken into account, since the bulk

Table 9.1. Projected semiconductor raw material consumption in 2020 for different PV technologies

	Raw material	2006 World production total	2020 Raw material needed for 100 GWp PV
1st Generation	c-Si	40,000 t/a	600,000 t/a
2nd Generation	a-Si/µc-Si	20,000 t/a	20,000 t/a
	CdTe	300 t/a	5,000 t/a
	CIGS	300 t/a	3,000 t/a
3rd Generation	Ge	100 t/a	600 t/a

material amount is the cost driver. All other materials – such as the front and back electrodes, buffer layers and the very thin junction material in the case of concentrator solar cells – have been neglected.

9.2.2 Thin-Film PV in Comparison to Crystalline Silicon PV: Advantages in Price, Performance and Large Size

Although conversion efficiencies are not as high as crystalline silicon PV, thin-film PV shows superior performance in hot and overcast climates because of the multiple p/n-junctions that can absorb different wavelengths of sunlight. Thin film layers can be deposited on large glass substrates, a technology introduced by Applied Materials on 5.7 m^2 large modules. This module size is ideal for incorporation into building-integrated photovoltaic (BIPV). The incremental costs of the system are reduced, the building owner is provided with energy and cost savings, and return on investment is increased. BIPV enables thin-film PV to serve as a platform for products that cannot easily be created with conventional crystalline silicon PV.

Thin-film PV will likely win over crystalline silicon PV for projects in locations where space is not a constraint, due to its lower cost and the ability to use large plots of land. Emerging economies that establish solar programs will be drawn to the cost savings of thin-film PV as well, unless feed-in tariffs are set high enough to suit crystalline silicon costs, as is currently the case in, e.g., Spain, Italy and Greece. In Germany, however, all major multi-MWp power plant projects in 2008 will use thin-film technology because of price pressure from the digression of the EEG. Thin-film PV also works better in Germany due to the comparatively low insulation in comparison to the Mediterranean countries.

Besides these side advantages of thin-film PV, the most important argument will be the lower price in the market due to a more favorable cost structure. Table 9.2 illustrates the expected module production cost for crystalline silicon PV, CdTe, and a-Si technologies in 2007 and 2010.

Although we expect polysilicon cost/watt to decrease by about 50% until 2010 and nonpolysilicon costs to decrease by about 20%, c-Si modules still remain more expensive than thin-film products. Crystalline silicon PV modules involve a series of production steps and costs that can each be performed in-house or by a third

Table 9.2. Module cost analysis: crystalline vs. thin-film 2007E and 2010E

($ per Watt)	2007E			2010E		
	c-Si	a-Si	CdTe	c-Si	a-Si	CdTe
Polysilicon	1.65			0.85		
Ingot / Wafering	0.35			0.25		
Solar Cells	0.25			0.20		
Modules	0.45	2.00	1.25	0.40	1.25	0.90
Total Cost	$2.70	$2.00	$1.25	$1.70	$1.25	$0.90

Source: Company reports and CIBC World Markets Corp

party. Since a-Si and CdTe production processes are continuous and all executed by the manufacturing firm, the pricing is not broken down into different steps; only the cost of producing the module is measured. With regards to CdTe module costs, we use First Solar's projected cost of $0.70/W in 2010 as recently reported in Photon International. However, we believe $0.90/W is more likely in 2010 and that First Solar will achieve its goal of $0.70/W in the following years.

9.2.3 CPV in Comparison to Crystalline Silicon Flat-Plate PV

Of the three generations, CPV exhibits the steepest increase in efficiency of all three generations. Therefore the steeper learning curve opens the potential for faster cost reduction. The overall higher efficiency potential of CPV leads to a cost reduction of all BOS (balance of system) components. Even at the currently low production volume of concentrator solar cells the cost of the concentrator solar cell per Wp under high concentration is already only around one third of the crystalline silicon cell cost. But one obviously has to take the increased complexity of the concentrator portion of system cost, i.e. the optics as well as the tracker, into account. For comparison the LED industry, which uses technologies similar to concentrator solar cells, has achieved 90% price reductions of LEDs within six years through mass production and learning curve effects. Since LED manufacturers are still profitable, it has to be assumed that the cost reduction will be very similar. This shows the enormous potential of the steep CPV learning curve. If CPV manages to create a learning curve similar to LED technology, then solely the concentrator solar cell cost under concentration can drop below 10 €ct/Wp in the near future.

9.2.4 Conclusion: Cost Potential to Reach "Grid Parity"

All three technologies show considerable potential for cost reduction. However, the second- and third-generation technologies – with low consumption of expensive semiconductor material and the option for fully automated production processes – show a much greater potential to considerably lower the costs of PV systems. CPV uses approximately 1,000 times less, and thin-film 100× less semiconductor material in comparison to crystalline silicon. But the market for CPV is geo-

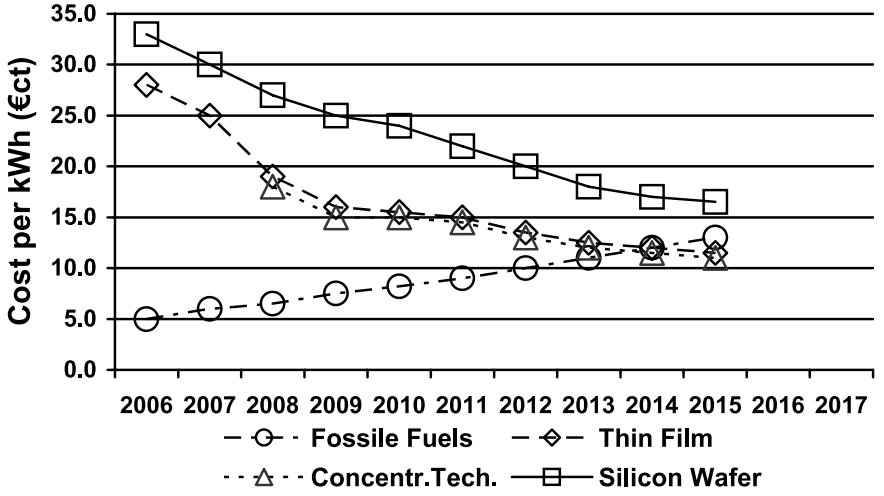

Fig. 9.2. Costs per KWh produced in sun-rich areas with the three PV generations. Source: IEA and company calculations

graphically limited to the sun-belt region on Earth and the technology is applicable only to large-scale power plants. In comparison, thin-film technologies are best suited for BIPV applications as well as power plant applications, in which there are no area constraints. Crystalline silicon, however, can be applied in all markets.

Grid parity will be achieved by these technologies within the next five to nine years. In our view the first-generation crystalline silicon technology might have difficulties following the cost reduction curves of the second and third generation, unless step changes in efficiency or cheaper feedstock sources can be realized. Sanyo's HIT as well as Sunpower's back contact cell concepts show that step changes in efficiency in the first generation are still possible, and initial results using metallurgical-grade silicon are promising. Another possible step for crystalline silicon might be application to low- and medium-concentration systems, which would reduce material consumption significantly. If those technologies are combined with increased pressure from reduced feed-in tariffs, then the first generation might also be able to reach grid parity faster than shown in Fig. 9.2.

The cost potential of the three technologies is shown in Fig. 9.2.

Table 9.1 shows that the amount of semiconductor material necessary to produce 100 GWp of power is 600,000 t/a in the case of crystalline silicon flat-plate technology, but only 600 t/a for germanium as used in CPV systems. At a concentration factor of 100, which is technically still feasible for silicon, the raw material requirement would be reduced to 6,000 t/a. At 100 GWp production volumes the cost will be driven by the material cost. Therefore crystalline silicon flat plate has an inherent disadvantage in comparison to thin-film and CPV technologies as long as silicon feedstock prices are high. CPV especially has the overall lowest semiconductor ma-

terial requirement of all PV technologies, but this comes with the added cost of both optical and tracking systems.

9.3 Meeting the Tremendous Growth Perspective

9.3.1 Growth Beyond all Imagination

The latest market forecast by M. Rogol of Photon Consulting expects the world market to hit 14 GWp by 2010 [2]. At 45% CAGR (compound annual growth rate) the market would be in excess of 40 GWp by 2013!

To satisfy this enormous demand, the industry will have to change considerably. Investments in the sub-GWp manufacturing capacity are common today (e.g. 250 MWp, Conergy; 500 MWp, SolarWorld and Solon for 2010; First Solar expects 900 MWp for 2009), but in the future multi-GWp facilities are mandatory. REC, one of the largest silicon producers from Norway has already announced construction of a 1.5 GW facility in Singapore – all in first-generation technology. In comparison to today's production processes, the industry will have to change the way it is thinking about manufacturing expansions. Logistic problems will play a much more important role in the future. Production lines, which fully integrate all process steps virtually from sand for solar glass production until the delivery of modules to the sites for power plants, will have to become mainstream in the future. Enormous quantities have to be moved in those factories. To ship 1 GW of modules, approx. 10,000 containers are needed. This means about 40 containers a day or one full 40-ft container every 15 minutes during daytime.

Companies need an enormous volume just to defend their market share.

Two simple examples (based on conservative market expectations) are given below to explain this fact:

1. According to the latest Sarasin Forecast, in 2020, the world market will be at 65 GWp (Study Nov. 2007 [3]). Ten percent of the market share represents a production capacity of 6.5 GWp. At the average forecast of 50% CAGR, the company would have to add 3.25 GWp of additional production capacity in 2021 just to maintain market share!
2. Let's say a company plans to acquire 10% of the market share in 2030. Given the conservative estimate of 180 GWp for the market, the companies needs a production capacity of 18 GWp. At 33% CAGR the company would have to add 6 GWp of additional production capacity in 2031 just to maintain market share!

9.3.2 Multi-GWp Capability

A GE-Matrix can be used to assess the future potential of the different PV technologies. For this one needs to assess the technological readiness of all candidates. To assess the technological readiness, one has to distinguish between material availability and actual manufacturability in the GWp range. Manufacturability issues include

in-line process capability, material logistics as well as number of devices handled per MWp.

The current three generations of PV technologies – i.e. crystalline flat-plate, thin-film technologies as well as concentrator PV – can be viewed along a two-axis coordination system, i.e. the technological multi-GWp capability and their cost reduction potential, as shown in Fig. 9.3.

Today's dominating silicon flat-plate technology has much higher technological barriers to overcome compared to the second- and third-generation technologies. The fact that thin-film technologies currently grow faster than crystalline silicon and that in markets with high price pressure like Germany, large PV power plants are realized only in thin-film technologies confirm that the market believes in the superior cost-reduction potential of thin-film technologies. A similar development can be expected when CPV technologies start to enter the market.

All thin-film (TF) technologies have a high cost reduction potential, but non-silicon technologies like CIS and CdTe use rare metals like indium and tellurium, which are a significant constraint for their muli-GWp capabilities. All silicon technologies have the advantage of using the second-most abundant element on Earth and therefore have basically unlimited supplies of raw materials. But crystalline silicon flat-plate has the disadvantage, in comparison to TF technologies, that it uses approximately 100 times more semiconductor material and needs to handle 100 times more devices per MWp.

CPV has the lowest semiconductor material consumption per Wp and the highest efficiency potential of all technologies, which shows up in the highest cost re-

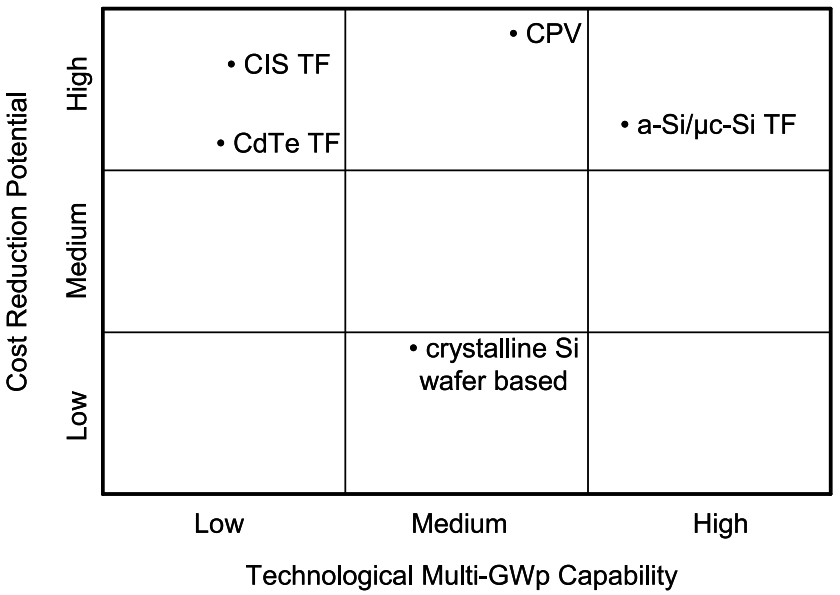

Fig. 9.3. Assessment of the technological readiness of different PV technologies

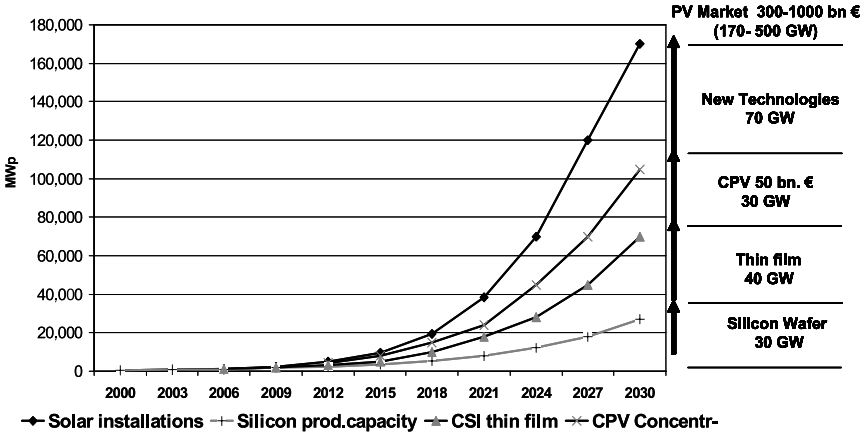

Fig. 9.4. Conservative estimate of PV world market development to 2030 distinguished between different technologies

duction potential. However, at present the technology requires the handling of even more devices per MWp than crystalline silicon, which impacts on its multi-GWp capability. Therefore, from Fig. 9.3 we can conclude that the two technologies with the best multi-GWp capability and the highest cost reduction potential are silicon-based thin-film and concentrator PV, albeit for different reasons (as explained earlier).

9.3.3 The Market in 2030: Will There Be a Winning Technology?

The prediction of the growing worldwide energy demand requires the PV industry to prepare for enormous growth. A conservative estimate of a market demand of 170 GWp in 2030 is shown in Fig. 9.4.

In comparison to today's market, in which the silicon flat-plate technology still dominates and has around 90% market share, we expect the market to change in the future. Both thin-film and CPV technologies will gain significant market share due to their superior multi-GWp capabilities, i.e. their cost-reduction potential as well as their multi-GWp manufacturability. But in general all three generations will prevail due to the fact that they serve partly different markets and applications. It is also anticipated that a large part of the future growth up to 2030 will come from technologies which are still to be developed.

9.4 Cost Barriers for Leaving the Niche

9.4.1 Explosive Growth of PV – Low Rate of Innovation

Installations of photovoltaic power systems have achieved tremendous growth rates in Germany and Japan, with high double-digit growth rates for many years. These

two countries alone account for 88% of installed systems. Other countries in Europe and around the world are only slowly catching up.

The growth of the PV industry is strongly related to public subsidies for either investments or for each unit of electricity fed into the grid. One of the "success stories" is the German EEG, which strongly supports the production of solar energy fed into the grid. Similar laws have been passed by other European governments. Feed-in laws are even on the way to becoming adopted worldwide. Although this policy has proven to be successful in bringing a small-scale industry to an industrial level, it has shortcomings, too. The most important are:

- Prices are much higher in countries with high subsidies.
- There is no real pressure on prices and costs.
- No innovation is required to reach a comfortable profit and relax on the pillow provided by subsidies.
- Lack of innovation shows serious side effects with the shortage of silicon halting some of the growth expectations.
- No serious alternative to the high-price silicon-wafer technology has been investigated after 2004.
- Thin-film technology has tried to solve this problem for the last 15 years, with thus far limited success; in 2007, however, thin-film has grown faster than crystalline silicon for the first time.

In case of a significant cut in subsidies the market for PV systems will break down because its economic viability so far is based on subsidies.

9.4.2 High Growth at High Price Levels – the Problem of a Subsidized Industry

Most of today's PV technology concepts have been started without the shortcomings mentioned above.

This is true for the traditional flat-plate solar industry, which started with a feedstock that was available in large enough quantities for a long time. However, any serious forecast will project that permanent subsidies cannot be the solution to the energy problems the world is facing. The basic problem is that the dominating flat-plate silicon technology is consuming huge quantities of expensive semiconductor material to collect the sun's energy at low-density levels. It is very hard to believe that there will be enough low-cost, high-purity silicon to cover the 100 to 500 times higher demand in the year 2030 or 2050. The investment costs for solar silicon production facilities are above 100 million Euro per 1,000 tons annual capacity and the high consumption of energy for the complex production process limit the price reduction potential.

Different but similar problems in concept can be seen in other areas of the PV industry. Looking into concentrator PV concepts we have to conclude that most of today's CPV prototypes have been developed by research institutes, mostly subsidized through government projects.

Basic errors in concept are:

- Materials which are either not suitable or too expensive for mass production cost targets.
- High consumption of material in relation to the peak production of power.
- High maintenance costs.
- Lack of concerns for the necessities of mass production processes, long-term stability and the standard qualification procedures.

9.4.3 Solar Energy: Abundant Quantity but Low Density

The main reason for the high costs of today's solar installations is the poor use of the huge but dispersed solar resource. Traditional flat-plate silicon has shown a very poor increase in efficiency over the last 50 years, from 6% reached by Bell Laboratories in 1955 to an average of less than 14% in today's installations. The PV industry has failed to prove their capability of providing a competitive system for the production of electricity. The respectable growth of the industry was achieved only through huge subsidies.

PV will pick up the role it has to play in the energy sector only if new technologies and innovations emerge with the potential for high conversion rates of the solar spectrum and a high cost-reduction potential. CPV under certain conditions has this potential.

9.5 The Learning Curve of CPV: Quick or Slow

9.5.1 Concentration on the Strength Factors

CPV will be successful only if it concentrates its activities on some basic principles:

Replace expensive semiconductor material through inexpensive optics and use a module construction concept suitable for mass production. Use wherever possible proven commercial manufacturing technologies instead of relying on prototyping. Always calculate the cost down to the complete system. Do not stop at the module. Only the complete system cost allows us to assess the cost of electricity generation. Have the application and the market in mind, not just the technology.

However, we cannot see that the CPV concepts on the market follow this approach very well. In spite of almost 20 years of developments and huge amounts of public-sponsored research and development, no concept is really ready for industrial mass production with a serious potential of reducing costs below the one Euro per watt target for modules.

9.5.2 Learning from the LED and Photonic Industries

The LED industry has been developing at a remarkable technological rate of innovation. The first white LEDs were introduced in 1996 with an efficiency of approximately 5 lumen per watt. This efficiency is comparable to the Edison light bulb

around the year 1880. During the following 90 years the efficiency of the incandescent lamp has increased at a poor rate of less than 1% per year, reaching little over 10 Lm/W in 1970.

The technological development of the white LEDs shows a completely different picture, one of fast development: 108 Lm/W were reached by Osram in 2005 after only nine years; 200 Lm/W are expected for 2012. Since LEDs use basically the same – only in reverse – principle, they show up a technological pathway which is suitable for CPV.

LEDs and concentrator solar cells are, in principle, the same device. An LED produces light from electricity, whereas a concentrator solar cell produces electricity from sunlight. When a concentrator solar cell is run in reverse, it emits light and glows red. Both devices are produced by the same production technology: MOCVD (metal organic vapor deposition). Whereas the worldwide demand for space and concentrator solar cells is covered by approximately five MOCVD reactors, the largest LED manufacturer in the world runs 115 such reactors in production alone. Even today the efficiency increase in concentrator solar cells is remarkable. But in comparison to what was achieved in LED manufacturing, it looks rather mediocre. The cost reductions in the LED industry of 90% over a six-year period were achieved by a combination of efficiency gains and economy of scales from volume production. There is no technological reason why the same result cannot be achieved in concentrator solar cell production. Even at today's low production volume for concentrator solar cells, those cells are already at one third of the cost per watt in comparison to silicon solar cells. With the cost reduction potential shown in the LED industry, the concentrator solar cell cost can be decreased to a few cents per watt. When tight cost control is applied in the selection of module materials and concept, then a concentrator module price below one Euro per watt can be achieved. Together with the balance of system cost this would be sufficient to reach grid parity in the sun-belt region on earth.

9.5.3 Solar*Tec AG's Approach to CPV

SolarTec AG is currently developing its proprietary third-generation CPV technology in close collaboration with the Ioffe Institute in St. Petersburg, Russia. Ioffe's original idea of using micro Fresnel lenses and micro solar cells has been adopted by SolarTec, but the all-glass module design has been replaced by materials that are easier to adapt to volume manufacturing.

Key features of the SolarTec approach are:

1. The micro Fresnel lens approach with micro concentrator cells allow the application of a simple, passive heat-sink technology, which leads to similar cell temperatures under operation as can be observed for standard silicon flat-plate modules.
2. A short focal distance increases the acceptance angle of the module, which is a very important parameter for the overall, yearly performance ratio of the system, and reduces the specification for the tracker accuracy. The short focal

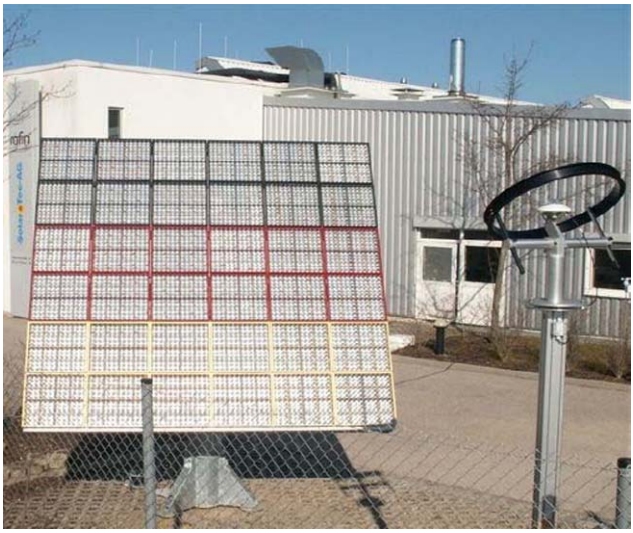

Fig. 9.5. SolarTec AG's test tracker with CPV modules and weather station in front of the R&D facility in Aschheim near Munich, Germany

distance also reduces the amount of material required for the housing frame of the module and reduces the overall weight of the module, which also decreases tracker specifications. But the reduced focal distance comes at the cost of a slightly reduced theoretical maximum optical efficiency of the Fresnel lens.

3. The Fresnel lens array is produced by injection moulding, a technology well known for volume production in other industries.
4. A high concentration ratio of 700× reduces the cell area and therefore the semiconductor material consumption.
5. The module housing is also produced by injection moulding of low-cost, environmentally enduring plastic material, which reduces the module weight in comparison to most other materials and allows for optimal fit of thermal expansion coefficients between the front glass and the module frame, which is required for the module's long lifetime.
6. Each single solar cell is measured and binned according to its electrical parameters in order to reduce mismatch losses during interconnection.
7. High accuracy pick-and-place technology, frequently used in the LED industry, has been adapted for the production of the receivers.
8. Standard bonding technology has been adapted for the automated interconnection of all solar cells. Bond wires and bond parameters have been optimized together with the solar cell metallization with respect to resistance losses and adhesion properties in collaboration with SolarTec's subsidiary ENE, which provides the concentrator cells.
9. Process control tools have been developed for each process step to assure the highest quality during production.

10. SolarTec has an in-house tracker development, which realizes the required accuracy at low cost.
11. SolarTec's own PV power plant business, which has already realized more than 10 MWp of power plants with conventional first-generation silicon flat-plate modules in 2007 and plans to increase this business to more than 70 MWp in 2008, ensures that the overall system for CPV is designed for highest performance ratio.

SolarTec is currently preparing for certification according to IEC 62108, which is a necessity for the sale of CPV power plants to investors.

The result of SolarTec's and Ioffe's joint effort on the development of the technology can be seen in Fig. 9.5, which shows a fully functional test tracker at SolarTec's R&D facility in Aschheim near Munich, Germany.

References

1. Fortune, 15 Oct. 2007, p. 62
2. Rogol, Solar Annual 2007, Photon Consulting, Solar Verlag, 2007
3. Sarasin, Solar Energy 2007, Bankhaus Sarasin, 2007
4. Umicore, The role of the germanium substrate manufacturer in the CPV market, Ralf Dessein, CPV Workshop, Marburg 2007

10 Fluorescent Solar Energy Concentrators: Principle and Present State of Development

A. Goetzberger

10.1 Principle

The use of transparent sheets doped with fluorescent dyes for the concentration of sunlight was suggested first in the 1970s [1, 2]. The principle itself is much older; it was first used in scintillation counters for atomic physics [3, 4]. Although significant advances were made in early work, after some years further progress was limited by the materials available at that time – in particular the dyes – and interest was dormant for decades. Only recently new progress in materials as well as theoretical advances rekindled interest. In this article the historic work and the present state of the art will be reviewed.

Figure 10.1 shows the principle of the fluorescent concentrator, sometimes also called the luminescent solar concentrator: I represent an incident beam of light interacting with a dye molecule dissolved in a matrix of index of refraction n. The incident light will be absorbed and emitted at a different wavelength. (In the normal case of Stokes fluorescence, the emitted wavelength will be shifted to a longer wavelength.) If the probability of emission is equal in all directions, part of the light will leave the transparent medium (F_1) while another part (F_2) will be reflected back because it intersects the surface at an angle leading to total internal reflection. It is important to note that this reflection is in principle *lossless.* Thus the captured light is guided within the transparent sheet which will be also called the collector. Concentrated light can thus be obtained at the edge of the concentrator. The edges of the concentrator not contacted by solar cells have to be covered with mirrors. The fraction of light contained in the concentrator can be quite high. The fluorescent concentrator is the only concentrator known that can achieve high values of concentration without tracking. In contrast, concentrators based on geometric optics have to be tracked in order to achieve concentration of more than about 2 and they can only use direct sunlight. This is a fundamental limitation following from nonimaging optics.

In [5, 6] it has been shown that loss due to light leaving the concentrator through the two boundary planes is given by:

$$L = 1 - (n^2 - 1)^{1/2}/n \tag{10.1}$$

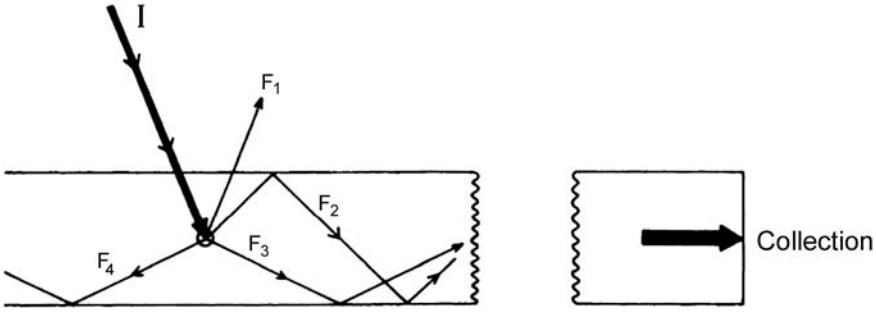

Fig. 10.1. Principle of fluorescent collection. Dye molecule D interacts with incoming light beam I. Secondary beams are partly lost (F_1) and partly guided in transparent material (F_2–F_4)

where n is the index of refraction of the concentrator. For $n = 1.5$ for instance, $L = 0.2546$, for $n = 2$, L is 0.134 (it will be shown below that by optimized design of concentrators these losses can be reduced significantly). The solid angle determined by the onset of total internal reflection is called the loss cone.

A basic requirement for efficient collection is that the incident wavelength has to have a short absorption length, the emitted wavelength a very long absorption length. This is accomplished by selecting a dye whose absorption and emission wavelengths are well separated. Also the fluorescence efficiency has to be high. The latter requirement is more easily met than the former. Quite a number of dyes are known having a fluorescence efficiency of close to 100%. New dyes with better spectral properties and stability are being developed by the chemical industry. The emission and absorption characteristics are not only dependent on the nature of the molecule but also on that of the solvent. The material of the collector has to be highly transparent and a good solvent for dyes. Plastics, glass, or organic solvents contained between plastic or glass sheets are possible candidates for this purpose. It is also possible to apply the dye dissolved in a thin film on the surface of a completely transparent sheet.

Although prices for solar cells have come down considerably in recent years, the cells are still the most expensive part of a flat plate solar generator.

Fluorescent concentrators have the following advantages:

- Concentration of Sunlight without tracking
- Concentration of direct *and* diffuse light. The concentrators are particularly well adapted to overcast conditions that occur frequently in temperate climates
- Possibility of spectrum splitting use of several sheets doped with different dyes shown below

A single semiconductor can never convert sunlight with the highest possible efficiency because quanta with higher energy than the band gap lose their energy by thermalization and those with lower energy are not absorbed. Therefore multijunction cells employing different semiconductors achieve the highest efficiency today.

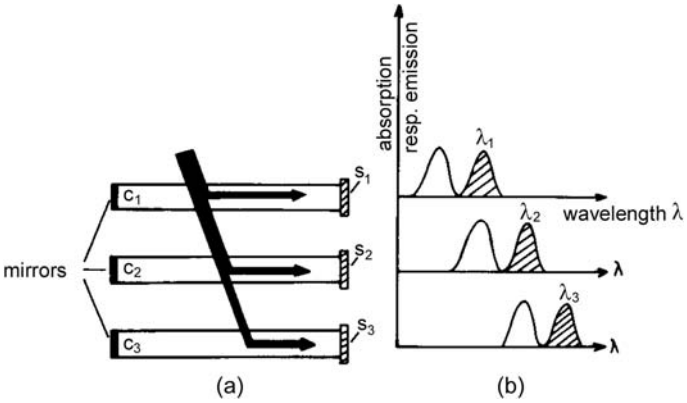

Fig. 10.2. (**a**) Fluorescent concentrator stack. Collectors c_1, c_2, c_3 are combined with solar cells S_1, S_2, S_3 of different bandgaps. (**b**) Absorption and emission (*shaded*) spectra of dyes in c_1–c_3, λ_1–λ_3 are peak emission wavelengths of c_1–c_3

They consist of complex layers of III–V compounds but are very expensive and so they can only in be used concentrating systems.

10.2 Concentrator Stacks

Fluorescent concentrators offer the possibility to separate different portions of the solar spectrum just like multijunction cells and concentrate them at the same time [2]. Figure 10.2(a) shows a stack of three collectors c_1–c_3 contacted by three different solar cells S_1–S_3. The ideal absorption and emission spectra of the fluorescent molecules in the collectors are sketched in Fig. 10.2(b). Because every collector is fully transparent to the unabsorbed part of the spectrum a rather complete separation of the solar spectrum is possible in this manner. The solar cells S_1–S_3 have band gaps adjusted to the emission bands of the collectors. A more detailed analysis carried out below demonstrates that the theoretical energy conversion efficiency is greater than 30% versus 24% for single junction silicon cells (for AM 1.5).

1. Quantum Efficiency of Fluorescent Concentrators

1.1 *Quantum Efficiency of Sequential Stack*

For the calculation of quantum efficiency we put aside the energy loss due to Stokes shift and are only interested in quantum losses. It is assumed that the quantum efficiency of fluorescence is 100%. Reflection losses can be minimized with antireflection layers but even without antireflection coatings the stack offers possibilities for minimizing reflection losses.

Much progress has occurred with antireflective coatings in the last 30 years. They have become more efficient and also more economical. Although such coatings have a lower index of refraction than the collector sheet they do not interfere with total internal reflection because only the difference between medium in which the light is emitted and air is of importance.

For collector stacks the following facts apply: The spectral range for these antireflective coatings becomes narrower and therefore easier to realize for the lower plates of the stack. It can be seen that whereas c_1 has to be transparent for the entire solar spectrum, c_3 only has to operate in the long wavelength range. An additional possibility is use of photonic structures to decrease the loss cone angle as will be described below.

Now the quantum efficiency for a stack of collectors will be calculated. Again normal incidence is assumed. The procedure applied here is the following: The incident spectrum is assumed to be divided into m parts such that each part contains an equal number of photons. This requirement is convenient for computation but not necessary for practical applications. An advantage of the stack is the fact that one half of the escape cone losses of the preceding plate are recovered by the following one. This is seen from Fig. 10.2(b). Collector c_1 emits at wavelength λ_1. If the absorption band of c_2 is arranged as shown in Fig. 10.2(b), c_2 absorbs not only the solar radiation at the wavelength band λ_1 coming from above but also the radiation emitted by the dye in c_1 in the direction of c_2. The same is true for the lower parts of the stack. A recursion formula will now be derived for the quantum efficiency of a stack versus the number of collector plates in the stack. The symbols used in this calculation are given in Fig. 10.3.

The incident radiation S suffers reflection losses R at every interface traversed. Loss of fluorescent radiation not retained in the collectors is indicated by L. As was pointed out already, the loss cone losses directed towards c_2 are recoverable. A minor detail, also indicated in Fig. 10.3 is the fact that reflection of this radiation in leaving c_1 does not have to be taken into account because exactly the same loss occurs at the top surface of the collector thus cancelling the former loss (dashed lines in Fig. 10.3).

Let S_1 be the amount of radiation entering collector c_1 at the absorption band of this collector and C_1 be radiation collected there $S_2, \ldots, S_m$ and $C_2, \ldots, C_m$ are defined accordingly. Then $S_1(\lambda_1) = (1 - R)/m$

$$C_1 = S_1(1 - L).$$

The amount of radiation entering the second collector in the appropriate band is one mth of the incident spectrum attenuated by reflection (multiple reflections are neglected) and augmented by half of the loss from the preceding collector attenuated by reflection upon entering the second collector and so on:

$$S_2(\lambda_2) = (1 - R)^3/m + (1 - R)S_1L/2; \qquad C_2 = S_2(1 - L);$$
$$S_3(\lambda_3) = (1 - R)^5/m + (1 - R)S_2L/2; \qquad C_3 = S_3(1 - L);$$
$$S_4(\lambda_4) = (1 - R)^7/m + (1 - R)S_3L/2; \qquad C_4 = S_4(1 - L);$$
$$\vdots$$
$$S_m(\lambda_m) = (1 - R)_{2m-1}/m + (1 - R)S_{m-1}L/2; \qquad C_m = S_m(1 - L).$$

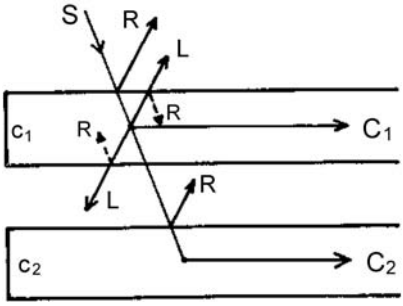

Fig. 10.3. Definition of quantities used in calculation of quantum efficiency. For details see text

Table 10.1. Quantum efficiency η_Q of collector stack

m	1	2	3	4
η_Q	0.7126	0.7299	0.7204	0.7030

The quantum efficiency is the sum:

$$\eta_Q = \sum_{k=1}^{m} C_k. \tag{10.2}$$

Equation (10.5) will now be evaluated for a realistic case. A common high transparency plastic like Plexiglas with an index of refraction of 1.49 without antireflection coating and $L = 0.2587$.

Obviously the stacking of collectors does not degrade quantum efficiency.

It should be pointed out that the order of dyes in the different sheets as shown in Fig. 10.2 can also be reversed – the longest wavelength on top and the highest at the bottom. This may be advantageous. In this case a band pass mirror as described in the next section can be applied.

10.3 Light Guiding by Photonic Band Pass Mirrors

The loss of fluorescent light through the surfaces of the collector can be entirely avoided by covering the front surface with a wavelength selective mirror (hot mirror) [7, 8]. This mirror should have the following properties:

- A sharp cut-off edge at the onset-wavelength of the dye's emission. All light below this wavelength should be transmitted, all above should be reflected.
- Near 100% reflection for light coming from all directions.

A band pass mirror with non-ideal properties can been realized with commercial hot mirrors [8, 9]. Better results can be expected from photonic structures. First experiments with Rugate structures have shown promising results [10]. It features a continuously varying refractive index profile in contrast to the discrete structure

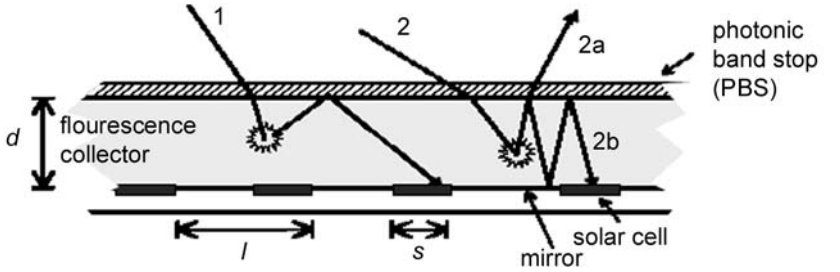

Fig. 10.4. Optimal design of fluorescent collector with band pass mirrors [9]. The coverage factor $f = s^2/l^2$

of normal Bragg reflectors. This results in the suppression of side loops, which would cause unwanted reflection and loss of usable radiation. In [9, 11] it was shown that the ultimate efficiency limits of fluorescent concentrators can only be reached with selective mirrors. On the other hand, light within the loss cone has a long path length before reaching the edges of the concentrator. In this case an arrangement as depicted in Fig. 10.4 is more advantageous.

10.4 Factors Determining Energy Efficiency of Fluorescent Concentrators

For the energy conversion efficiency all energy losses in the collection process have to be taken into account. These are in detail

- R Surface reflection coefficient. This is either the Fresnel reflection coefficient or a lower value if an antireflection coating is applied
- η_{abs} Absorption efficiency of the dye due to its absorption spectrum with respect to the solar spectrum
- η_{qua} Quantum efficiency of dye
- η_{stok} "Stokes efficiency"; $(1 - \eta_{\mathrm{stok}})$ is the energy loss due to Stokes shift
- η_{trap} Efficiency of light trapping by total internal reflection (Loss cone)
- η_{dye} Efficiency of light conduction limited by self-absorption of dye
- η_{mat} "Matrix efficiency"; $(1-\eta_{\mathrm{mat}})$ is the loss caused by light scattering or absorption in the matrix. η_{dye} and η_{mat} determine the mean free path of the emitted light in the collector
- η_{tref} Efficiency of light guiding by total internal reflection. This depends on the surface quality of the matrix

The overall optical efficiency can then be written as:

$$\eta_{\mathrm{opt}} = (1 - R)\eta_{\mathrm{abs}}\eta_{\mathrm{qua}}\eta_{\mathrm{stok}}\eta_{\mathrm{trap}}\eta_{\mathrm{dye}}\eta_{\mathrm{mat}}\eta_{\mathrm{tref}}. \tag{10.3}$$

These loss factors will now be discussed.

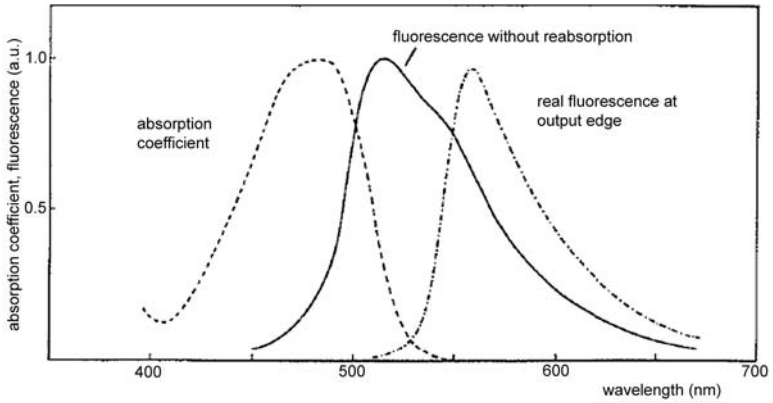

Fig. 10.5. Absorption and emission spectrum of typical dye. Output spectrum is modified by reabsorption

The *surface reflection loss* R is usually the Fresnel reflection loss. It is given by $[(n-1)/(n+1)]^2$ where n is the refractive index. For most transparent materials it amounts to about 4% per surface. It can be minimized by employing an antireflection coating. If it has a sooth surface it will not interfere with total internal reflection.

The *absorption loss* η_{abs} is determined by the fraction of the solar spectrum absorbed by the dye. Practically all dyes absorb only part of the solar spectrum. It is possible to incorporate more than one dye into a collector, leading to a cascade of absorption and reemission. A disadvantage is that at every emission part of the radiation escapes through the loss cone. If the dyes are located very close to one another radiationless energy transfer can occur via the Förster mechanism. Therefore doping of a thin surface region of the collector with a high concentration of dyes may have advantages.

The *quantum efficiencies* η_{qua} of the dyes can vary considerably. Only dyes with efficiency close to unity are usable. Fortunately dyes with such efficiency and good stability are available but this refers only to the visible range.

The *Stokes loss* η_{stok} is caused by the frequency shift between absorbed and emitted light. It is inherent in the fluorescence process. On one hand this shift should be small to minimize the energy loss, on the other it should be large enough to avoid overlap of absorption and emission loss (related to η_{dye}).

The light trapping efficiency η_{trap} is given by L (from (10.1)). It increases with increasing refractive index of the collector material. In practice there are only little differences of available materials.

η_{dye} designates the efficiency limitation caused by *self absorption of the dye*. All known dyes have a certain overlap of absorption and emission spectrum as shown in Fig. 10.5. Also shown in this Figure is how the spectrum is modified by multiple reabsorption and emission. The spectrum at the output is then red shifted. It has also been found that dyes cause a very small absorption within the emission region and

beyond [12]. This absorption is difficult to determine but can have great influence on the overall efficiency. A further effect causing unwanted absorption are photodegradation products caused by degradation of dyes [13]. These products can be annealed by heating in the dark.

η_{mat} is the *efficiency due to scattering or absorption in the matrix*. It depends strongly on purity and preparation of the matrix.

Total internal reflection is theoretically lossless but in practice it depends on the surface finish of the matrix. This loss η_{tref} can in principle be completely avoided by employing a reflecting band pass filter at the surface of the collector as pointed out above. Ideally this filter should also serve as an antireflection coating for the wavelength region absorbed by the dye to reduce R.

10.5 Theoretical Limits of Concentration and Efficiency

10.5.1 Limit of Concentration

Let us first consider a conventional concentrator based on geometric optics. In this case the concentration is limited by the conservation of étendue or Liouville's theorem which relates the beam divergence at the input and output aperture. The most efficient concentrator is the Compound Parabolic Concentrator (CPC) that can approach the theoretical limits.

The concentration ratio C is given (for three dimensions) by:

$$C \leq \frac{n \sin^2 \theta_2}{\sin^2 \theta_1} \tag{10.4}$$

where C is the concentration factor, θ_1 = input angle of light, and θ_2 = output angle at receiver. If diffuse light is to be concentrated, $\theta_1 = 90°$ and therefore the maximum concentration is limited to n^2 which is about a factor of two for most available transparent materials.

On the other hand, geometrical concentration can be very effective at very small input angles. For solar radiation the limiting input angle is given by the viewing angle of the sun. Therefore tracking concentrators for direct radiation permit very high concentration.

The maximum concentration of the fluorescent concentrator has been determined by Yablonovitch [14] and Smestad et al. [7]. They point out that because of the energy loss due to the Stokes effect the system operates like an optical heat pump. The radiance at a given energy is increased by changing some of the incoming energy to heat.

For fluorescent concentrators the concentration factor is determined by:

$$C \leq \frac{(\nu_2)}{(\nu_1)} \exp\left(\frac{h(\nu_1 - \nu_2)}{KT}\right) \tag{10.5}$$

where ν_1 = frequency of absorbed light, ν_2 = frequency of emitted light. The concentration factor depends only on the magnitude of the Stokes shift. So concentration occurs at the sacrifice of energy efficiency.

10.5.2 Limit of Efficiency

The limits of efficiency were examined by Rau et al. [9], Glaeser and Rau [10] and Markvart et al. [15, 16]. They showed that the detailed balance principle introduced into solar cell physics by Shockley and Queisser [17] can also be used for the fluorescent concentrator-solar cell system. They investigated a single stage concentrator and found that very high efficiency is possible provided the concentrator surface is covered by a perfect band pass mirror. In [9, 10] Monte-Carlo simulations were employed to obtain relations between efficiency, band gap energy and coverage fraction. In Fig. 10.6 are presented the results of these calculations.

The simulated efficiencies for a fluorescent concentrator ($f = 1$) *with PBS* (open squares) follow the radiative Shockley–Queisser efficiency limit η_{rad} (solid line) when calculated with reference to the photonic threshold energy E_{th}. The efficiencies *without PBS* (open circles) are at about $0.88 \times \eta_{\mathrm{rad}}$ (dashed line) calculated with reference to the band gap energy $E_{\mathrm{g}} = E_{\mathrm{th}} - 0.2$ eV of the underlying solar cell. (b) Efficiencies for a band gap energy $E_{\mathrm{g}} = 1.12$ eV and threshold energy $E_{\mathrm{th}} = 1.32$ eV for ideal (rad.) and non-ideal (nonrad.) solar cells. *Without* photonic band stop (PBS) the efficiencies degrade monotonically with decreasing coverage fraction f (full and open circles, for the radiative and the non-radiative case). *With* PBS the system's efficiency drops much slower for an ideal solar cell (open squares) and even achieves an optimum at $f \approx 10^{-2}$ in the non-radiative case (full squares).

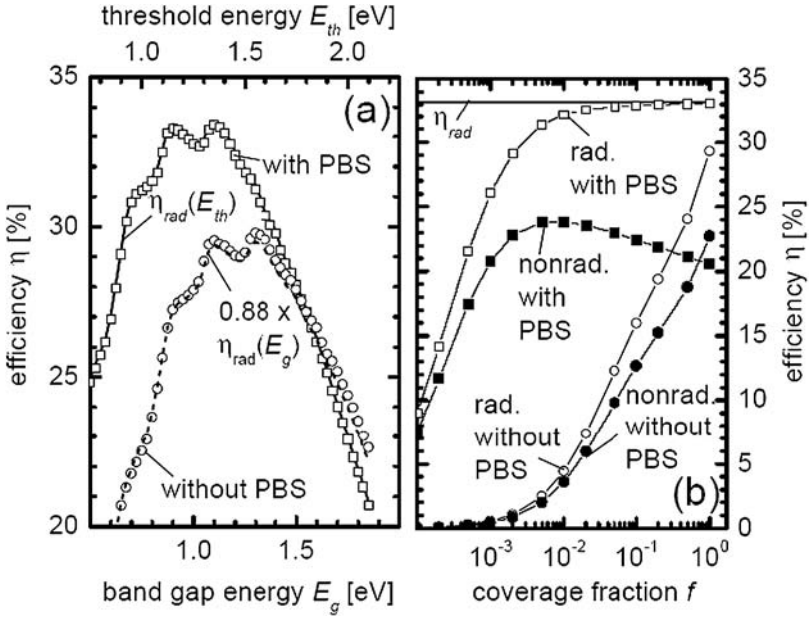

Fig. 10.6. Monte-Carlo simulations [9, 10]. For explanations see text

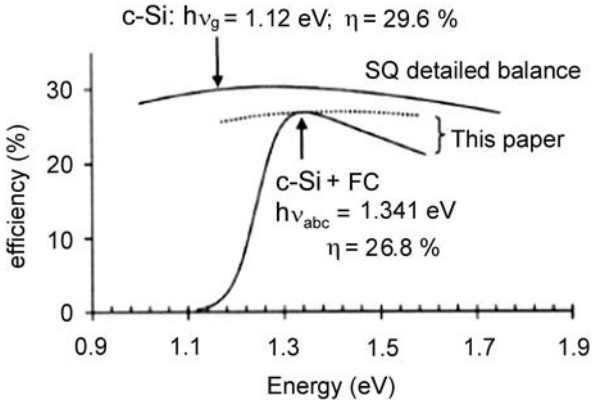

Fig. 10.7. Conversion efficiency of an ideal Si cell with and without a fluorescent concentrator

Comparable results were obtained by Markvart [15, 16] as shown in Fig. 10.7. It is seen that ideal efficiency is 26.8% vs. 29.6% without concentrator.

10.6 Improvements of Basic Design

10.6.1 Optical Concentrators at the Collector Output

This is a very old proposal [18]: At the edge of a collector plate a concentrating element (taper or more effective a CPC) is attached before the solar cell (Fig. 10.8). The additional concentration possible in this manner is given by (4). This additional concentration rests on two facts: The divergence angle of incoming rays is limited by the onset angle of total internal reflection and can then further be converted to 90°. The collector material can be made of a material of higher index of refraction than the collector material. A concentration factor between 1.5 and 2 is thus possible.

10.6.2 Combination of Fluorescent Collector with Large Area Si-Solar Cell

Because at present no dyes emitting in the IR with acceptable properties are available, a good compromise is the following concept [10] (Fig. 10.9).

A fluorescent concentrator doped with a dye emitting in the red or orange is equipped with a GaInP cell that has its maximum response in this range. The collector is transparent to all radiation not absorbed by the dye that is converted by a large area silicon cell at the bottom. Figure 10.10 shows the efficiencies of the silicon cell alone and the combined system. The silicon cell *without the concentrator had an efficiency of* 16.7%. *Under the fluorescent concentrator the efficiency dropped to* 14.0%. *The total system efficiency was* 17.7%, *which is significantly higher than the silicon solar cell alone.*

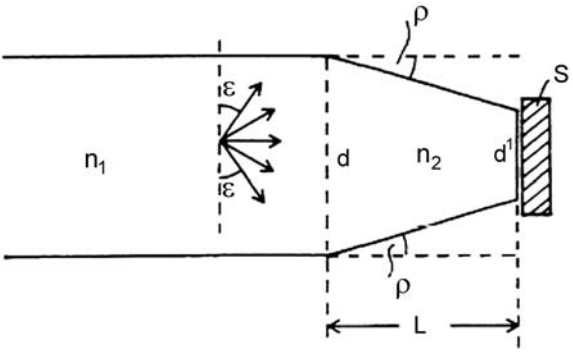

Fig. 10.8. Fluorescent collector with two stage concentration by attached taper with refractive index $n_2 > n_1$

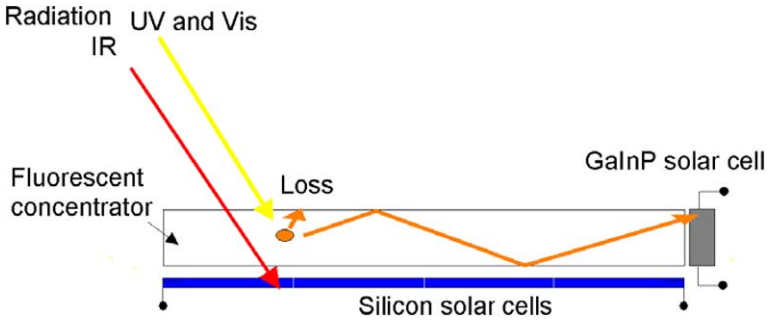

Fig. 10.9. Combination of a short wavelength fluorescent concentrator with attached GaInP cell and Si bottom cell [10]

10.6.3 Combination of Fluorescent Concentrator with Up-Conversion

Recently great progress has been achieved with up-converters – compounds that combine two or more quanta to a higher energy quantum [19].

This effect can also be useful for fluorescent concentrators as indicated in Fig. 10.11.

Below the fluorescent collector an up-converter and a mirror is arranged. The spectral properties of the fluorescent collector and the up-converter are shown below. The dye in the collector shifts the absorbed wavelength range to longer wavelength above the band energy of the solar cell. So the photons emitted downwards are converted by the up-converter to shorter wavelength to be reabsorbed by the collector. Furthermore the collector is transparent to the solar spectrum within the emission range of the dye in the collector. These photons will also be converted to higher wavelengths.

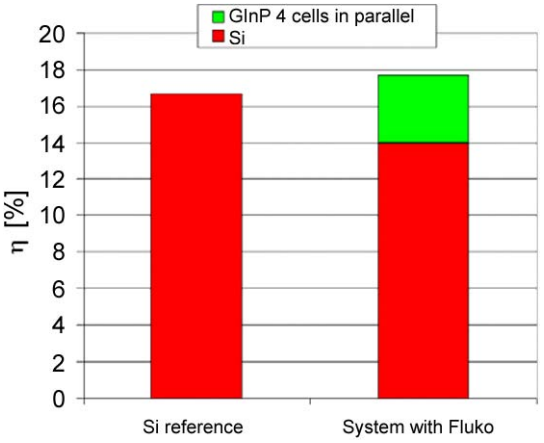

Fig. 10.10. Efficiency of silicon cell alone and of total system

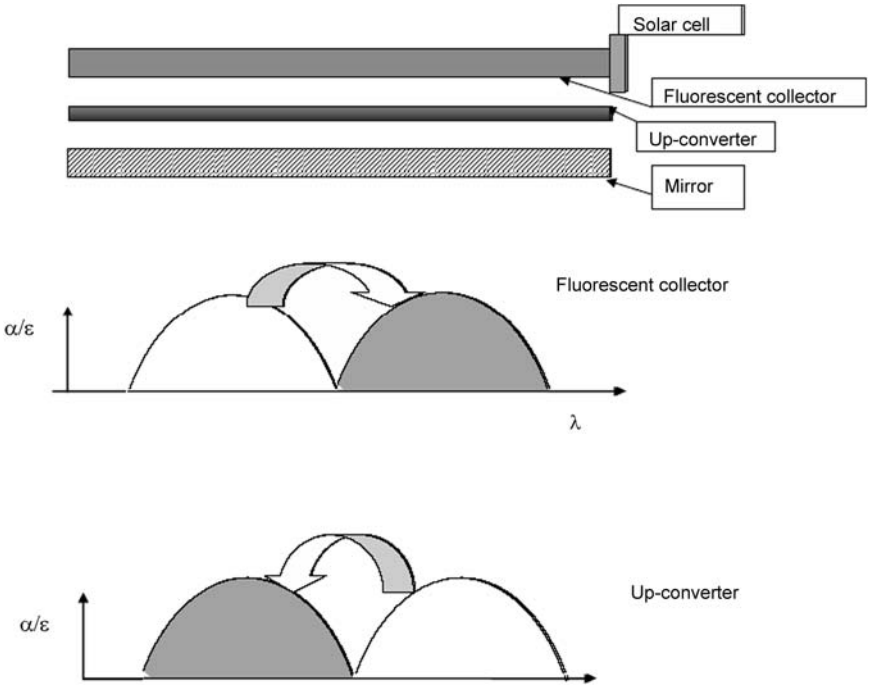

Fig. 10.11. Fluorescent collector combined with up-converter. For explanation of function see text

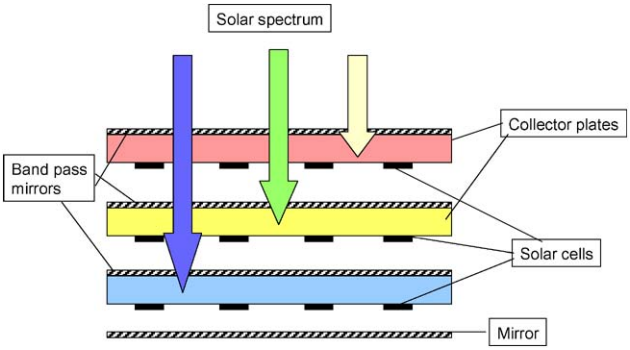

(a)

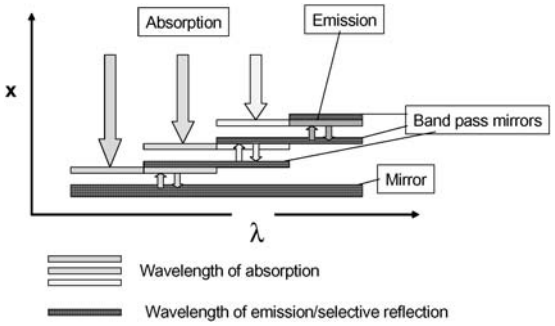

(b)

Fig. 10.12. Fluorescent collector stack with band pass reflectors. (**a**) Geometrical arrangement, (**b**) wavelength representation

Table 10.2. Electrical efficiencies for 40×40 cm^2 collectors with Si and GaAs cells. Highest efficiency of 4.0% was obtained with a double stack and GaAs cells

Dimension (cm^3)	Absorption range (nm)	Efficiency		
		Si	(%)	GaAs
$40 \times 40 \times 0.3$	360–550	2.1		2.5
$40 \times 40 \times 0.3$	490–610	1.4		2.5
Stack of both	360–610	3.0		4.0

10.6.4 Combination of Collector Stack with Band Pass Mirror

The collector stack can also be combined with a band pass mirror as described in Sect. 10.3 if conditions are chosen appropriately. For this purpose the following conditions apply:

- Longest wavelength dye on top
- Solar cells placed below each other
- Transparent electrical connections

In Fig. 10.12(a) the stacking of the collectors is sketched, in Fig. 10.12(b) we see the wavelength diagram. Consider the top plate: The dye absorbs in the yellow and emits in the red. (In reality it would be infrared.) The upper mirror reflects the emitted radiation but is transparent for all other wavelengths, downward emitted radiation is reflected by the lower mirror which extends into this wavelength region as indicated by the short arrows. The lower plates operate in the same manner.

The collector stack with band pass mirrors offers intriguing prospects: It is the only device that can concentrate diffuse radiation and could also approach highest conversion efficiency. While the original fluorescent concentrator shown in Fig. 10.2 has a theoretical efficiency of about 30%, the new design can go much higher. From Fig. 10.7 we derive that a one plate concentrator with a silicon cell has a theoretical efficiency of 90% of the thermodynamic efficiency. A collector stack is a spectrum splitting device and can now achieve an efficiency close to that of a multi-junction cell. If we assume the theoretical efficiency to be 60%, the multi-stage fluorescent concentrator has a theoretical efficiency of 54%.

Obviously, many difficulties have to be overcome to reach this goal, such as: Near ideal band pass mirrors are needed, the dyes should have well defined absorption bands without absorption in the shorter wavelengths and appropriate wide gap solar cells have to be available. In addition the cost should be competitive.

10.7 Experimental Results

10.7.1 Results of the Initial Period

Experimental work can be divided into two periods: The initial period from 1977 to about 1985 and the more recent period which started about 2000. The older results are still meaningful because they represent benchmarks to be reached and exceeded in present work. The most interesting parameters are the overall electrical efficiency and the long term stability of the collectors. These are in turn influenced by the properties of matrix and dye. In comparing efficiencies the dimensions of the samples are very important. Results of the early period are summarized in review papers by Wittwer et al. [20] and Zastrow [21].

The efficiency of 4% is still the highest value that has been realized for such a large area. The second most important issue is stability of the collector dye-system under illumination. It could be observed that by continued development the stability of the dyes improved during the course of the work. A representative measurement is shown in Fig. 10.13. The cumulative illumination corresponds to more than two years of outdoors exposure. Also clearly seen is the recovery of fluorescence during periods of darkness.

A problem that continues to limit efficiency is the lack of useful long wavelength dyes. They still have low quantum efficiency and are not very stable. Figure 10.14 gives a compilation of quantum efficiencies found until 1984. It is evident that there is a general tendency is towards lower efficiency when emission wavelength increases.

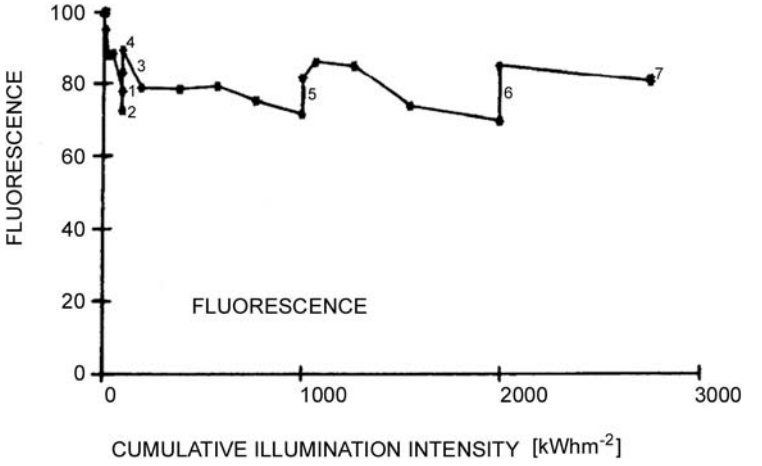

Fig. 10.13. Fluorescence during long term light exposure in kWh/m^2. Fluorescence is normalized to maximum value

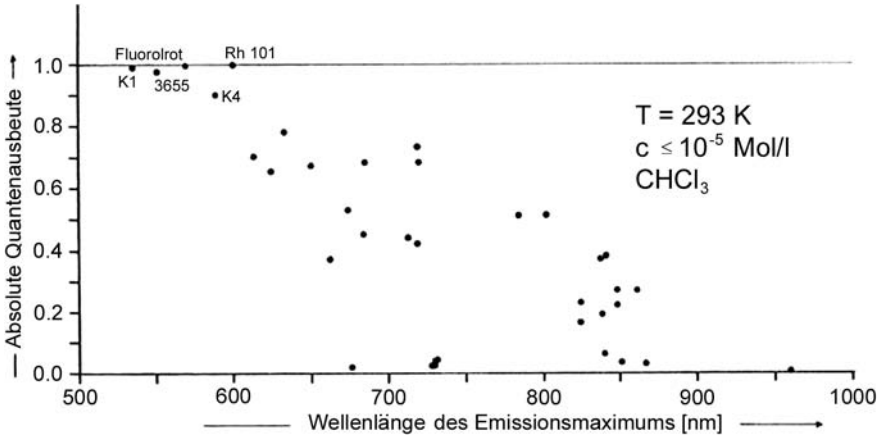

Fig. 10.14. Quantum efficiencies of different dyes vs. peak emission wavelength

10.7.2 Recent Experimental and Theoretical Work

L. Danos et al. [22] characterized fluorescent concentrators based on solid, liquid and Langmuir Blodget films. A. Chatten et al. [23] have developed a self-consistent 3D thermodynamic model for planar concentrators, modules and stacks. The results for test concentrators containing both quantum dots and organic dyes as the luminescent species show excellent agreement with experiment.

Organic dyes are still the best choice for fluorescent concentrators as shown in [24]. In this paper by Richards and McIntosh collectors doped with multiple dyes were investigated by ray tracing using experimental data from newly available dyes. In such a collector multiple dyes are absorbed and reemitted by increasingly longer

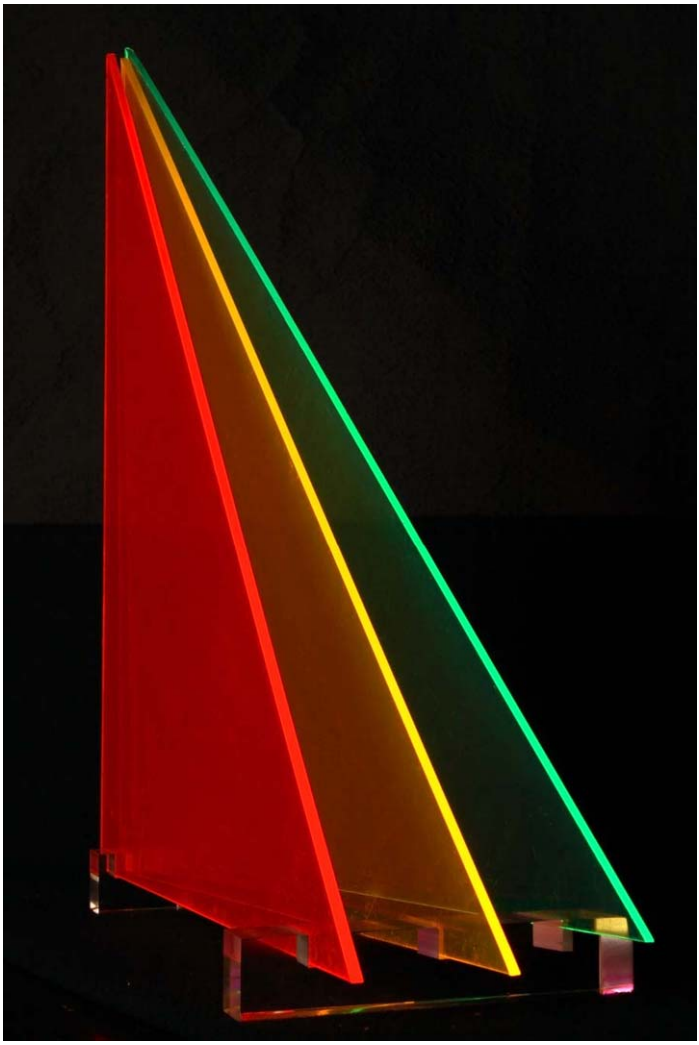

Fig. 10.15. Three PMMA plates doped with different color dyes. These plates are about 25 years old but not degraded, they were however mostly stored in the dark. Although the light output looks very spectacular only part of the light arriving at the edges is emitted because a big part is reflected back by total internal reflection

wavelength dyes. In this manner a large part of the solar spectrum is absorbed and emission occurs at a wavelength which is more suitable for silicon cells. They found that a mixture of five dyes including a near IR dye of 85% quantum efficiency gave the best result of 44% electrical efficiency. Only radiative transfer and high efficiency solar cells were studied. They also state that all dyes show photostability

under sunlight for at least 10 years. Lower stability was found by Reda with more conventional dyes [25].

A new possibility to obtain better performing luminescing centers consists in quantum dots as has been pointed out by Barnham et al. [26]. These are nanometer sized semiconductor crystallites. Because they are anorganic there is hope that they exhibit greater light stability than organic dyes. Another advantage is that the absorption threshold can be tuned by choice of the dot diameter. Furthermore, Chatten et al. [27] showed by a thermodynamic model that the red shift of emission is related to the spread of quantum dot sizes.

In view of these advantages there is considerable interest in developing fluorescent concentrators doped with quantum dots. Numerous investigations were carried out in recent years. Mainly quantum dots based on CdS were used. Schüler [28] applied the dots by the sol-gel technique to glass surfaces but also core-shell quantum dots consisting of CdSe cores with CdS or ZnS shell were studied [29, 30]. So far the quantum dots show continued improvement but quantum efficiency is not yet as high as for the best organic dyes. Also some instability has been observed.

Further, it should be remarked that fluorescent concentrators have applications beyond photovoltaics. They have been in use for advertising for many years. They can also be used in green houses to convert the green light to red light which can be better absorbed by plants [20]. Application for daylighting has been studied in the early days [31] and recent work with newer dyes appears very promising [12].

Finally in Fig. 10.15 I present a photograph of three collector plates as they appear in daylight.

References

1. W.H. Weber, J. Lambe, Appl. Opt. **15**, 2299 (1976)
2. A. Goetzberger, W. Greubel, Solar energy conversion with fluorescent collectors. Appl. Phys. **12**, 123 (1977)
3. W.A. Shurcliff, R.C. Jones, J. Opt. Soc. Am. **39**, 912 (1949)
4. J.B. Birks, *The Theory and Practice of Scintillation Counting* (Pergamon, London, 1964)
5. G. Keil, J. Appl. Phys. **40**, 3544 (1969)
6. G. Keil, Nucl. Instrum. Methods **87**, 111–123 (1970)
7. G. Smestad, H. Riess, R. Winston, E. Yablonovitch, Sol. Energy Mater. **21**, 99 (1990)
8. B.S. Richards, A. Shilav, R. Corkish, 19. EU PV Sol. En. Conf. 113 (2004)
9. U. Rau, F. Einsele, G.C. Glaeser, Appl. Phys. Lett. **87**, 171101 (2005)
10. J.C. Goldschmidt, S.W. Glunz, A. Gombert, G. Willeke 21, EU PV Sol. En. Conf. 107 (2006)
11. G.C. Glaeser, U. Rau, Proc. SPIE **6197**, 143 (2006)
12. A.A. Earp, G.B. Smith, P.D. Swift, J. Franklin, Sol. Energy **76**, 655 (2004)
13. A. Zastrow, H.R. Wilson, K. Heidler, V. Wittwer, A. Goetzberger, *6th EU PV Conf. 202* (1983)
14. E. Yablonovitch, J. Opt. Soc. Am. **70**, 1362 (1980)
15. T. Markvart, J. Appl. Phys. **99**, 026101 (2006)
16. T. Markvart, L. Danos, P. Kittidachachan, R. Greef, *20. EU PV Sol. En. Conf. 171* (2005)

17. W. Shockley, H.J. Queisser, J. Appl. Phys. **32**, 510 (1961)
18. A. Goetzberger, O. Schirmer, Appl. Phys. **19**, 53 (1979)
19. S. Balushev, T. Miteva, V. Yakutin, G. Nelles, A. Yasuda, G. Wegner, Appl. Phys. Lett. **14**, 143903 (2006)
20. V. Wittwer, W. Stahl, A. Goetzberger, Sol. Energy Mater. **11**, 187 (1984)
21. A. Zastrow, SPIE **2255**, 534 (1993)
22. L. Danos, P. Kittidachachan, P.J.J. Meyer, R. Greef, T. Markvart, *21. EU PV Sol. En. Conf. 443* (2006)
23. A.J. Chatten, D.J. Farrell, B.F. Buxton, A. Büchtemann, K.W.J. Barnham, *21. EU PV Sol. En. Conf. 315* (2006)
24. B.S. Richards, K.R. McIntosh, *21. EU PV Sol. En. Conf. 185* (2006)
25. S.M. Reda, Sol. Energy **81**, 755 (2007)
26. K. Barnham, J.L. Marques, J. Hassard, P. O'Brien, Appl. Phys. Lett. **76**, 1197 (2000)
27. A.J. Chatten et al., Sol. Energy Mater. Sol. Cells **75**, 363 (2003)
28. A. Schüler, M. Python, M. Valle del Olmo, E. de Chambrier, Sol. Energy **81**, 1159 (2007)
29. S.J. Gallagher, B. Norton, P.C. Eames, Sol. Energy **81**, 813 (2007)
30. S.J. Gallagher, B.C. Rowan, J. Doran, B. Norton, Sol. Energy **81**, 540 (2007)
31. A. Zastrow, V. Wittwer, Proc. SPIE **653**, 93 (1986)

11 Hybrid Photovoltaic/Thermal Collector Based on a Luminescent Concentrator

V. Petrova-Koch and A. Goetzberger

11.1 Introduction

The efficiency of a single-junction PV cell – for example, a c-Si solar cell – has a theoretical limit of around 27%–30% [1]. This means that, in the best-case scenario, the device harvests around one-fourth of the solar energy. This relatively low efficiency is due to the impossibility of converting the broad solar spectrum with one semiconductor material. The single-junction cell represents a relatively narrow band, two-terminal device. The spectrally distributed solar radiation requires, in principle, a many-terminal or multijunction device in order to reach a high conversion efficiency. When the single junction is replaced by a multijunction cell in practice, efficiency rises substantially (to about 40% in the last few years, for the triple-junction III–V-based PV cells [2]). But even then it remains relatively low.

The introduction of an intermediate band into the semiconductor band gap [3], or solar thermophotovoltaics [4] are other innovative ways to increase the efficiency of a PV cell, but again the efficiency improvement is about the same.

Concentration of solar radiation is a prerequisite to achieve these high efficiencies. [5], and concentrator photovoltaics (CPV) have good prospects for terrestrial applications. There are two principally different ways to concentrate solar radiation. One is CPV based on geometrical optics using, for example, an array of Fresnel lenses with a tracking system [5], and is suitable for concentration of direct solar radiation only. The other type of CPV is based on the luminescent concentrator (LuCo), which is the only device known with a chance to concentrate not only direct but also diffuse solar radiation without need of a tracking system [6].

Hybrid solar collectors are an attractive approach to harvesting electricity and heat simultaneously. This will reduce the cost of the modules, and will increase significantly the total efficiency of the system. Numerous attempts have been made in the past to develop such collectors, but there was little commercial success.

In principle, all the absorbed solar radiation which does not undergo conversion to electricity in a solar cell gets converted to heat. It is well known that the conversion efficiency of a solar cell drops as temperature increases. The temperature dependence depends on band gap: Solar cells with a large band gap are less sen-

sitive than those with lower gap. Therefore crystalline Si has a higher temperature coefficient than amorphous silicon.

The common practice is to integrate the solar module into the thermal absorber. This concept causes the well-known discrepancy that higher absorber temperature is not compatible with good performance of the solar cells. Furthermore, the solar cells do not provide a selective surface that is best for the absorber. As a result, hybrid collectors provide only relatively low temperatures. Nevertheless, many applications can be envisioned for such collectors. There is an IEA task 35 (PV/T) that is devoted to the promotion of hybrid collectors. The most recent information on this subject can be found at its website [7].

11.2 PV/T Hybrid Collector Based on a Luminescent Concentrator

If a luminescent concentrator is used in a PV/T hybrid collector, it offers a unique possibility to separate electrical and thermal conversion spectrally and in space. The incident solar radiation is split by the luminescing plate spectrally and spatially into two parts, as shown in Fig. 11.1.

The collector is constructed like a common thermal collector with the addition of a luminescing concentrator plate inserted between the cover glass and the absorber. Silicon PV Cells (mono- or bifacial, as presented in Chaps. 6 and 7) are positioned on one or several side edges of the plate. The other edges of the plate are mirrored. The luminescent plate is assumed to be doped with one or several dyes that transform the solar radiation into the red or near infrared fluorescence or phosphorescence that is best used by the silicon solar cell. It is possible to use a single dye or quantum dots with a broad absorption spectrum or a multistage sequence of dyes. The solar cells are positioned outside of the collector and thus are not exposed to high temperature.

The thermal energy reaching the absorber comes from several sources:

- The luminescent plate acts as a heat source because heat is generated by Stokes losses in the plate. Dependent on the temperature difference between LuCo plate

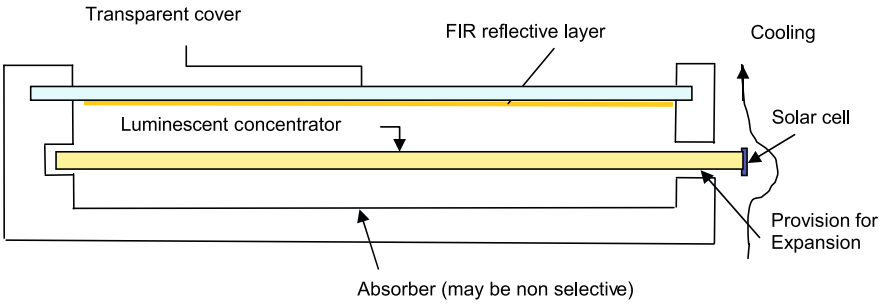

Fig. 11.1. The concept of a PV/T hybrid collector based on the luminescent solar concentrator

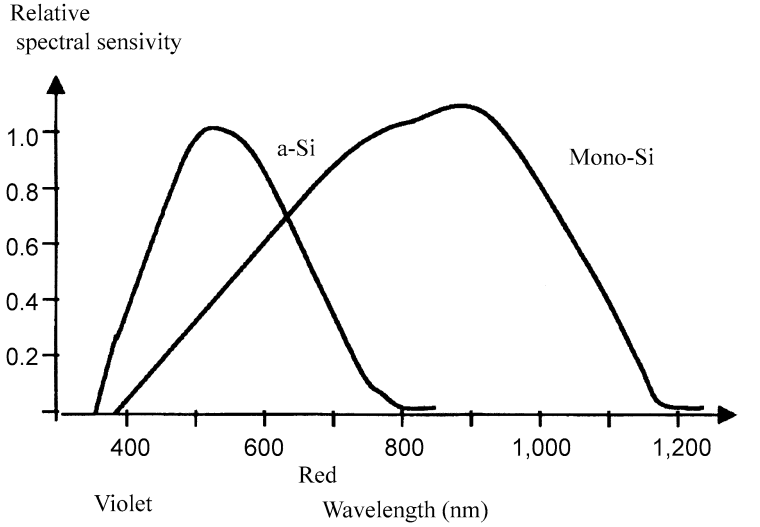

Fig. 11.2. Spectral response curves of amorphous and crystalline silicon

and absorber thermal radiation and heat flowing by conduction and convection reaches the absorber. Nonselectivity of the absorber may be advantageous.

- The luminescent plate is transparent to the infrared part of the solar spectrum. This radiation reaches the absorber directly. Onset of transmission of the LuCo plate is at the long wavelength edge of the dye absorption.
- As pointed out in the preceding article, about 25% of luminescent radiation is emitted to the outside of the plate. One half of this radiation emitted downwards will also reach the absorber. If radiation is reabsorbed by the same or other dyes in the matrix, the loss is repeated.

In order to reduce heat losses through the front plate its inside can carry an FIR reflecting coating.

The PL spectrum of the luminescent concentrator should be designed to match the spectral sensitivity curve of the solar cells (Fig. 11.2). By making use of only this part of the solar spectrum, heating of the cell will be suppressed substantially. Both crystalline and amorphous silicon are feasible. In the amorphous case, a larger part of the long wavelength spectrum would be transmitted to the absorber. From an efficiency standpoint, however, crystalline silicon is preferred.

A very rough estimate of the efficiency of the LuCo hybrid collector is now possible.

The PV efficiency can be expected to be between 5% and 10%, referred to as total collector area. This depends on the availability of suitable dyes.

The thermal efficiency of the collector (excluding system efficiency) can be expected to be between 50% and 60% in the temperature range used for water heating.

The advantages of the LuCo hybrid collector are as follows:

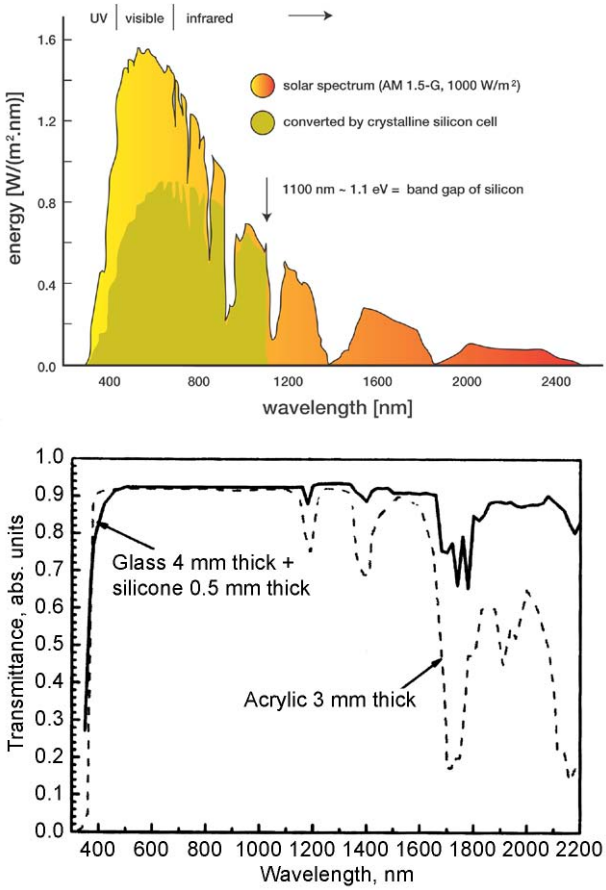

Fig. 11.3. A typical transmittance spectrum of a solar glass plate compared with that of an acrylic plate with similar thickness together with the terrestrial solar AM1.5 spectrum [5]

- High combined thermal plus electrical conversion efficiency.
- High geometrical PV concentration, thus the cost of solar cells is reduced.
- Solar cells can operate at close to ambient temperature.

Several difficulties associated with this concept should not be overlooked. They refer mostly to materials such as:

Thermal stability of the LuCo plates. So far only plastic materials have been used because very high transparency is required. Polycarbonate rather than PMMA is advised. Even better would be glass if it can be made with comparable transparency. It should be noted that the dye does not have to be distributed throughout the matrix but can also be incorporated in a thin surface film at much higher concentration, as reported recently in Scince [8].

For the present application, transparency of the matrix in the near infrared is important because it has to be transmitted within the matrix to the solar cell. Figure 11.3 shows the solar spectrum and transparency of glass and acrylic. Glass is more transparent than plastic beyond 1,200 nm.

11.3 Conclusions

This chapter describes a novel concept for a PV/T hybrid based on the luminescent solar energy collector, particularly suitable for application with highly efficient c-Si solar cells, mono- or bifacial. This collector separates electrical and thermal conversion and thus allows the solar cells to operate at lower temperature while the thermal absorber is at high temperature.

References

1. A. Goetzberger, V.U. Hoffmann, in *Photovoltaic Solar Energy Generation*. Springer Series Optical Science, vol. 12 (2005), p. 58
2. A.W. Bett, F. Dimroth, G. Siefer, Multi-junction concentrator solar cells, in *Concentrator Photovoltaics*. Springer Series in Optical Sciences, vol. 130 (2007), p. 67
3. A. Luque, A. Marti, A metallic intermediate band high efficiency solar cell, in *Prog. Photovoltaics*, vol. 9 (2001), pp. 73–86
4. V. Andreev, V. Khvostikov, A. Vlasov, Solar thermophotovoltaics, in *Concentrator Photovoltaics*. Springer Series in Optical Sciences, vol. 130 (2007), p. 175
5. V.D. Rumyantsev, Terrestrial concentrator PV systems, in *Concentrator Photovoltaics*. Springer Series in Optical Sciences, vol. 130 (2007), p. 150
6. A. Goetzberger, Fluorescent Solar Energy Concentrator: Present State of Development. Chapter in this book
7. www.iea-shc.org
8. M.J. Curie, J.K. Mapel, T.D. Heiden, Sh. Goffri, M.A. Baldo, *High Efficiency Organic Solar Concentrator for Photovoltaics in Scince*, vol. 321 (2008), p. 226

12 Installation Concept and Future Applications

O. Mayer

12.1 PV from the Customer Perspective

With annual growth rates exceeding 30%, photovoltaic (PV) energy is now firmly established as a decentralized source for generating power. Due in particular to German legislation promoting renewable energies (Renewable Energy Sources Act/EEG), PV has in recent years made triumphant advances.

If one considers the technology currently in deployment (in 2008), the following is ascertainable:

Roof-mounted installation is used for the vast majority of PV systems (that is to say, the system is mounted on top of an existing roof). The preponderance of this method is due to the current preference for "retrofitting" PV systems onto existing roofs. In such cases, dual functionalities are not exploited.

The criterion for a PV system is the maximum possible degree of generator efficiency. This is necessitated by the target of obtaining the maximum possible packing density on a limited roof area in order to reap maximum energy yields.

For the time being, building-integrated PV (BIPV) continues to play a subordinate role.

Consideration of the product range available at present (in 2008) shows that the majority of products consist of flat PV modules in which the blue silicon cells are clearly visible; when installed on a roof, the aesthetic effect is not particularly pleasing (Fig. 12.1).

This understandable lack of attention to aesthetic considerations was also expedient in view of the time frame in which the technology was developed. The target was to introduce and advance PV as a power-generation technology. In order to ensure competitive ability with existing systems, efficiency was the primary concern.

However, now that even the general public is familiar with PV technology, the target course of PV must be altered. Until now, the direction taken by PV was "dictated" by engineers in line with the following objectives:

High efficiency
High reliability
Simple installation
Low costs/Wp

Fig. 12.1. Typical roof-mounted installation of a solar-thermal and PV system. (Source: Mayer, private photograph)

"Maximum output on the smallest space" – the perspective of the power engineer – was decisive in the development process. In view of the fact that contemporary PV systems are no longer in their technological infancy, the technology must be viewed from a new perspective. The crucial question to be asked is:

What do customers want, and for what are they willing to pay?

This question may be viewed analogously with developments in the automobile industry. While technical attributes (performance, reliability, costs, and so forth), were formerly crucial selling points for vehicles, contemporary advertising promotes wholly different characteristics (motoring experience, emotion, safety, and so forth). It is universally assumed that the performance attributes of a car are delivered automatically, and need not be queried. For the manufacturer, this leads to the question of how his or her product can be distinguished from those of the competition – the question of the differentiators or Unique Selling Points (USPs).

The KANO model (Fig. 12.2) reflects this view of customer satisfaction. Many functionalities are taken as given, and not even addressed by the customer. If only these functionalities are delivered, then customer satisfaction is scarcely achievable (red arrow). Performance characteristics desired by and imaginable to the customer lead to customer satisfaction (yellow arrow). The truly interesting attributes, however, are those which surpass the customer's conceptions and are unexpected (green arrow). They are the ones which produce enthusiasm for the product and amount to a differentiator, or unique selling point (USP). However, it must be noted that in the course of time such attributes likewise turn into ones which are automatically expected and assumed to be given.

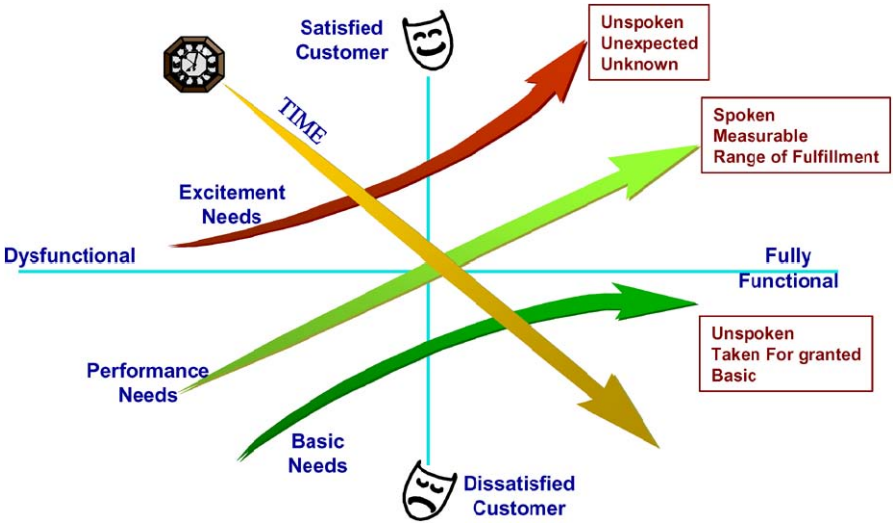

Fig. 12.2. KANO model for customer requirements. (Source: SixSigma, modified)

If one considers those applications at present feasible for PV as systems technology, there exist a number of customer requirements that do not simply translate into €/Wp. Figure 3.2 shows an overview of possible applications of PV.

When a PV system is used to feed energy to the grid in accordance with the EEG, the foremost concern is to obtain the maximum possible power yield per capital investment (distributed over the life of the system). In comparison with the efficiency of the modules, this aspect attributes a new status to parameters such as useful life of the components, costs of the balance of system (BOS), and maintenance costs. Efficiency is not directly relevant, but becomes significant due to the limited space for the installation (e.g. roof area). All these variables –and not just the cell/module efficiency – must be cooptimized.

In the case of standalone systems, a high peak output (depending on application) may be necessary alongside a high energy yield – for example, if information is required to be transmitted at a specific, periodic time or, like in the case of a pumping system, high midday water requirements simultaneously entail the need for disinfecting.

Other applications such as motor vehicles offer only very limited space on which to generate power. Therefore, the high efficiency of PV cells/modules becomes the dominant parameter. This is especially true when the power requirement is predefined by the existing ventilation system, for example in the case of vehicle air-conditioning systems.

When PV is used to provide power in extraterrestrial applications, the important aspects in addition to high efficiency are useful life, maintenance-freedom (reliability), and low weight. These parameters may well be more important than high efficiency, since the advantage gained by the latter is questionable if reliability is

low. Due to technical considerations and the costs, the possibility of repairs in outer space is more or less ruled out.

When PV is used in the form of facade elements, then this technology competes with other facade constructions, whereby the comparative costs per square meter are decisive. The fact that a PV facade also allows electricity to be generated is, in this case, a secondary sales argument – a unique selling point (USP) or "differentiator" over competitive products.

When PV is deployed as an architectural element, the efficiency aspect moves almost entirely into the background. The dominant aspects are aesthetic in nature: the "look" and the impression are crucial.

In the case of other applications (garden lights, pond fountains, etc.), the flexibility of PV is decisive. The PV must be able to adapt to the product requirements, above all in regard to form and color. High efficiency is secondary in importance.

In the case of concentrator systems, a high degree of thermal endurance must be guaranteed, and tracking mechanism and inverter performance have to comply with precision requirements.

Especially relevant in the case of PV water supply are the costs per cubic meter of water. While cell/module efficiency likewise plays a role, it is merely one aspect among several (drilling costs, space requirement, reliability, 24-hour maximum permissible failure duration, BOS, etc.).

12.2 PV Deployment Today

Contemporary terrestrial PV systems may be divided into the following groups:

- Nondomestic stand-alone systems
- Domestic standalone systems
- Grid-connected centralized PV systems
- Grid-connected decentralized PV systems

Figure 12.3 shows the development of PV in countries which are members of the International Energy Agency. Grid-connected systems represent the largest share.

12.2.1 Nondomestic Standalone Systems

Nondomestic standalone systems are mainly systems supplying electricity to villages in regions formerly lacking grid electricity. Solar generators and/or windturbine systems are deployed as power generators, and an energy-management system provides the grid supply to a village, for example (Fig. 12.4).

In such applications a subordinate role is played by space requirements or aesthetics. At the present time, there is little demand for multifunctional characteristics; with such systems, the crucial criterion is price per Wp.

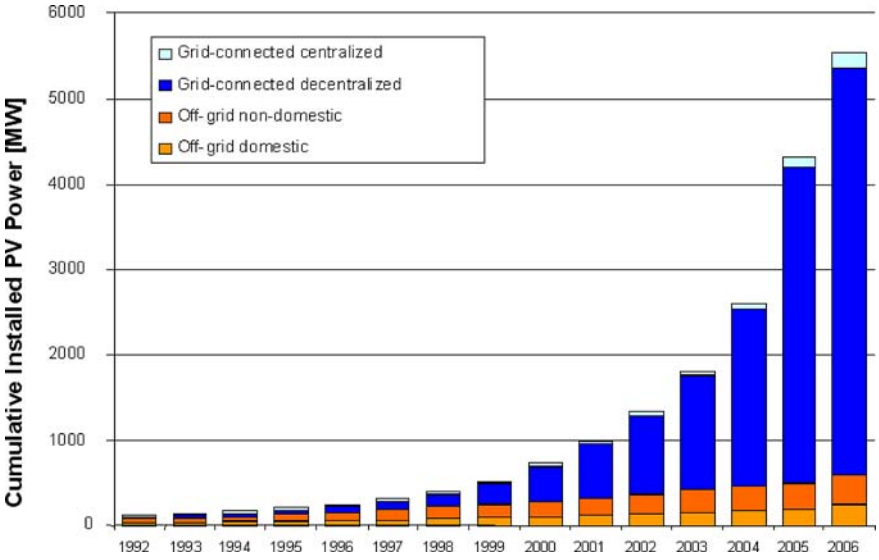

Fig. 12.3. Different applications of PV and installed Power (based on IEA data). (Source: IEA)

Fig. 12.4. PV generator for a village electricity supply. (Source: SMA)

12.2.2 Domestic Standalone Systems

Domestic standalone systems are also knows as solar home systems (SHS). These small PV systems are mainly used to supply homes with light, radio, and possibly also television (Fig. 12.5). With a generator output of generally 10 W to 200 W,

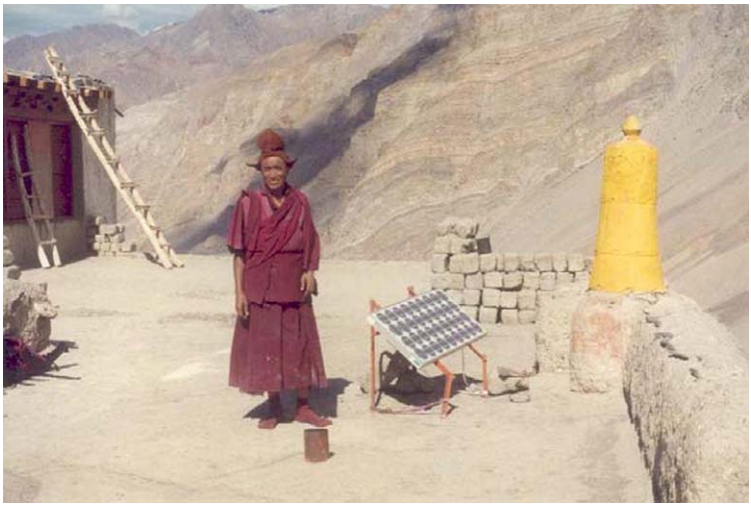

Fig. 12.5. SHS in Tibet. (Source: LBST)

Fig. 12.6. Central PV field in Germany. (Source: Shell Solar)

they take the place of petroleum lamps or battery-driven equipment. The price paid for the supply of nonphotovoltaic electric current is on the order of 8 to 10 dollars per month. Once again, price is the decisive criterion in determining the expedience of substituting a SHS. Aesthetics or multifunctionality remain secondary considerations.

12.2.3 Grid-Connected Central PV Systems

Figure 12.6 shows a central PV field of the kind typically installed in Europe (Germany or Spain) at the present time. These systems are generally operated like power stations. The functionality required is above all high power density (high efficiency, low space requirements). As yet, aesthetic requirements are not relevant, although

the optical impression will become increasingly important as these systems increase in number.

12.2.4 Grid-Connected Decentral Systems

The vast majority of photovoltaic applications are installed in the form of grid-connected decentral systems. These systems are for the most part roof-mounted installations (Fig. 12.7(a)). This mode of installation offers several advantages:

(a)

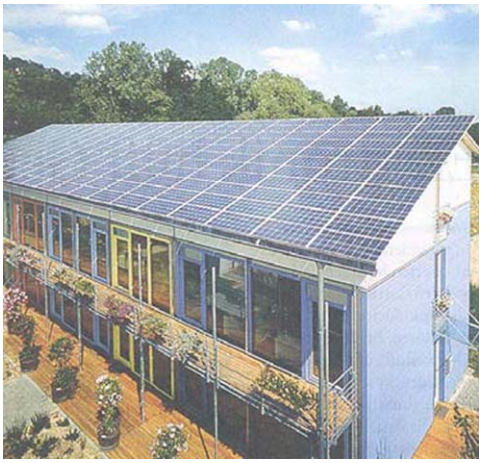

(b)

Fig. 12.7. (**a**) Roof-mounted PV System. (Source: Mayer, private photograph.) (**b**) Roof-integrated. (Source: Photon)

- The waterproofness of the roof is not dependent on the PV.
- Easier compliance with fire-protection or building regulations for roofs.
- Subsequent installation is simple.
- The generator size can be chosen without reference to the roof area.

In order to reduce costs, however, multifunctional usage of the PV modules is expedient, for example simultaneously as substitute roofing material and as power generator. This method simultaneously reduces roofing costs and the expenditure for electricity which would otherwise be purchased at commercial rates (including the cost saved on the normal roof tiling, Fig. 12.7(b)). However, contemporary systems continue to be based on the predominant consideration of *primarily* generating electric energy. All other functionalities are viewed as less important.

The possibility of introducing a dual-layered perspective is particularly manifest in the case of the decentral grid-connected systems, that dual perspective can be summed up as

"Power engineer" ↔ "Aesthete / Architect".

The "power engineer" discerns in photovoltaics above all the potential for generating electricity. The main criteria are high power density, optimum positioning, high system yield, low maintenance costs, long useful life, and so on. The objective is to produce the lowest possible energy costs in order to be able to compete with current electricity prices. Little consideration is given to optical characteristics, aesthetics, and so forth.

The "aesthete/architect" focuses on these otherwise secondary attributes, with electricity production being of subordinate importance. Solar panels are viewed as a desirable design element allowing a building to be given a particular optical effect. Figure 12.8 shows the example of a house into which the conventional PV modules have been integrated in optically compatible form.

If generation of electricity no longer occupies the foreground of considerations, then other criteria must be applied when evaluating a system. If PV is used as a facade element, the €/kWh relationship becomes less important than the cost per

Fig. 12.8. Facade-integration of conventional PV modules. (Source: Photon)

square meter in comparison with other facade elements. Power generation is viewed as a cost-reducing factor not given in the case of conventional facade elements, with which no savings are made over the course of time. Thus, the efficiency of the system is not critically important, but the overall costs must add up:

$$\begin{aligned}&\text{Invest}_{\text{PV facade}} - \text{Power yield}_{\text{useful life}} \cdot €/\text{kWh}\\ &< \text{Invest}_{\text{conventional facade}} \cdot F_{\text{aesthetic impression}}.\end{aligned}$$

$F_{\text{aesthetic impression}}$ is here a quality factor dealing with the optical impression:

$$F_{\text{aesthetic impression}} = \frac{\text{Evaluation of PV facade}}{\text{Evaluation of conventional facade}}.$$

In this way, the multifunctionality of PV modules widens the spectrum of market approaches when energy generation is no longer in the foreground. Figure 12.9 illustrates the functions of a PV facade element as a substitute for conventional elements.

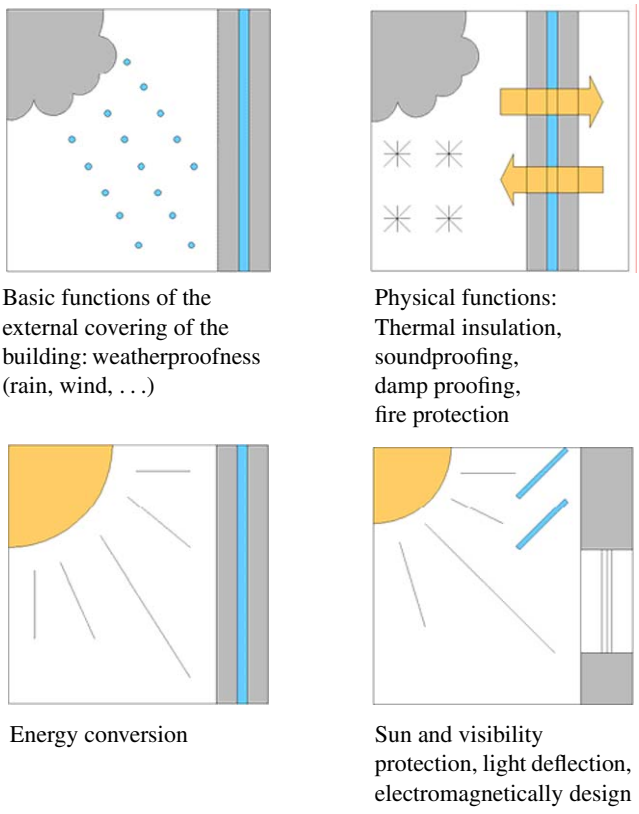

Fig. 12.9. Multifunctionality of PV facades. (Source: Ingrid Lützkendorf, IFF Weimar)

The PV module must assume basic functions of the external covering of the building; these functions include weatherproofing, protection against mechanical impacts (e.g. hailstones), optical impression, and so forth. Alongside these basic functions, a number of physical functions must be given. Thermal protection and damp proofing are essential to the energy use, fireproofing is a safety consideration, and soundproofing heightens the quality of life. In locations close to airports, and particularly in the case of tall buildings, it may be important to consider electromagnetic damping properties in order to reduce radar radiation.

Contemporary PV modules are not designed for the above-mentioned functionalities. For more than 20 years now, form and structure have been dictated by the need to obtain maximum yields from minimal space. All the same, such modules are being deployed as facade elements after undergoing slight alterations. Thanks to resourceful architecture combined with considerable efforts, such attempts are rewarded with success. However, present-day modules are less suitable for widespread deployment as facade elements that also work as decentral grid-connected systems, since they lack the functionalities necessary for this purpose.

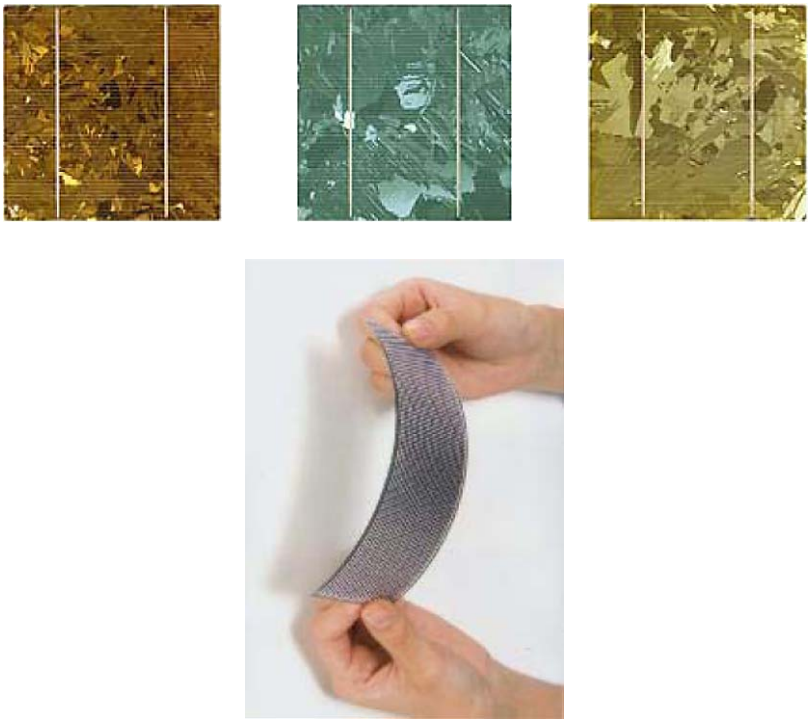

Fig. 12.10. Colored PV cells/Spherical cells. (Source: Sunways, Nikkei BP)

12.3 PV Developments in the Future

Since contemporary PV modules are not purpose-designed for deployment as facade elements, new criteria are necessary for this application. The main requirements may be seen to be coloration and shaping.

The market already offers solutions in regard to coloration (Fig. 12.10). Special coatings allow colored cells to be produced, whereby efficiency is reduced at the same time.

These cells continue to be flat. In the future, reduced cell thickness could produce flexible cells adaptable to curve forms. Another alternative is represented by spherical cells, which are embedded in a matrix. In this case, the matrix can likewise comply with a predefined form.

13 Design Rules for Efficient Organic Solar Cells

Z. Zhu, D. Mühlbacher, M. Morana, M. Koppe, M.C. Scharber, D. Waller,
G. Dennler, and C.J. Brabec

13.1 Introduction

There has been an intensive search for cost-effective photovoltaics since the development of the first solar cells in the 1950s [1–3]. Among all the alternative technologies to silicon-based pn-junction solar cells, organic solar cells are the approach that could lead to the most significant cost reduction [4]. The field of organic photovoltaics (OPV) is composed of organic/inorganic nanostructures, like the dye-sensitized solar cell, multilayers of small organic molecules and mixtures of organic materials (bulk-heterojunction solar cell). A review of several so-called organic photovoltaic (OPV) technologies was recently presented [5].

Unlike conventional inorganic solar cells, light absorption in organic solar cells leads to the generation of excited bound electron–hole pairs (often called excitons). To achieve substantial energy-conversion efficiencies, these excited electron–hole pairs need to be dissociated into free charge carriers with a high yield. Excitons can be dissociated at interfaces of materials with different electron affinities, by electric fields or the dissociation can be trap- or impurity-assisted. Blending conjugated polymers with high electron affinity molecules like C_{60} (bulk-heterojunction solar cell) has proven to be an efficient way for rapid exciton dissociation. Conjugated polymer/C_{60} interpenetrating networks exhibit an ultra-fast charge transfer ($\sim$40 fs) [6, 7]. As there is no competing decay process of the optically excited electron–hole pair located on the polymer, in this time regime an optimized mixture with C_{60} converts absorbed photon to electron with an efficiency close to 100% [8]. Besides the efficient charge carrier generation process, the bulk-heterojunction solar cell has attracted a lot of attention because of its potential to be a true low-cost photovoltaic technology. It is believed that a simple coating or printing process will allow a roll-to-roll manufacturing of flexible, lightweight PV modules which should allow for cost-efficient production and the development of products for new markets, e.g. in the field of portable electronics. One major obstacle to an immediate commercialization of the bulk-heterojunction solar cell are the relatively small device efficiencies demonstrated up to now [5]. The best energy conversion efficiencies published for small-area devices are in the range of 5–6% [9–12]. A detailed analysis of state-of-the-art bulk-heterojunction solar cells [8] reveals that efficiency loss

stems primarily from the low open-circuit voltage (V_{oc}) delivered by these devices under illumination. Typically, organic semiconductors with a bandgap of about 2 eV are applied as photoactive materials but the observed open circuit voltages are only in the range between 0.5 V and 1 V.

Here, we discuss the design rules for polymer donors, allowing high power efficiencies when processed in composites with a prototype acceptor PCBM ([6, 6]-phenyl-C_{61}-bytric acid methyl ester). Specifically, one class of low bandgap donors will be discussed in more detail, as we outline the important interplay between material design, synthesis, optical, morphological and transport related properties to the power conversion of solar cells. The chapter is closely related to a series of papers on these topics, which were published recently [13–16].

13.2 Material Design Rules for Donors in Single-Junction Solar Cells

In Fig. 13.1 the open circuit voltage of different bulk-heterojunction solar cells is plotted versus the oxidation potential of the conjugated polymers used in these devices. More than 26 different polymeric donors from various material classes (thiophenes, fluorenes, phenylene-vinylenes. . .) were investigated in bulk-heterojunction (BHJ) composites with PCBM. A linear relation between V_{oc} and the conjugated

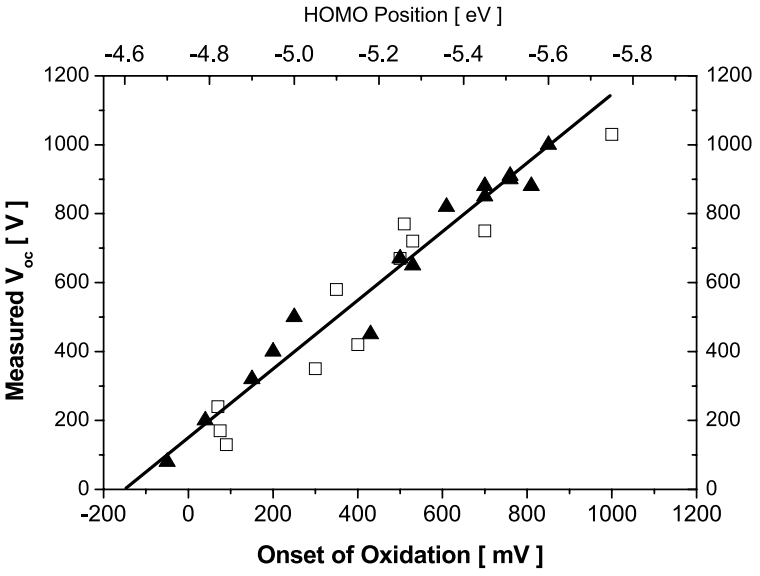

Fig. 13.1. Open-circuit voltage of different bulk heterojunction solar cells plotted versus the oxidation potential/HOMO position of the donor polymer used in each individual device. The straight line represents a linear fit with slope 1

polymer oxidation potential is found, with an x-axis offset of −140 mV, corresponding to a HOMO level of 4.6 eV. The offset suggests that the donor materials with lower lying HOMOs will not function in solar cells with PCBM. The LUMO of PCBM is assumed with 4.3 eV, and the difference between the PCBM LUMO and the smallest polymer HOMO value represents the energy which is obviously lost during the photo-induced charge-generation process. In our case, this number is 0.3 eV. According to Fig. 13.1 the open circuit voltage of a conjugated polymer/PCBM solar cell can be estimated by

$$V_{\mathrm{oc}} = \left|E_{\mathrm{HOMO}}^{\mathrm{Donor}}\right| - \left|E_{\mathrm{LUMO}}^{\mathrm{PCBM}}\right| - 0.3\,\mathrm{V}. \tag{13.1}$$

Based on this finding one can calculate the efficiency of a bulk-heterojunction solar cell solely as a function of the bandgap and the lowest unoccupied molecular orbital (LUMO) level of the donor. For simplicity we assume a constant external quantum efficiency of the solar cell for photon energies equal to or larger than the bandgap energy of the donor and neglect possible contribution to the short-circuit current from photons absorbed by the fullerene. Under these assumptions the short circuit current is calculated by

$$i_{\mathrm{sc}} = e \cdot \int_{E_{\mathrm{g}}}^{\infty} \mathrm{EQE}(E) \cdot n_{\mathrm{AM1.5}}(E)\,\mathrm{d}E, \tag{13.2}$$

where e is the electric charge of an electron, $n_{\mathrm{AM1.5}}$ is the number of photons arriving on the surface of the earth under AM1.5 illumination, E is the photon energy and E_{g} corresponds to the bandgap energy of the donor polymer. For simplicity, the calculations assumed an $\mathrm{EQE}(E) = 0.65$ for energies larger than E_{g} and a FF of 0.65, values which are typical for optimized devices [17]. In combination with (13.1) and (13.2) the efficiency of a bulk-heterojunction device given by

$$\begin{aligned}\eta &= \frac{i_{\mathrm{sc}} \cdot V_{\mathrm{oc}} \cdot \mathrm{FF}}{P_{\mathrm{light\_in}}} \\ &= \frac{e \cdot \int_{E_{\mathrm{g}}}^{\infty} 0.65 \cdot n_{\mathrm{AM1.5}}(E)\,\mathrm{d}E \cdot (|E_{\mathrm{HOMO}}^{\mathrm{DONOR}}| - |E_{\mathrm{LUMO}}^{\mathrm{ACCEPTOR}}| - 0.3) \cdot 0.65}{P_{\mathrm{light\_in}}},\end{aligned} \tag{13.3}$$

where $P_{\mathrm{light\_in}}$ is the incident light power per unit area. The result is shown in Fig. 13.2 as a contour plot where the x and y axis are the bandgap and the LUMO level of the donor and the contour lines indicate constant power conversion efficiencies.

Figure 13.2 shows that the donor LUMO-level determines the maximum energy conversion efficiency of a bulk-heterojunction device. Surprisingly the variation in the efficiency is rather small upon changing the bandgap of the donor when the LUMO level is kept constant. The relative position of the polymer's LUMO is much more relevant to achieving highest efficiencies. For energy conversion efficiencies exceeding 10%, the donor polymer must have a bandgap <1.74 eV and a LUMO level <-3.92 eV always assuming a fill factor (FF) and the average EQE equal to 0.65. Again the calculated value is almost constant upon decreasing the donor bandgap down to 1.3 eV.

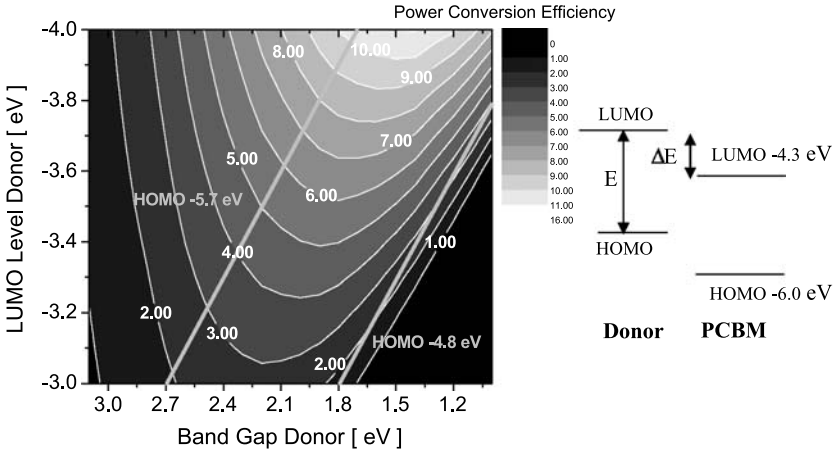

Fig. 13.2. (*Left*) Contour plot showing the calculated energy conversion efficiency (contour lines and colors) versus the band gap and the LUMO level of the donor polymer according to the model described earlier. Straight lines starting at 2.7 eV and 1.8 eV indicate LUMO levels of −5.7 eV and −4.8 eV, respectively. (*Right*) Schematic energy diagram of a donor PCBM system

Besides a reduction of the bandgap, new donor materials must be designed to optimize the LUMO as this parameter dominantly drives the solar cell efficiency.

It is important to note that an optimized open-circuit voltage is a prerequisite to achieve certain device efficiencies; however, it is not sufficient. In addition, the charge carrier mobility of electrons and holes in the donor acceptor blend must be high enough to allow an efficient charge extraction and an electrical fill factor (FF) of 0.65. The relation between charge carrier mobility and FF can be deduced from a recently presented model [17]. The main feature of this extended pn-junction model is that the photocurrent is dominantly field driven. For devices with an active layer thickness of several hundred nanometers, mobilities of $\sim 10^{-3}$ cm^2/Vs are required to prevent significant electrical and recombination losses. The model can also be used to analyze V_{oc} losses of bulk heterojunction solar cells. The overall theoretical limit of the open-circuit voltage is given by the difference between the acceptor LUMO level and the donor HOMO level, which also defines the built-in field V_{BI}. As discussed earlier and shown in Fig. 13.1, we find deviations of the theoretical maximum V_{oc} in the order of 0.3 V.

In Fig. 13.3 the current voltage curve of a poly-3-hexyl-thiophene/PCBM bulk-heterojunction solar cell acquired in the dark (full line) and the idealized field-driven photocurrent are plotted. The superposition of both curves gives the current–voltage curve under illumination. The open-circuit voltage of the solar cell is defined as the voltage which compensates the current flow through the external circuit (indicated by the vertical line in Fig. 13.3). Figure 13.3 shows that a main loss mechanism for V_{oc} is dominated by the dark current–voltage curve of the diode which is determined by the ideal factor n and the reverse dark current i_0 of the diode. This loss is typi-

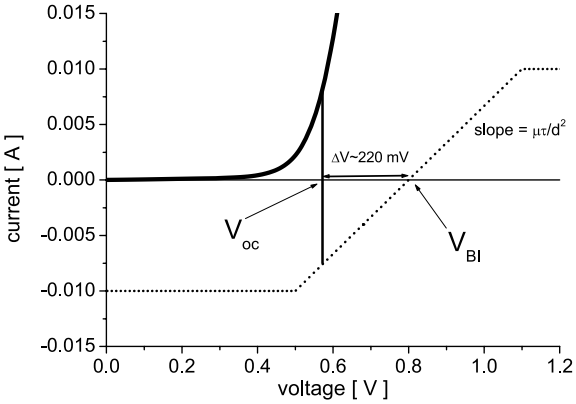

Fig. 13.3. Current-voltage curve of poly-3-hexyl-thiophene (P3HT)/PCBM solar cell measured in the dark (*full line*) and field-driven photocurrent (*dotted line*). VBI is given by ELUMO (PCBM) minus EHOMO (P3HT) (−4.3 V–(−5.1 V)) = 0.8 V

cally of the order of 200 mV. A smaller part of the V_{oc} loss can originate from the fact that the photocurrent in bulk-heterojunction devices is dominantly field-driven. The open-circuit voltage depends on the slope ($=\mu\tau/d^2$) of the field-driven current around V_{BI}. A steeper slope moves the V_{oc} closer to V_{BI}.

In summary, OPV can easily reach 10% efficiency with the outlined BHJ concept. There is a distinct relation between energy conversion efficiency of a bulk-heterojunction solar cell, bandgap and the LUMO level of the donor, which can be summarized in a 2D contour diagram.

Most interestingly, these investigations give a fundamental insight into the losses of BHJ solar cells and clearly outline how to go beyond 10% efficiency. First, the EQE and the FF have to be improved. There have been reports on so-called hero solar cells with a maximum EQE of more than 80%, and a FF of more than 70% has been published as well. Obviously, there is still significant potential to improve the performance of single-junction cells by further fine tuning on the EQE and FF values. Second, BHJ solar cells exhibit two quite fundamental losses – on the one hand the energetic loss due to the photo-induced charge transfer, on the other hand the V_{oc} losses due to dark current contributions. One might be interested in understanding the efficiency potential of single-junction cells in dependence on these two losses, and that is plotted in Fig. 13.4. Here, the CT loss as well as the V_{oc} loss were modeled with 0.25 V each. The calculations were run for a FF of 0.7 and an EQE of 90%. Both are challenging but realistic values for fully optimized organic solar cells. The loss-free scenario yields a maximum possible efficiency of about 30%. Each loss reduces the efficiency potential by about 5% points, so that in the case of CT and V_{oc} losses, a maximum efficiency of about 20% can be expected. A reduction in the optimum bandgap accompanies these losses. Although the loss-free case shows little sensitivity to the bandgap of the donor, a clear maximum in the 1.5 eV (900 nm regime) is observed for the scenario with V_{oc} and CT losses.

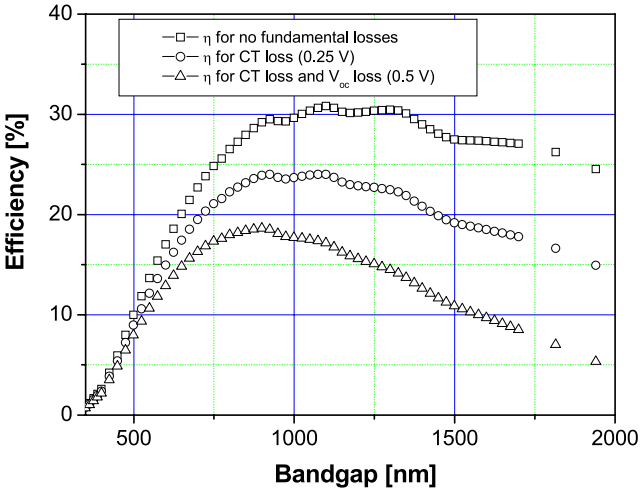

Fig. 13.4. Efficiency of organic BHJ independent of the donor's bandgap. The three different curves assume (**a**) the loss-free case (*top curve*), (**b**) energetic losses (0.25 eV) due to the photo-induced charge transfer (CT) (*middle curve*) and (**c**) losses due to CT and the V_{oc} (0.5 V) (*lower curve*)

In summary, today's single-junction organic solar cells have the performance potential to overcome 10% by fine tuning the material properties of the donor. Increasing the FF to over 70% and the EQE to 90% will pave the way to 20% power efficiency; for 30% power efficiency, though, the two fundamental losses – the V_{oc} as well as the CT loss – have to be overcome. Compared to today's efficiency of 5% [18–22], there is still some development to be done.

13.3 Toward Novel Polymeric Donors: Poly-Cyclic-Bridged-DiThieno Copolymers (PCPDT)

After more than 10 years of trying to find acceptors better than PCBM, all the alternative approaches – including other fullerenes, TiO2, ZnO, n-type polymers, and small molecular acceptors – did not outperform PCBM, despite their large potential for future performance improvements. Following the design rules discussed in the previous section, there is a huge demand for polymers with a bandgap between 1.3 and 1.6 eV. Besides bandgap, several other characteristics of conjugated polymers, including HOMO/LUMO levels and carrier mobility, need to be optimized simultaneously in order to achieve high photovoltaic performance [13]. In general, the gap between the HOMO of the electron donating polymer and the LUMO of the electron acceptor should be maximized in order to increase the open-circuit voltage, and at the same time the bandgap of the polymer should be minimized to increase photon absorption and thus short-circuit current. In addition the LUMO of the polymer

(donor) should be positioned above the LUMO of the fullerene derivative (acceptor) by at least 0.2–0.3 eV to ensure efficient electron transfer. All of that was discussed in the previous section. In addition to these design rules, a high charge-carrier mobility of holes and electrons is essential for efficient charge extraction and a good fill factor. To prevent significant photocurrent loss in cells with an active layer thickness of several hundred nanometers, a carrier mobility of 10^{-3} cm^2 V^{-1} s^{-1} is desired.

In the next two sections we will review a novel class of low bandgap polymers which has a high potential to fulfill all our requirements for higher efficiencies.

13.3.1 Structural and Optical Properties of PCPDT

The employment of materials absorbing the red and near-IR part of the solar spectrum has been one of the fundamental strategies in improving the performance of organic solar cells [23, 24]. It has been well known that coupling together electron-donors and acceptors leads to effective expansion of absorption wavelength. For example, the electron withdrawing 2, 1, 3-benzothiadiazole when coupled with electron-donating thiophenes or pyrroles resulted in a number of low-bandgap polymers [25–36]. Many structures have been designed and investigated, but most of them delivered only very low device performance [37–46]. The photovoltaic performances of these polymers is typically lower than 1%, significantly inferior to what is realized with a prototype wide bandgap polymer, poly-(3-hexylthiophene) (P3HT), and only a few polyfluorene-based copolymers showed efficiencies over 1%. One of the main reasons for this, we believe, is that these polymers usually lack solubility and their building blocks do not provide suitable anchoring sites for solubilizing side chains without causing further twisting between adjacent repeating units; this causes loss of conjugation. The carbon-bridged 4H-cyclopenta[2, 1-b:3, 4-b′]dithiophene was found to be a superior building block for conjugated polymers due to the forced co-planarity of the two thienyl subunits [47, 48]. The 4-carbon of the 4H-cyclopenta [2, 1-b:3, 4-b′]dithiophene can be readily functionalized by alkyl groups to increase solubility without causing additional twisting of the repeating units in the resulting polymers. In order to further increase the absorption wavelength and lower the bandgap of the polymer, a polymer containing the combination of cyclopentadithiophene as electron-donating and 2, 1, 3-benzothiadiazole as electron-accepting units (7, Fig. 13.5) was designed and synthesized.

The absorption spectra of the polymer 8 ($M_n = 28$ kDa) was recorded in both solution and solid state (Fig. 13.6). The optical band gap at solid state was estimated to be 1.4 eV from its absorption edge. It has a HOMO level of −5.3 eV and a LUMO level of −3.55 eV and bandgap of 1.75 eV as determined by cyclic voltammetry.

These physical parameters make this polymer a very promising material for high-performance organic solar cells though it is noted that there is a transmission window in the solid-state absorption spectrum of 8 around 500 nm which will reduce light harvesting, and, consequently cell performance. To increase light harvesting across the solar spectrum in the visible region, further random polymers copolymers 9(a–d) were prepared. The copolymer of bithiophene and cyclopenta[2, 1-b;3, 4-b′]dithiophene (10) was also synthesized for comparison purposes.

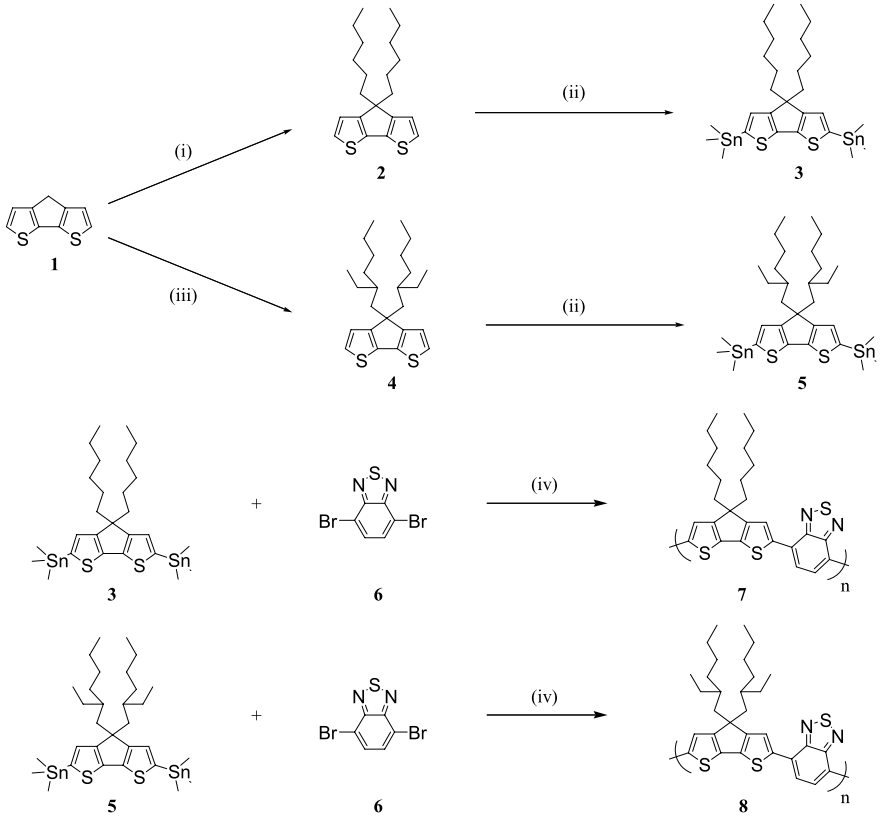

Fig. 13.5. Synthesis of poly[2, 6-(4, 4-dialkyl-4*H*-cyclopenta[2, 1-b; 3, 4-b′]dithiophene)-*alt*-4, 7-(2, 1, 3-benzothiadiazole)]

These polymers are shown in Fig. 13.7 and their corresponding optical properties compiled in Fig. 13.6. As expected, the incorporation of unbridged [2, 2′]bithiophene shifts the absorption maxima to the shorter wavelength region. With a ratio of the two electron-donating units, (4, 4-bis-(2-ethylhexyl)-4*H*-cyclopenta[2, 1-b;3, 4-b′]dithiophene) and 5, 5′-[2, 2′]bithiophene, between 2:1 and 1:2, the copolymer absorption covers broad range of the visible spectrum, and the dominant task – to find absorbers covering the whole visible spectrum – can be fulfilled by blends of these polymers.

An additional attractive feature of these polymers is that they have significantly higher absorptivity than the well-known regio-regular P3HT polymer. The optical densities of these polymers in chlorobenzene are normalized to the same polymer concentration (1 g/L) and their comparison is shown in Fig. 13.8. As can be seen from the spectra, the polymers 8–10 not only absorb at longer wavelength, but also exhibit higher absorptivity than P3HT. Electrochemical analysis (cyclic voltammetry) was conducted on these polymers to determine their LUMO and HOMO positions. All the polymers (8–10) have a HOMO of between −3.25 eV and −3.38 eV.

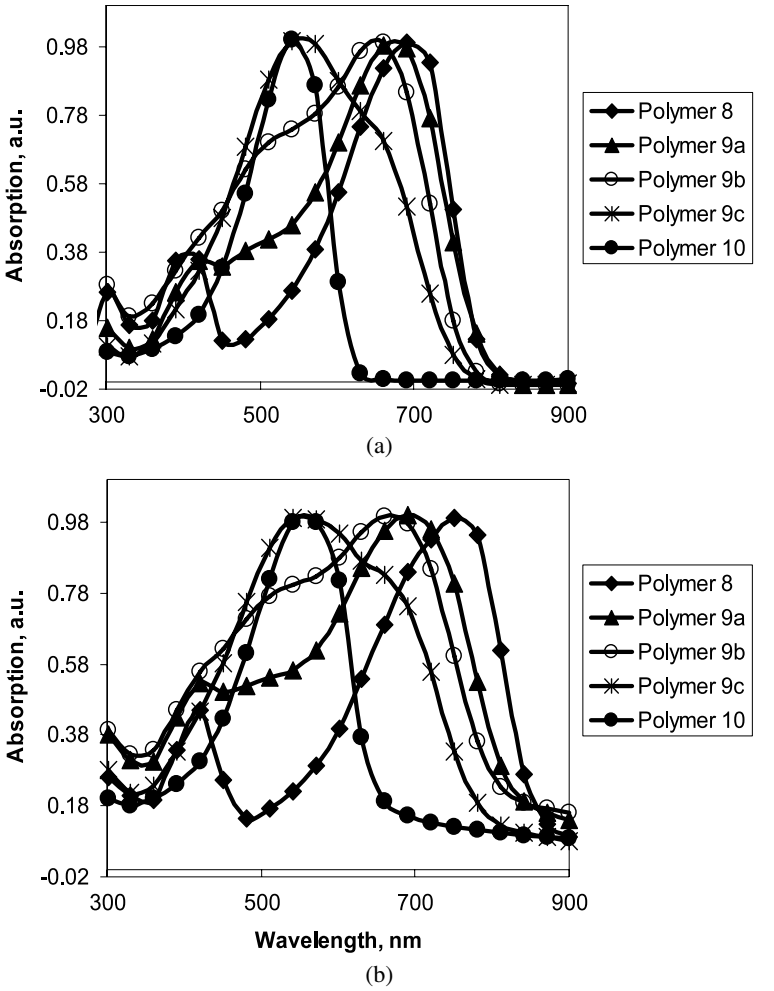

Fig. 13.6. The normalized absorption spectra of the polymers in chloroform (**a**) and in solid state (**b**)

The LUMOs of all the benzothiodiazole containing polymers (8, 9a–c) are around −3.55 eV. The LUMO of polymer 10 is around −3.0 eV. All these characteristics of PCPDT copolymers are within the desirable range for an ideal polymer for organic photovoltaic applications.

13.3.2 Transport and Electrical Properties of PCPDT-BT

The optical and electrochemical properties of the PCPDT copolymers, especially of the copolymer with benzothiadiazole (PCPDT-BT), clearly point to the potential of this material and presented the current limitations with respect to the power conversion efficiency. For high solar cell performance, the electrical transport properties of

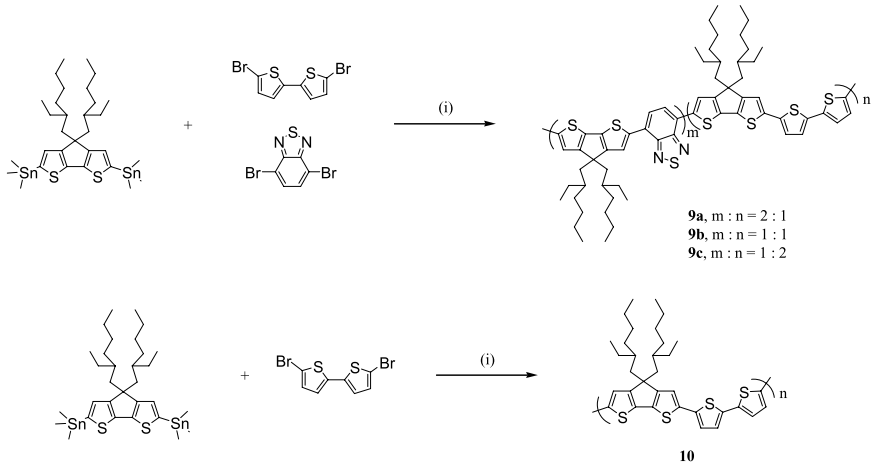

Fig. 13.7. The synthesis of both [2, 2′]bithiophene and cyclopenta[2, 1-b; 3, 4-b′]dithiophene containing copolymers

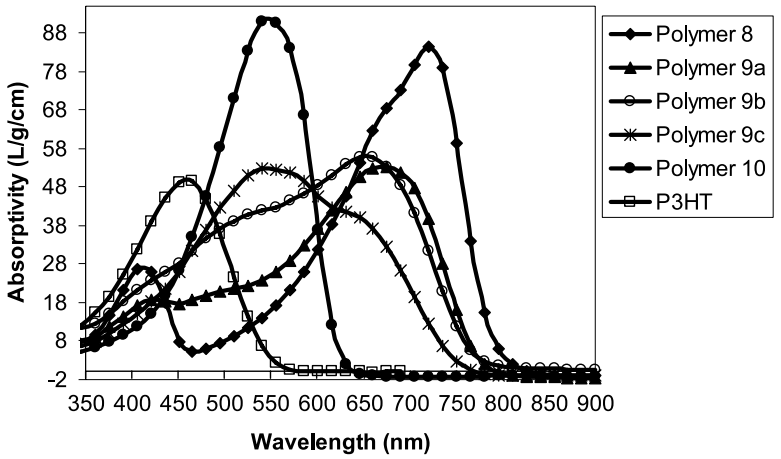

Fig. 13.8. A comparison of the absorptivity of the polymers with that of region-regular P3HT. All spectra were recorded in chlorobenzene

the donor/acceptor blend have to be sufficient to guarantee recombination-free transport. On the one hand, the ambipolar mobility and the related carrier drift length need to be larger than the device thickness. On the other hand, defects, traps and isolated or strongly phase-separated domains may significantly reduce the carrier lifetime as well. Recent steady-state and transient photoconductivity studies [49] on PCPDT-BT and PCPDT-BT:PCBM films in direct comparison with a P3HT reference system have confirmed efficient photogeneration of charges in the PCPDT-BT:PCBM blend and showed evidence of a quite comparable, though slightly lower

carrier lifetime compared to the one in P3HT:PCBM blends. Besides, lifetime, mobility and transport is equally important. Both of these parameters are related to the morphology of the donor–acceptor network. Transport losses, morphological as well as trap-induced, can be investigated by bipolar field effect transistor measurements (OFET). Phase separation and subsequent crystallization can be investigated by X-ray spectroscopy.

The grazing incidence X-rays spectroscopic profiles in thin films of PCPDT-BT (Fig. 13.9) show three distinct peaks at $2\theta \sim 24$ deg, $2\theta \sim 9.6$ deg and $2\theta \sim 3$ deg, respectively, whose intensity is rather low. The higher angle peak corresponds to a distance of approximately 3.7 Å that can be assigned to the π-orbital stacking between chains. Interestingly this lattice distance is the same as found for P3HT films [50]. The higher intensity 9.6 deg peak corresponds to a distance of 9.15 Å. In RR-P3HT this peak corresponds to the interchain spacing between chains interdigitated through the side chains. The XRD pattern of PCPDT-BT could therefore correspond to a lamellar structure similar to the one found in P3HT with the lamellae being perpendicular to the substrate. The intensity of the π-stacking peak is, however, much lower with respect to ordered RR-P3HT samples (not shown). This could be due to a rather low crystalline fraction present in the PCPDT-BT film measured. However, since a π-stacking perpendicular to the substrate cannot be detected by a θ–2θ scan, the possibility of having a significant volume of lamellar structure parallel to the substrate cannot be excluded. The third peak whose intensity is rather high corresponds to a spacing of ~37 A, indicating the presence of a significant long-range order.

The dynamics of film drying in relation to the crystalline order was investigated for drop-cast films dried in nitrogen atmosphere at room temperature versus 80 °C. Interestingly the slowly drying films showed a smaller signal at $2\theta \sim 24°$, which suggests a lower degree of π-orbital delocalization. In addition, films prepared from a bend of PCPDT-BT:PCBM = 1:1 were also studied to observe the changes induced in the polymer crystalline structure upon the addition of PCBM in Fig. 13.9(b). Interestingly, in this case a faster dying (80 °C) reduces the intensity of the π-stacking peak in the blend. In both cases the long-range order peak at low incidence angles is strongly reduced in films dried at 80 °C. The data presented here seem to indicate a rather low crystalline order in PCPDT-BT, in comparison with that observed in high-mobility conjugated homopolymers like RR-P3HT [51], which is only slightly dependent on the film processing conditions. However, the high in-plane hole mobility observed in this material poses new questions concerning the relation between morphology and charge transport associated with the structure of alternating donor–acceptor copolymers.

The transport of pristine PCPDT-BT was investigated by the field-effect transistor method (FET), and the hole mobility was deduced from the slope of the transfer-characteristic [52] using a DC dielectric constant of $\varepsilon_r = 2.7$ that was determined from MOS capacitance measurements, and is in the range 5×10^{-3}–2×10^{-2} cm^2/Vs ($C_{ox} \sim 1.4 \times 10^{-4}$ F/m).

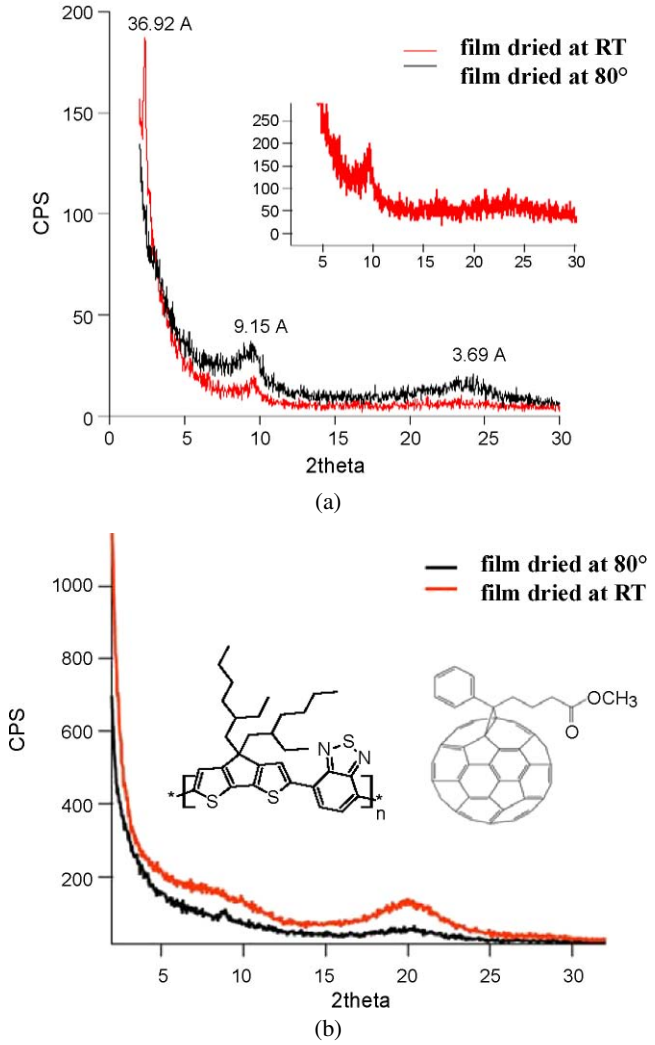

Fig. 13.9. (**a**) XRD pattern of a pristine PCPDT-BT film drop-cast from chlorobenzene slowly dried at room temperature (*grey line*) in N2 atmosphere compared to a film dried at 80 °C (*black line*). (**b**) XRD pattern of a PCPDT-BT:PCBM = 1:1 film drop-cast from chlorobenzene slowly dried at room temperature (295 K, *grey line*) in N2 atmosphere compared to a film dried at 80 °C (*black line*). The inset shows the chemical structure of PCPDT-BT (*left side*) and PCBM (*right side*)

As already known from other polymers, the processing conditions can influence the transport properties. Drying time, choice of the solvent, drying temperatures, etc. – all these parameters are known to impact the mobility of organic semiconductors. From the XRD data discussed in the previous paragraph, a dependence of

Table 13.1. Field-effect mobility data for films obtained using different coating process and temperature

Coating process	Hole mobility (cm^2/Vs)
Drop cast – r.t. drying	1.7×10^{-3}
Drop cast – 80 °C drying	1.8×10^{-3}
Spin coated – r.t. drying	5.1×10^{-3}
Spin coated – 80 °C annealing	4.2×10^{-3}

Table 13.2. Field-effect mobility data for PCPDTBT films cast using different solvents

Solvent	μ_h (cm^2/Vs)	μ_e (cm^2/Vs)
$CHCl_3$ – pristine	6×10^{-3}	2×10^{-5}
$CHCl_3$ – blend	4.8×10^{-3}	4×10^{-5}
oDCB – pristine	5×10^{-3}	9×10^{-5}
oDCB – blend	5.5×10^{-3}	4.5×10^{-4}
toluene – pristine	1.5×10^{-2}	2×10^{-4}
toluene – blend	5×10^{-3}	2×10^{-5}

the intermolecular order on the coating and drying process is expected. FETs were produced according to the conditions of the X-ray samples, and the data are summarized in Table 13.1, while Table 13.2 summarizes the impact of the solvent on the mobility. It is found that drop cast films show an almost three times lower mobility than the spin cast ones, while overall the mobility is only slight dependent on the processing and drying conditions. Also, fast and slow drying solvents do give quite comparable mobility. Highest mobility was observed for toluene-based solutions. Electron mobility of the pristine polymer is typically two orders of magnitude lower than the hole mobility.

By using the same solvents used for the pristine materials, we investigated OTFTs from blend solutions of PCBM:PCPDT-BT with a weight ratio of 1:1. The bipolar mobility was calculated as described in [53] from the measured transfer characteristics in the saturation region. The results are reported in Table 13.2 and depicted in Fig. 13.10. One can observe that the hole mobility in the blend is almost independent of the processing solvent while its value is very close to the pristine material. Considering the electron transport, we found that the blend processed from oDCB represents the only case that shows electron mobility above $10^{-4}\,cm^2/Vs$, while μ_e in the toluene blend is even lower compared to the pristine material. In blended films cast from $CHCl_3$ or toluene the electron field-effect mobility is up to two orders of magnitude lower than that for the holes.

The presence of a homogeneously mixed PCBM phase can cause a reduction of the hole mobility. This happens due to a reduced volume occupied by the polymer in combination with changes in the molecular arrangement of the polymer chains due to the presence of PCBM. The lack of changes on μ_h in our case suggests two main possibilities: (a) polymer segregation at the bottom interface inducing a low density of PCBM at the bottom interface or (b) a rather homogeneous molecular mixing of PCBM with the polymer matrix. An investigation of the field effect

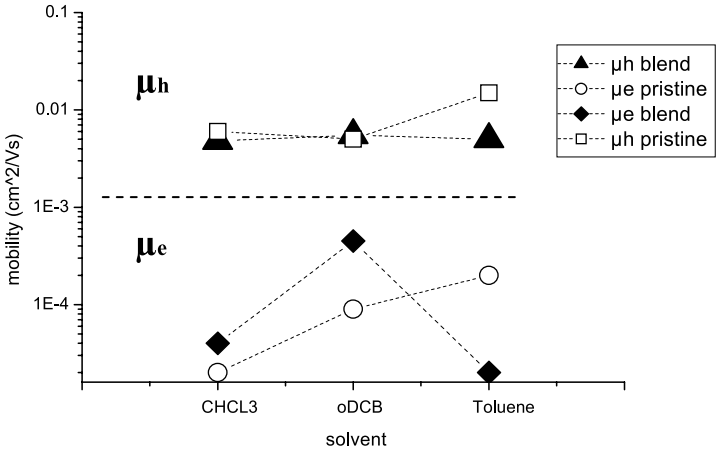

Fig. 13.10. Comparison of electron and hole mobility in pristine PCPDTBT and in blend with PCBM (1:1 ratio) for different solvents

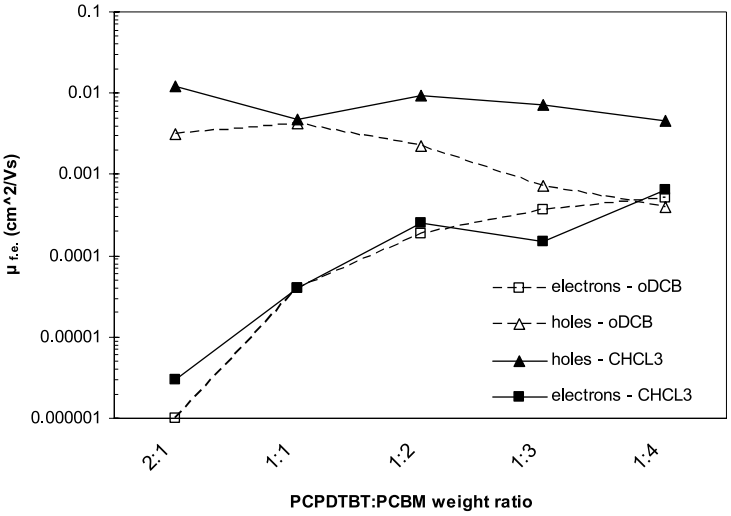

Fig. 13.11. Comparison of electron and hole field effect mobility in PCPDTBT:PCBM blend with different polymer:fullerene weight ratios for different solvents: oDCB and chloroform

mobility of holes and electrons versus the polymer:fullerene ratio for films spin-cast and doctor-bladed from various solvents helps to distinguish between these two phenomena. The results (Fig. 13.11) relative to spin-coated films clearly show that the high fullerene content in the blend is required to achieve a sufficient electron mobility to reduce transport losses. We found that the electron mobility matches the hole mobility at a fullerene weight content that is at least four times higher than the polymer content which indicates a rather homogeneous mixing of PCBM in the

polymer matrix. In this case the field-effect mobility of both charge carriers is balanced and is in the range 4×10^{-4}–7×10^{-4} cm^2/Vs when oDCB is used as solvent. Generally, in the range of investigated ratios the hole mobility only varies slightly with the PCBM content. The optimal composition for charge transport is found at 1:4 ratios, which is an important design rule to optimize the performance of solar cell devices from these composite.

In summary, PCPDT-BT is one of the highly promising low-bandgap polymers with good optical and electrical properties. Following the design rules for efficiency prediction, this polymer has the potential to show a performance around 7%, with more at reasonable FF and EQE values. Morphology investigations, however, open up the concern of a poor electron percolation of the PCBM network with respect to the holes of the polymer, resulting in a design rule that demands high fullerene contents, around 80wt.%, to overcome the electron transport limitation and to achieve optimal performances.

13.4 Photovoltaic Performance of PCPDT-Based Solar Cells

In this section we present and discuss the device performance of PCPDT-BT:PCBM composites. Before embedding them into devices, the thin-coated films were investigated by absorption and luminescence spectroscopy (Fig. 13.12). The solid-state absorption peaks at 775 nm (1.6 eV) and has an onset at approximately 890 nm (1.40 eV) with a strong tailing in the solid state, which makes determination of the onset difficult. Interestingly, PCPDT-BT exhibits a quite strong bathochromic shift in the absorption of approximately 70 nm between solution and solid-state films. Such shifts [54] have been frequently observed for rigid conjugated polymers with

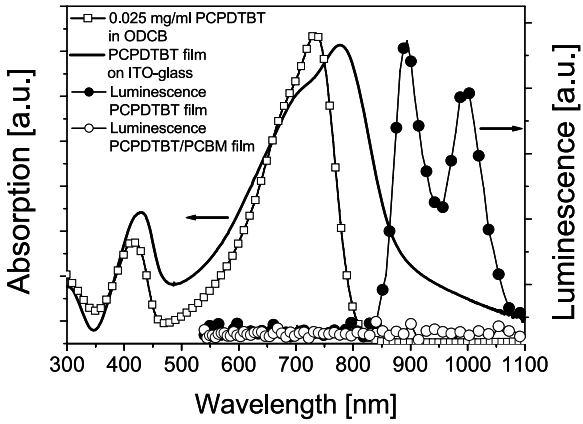

Fig. 13.12. Comparison of solid state absorption (*black line*) and solution absorption (*open squares*) to the solid state luminescence of PCPDTBT and the luminescence quenching for the blend with PCBM, EgOpt $\sim$ 1.38 eV

a strong interchain interaction and are a sign of two-dimensional stacking and extension of the conjugation over two dimensions. As expected from the small optical bandgap, the photoluminescence of PCPDTBT lies in the infrared (IR), between 1.2 eV and 1.4 eV and can be almost completely quenched by addition of PCBM. Very efficient photoluminescence (PL) quenching is the signature of the ultrafast photo-induced charge transfer from PCPDTBT to PCBM, a prerequisite for efficient solar cells, in good accordance with the position of the electrochemical levels as depicted in Fig. 13.13(a).

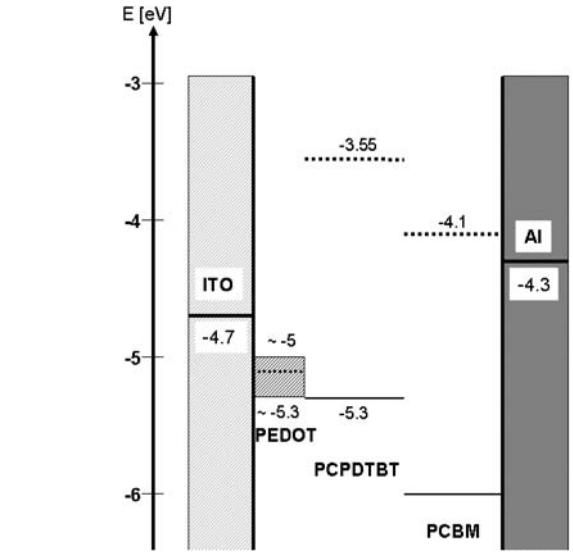

(a)

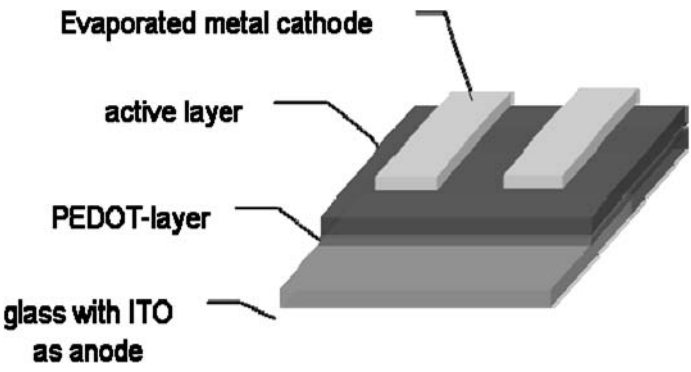

(b)

Fig. 13.13. (**a**) Energy scheme for a PCPDTBT/PCBM device; (**b**) build-up of device layers and (**c**) comparison of device characteristics PCPDTBT/PC61BM and PCPDTBT/PC71BM

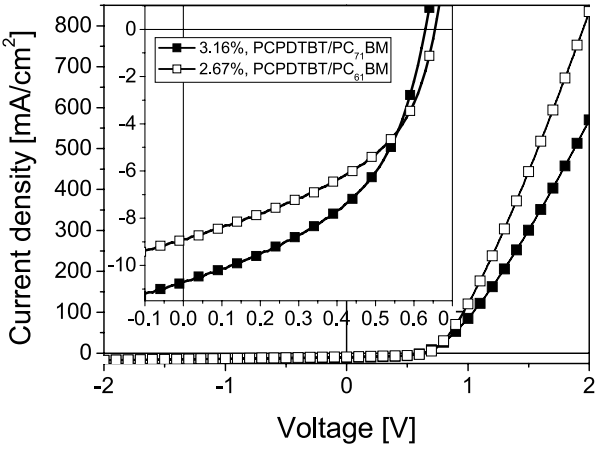

(c)

Fig. 13.13. Continued

Photovoltaic devices were produced according to the scheme shown in Fig. 13.13(b). The active layer, processed from solutions with and without additives like mono or dithiols, was embedded between PEDOT and LiF/Al [14] or TiOx/Al [11, 12] interfaces. ITO on glass was used as a transparent bottom electrode. Figure 13.13(c) shows the current voltage (jV) characteristics of PCPDTBT/PC_{61}BM and PCPDTBT/PC_{71}BM devices. Under AM1.5 illumination of 100 mW/cm^2, outstanding high photocurrents up to 10 mA/cm^2 [14] are reached for the blend with PC_{61}BM and more than 15 mA/cm^2 [11, 12] are observed for blends with PC_{71}BM. PC_{71}BM was used to further broaden the effectively used spectral range for the photocurrent, as can be seen from the EQE spectra shown in Fig. 13.14(a).

A clear additional contribution arising from PC_{71}BM around 500 nm results in an additional peak of the photocurrent spectrum reaching 35% EQE in the case of semiconductors layers processed without additives. Clearly, the usage of PC_{71}BM accounts for the higher I_{SC} of the PCPDTBT/PC_{71}BM device. The open-circuit voltage V_{OC} is typically at 650 mV; the highest observed values were close to 700 mV. These values fulfill the expectations derived from the position of the electrochemical potentials.

While the observed photocurrent and also the photovoltage are already satisfyingly high, the low fill factor (FF) of the device limits the overall performance. From the high-injection currents at low voltages and the good diode behavior (see Fig. 13.13) the presence of a large serial resistivity can be ruled out as responsible for the limitation of the FF. In addition, the high mobilities of PCPDTBT and PCBM allow exclusion of transport limitation of the individual components. In accordance to the earlier discussions, two possible underlying mechanisms with relevance to this observation are suggested: first, and most likely, an unfavorable morphology of the polymer/fullerene blend leads to recombination. The slope of

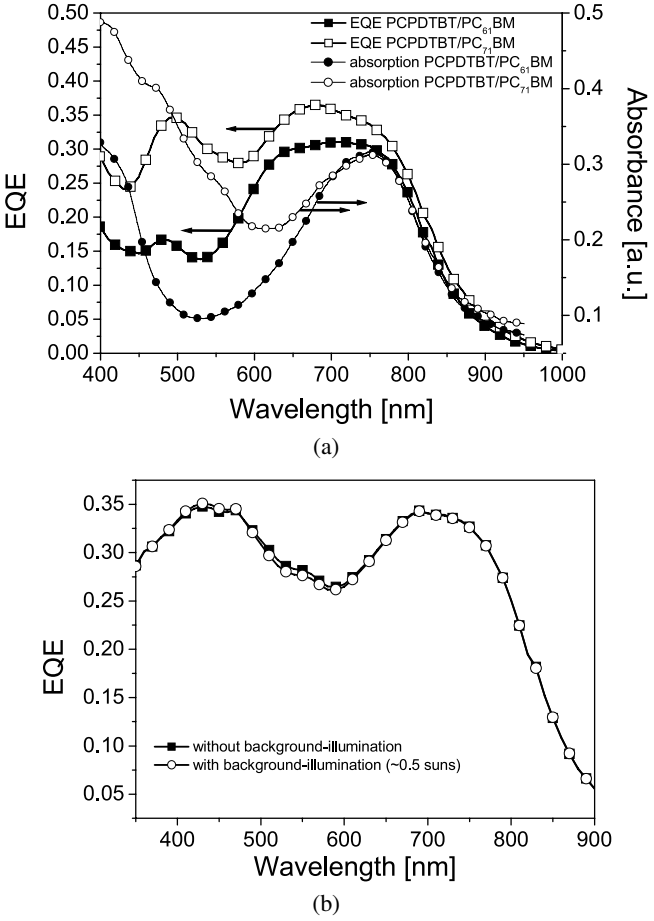

Fig. 13.14. (**a**) EQE and absorption spectra of a blend of PCPDTBT/PC_{61}BM and PCPDTBT/PC_{71}BM, the EQE shows similar differences as the absorption profile for the two blends. (**b**) EQE of a typical blend of PCPDTBT/PC_{71}BM with and without background light. (**c**) EQE of typical blends of PCPDTBT/PC_{71}BM under reverse bias. (**d**) Temperature dependence of the photocurrent of a typical PCPDTBT/PCBM solar cell

the photocurrent curve under reverse bias then indicates that higher electrical fields are necessary to collect the charge carriers and in that way diminish the recombination losses. This recombination can be of first or of second order. Second, the close energetic proximity of the donor and acceptor LUMO levels (∼3.55 eV for PCPDTBT and ∼4.1 eV for PCBM, respectively; see Fig. 13.13(a)) may diminish the selectivity of the metal electrode contacts, lowering the diode quality by loss mechanisms such as enhanced interface recombination or tunnel injection under reverse bias. In addition, the slightly unfavorable field dependence of the PCPDTBT composites suggests transport-induced losses in the low field regions, i.e., close

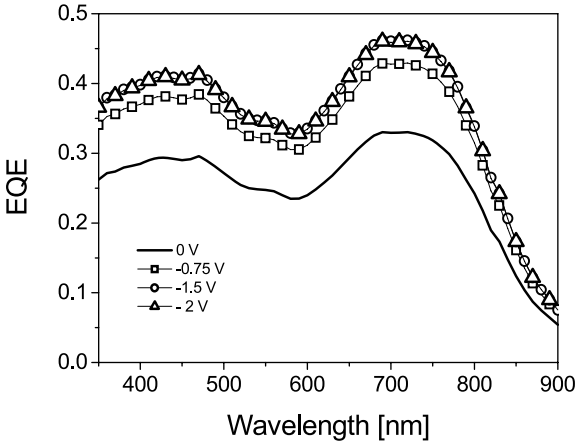

(c)

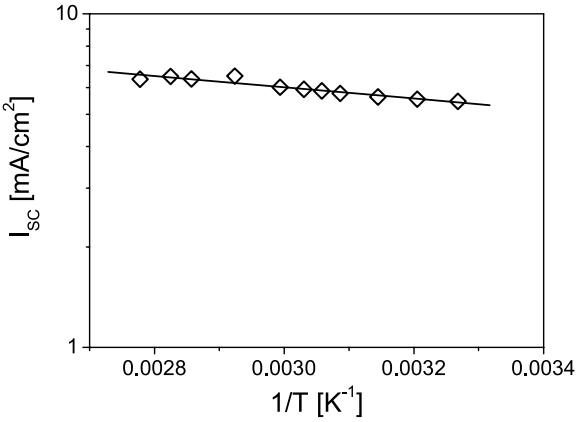

(d)

Fig. 13.14. Continued

to and around V_{oc}. In order to learn more about the recombination mechanisms in PCPDTBT/PCBM composites, white-light bias and field-dependent EQE measurements were executed and analyzed on typical PCPDTBT/PC_{71}BM devices. The EQE of a PCPDTBT/PC_{71}BM device (Fig. 13.14(a)) has two dominant features – a near-IR peak between 700 nm and 800 nm as well as a UV/Vis peak around 500 nm. The onset of photocurrent starts beyond 900 nm is in excellent agreement with the optical data. The EQE is absolutely symbatic and peaks at ∼38% in the 700–800 nm region. Using dithiol as an additive to the semiconductor blends, EQE values as high as 50% could be demonstrated, which is by far the highest value for any organic low bandgap material [11, 12].

While the near-IR peak is unambiguously identified with the PCPDTBT absorption, the UV/Vis peak is dominated by the absorption of the fullerene PC_{71}BM or

$PC_{61}BM$. The reduced absorption of $PC_{61}BM$ in the 500 nm region leads to reduction of the photocurrent by approximately 40 to 50%. Figure 13.14(b) shows the spectral shape of the EQE with background illumination. In case of classical second-order recombination dominating the device performance of PCPDTBT/PCBM, one would expect a major difference between these two measurement conditions. Due to charge density under white light bias that is orders of magnitude larger, the presence of bimolecular recombination would lead to a reduction of the EQE. This effect is not observed and we can safely conclude that second-order recombination mechanisms are not relevant at Jsc. Figure 13.14(c) shows the field dependence of the EQE. A white light background bias is applied to compensate for the influence of photoconductivity. Under reverse bias, the EQE continuously rises and saturates at a bias of approximately −2 V. At that bias level, the EQE has increased by a factor of approximately 1.5, from 35% to almost 50%. In parallel, the quasi-steady state photocurrent at −2 V is a factor of 10 higher than under I_{SC} conditions. This phenomenon, which is a peculiar property of most BHJ solar cell systems, is called photo shunting and was introduced in detail recently [55]. Such a strong photo shunt effect as observed for PCPDTBT/$PC_{71}BM$ devices indicates a nonselective electrode interface.

In addition, the temperature dependence of PCPDTBT/$PC_{71}BM$ devices was studied. From previous studies it is well known that the photocurrent of polymer/fullerene solar cells is determined by the choice of the polymer. For instance, devices from MDMO-PPV/PCBM [56] show distinct positive temperature dependence while devices from P3HT/PCBM [57] can be almost temperature independent. Figure 13.14(d) shows the temperature dependence of the photocurrent of PCPDTBT/$PC_{71}BM$ devices. We chose an Arrhenius-like plot to quantitatively evaluate the temperature dependence. Figure 13.14(d) clearly indicates that PCPDTBT/$PC_{71}BM$ devices have a quite strong temperature dependence of the photocurrent, comparable to earlier observations for MDMO-PPV/PCBM devices. It is a clear indication that transport on one or both of the materials in the composite suffer from the presence of shallow traps, likely connected to enhanced energetical disorder in the blend.

Taking into account all data acquired so far, the efficiency of PCPDT-BT/PCBM cells can be predicted quite well once the morphology is optimized. The EQE under reverse bias as well as the recently published model [11, 12] suggest short-circuit currents on the order of 17 mA/cm^2. In combination with more selective electrodes, a polymer with such a high mobility will show FF higher than 0.6. Together with a V_{oc} of 700 mV, these parameters qualify PCPDTBT as a candidate for exceeding 7% efficiency [11, 12, 14]. For a polymer closely related to PCPDT, with a similar structure, indeed better performance was observed. The NREL certificate shown in Fig. 13.15 rates this polymer at over 5%. Here, the current densities of 15 mA/cm^2 and the FF of 61% are already quite close to the expected maximum. Only the slightly lower V_{oc} of 580 mV reduces the efficiency to the 5–6% regime instead of the 6–7% regime.

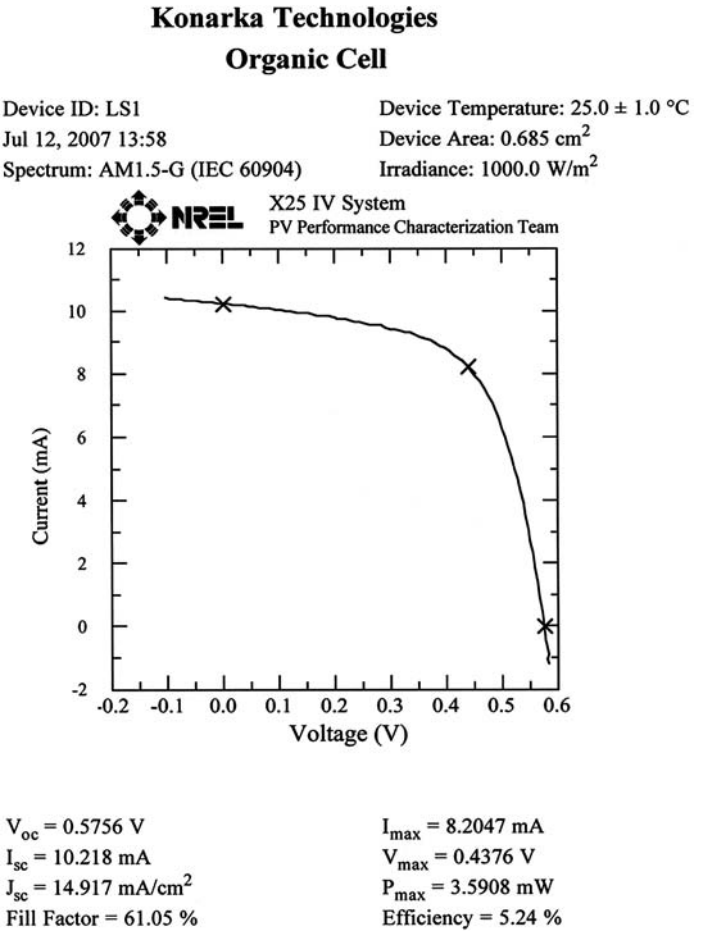

Fig. 13.15. NREL certificate for a polymer/fullerene solar cell using a low-bandgap polymer as donor

13.5 From Single-Junction to Multijunction Solar Cells

With the existence of a well-performing low-bandgap polymer, the realization of multijunction solar cells becomes possible. The PCPDT-BT series, with a bandgap of about 1.4 eV, is certainly suitable for the incorporation into multijunction solar cells. Another reason why PCPDT-BT perfectly suits the tandem approach is the reduced transport properties induced by a nonideal morphology, which limits the active layers thickness to below 200 nm and external quantum efficiencies (EQE) less than 35% [14] and 50%, respectively [11, 12]. Thus, combining P3HT and PCPDTBT in a series connected tandem solar cells appears likely to push forward the performance of devices based on the individual materials. There has been

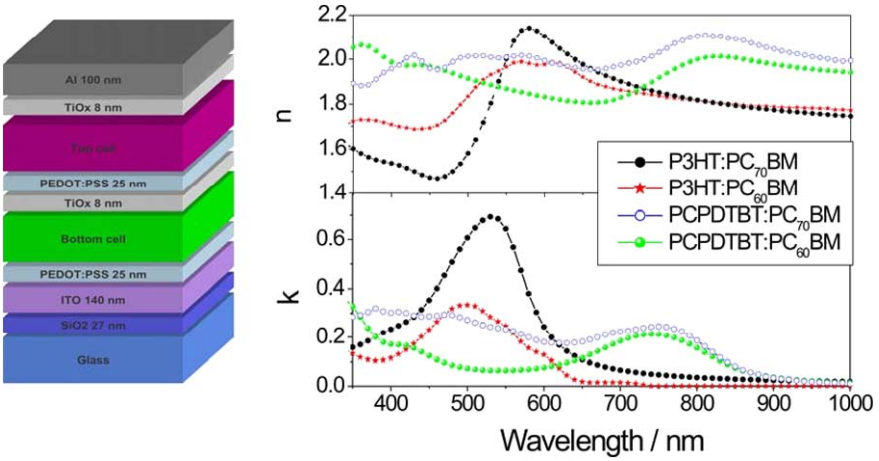

Fig. 13.16. Scheme of the structure of the tandem cells simulated, and real and imaginary parts of the complex refractive indexes of the various active materials used for the simulations

tremendous progress in the design and in the realization of tandem cells. While the first tandem concepts and interfacial layers suffered from either high absorption, nonideal transport properties, or recombination losses [58–60] leading to either unmatched current densities or to low FF, Kim et al. [61] recently presented a tandem architecture with which he reported an FF of more than 65% and efficiencies as high as 6.5%. The structure of a tandem cell from Kim, based on two half cells with P3HT and PCPDT-BT, respectively, is shown in Fig. 13.16. It is composed of a thick (thicker than the coherence length of the light) glass substrate, followed by 27 nm of SiO_2, 140 nm of indium tin oxide (ITO), 25 nm of poly(3, 4-ethylenedioxythiophene) doped with poly(styrene sulfonate) (PEDOT:PSS), a variable thickness bottom active layer, 8 nm of sol-gel TiOx, 25 nm of PEDOT:PSS, a variable thickness top active layer, 8 nm of sol-gel TiOx, and finally 100 nm of Al. The optical parameters of the four active blends that have been treated are displayed in Fig. 13.16. The TiOx/PEDOT layer is called the recombination layer, and serves the function to interconnect the two half cells in series.

It appears that the usage of PC70BM instead of PC60BM permits enlarging the imaginary part of the complex refractive index and therefore the extinction coefficient of the blends, especially in the range 350–700 nm. It is interesting to note that the PCPDTBT:PC60BM blend shows a minimum in absorption at 550 nm, exactly where the P3HT:PC70BM shows a maximum.

Looking to the structure of the tandem cell, one immediately realizes that the low bandgap polymer is the front absorber, while the wide bandgap polymer is the back absorber. This is opposite to inorganic solar cells, where the wide bandgap absorber is always placed in front. However, due to the specific optical absorption profiles of the two polymers, it turns out that the configuration with the wide bandgap polymer as the front absorber allows higher performance compared to the other layer

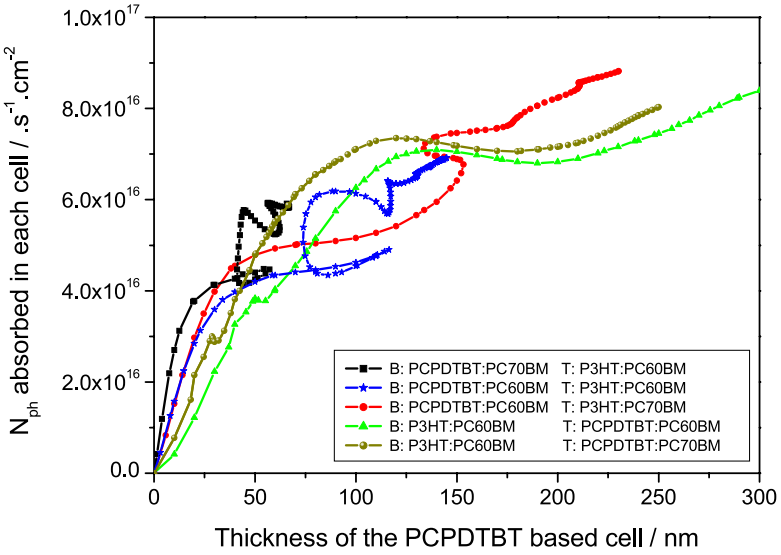

Fig. 13.17. Number of photons absorbed in both active layers (isoline 1) versus the thickness of the PCPDTBT based active layer for various material combinations under AM1.5G

architecture. The optical methodology used to analyze and predict the tandem architecture is close to the approach employed by Persson et al. [62] and is described in detail elsewhere [63]. For each active layer couple, the thickness of both the bottom (between 0 and 300 nm) and the top (between 0 and 600 nm) active layers and calculated the number of photons absorbed (N_{ph}) in those layers under AM1.5G. The design rule for tandem cells requires that the current density in the two half cells needs to be identical. Under the assumption of identical quantum efficiencies, the number of absorbed photons N_{ph} in each layer has to match. The pairs of film thicknesses, where the N_{ph} in both layers is identical, is called the isoline 1. Valuable information can be deducted from the N_{ph}, plotted versus the thickness of the single layers as shown in Fig. 13.17. This one displays the N_{ph} along the isolines 1 versus the thickness of the PCPDTBT-based cell. This way of plotting was chosen because PCPDT-BT cannot be processed in thick layers without losing its performance. As such, it is more critical to optimize the thickness of this cell. This plot yields quite unusually shaped curves, since N_{ph} of a single film thickness of the PCPDT-BT layer can be matched by multiple layer thicknesses of the P3HT layer due to optical interference effects. The precise information on the absorbed photon density now allows us to distinguish and rate the first and the last cases. Specifically one case, where PCPDT-BT/PC60BM is used as the bottom layer and P3HT/PC70BM is used as the top layer appears to be the most promising for reasonable thicknesses of the PCPDT-BT layer – between 130 and 230 nm. Under these conditions, the number of absorbed photons becomes maximized, which should be reflected in higher current densities compared to the other scenarios.

Having established and verified the optical model for organic tandem cells, one is able to answer the question of the ultimate efficiency potential of these two materials. According to the above calculations, the blends chosen by Kim et al. to realize their highly efficient organic tandem cell is the very one identified here as being the most promising by optical simulation. The combination of film thicknesses chosen for the realization of the tandem cell were about 135 nm for the PCPDT-BT layer and 155 nm for the P3HT layer, resulting in an absorbed photon density of 7.3×10^{16} photons $s^{-1}\,cm^{-2}$. Assuming an IQE of 100%, this N_{ph}, folded with the solar spectrum, would yield a short-circuit current density of 11.7 mA cm^{-2}, while the current reported for this device is about 7.8 mA cm^{-2}. This indicates that the limiting subcell driving the Jsc in the tandem has an IQE of 67%, a value in good accordance with the IQE values we have determined for PCPDTBT:PC60BM single devices. Hence this suggests that the performance of the device is limited by the PCPDTBT subcell and one can not expect efficiencies beyond 7% for this combination. Assuming an EQE of over 50% and an IQE of about 85% as was reported for PCPDT-BT when processed with additives [11, 12], one calculates a short-circuit current density of almost 10 mA cm^{-2} for the tandem cell. With a FF of 0.65 and a V_{oc} of 1.2 V, an efficiency of nearly 8% is expected for such a tandem cell.

Finally, it is interesting to discuss the efficiency potential of tandem cells versus single-junction solar cells. Again, we discuss this by way of a simplified picture, where we assumed fixed FF and fixed EQE values. The same model as suggested in the first part of this paper was expanded to tandem cells. In order to fulfill the tandem design rule – i.e. matching of the current densities – it is necessary to describe the integrated AM1.5 photon density by a linear fit. Using a simple linear fit, and again assuming that the EQE has a rectangular profile, the current density can be given as a function of the bandgap. In order to calculate the maximum possible efficiency of a tandem cell in dependence of the lower bandgap absorber, the tandem design rule was applied. Each of the half cells was assigned to absorb half of the photon density compared to the single-junction solar cell. The bandgap of the wide-bandgap material was calculated according to matching the photon density of the low bandgap solar cell to the current density. The V_{oc} was calculated directly from the bandgap, assuming the CT and V_{oc} losses of 0.5 V as assumed above. One has to keep in mind that the linear fit of the integrated photon density does deviate from the real situation, especially at very low and very high wavelengths. Nevertheless, the model is very useful to understand how a tandem cell can reach higher efficiencies compared to single junction cells. Figure 13.18 summarizes the scenario by plotting the maximum possible efficiency of single-junction solar cells versus the bandgap and of tandem junction solar cells versus the bandgap. In the case of the tandem junction solar cell, the bandgap is, of course, the bandgap of the low bandgap absorber, while the bandgap of the wide bandgap absorber is calculated to fulfill the current matching condition. As such, the calculated tandem efficiency can be regarded as the highest possible tandem efficiency which can be gained with that low bandgap polymer. Figure 13.18 clearly points out that tandem cells benefit from even lower bandgap polymers as single-junction solar cells. While the efficiency of

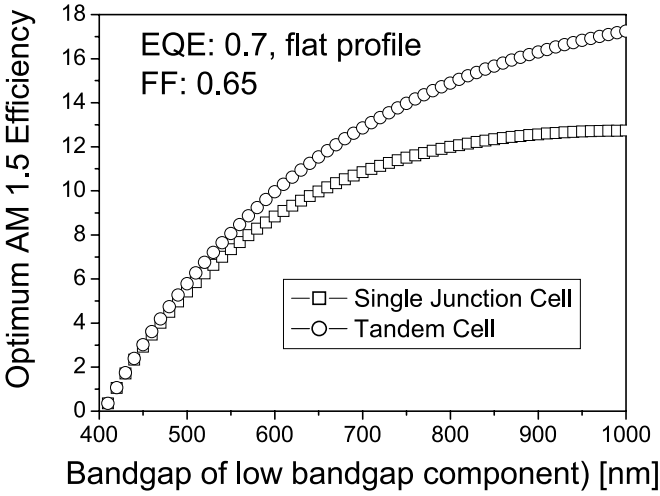

Fig. 13.18. Plot of the max efficiencies for single-junction cells versus tandem cells versus the bandgap of the low-bandgap absorber

single-junction solar cells flattens out at a bandgap of about 900–950 nm, the tandem efficiency still would further increase with lower bandgaps. Also interesting to note is that the tandem cell has nearly no benefit compared to single-junction solar cells for polymers with a bandgap below 600–650 nm.

13.6 Summary

Organic bulk heterojunction solar cells have overcome the 5% efficiency barrier, with current efficiencies rated between 5–6%. For single-junction BHJ solar cells, there are no obstacles to prevent reaching the 10% milestone. To increase the efficiency beyond 10% cell efficiency, various scenarios are currently being discussed and developed. Tandem cells certainly have the potential to reach efficiencies of up to 15%. An alternative path is to reduce the current intrinsic losses of the single-junction solar cells. One the one hand, the energy losses of about 0.25 eV are due to the photo-induced charge transfer. On the other hand the V_{oc} losses of about 0.25 V are due to the dark current injection. Overcoming each of these losses would significantly increase the efficiency potential of the organic solar cells. Assuming no energetic losses at all, an FF of 0.7 and a rectangular EQE as high as 90%, the maximum efficiency of almost 30% is predicted for a bandgap between 1–1.25 eV. All of these approaches rely on high-performing, low-bandgap polymers and underline the importance and necessity of developing such polymers. Copolymers from bridged bithiophenes and acceptors, the so-called PCPDT-X series, may be the polymers that enable these new efficiency concepts.

References

1. D.M. Chapin, C.S. Fuller, G.L. Pearson, J. Appl. Phys. **25**, 676–677 (1954)
2. M.D. Archer, R.R Hill (eds.), *Clean Electricity from Photovoltaics*. Series on Photoconversion of Solar Energy, vol. 1 (Imperial College Press, London, 2001)
3. A. Goetzberger, C. Hebling, Sol. Energy Mater. Sol. Cells **62**, 1–19 (2000)
4. C.J. Brabec, J. Hauch, P. Schilinsky, C. Waldauf, MRS Bull. **30**(1), 50–52 (2005)
5. Organic-based photovoltaics. MRS Bull. **30**(1), 10–52 (2005)
6. N.S. Sariciftci, L. Smilowitz, A.J. Heeger, F. Wudl, Science **258**, 1474 (1992)
7. C.J. Brabec, G. Zerza, N.S. Sariciftci, G. Cerullo, S. DeSilvestri, S. Luzatti, J.C. Hummelen, Chem. Phys. Lett. **340**, 232–236 (2000)
8. P. Schlinsky, C. Waldauf, C.J. Brabec, Appl. Phys. Lett. **81**, 3885–3887 (2002)
9. J. Xue, S. Uchida, B.P. Rand, S.R. Forrest, Appl. Phys. Lett. **85**, 5757–5759 (2004)
10. L. Schmidt-Mende et al., Adv. Mat. **17**, 813–815 (2005)
11. J. Peet, J.Y. Kim, N.E. Coates, W.L. Ma, D. Moses, A.J. Heeger, G.C. Bazan, Nat. Mater. **6**, 497 (2007)
12. J.Y. Kim, K. Lee, N.E. Coates, D. Moses, T.-Q. Nguyen, M. Dante, A.J. Heeger, Science **317**, 222 (2007)
13. M. Scharber, D. Mühlbacher, M. Koppe, P. Denk, C. Waldauf, A.J. Heeger, C.J. Brabec, Adv. Mater. **8**, 789 (2006)
14. D. Muehlbacher, M. Scharber, M. Morana, Z. Zhu, D. Waller, R. Gaudiana, C.J. Brabec, Adv. Mater. **18**, 2884–2889 (2006)
15. Z. Zhu, D. Waller, R. Gaudiana, M. Morana, D. Mühlbacher, M. Scharber, C.J. Brabec, Macromolecules **40**(6), 1981–1986 (2007)
16. M. Morana, Z. Zhu, D. Waller, R. Gaudiana, M. Scharber, C.J. Brabec, Adv. Funct. Mat. **18**, 1757–1766 (2008)
17. P. Schilinsky, C. Waldauf, J. Hauch, C.J. Brabec, J. Appl. Phys. **95**, 2816–2819 (2004)
18. Konarka NREL certificate from July 2005, October 2006 and August 2007
19. Plextronics NREL certificate from August 2007
20. W. Ma, C. Yang, X. Gong, K. Lee, A.J. Heeger, Adv. Funct. Mater. **15**, 1617 (2005)
21. M. Reyes-Reyes, K. Kim, D.L. Carrol, Appl. Phys. Lett. **87**, 083506–08350611 (2005)
22. G. Li, V. Shrotriya, J. Huang, Y. Yao, T. Moriarty, K. Emery, Y. Yang, Nat. Mater. **4**, 864 (2005)
23. C. Winder, N.S. Sariciftci, Mater. Chem. **14**, 1077–1086 (2004)
24. B.P. Rand, J. Xue, F. Yang, S.R. Forrest, Appl. Phys. Lett. **87**, 233508/1–233508/3 (2005)
25. E. Bundgaard, F.C. Krebs, Macromolecules **39**, 2823–2831 (2006)
26. F. Huang, L. Hou, H. Shen, J. Jiang, F. Wang, H. Zhen, Y.J. Cao, Mater. Chem. **15**, 2499–2507 (2005)
27. M. Velusamy, K.R.J. Thomas, J.T. Lin, Y.C. Hsu, K.C. Ho, Org. Lett. **7**, 1899–1902 (2005)
28. R. Yang, R. Tian, J. Yan, Y. Zhang, J. Yang, Q. Hou, W. Yang, C. Zhang, Y. Cao, Macromolecules **38**, 244–253 (2005)
29. Q. Hou, Q. Zhou, Y. Zhang, W. Yang, R. Yang, Y. Cao, Macromolecules **37**, 6299–6305 (2004)
30. F. Huang, L. Hou, H. Wu, X. Wang, H. Shen, W. Cao, W. Yang, Y. Cao, J. Am. Chem. Soc. **126**, 9845–9853 (2004)
31. M. Chen, E. Perzon, M.R. Andersson, S. Marcinkevicius, S.K.M. Jonsson, M. Fahlman, M. Berggren, Appl. Phys. Lett. **84**, 3570–3572 (2004)
32. D. Muhlbacher, H. Neugebauer, A. Cravino, N.S. Sariciftci, Synth. Met. **137**, 1361–1362 (2003)

33. C.J. Brabec, C. Winder, N.S. Sariciftci, J.C. Hummelen, A. Dhanabalan, P. Van Hal, R.A.J. Janssen, Adv. Funct. Mater. **12**, 709–712 (2002)
34. Q. Hou, Y. Xu, W. Yang, M. Yuan, J. Peng, Y. Cao, J. Mater. Chem. **12**, 2887–2892 (2002)
35. H.A.M. Van Mullekom, J.A.J.M. Vekemans, E.W. Meijer, Chem. Eur. J. **4**, 1235–1243 (1998)
36. M. Karikomi, C. Kitamura, S. Tanaka, Y. Yamashita, J. Am. Chem. Soc. **117**, 6791–6792 (1995)
37. J. Roncali, Chem. Rev. **97**, 173–205 (1997)
38. S.E. Shaheen, D. Vangeneugden, R. Kiebooms, D. Vanderzande, T. Fromherz, F. Padinger, C.J. Brabec, N.S. Sariciftci, Synth. Met. **121**, 1583–1584 (2001)
39. C. Winder, G. Matt, J.C. Hummelen, R.A.J. Janssen, N.S. Sariciftci, C.J. Brabec, Thin Solid Films **403–404**, 373–379 (2002)
40. A. Dhanabalan, J.K.J. Van Duren, P.A. Van Hal, J.L.J. Van Dongen, R.A.J. Janssen, Adv. Funct. Mater. **11**, 255–262 (2001)
41. A.P. Smith, R.R. Smith, B.E. Taylor, M.F. Durstock, Chem. Mater. **16**, 4687–4692 (2004)
42. X. Wang, E. Perzon, F. Oswald, F. Langa, S. Admassie, M.R. Andersson, O. Inganaes, Adv. Funct. Mater. **15**, 1665–1670 (2005)
43. X. Wang, E. Perzon, J.L. Delgado, P. De la Cruz, F. Zhang, F. Langa, M.R. Andersson, O. Inganas, Appl. Phys. Lett. **85**, 5081–5083 (2004)
44. F. Zhang, E. Perzon, X. Wang, W. Mammo, M.R. Andersson, O. Inganaes, Adv. Funct. Mater. **15**, 745–750 (2005)
45. L.M. Campos, A. Tontcheva, S. Guenes, G. Sonmez, H. Neugebauer, N.S. Sariciftci, F. Wudl, Chem. Mater. **17**, 4031–4033 (2005)
46. E. Perzon, X. Wang, S. Admassie, O. Inganäs, M.R. Andersson, Polymer **47**, 4261–4268 (2006)
47. M. Kalaji, P.J. Murphy, G.O. Williams, Synth. Met. **101**, 123 (1999)
48. C.A. Mills, D.M. Taylor, P.J. Murphy, C. Dalton, G.W. Jones, L.M. Hall, A.V. Hughes, Synth. Met. **102**, 1000–1001 (1999)
49. C. Soci, I.-W. Hwang, D. Moses, Z. Zhu, D. Waller, R. Gaudiana, C.J. Brabec, A.J. Heeger, Adv. Funct. Mater. **17**, 632–636 (2007)
50. T. Erb, U. Zhkavhets, G. Godch, S. Raleva, B. Stuhn, P. Schilinsky, C. Waldauf, C.J. Brabec, Adv. Funct. Mat. **15**, 1193–1196 (2005)
51. R.A. Street, J.E. Northrup, A. Salleo, Phys. Rev. B **71**, 165202 (2005)
52. G. Horowitz, J. Mater. Res. **19**, 7 (2004)
53. M. Morana, P. Koers, C. Waldauf, M. Koppe, D. Muehlbacher, P. Denk, M.C. Scharber, D. Waller, C.J. Brabec, Adv. Funct. Mat. **17**(16), 3274–3283 (2007)
54. P.J. Brown, D.S. Thomas, A. Köhler, J.S. Wilson, J.-S. Kim, C.M. Ramsdale, H. Sirringhaus, R.H. Friend, Phys. Rev. B **67**, 0642031 (2003)
55. P. Schilinsky, C. Waldauf, J. Hauch, C.J. Brabec, J. Appl. Phys. **95**, 2816 (2004)
56. E. Katz, D. Faiman, S.M. Tuladhar, J.M. Kroon, M.M. Wienk, T. Fromherz, F. Padinger, C.J. Brabec, N.S. Sariciftci, J. Appl. Phys. **90**, 5343 (2001)
57. I. Riedel, V. Dyakonov, Phys. Stat. Sol. A **201**, 1332 (2004)
58. A. Hadipour, B. de Boer, J. Wildeman, F.B. Kooistra, J.C. Hummelen, M.G.R. Turbiez, M.M. Wienk, R.A.J. Janssen, P.W.M. Blom, Adv. Funct. Mater. **16**, 1897 (2006)
59. J. Gilot, M.M. Wienk, R.A.J. Janssen, Appl. Phys. Lett. **90**, 143512 (2007)
60. G. Dennler, H.-J. Prall, R. Koeppe, M. Egginger, R. Autengruber, N.S. Sariciftci, Appl. Phys. Lett. **89**, 073502 (2007)

61. J.Y. Kim, K. Lee, N.E. Coates, D. Moses, T.-Q. Nguyen, M. Dante, A.J. Heeger, Science **317**, 222 (2007)
62. N.-K. Persson, O. Inganas, Sol. Energy Mater. Sol. Cells **90**, 3491 (2006)
63. G. Dennler, T. Ameri, C. Waldauf, P. Denk, K. Hingerl, K. Forberich, A.J. Heeger, C.J. Brabec, J. Appl. Phys. **102**, 123109 (2007)

Index

Springer Series in
OPTICAL SCIENCES

Volume 1

1 **Solid-State Laser Engineering**
By W. Koechner, 5th revised and updated ed. 1999, 472 figs., 55 tabs., XII, 746 pages

Published titles since volume 110

110 **Kramers-Kronig Relations in Optical Materials Research**
By V. Lucarini, J.J. Saarinen, K.-E. Peiponen, and E.M. Vartiainen, 2005, 37 figs., X, 162 pages

111 **Semiconductor Lasers**
Stability, Instability and Chaos
By J. Ohtsubo, 2nd edn. 2007, 169 figs., XIII, 475 pages

112 **Photovoltaic Solar Energy Generation**
By A. Goetzberger and V.U. Hoffmann, 2005, 139 figs., XII, 234 pages

113 **Photorefractive Materials and Their Applications 1**
Basic Effects
By P. Günter and J.P. Huignard, 2006, 169 figs., XIV, 421 pages

114 **Photorefractive Materials and Their Applications 2**
Materials
By P. Giinter and J.P. Huignard, 2006, 370 figs., XVII, 640 pages

115 **Photorefractive Materials and Their Applications 3**
Applications
By P. Günter and J.P. Huignard, 2007, 316 figs., X, 366 pages

116 **Spatial Filtering Velocimetry**
Fundamentals and Applications
By Y. Aizu and T. Asakura, 2006, 112 figs., XII, 212 pages

117 **Progress in Nano-Electro-Optics V**
Nanophotonic Fabrications, Devices, Systems, and Their Theoretical Bases
By M. Ohtsu (Ed.), 2006, 122 figs., XIV, 188 pages

118 **Mid-infrared Semiconductor Optoelectronics**
By A. Krier (Ed.), 2006, 443 figs., XVIII, 751 pages

119 **Optical Interconnects**
The Silicon Approach
By L. Pavesi and G. Guillot (Eds.), 2006, 265 figs., XXII, 389 pages

120 **Relativistic Nonlinear Electrodynamics**
Interaction of Charged Particles with Strong and Super Strong Laser Fields
By H.K. Avetissian, 2006, 23 figs., XIII, 333 pages

121 **Thermal Processes Using Attosecond Laser Pulses**
When Time Matters
By M. Kozlowski and J. Marciak-Kozlowska, 2006, 46 figs., XII, 217 pages

122 **Modeling and Analysis of Transient Processes in Open Resonant Structures**
New Methods and Techniques
By Y.K. Sirenko, N.P. Yashina, and S. Ström, 2007, 110 figs., XIV, 353 pages

123 **Wavelength Filters in Fibre Optics**
By H. Venghaus (Ed.), 2006, 210 figs., XXIV, 454 pages

124 **Light Scattering by Systems of Particles**
Null-Field Method with Discrete Sources: Theory and Programs
By A. Doicu, T. Wriedt, and Y.A. Eremin, 2006, 123 figs., XIII, 324 pages

Springer Series in
OPTICAL SCIENCES

125 **Electromagnetic and Optical Pulse Propagation 1**
Spectral Representations in Temporally Dispersive Media
By K.E. Oughstun, 2007, 74 figs., XX, 456 pages

126 **Quantum Well Infrared Photodetectors**
Physics and Applications
By H. Schneider and H.C. Liu, 2007, 153 figs., XVI, 250 pages

127 **Integrated Ring Resonators**
The Compendium
By D.G. Rabus, 2007, 243 figs., XVI, 258 pages

128 **High Power Diode Lasers**
Technology and Applications
By F. Bachmann, P. Loosen, and R. Poprawe (Eds.), 2007, 543 figs., VI, 548 pages

129 **Laser Ablation and its Applications**
By C.R. Phipps (Ed.), 2007, 300 figs., XX, 586 pages

130 **Concentrator Photovoltaics**
By A. Luque and V. Andreev (Eds.), 2007, 250 figs., XIII, 345 pages

131 **Surface Plasmon Nanophotonics**
By M.L. Brongersma and P.G. Kik (Eds.), 2007, 147 figs., VII, 271 pages

132 **Ultrafast Optics V**
By S. Watanabe and K. Midorikawa (Eds.), 2007, 339 figs., XXXVII, 562 pages.
With CD-ROM

133 **Frontiers in Surface Nanophotonics**
Principles and Applications
By D.L. Andrews and Z. Gaburro (Eds.), 2007, 89 figs., X, 176 pages

134 **Strong Field Laser Physics**
By T. Brabec, 2007, approx. 150 figs., XV, 500 pages

135 **Optical Nonlinearities in Chalcogenide Glasses and their Applications**
By A. Zakery and S.R. Elliott, 2007, 92 figs., IX, 199 pages

136 **Optical Measurement Techniques**
Innovations for Industry and the Life Sciences
By K.E. Peiponen, R. Myllylä and A.V. Priezzhev, 2008, approx. 65 figs., IX, 300 pages

137 **Modern Developments in X-Ray and Neutron Optics**
By A. Erko, M. Idir, T. Krist, and A.G. Michette, 2008, 299 figs., XXIII, 533 pages

138 **Optical Micro-Resonators**
Theory, Fabrication, and Applications
By R. Grover, J. Heebner, and T. Ibrahim, 2008, approx. 100 figs., XIV, 266 pages

139 **Progress in Nano-Electro-Optics VI**
Nano Optical Probing, Manipulation, Analysis, and Their Theoretical Bases
By M. Ohtsu (Ed.), 2008, 107 figs., XI, 188 pages

140 **High-Efficient Low-Cost Photovoltaics**
Recent Developments
By V. Petrova-Koch, R. Hezel, and A. Goetzberger (Eds.), 2008, 100 figs., XVI, 232 pages

141 **Light-Driven Alignment**
By B.P. Antonyuk, 2008, approx. 120 figs., XI, 330 pages